

**Autocrine and paracrine signaling contributes to acquired chemotherapeutic resistance in
Group 3 medulloblastoma**

by

Lakshana Sreenivasan

B.S., The University of Arizona, 2014

A THESIS SUBMITTED IN PARTIAL FULFILLMENT OF
THE REQUIREMENTS FOR THE DEGREE OF

DOCTOR OF PHILOSOPHY

in

THE FACULTY OF GRADUATE AND POSTDOCTORAL STUDIES
(Experimental Medicine)

THE UNIVERSITY OF BRITISH COLUMBIA

(Vancouver)

November 2021

© Lakshana Sreenivasan, 2021

The following individuals certify that they have read, and recommend to the Faculty of Graduate and Postdoctoral Studies for acceptance, the dissertation entitled:

Autocrine and paracrine signaling contributes to acquired chemotherapeutic resistance in Group 3 medulloblastoma

submitted by Lakshana Sreenivasan in partial fulfillment of the requirements for

the degree of Doctor of Philosophy

in Experimental Medicine

Examining Committee:

Dr. Chinten James Lim, Associate professor, Department of Pediatrics, UBC

Supervisor

Dr. Stephen Yip, Associate professor, Department of Pathology and Laboratory Medicine, UBC

Supervisory Committee Member

Dr. Michael R. Gold, Professor, Department of Microbiology and Immunology, UBC

Supervisory Committee Member

Dr. Amina Zoubedi, Professor, Department of Urologic Sciences, UBC

University Examiner

Dr. Marcel Bally, Professor, Department of Pathology and Laboratory Medicine, UBC

University Examiner

Additional Supervisory Committee Members:

Dr. Christopher A. Maxwell, Associate professor, Department of Pediatrics, UBC

Supervisory Committee Member

Abstract

Group 3 medulloblastoma (MB) is the most aggressive type of MB with the least favourable outcome. Although enhanced STAT3 signaling is implicated in acquired chemoresistance of multiple cancers, a role for STAT3 in MB chemoresistance is not known. Here, I evaluated if IL-6/STAT3 signaling contributes to acquired chemoresistance in Group 3 MB. Group 3 MB cells that are initially chemosensitive were rendered chemoresistant either by incremental drug selection, or by conditioning with IL-6 family cytokines. IL-6 cytokines robustly stimulated the activation of JAK/STAT3 activity, and the chemoresistant variants exhibited increased STAT3 phosphorylation when transiently treated or conditioned with IL-6. Abrogation of STAT3 or IL6R expression in the chemoresistant cells successfully restored the chemosensitivity, highlighting the requirement of IL-6/STAT3 signaling in acquired chemoresistance. MB cells rendered chemoresistant following IL-6 conditioning secreted high levels of IL-6, indicating that an IL-6 autocrine feedback loop forms an important stimulus able to sustain enhanced STAT3 signaling. Furthermore, IL-6 secreted by chemoresistant cells also stimulated phosphorylated STAT3 in treatment-naïve chemosensitive cells, suggesting acquired chemoresistance may be propagated through the tumour microenvironment via a paracrine mechanism.

I postulated that immune cells in the TME could initiate paracrine cytokine signaling. Indeed, microglia co-cultured with MB cells secreted cytokines, including IL-6, that phosphorylated STAT3 and enhanced MB chemoresistance. Unexpectedly, IL6R^{-/-} MB cells co-cultured with microglia also exhibited enhanced STAT3 phosphorylation and chemoresistance, suggesting involvement of cytokines in addition to IL-6. I then demonstrated that IL-6 family cytokines effectively induced STAT3 phosphorylation and chemoresistance. Gp130 encodes the

common β subunit for the IL-6 family cytokine receptors required for activating JAK/STAT3 signaling. Abrogation of gp130 expression in MB effectively blocked STAT3 signaling and IL-6 cytokine mediated chemoresistance. Furthermore, combination chemotherapy that included inhibitors targeting gp130, JAKs or STAT3 effectively circumvented IL-6 mediated chemoresistance in Group 3 MB. Analysis of multi-layered GEO databases of MB unveiled certain gene expression changes in the IL-6/STAT3 signaling axis that correlated with poor outcomes associated with Group 3 MB. Overall, elucidation of the role of IL-6/STAT3 signaling in cell survival and acquired chemoresistance revealed strategies for molecular targeted therapies to combat chemoresistance in Group 3 MB.

Lay Summary

Group 3 medulloblastoma is an aggressive type of medulloblastoma associated with less than 60% survival. A major caveat of chemotherapy in medulloblastoma is the harmful long-term side effects observed in infants and children as a result of aggressive treatment. My thesis highlights the importance of certain “survival signals” made up of cytokines that enable cancer cells to resist chemotherapy. When exposed to these cytokines, medulloblastoma cells gradually become more resistant to the cytotoxic, or cell death inducing effects, of chemotherapy, that can eventually lead to treatment failure and disease relapse. My overall goal was to identify and understand the function of the molecular factors promoting the survival of the few cells that ultimately become treatment resistant. Once identified, I targeted these molecular factors with commercially available drugs. Blocking these survival factors made Group 3 medulloblastoma cells more susceptible to treatment and offers a novel approach to combat acquired chemotherapeutic resistance.

Preface

The contents of this dissertation are my original work. All experiments were designed and conducted by me in conjunction with my supervisor, Dr. Chinten James Lim, and the guidance of my supervisory committee.

A version of Chapter 2 entitled “Autocrine IL-6/STAT3 signaling aids the development of drug resistance in Group 3 medulloblastoma” by L Sreenivasan, H Wang, SQ Yap, P Leclair, A Tam, and CJ Lim, has been published in *Cell Death Disease* (2020) 11:1035. Dr. Lim and I conceptualized the study and designed the experiments that are detailed in Chapter 2. I performed all experiments, collected and analyzed data, and prepared figures/graphs with the assistance of Dr Lim. Dr Lim and I co-wrote the published manuscript. Specific contributions by other personnel are as follows: Dr H Wang and SQ Yap generated the Med8A-R chemoresistant cell line and performed the preliminary characterizations. Dr A Tam assisted with qPCR experimental design and data analysis. Dr Lim and I designed the CRISPR guide RNA targeting STAT3 and IL-6R. The BCCHR Flow Cytometry core’s Dr L Xu provided fluorescent activated cell sorting services to collect the CRISPR edited clones. The BCCHR DNA Sequencing core performed Sanger sequencing of the CRISPR plasmids and knockout clones. P Leclair and I analyzed the sequencing results to identify the mutations in each CRISPR-targeted allele to confirm the knock out clones.

Chapter 3 “Targeting IL-6/gp130 signaling axis attenuates tumour microenvironment mediated chemoresistance in Group 3 MB” contains the bulk of the data for a manuscript in a late stage of preparation. I will be the first author on this manuscript, along with co-authors L Li, P Leclair and CJ Lim. Dr. Lim and I conceptualized the study and designed the experiments that are detailed in Chapter 3. I performed all experiments, collected and analyzed data, and prepared figures/graphs with the following exceptions: Dr Lim designed the CRISPR guide RNA targeting

gp130. The BCCHR Flow Cytometry core's Dr L Xu performed fluorescent activated cell sorting to collect the CRISPR edited clones. The BCCHR DNA Sequencing core performed Sanger sequencing. L Li assisted in maintenance of the gp130 CRISPR knockout cell lines. Dr Lim and I are co-writing the manuscript that is in preparation.

Chapter 4 contains transcriptome microarray-based gene expression data obtained from publicly available databases, specifically the Gene Expression Omnibus (GEO). Dr C Konwar provided initial assistance in the navigation and analyses of the GEO databases. T Lam provided additional assistance in the survival analysis of MB subgroups. I acquired the GEO datasets, performed the analyses, and prepared figures/graphs as shown in Chapter 4. Some parts of Chapter 4 have been published in *Cell Death Disease* (2020) 11:1035.

Chapter 5 is a summary of the overall conclusions of my thesis, including limitations, significance to the field, future directions and closing remarks.

Table of Contents

Abstract.....	iii
Lay Summary	v
Preface.....	vi
Table of Contents	viii
List of Tables	xiv
List of Figures.....	xv
List of Symbols	xx
List of Abbreviations	xxi
Acknowledgements	xxiii
Dedication	xxiv
Chapter 1: Introduction	1
1.1 Brief history of medulloblastoma	1
1.2 Epidemiology	2
1.3 Diagnosis and therapeutic intervention.....	2
1.3.1 General symptoms	3
1.3.2 Risk stratification	3
1.3.3 Histological classification.....	5
1.3.4 Surgery	6
1.3.5 Radiotherapy	7
1.3.6 Chemotherapy	8
1.4 Molecular classification of medulloblastoma	9
1.4.1 WNT	11

1.4.2	SHH.....	13
1.4.3	Group 3	16
1.4.4	Group 4	17
1.5	Molecular targeted therapy	18
1.6	Chemoresistance	20
1.7	Brain tumour microenvironment.....	23
1.8	The IL-6/JAK/STAT3 signaling pathway	26
1.8.1	Interleukin-6 family cytokines	28
1.8.2	Glycoprotein 130	30
1.8.3	Janus kinase	31
1.8.4	Signal transducers and activators of transcription	33
1.9	Research objectives and hypothesis.....	34
1.9.1	Overview of the problem	34
1.9.2	Chapter 2: Rationale and hypothesis.....	35
1.9.3	Chapter 3: Rationale and hypothesis.....	36
1.9.4	Chapter 4: Rationale and hypothesis.....	37
Chapter 2: Autocrine IL-6/STAT3 signaling aids development of acquired drug resistance		
in Group 3 medulloblastoma.38		
2.1	Chapter Overview	38
2.2	Materials and methods	38
2.2.1	Cells and tissue culture	38
2.2.2	Cell viability assays	40
2.2.3	Radiation assay	40

2.2.4	Western blots	41
2.2.5	Plasmids and CRISPR.....	41
2.2.6	Flow cytometry	42
2.2.7	Real Time PCR.....	42
2.2.8	Cell proliferation and colony forming assay.....	43
2.2.9	Invasion and Migration assay	43
2.2.10	ELISA and cytokine array	44
2.2.11	Statistical data analysis	44
2.3	Results.....	45
2.3.1	Drug resistant MB is correlated with increased IL-6/STAT3 activity.....	45
2.3.2	Loss of STAT3 or IL-6R in drug resistant MB led to restored sensitivity to vincristine.....	49
2.3.3	Conditioning with exogenous IL-6 is sufficient to promote acquired drug resistance.....	52
2.3.4	MDR1 is positively associated with chemoresistant variants.....	56
2.3.5	IL-6 conditioned cells exhibit increased migration and invasion	57
2.3.6	Chemoresistant MB is susceptible to combination treatment of vincristine with cisplatin or niclosamide	59
2.3.7	Autocrine IL-6 signaling promotes drug resistance in MB	60
2.3.8	Pro-survival and pro-apoptotic signaling pathways in MB cells	64
2.3.9	IL-6 conditioning leads to increased STAT3 activity, IL-6R expression, and acquired drug resistance in other Group 3 MB cell lines.....	65
2.4	Discussion.....	68

Chapter 3: Targeting gp130/STAT3 signaling axis attenuates tumour microenvironment

mediated chemoresistance in Group 3 MB.....	73
3.1 Chapter overview	73
3.2 Materials and methods	73
3.2.1 Cells and tissue culture	73
3.2.2 Co-culture system and cytokine conditioning.....	74
3.2.3 Cell viability assays	74
3.2.4 Western blots	75
3.2.5 Plasmids and CRISPR.....	75
3.2.6 Flow cytometry	76
3.2.7 ELISA and cytokine array	76
3.2.8 Statistical data analysis	77
3.3 Results.....	78
3.3.1 MB cells co-cultured with microglia exhibit increased STAT3 activity and chemoresistance.	78
3.3.2 JAK inhibitor ruxolitinib diminishes STAT3 activity and reverts acquired drug resistance.....	81
3.3.3 The IL-6 family cytokines IL-6, LIF, OSM and IL-11 promote acquired resistance to vincristine treatment.....	83
3.3.4 MB cells conditioned with one IL-6 family cytokine promote secretion of multiple IL-6 family cytokines.....	85
3.3.5 Ruxolitinib overcomes chemoresistance of IL-6 family cytokine conditioned MB cells.....	87

3.3.6	Targeting gp130 mitigates MB chemoresistance resulting from exposure to microglia.	90
3.3.7	Gp130 is essential for driving chemoresistance in other Group 3 MB cell lines.	93
3.4	Discussion.....	95
Chapter 4: Data mining of MB transcriptional databases provides insight into components of the IL-6/STAT3 signaling cascade.		100
4.1	Chapter overview	100
4.2	Methods.....	101
4.2.1	Data mining of gene expression profiles from GEO datasets.....	101
4.2.2	Method of analysis	102
4.2.3	Statistical analysis.....	102
4.3	Results.....	103
4.3.1	<i>STAT3</i> expression is significantly enriched in Group 3 γ MB.....	103
4.3.2	Group 3 MB is associated with reduced <i>JAK1</i> expression.	109
4.3.3	Expression analyses of the IL-6 family cytokines and their receptors.	112
4.3.3.1	Expression analyses of <i>IL6</i> , <i>IL6R</i> and <i>E2F3</i>	112
4.3.3.2	Expression analyses of <i>LIF</i> , <i>LIFR</i> , <i>OSM</i> , <i>OSMR</i> , <i>IL11</i> , <i>IL11R</i> and <i>Gp130</i> . ..	115
4.3.4	Expression analyses of negative feedback regulators of IL-6/STAT3 signaling....	122
4.4	Discussion.....	125
Chapter 5: Conclusion.....		131
5.1	Chapter summaries and working models.....	131
5.1.1	Autocrine IL-6 signaling mediates chemoresistance in MB cells.	131
5.1.2	Paracrine IL-6 signaling originating from the brain TME.....	133

5.1.3	Correlative clinical evidence for IL-6/JAK/STAT signaling in subgroups of MB.	136
5.2	Significance of study.....	138
5.3	Limitations of study	140
5.4	Future perspectives	143
5.5	Closing remarks	145
Bibliography		147
Appendix A.....		167
A.1	167
A.2	167
A.3	168
A.4	168
A.5	169
A.6	170
A.7	170
A.8	171
A.9	171
Appendix B.....		172
B.1	172

List of Tables

Table 1.1: MB risk stratification. Adapted table detailing proposed risk stratification based on clinical and molecular characteristics of MB.....	5
Table 1.2: IL-6 family cytokines and their receptors.....	29
Table 4.1: Additional information of GEO datasets used in this study.	101
Table 4.2: Summary of <i>STAT3</i> , <i>STAT5A</i> and <i>STAT5B</i> expression in GSE85217, GSE21140 and GSE37418 in comparison to Group 3 MB.....	109
Table 4.3: Summary of <i>JAK1</i> , <i>JAK2</i> and <i>TYK2</i> expression in GSE85217, GSE21140 and GSE37418 in comparison to Group 3 MB.....	112
Table 4.4: Summary of <i>IL6</i> , <i>IL6R</i> and <i>E2F3</i> expression in GSE85217, GSE21140 and GSE37418 in comparison to Group 3 MB.	115
Table 4.5: Summary of <i>LIF</i> , <i>LIFR</i> , <i>OSM</i> , <i>OSMR</i> , <i>IL11</i> , <i>IL11R</i> and <i>Gp130</i> expression in GSE85217, GSE21140 and GSE37418 in comparison to Group 3 MB.....	121
Table 4.6: Summary of <i>SOCS1</i> , <i>SOCS3</i> and <i>PIAS3</i> expression in GSE85217, GSE21140 and GSE37418 in comparison to Group 3 MB.....	124

List of Figures

Figure 1.1: A summary of the molecular and clinical features of the subgroups of MB.....	10
Figure 1.2: WNT signaling pathway.....	13
Figure 1.3: SHH signaling pathway.....	15
Figure 1.4: Cells in the brain tumour microenvironment.	26
Figure 1.5: IL-6-JAK-STAT3 signaling pathway.....	27
Figure 1.6: Structural components of JAK protein.....	32
Figure 1.7: Structural components of STAT3 protein.	34
Figure 2.1: Derivation of a chemoresistant variant of Med8A MB.....	46
Figure 2.2: Chemoresistant MB is associated with enhanced STAT3 activity.....	48
Figure 2.3: CRISPR-Cas9 generation of STAT3 ^{-/-} or IL-6R α ^{-/-} in Med8A-R cells.....	50
Figure 2.4: Loss of STAT3 or IL-6R restores chemosensitivity in Med8A-R cells.....	51
Figure 2.5: Comparison of STAT3 expression in chemosensitive parental and chemoresistant derivatives of Med8A cell lines.....	53
Figure 2.6: Exogenous IL-6 conditioning promotes drug resistance.....	54
Figure 2.7: IL-6 conditioning promotes resistance to cisplatin, mitoxanthrone and idarubicin. ..	55
Figure 2.8 : Proliferation rate comparison of Med8A-S, Med8A-R and Med8A-IL6+ cells.	56
Figure 2.9: MDR1 expression in Med8A-S, Med8A-R and Med8A-IL6+.	57
Figure 2.10: Cell migration assays.....	58
Figure 2.11: Chemoresistant MB is susceptible to combination treatment of vincristine with cisplatin or niclosamide.	60
Figure 2.12: Autocrine IL-6 secretion promotes IL-6/STAT3 activity.	63

Figure 2.13: Survey of pro-survival and pro-apoptotic signaling in DAOY, Med8A-S and Med8A-R cells.	65
Figure 2.14: Comparison of STAT3 expression in chemosensitive parental and chemoresistant derivatives of D341 and D283 cell lines.	66
Figure 2.15: Group 3 MB cell lines D283 and D341 exhibit similar responses to IL-6/STAT3 signaling.	67
Figure 3.1: Exposure to microglia render Med8A cells chemoresistant concurrent with enhanced STAT3 activity.	80
Figure 3.2: JAK inhibitor suppresses STAT3 activity and overcomes microglia-induced chemoresistance of MB cells.	82
Figure 3.3: MB cells conditioned with IL-6 family cytokines enhance JAK1 and STAT3 activity and chemoresistance.	84
Figure 3.4: Chemoresistant MB cells secrete elevated levels of LIF, OSM and IL-11.	86
Figure 3.5: Combined treatment of vincristine with ruxolitinib in IL-6 family of cytokine conditioned Med8A-S cells.	88
Figure 3.6: Combined treatment of vincristine with ruxolitinib in IL-6 family of cytokine conditioned IL6R ^{-/-} cells.	89
Figure 3.7: Loss of gp130 prevents microglia co-culture induced STAT3 signaling and chemoresistance in Med8A cells.	91
Figure 3.8: Gp130 inhibitors mitigates microglia co-culture induced chemoresistance in Med8A cells.	92
Figure 3.9: Combination SC144 and vincristine treatment mitigates microglia co-culture induced chemoresistance in D283 and D341 cells.	94

Figure 4.1: Expression of <i>STAT3</i> was analyzed according to their subgroup and subtype categorization.....	104
Figure 4.2: Correlation of <i>STAT3</i> expression with overall survival in MB.....	106
Figure 4.3:Expression of <i>STAT5A</i> was analyzed according to their subgroup and subtype categorization.....	107
Figure 4.4: Expression of <i>STAT5B</i> was analyzed according to their subgroup and subtype categorization.....	108
Figure 4.5: Expression of <i>JAK1</i> was analyzed according to their subgroup and subtype categorization.....	110
Figure 4.6: Expression of <i>JAK2</i> was analyzed according to their subgroup and subtype categorization.....	111
Figure 4.7:Expression of <i>TYK2</i> was analyzed according to their subgroup and subtype categorization.....	111
Figure 4.8: Expression of <i>IL6</i> was analyzed according to their subgroup and subtype categorization.....	113
Figure 4.9:Expression of <i>IL6R</i> was analyzed according to their subgroup and subtype categorization.....	113
Figure 4.10: Expression of <i>E2F3</i> was analyzed according to their subgroup and subtype categorization.....	114
Figure 4.11: Expression of <i>LIF</i> was analyzed according to their subgroup and subtype categorization.....	116
Figure 4.12: Expression of <i>LIFR</i> was analyzed according to their subgroup and subtype categorization.....	116

Figure 4.13: Expression of <i>OSM</i> was analyzed according to their subgroup and subtype categorization.....	117
Figure 4.14: Expression of <i>OSMR</i> was analyzed according to their subgroup and subtype categorization.....	118
Figure 4.15: Expression of <i>IL11</i> was analyzed according to their subgroup and subtype categorization.....	119
Figure 4.16: Expression of <i>IL11R</i> was analyzed according to their subgroup and subtype categorization.....	119
Figure 4.17: Expression of <i>GPI30</i> was analyzed according to their subgroup and subtype categorization.....	120
Figure 4.18: Expression of <i>SOCS1</i> was analyzed according to their subgroup and subtype categorization.....	123
Figure 4.19: Expression of <i>SOCS3</i> was analyzed according to their subgroup and subtype categorization.....	123
Figure 4.20: Expression of <i>PIAS3</i> was analyzed according to their subgroup and subtype categorization.....	124
Figure 5.1: Graphical abstract depicts the experimental approach and mechanisms involved in autocrine IL-6/STAT3 signaling in the development of chemoresistance in Group 3 MB cells.	133
Figure 5.2: Graphical abstract depicts the experimental approach and mechanism involved in tumour microenvironment mediated chemotherapeutic resistance involving IL-6 family of cytokine signaling in Group 3 MB.....	135

Figure 5.3: Heat map summary depiction of gene expression involved in the IL-6/STAT3

signaling pathway. 138

List of Symbols

α - Alpha
 β - Beta
 γ - Gamma
 δ - Delta

List of Abbreviations

ADAM17 - a disintegrin and metalloproteinase 17
APC - Adenomatous polyposis coli
ATO - Arsenic trioxide
ATRT - Atypical teratoid rhabdoid tumour
AURKA - Aurora kinase A
BBB - Blood-brain barrier
BET - Bromodomain and extra terminal
CAF - Cancer associated fibroblasts
CK1 α - Casein kinase 1 α
CLCF1 - Cardiotrophin-like cytokine factor 1
CNTF - Ciliary neurotrophic factor
CT1 - Cardiotrophin 1
CTB – Cell titer blue
Dsh - Dishevelled
ERK1/2 - Extracellular signal-regulated kinase 1/2
FBS - Fetal bovine serum
Fz - Frizzled
GABAergic - Gamma aminobutyric acid-secreting
GANT - GLI antagonist
GFI1 - Growth factor independent 1
GP130 - Glycoprotein 130, also known as IL6ST, IL6 β or CD130
GSK3 β - Glycogen synthase kinase 3
GTR - Gross total resection
IL-6 - Interleukin 6
IL-6R - Interleukin 6 receptor
JAK1 - Janus kinase 1
LIF - Leukemia inhibitory factor
LIFR - Leukemia inhibitory factor receptor
LSD1 - Lysine demethylase 1
MAPK - Mitogen-activated protein kinases
MB - Medulloblastoma
OSM - Oncostatin M
OSMR - Oncostatin M receptor
OTX2 - Orthodenticle homeobox 2
PI3K - Phosphatidylinositol 3-kinases
PIAS3 - Protein inhibitor of activated STAT3
PLK - Polo-like kinase
PNET - Primitive neuroectodermal tumours

PTCH1 - Patched1
PTCH2 - Patched2
PVT1 - Plasmacytoma variant translocation 1
SHH - Sonic hedgehog
SMO - Smoothed homologue
SNV - Single nucleotide variants
SOCS - Suppressors of cytokines signaling
STAT3 - Signal transducer and activator of transcription 3
STAT5 - Signal transducer and activator of transcription 5
SUFU - Suppressor of fused
TAM - Tumour associated macrophages
TERT - Telomerase reverse transcriptase
TGF β - Transforming growth factor beta
TME - Tumour microenvironment
Tregs - Regulatory T-cells
TS - Turcot Syndrome
TYK2 - Tyrosine-protein activated kinase 2
WHO - World Health Organization
WNT - Wingless

Acknowledgements

First and foremost, I would like to express my gratitude to my supervisor, Dr. Chinten James Lim, for his continuous support during my Ph.D. work. I am grateful for his patience, guidance, motivation and for consistently inspiring me with his passion for science. Thank you for taking a chance on me and for investing all this time and effort to ensure my development as a student and scientist. I could not have imagined having a better advisor for my Ph.D. I would like to extend my appreciation to my supervisory committee members Drs. Christopher Maxwell, Stephen Yip and Michael Gold, for their time, encouragement and feedback that helped shape this thesis and my progress as a researcher.

I would also like to thank all members of the Lim lab. Thank you from the bottom of my heart for the countless hours you have spent training, teaching and troubleshooting with me. It is rare to find a lab where you not only enjoy the science, but also appreciate all the people you work with.

I would like to thank my friends from Tucson and Vancouver. I have met some amazing people and I am grateful for the lifelong friendships.

To my amazing partner and best friend, Manish, thank you for your unwavering support and for being my rock throughout this entire journey. Finally, to my parents, thank you for being the most encouraging, inspirational and supportive people in my life. Thank you for always believing in me and telling me that I can make all my dreams come true. Your generosity is truly amazing, and I would not have been able to survive this degree without your help. I am forever indebted to you and can only hope that I make you proud every day.

Dedication

To Appa and Amma,
for always believing in me.

Chapter 1: Introduction

1.1 Brief history of medulloblastoma

Less than a century ago, Harvey Cushing and Percival Bailey postulated that medulloblastoma (MB) arose from undifferentiated cells termed “medulloblasts” present in the cerebellar vermis, exhibited leptomeningeal dissemination, and histologically classified MB cells as small round nuclei with minimum cytoplasm [1-3]. Cushing and Bailey’s recognition and vast understanding of the disease provided basic clinical information, surgical techniques, and histopathological characteristics of MB. Although Cushing perceived MB as a subset of glioma, in early 1900’s MB was redefined as primitive neuroectodermal tumours (PNETs) due to the histologic similarity shared with small round blue cell tumours [4]. Even today, patients diagnosed with PNET are enrolled in the same clinical trials as MB patients. Since MB tumours were thought to arise from the posterior fossa of the brain, they were radiographically similar to other pediatric brain tumours such as ependymoma, pilocytic astrocytoma, embryonal tumours and atypical teratoid rhabdoid tumours [5,6].

During Cushing’s era, extensive surgical resection resulted in improved survival outcomes, but 30% of post-operative patients experienced mortality. A vital study published in 1953 revealed that surgery followed by craniospinal radiation significantly improved the 3-year survival rate to 65%. However, a severe consequence of craniospinal radiation was observed in infants and children below the age of 3 who developed neurocognitive impairments, endocrine dysfunction and second malignancies later in life [7]. In 1970’s, adjuvant chemotherapy in addition to surgery and radiation helped improve overall survival, and this combination has since remained the gold-standard in the treatment of MB [8]. Cushing and Bailey’s discovery and studies led by several groups around the world paved the way for further reformation of our knowledge of central

nervous system malignancies. Up until 2012, MB was regarded as a single disease entity, but recent advances in molecular genetics led to its classification into distinct molecular subgroups. In 2016, the World Health Organization (WHO) classified MB into the following four subgroups: Wingless (WNT), Sonic hedgehog (SHH), Group 3 and Group 4 [6,9]. The classification details and the clinical implications for these MB subgroups will be further discussed in Sections 1.3 and 1.4.

1.2 Epidemiology

MB is a high-grade pediatric brain malignancy comprising 20% of all childhood brain tumours and accounts for approximately 63% of intracranial embryonal tumours. MB is postulated to originate from neuronal precursors and progenitor cell populations located in the posterior cranial fossa [10]. These tumours occur in infants, children and adults with an overall annual incidence of 5 cases per million individuals. MB is more common in males than females with a 1.8:1 sex ratio, however sexual predominance varies between subgroups [11,12]. Age-specific incidence also varies by subgroup; children and infants under the age of 10 comprise 70% of all MB cases, with peak incidence at ages 3-9. Adults are rarely affected by MB, with an annual incidence of 0.5 cases per million individuals, and their prevalence is linked to specific subgroups [13,14]. Due to overall low incidence of MB, population-based studies are scarce and have not revealed any remarkable disparities across geographical regions and ethnicities so far [10,15].

1.3 Diagnosis and therapeutic intervention

Despite standard treatments such as surgery, radiotherapy and chemotherapy, about 30% of MB patients experience mortality. Aggressive therapy also leads to severe long-term complications and development of secondary tumours in individuals with MB. Herein, I will

discuss the symptoms, and the histopathological and molecular signatures used to diagnose and treat MB patients.

1.3.1 General symptoms

Generic symptoms such as headaches, nausea and fatigue are often experienced by MB patients in the initial stages of tumour. Other symptoms that emerge as the tumour progresses include ataxia, manifesting as issues with vision and motor coordination. Patients with MB, especially in infants and children, are often present with a delayed diagnosis due to the initial non-specific symptoms. By the time MB is diagnosed, the tumour is often enlarged, leading to increased intracranial pressure and spinal metastases. However, some individuals with a predisposition to MB are diagnosed early with the assistance of genetic screening [16-18].

1.3.2 Risk stratification

The recent molecular classification has facilitated stratification of MB tumours into distinct risk groups and calls for specific treatment paradigm for each molecular subgroup. MB patients are classified into 4 risk categories based on their subgroup, clinical and molecular features (Table 1.1). The age of the patient at diagnosis, metastatic stage and extent of surgical resection play a significant role in designing the risk stratification groups.

Low risk MB has an overall survival greater than 90%. Based on the current system, patients older than 3 years at diagnosis with localized tumour and near total resection (residual tumour $<1.5 \text{ cm}^3$) belong to the low-risk category [6,8,16,19]. Patients with localized WNT MB tumours and Group 4 MB tumours with loss of chromosome 11 are also stratified into this risk group due to their better survival outcomes.

MB patients with residual tumour post-surgery with or without metastatic disease are considered standard-risk or high-risk. Standard risk patients, with an overall survival of 75-90%, most likely develop localized SHH tumours without *TP53* mutation or *MYC* amplification, Group 3 tumours without *MYC* amplification, or Group 4 tumours without loss of chromosome 11. High-risk MB has an overall survival not exceeding 75%. This includes patients with SHH tumours with *MYCN* amplification and metastatic Group 4 tumours [6,8,16,19].

Infants and children below the age of three with metastatic disease at diagnosis belong to the very high-risk category that is associated with the lowest survival rate (<50%). This category consists of Group 3 tumours with *MYC* amplification and SHH group with *TP53* mutation. Very high-risk tumours have near fatal outcomes but a small subset of patients that survive succumb to secondary tumours later in life [16,20,21].

The proposed risk stratification attributed to the diverse molecular and clinical characteristics of MB necessitates de-escalation of therapy in some risk categories. Further reliable data and delineation of sub-categories is required across different patient cohorts to provide additional strata of information to develop a more robust and enhanced risk stratification system [16,20,21].

Table 1.1: MB risk stratification. Adapted table detailing proposed risk stratification based on clinical and molecular characteristics of MB.

Risk category	Low risk	Standard risk	High risk	Very high risk
Survival	>90%	75-90%	50-75%	<50%
Molecular profile	WNT Group	SHH group without <i>TP53</i> mutation or <i>MYC</i> amplification	SHH group with <i>MYCN</i> amplification	SHH group with <i>TP53</i> mutation
	Group 4 with loss of chromosome 11	Group 3 without <i>MYC</i> amplification Group 4 without loss of chromosome 11	Metastatic Group 4	Metastatic group 3 with <i>MYC</i> amplification
Metastatic?	No	No	Yes	Yes

1.3.3 Histological classification

MB is histologically classified into four subtypes: classic histology, nodular desmoplastic, MB with extensive nodularity and large-cell anaplastic. Classic MBs are poorly differentiated sheets of cells consisting of small round blue-cell tumours with minimal cytoplasm. The classic histological subtype is associated with a worse prognosis when compared to nodular desmoplastic tumours. Nodular desmoplastic MBs are made of nodular islands encased by neuronal differentiated cells and tightly packed hyperchromatic cells. They are mostly present in infants and adults with MB than in children [8,22,23]. MB with extensive nodularity histological subtype exhibits extensive lobular structures with enormous elongated reticulin-free zone between the nodules. Small, round neurocytic-like cells are often found in the internodular regions of MB with extensive nodularity variants. MB with extensive nodularity are commonly found in infants and associated with exceptional prognosis. Large-cell anaplastic MBs are defined by enlarged nuclei

with distinguished nucleoli and pleomorphism with variable cytoplasm. Large-cell anaplastic subtype is often difficult to diagnose as they may either present as large-cell or only anaplastic phenotypes. Compared to nodular desmoplastic, large-cell anaplastic histological subtype is considered a marker for high-risk disease that warrants aggressive therapy. The identification of these histological subtypes has clinical utility and is currently being used as a marker to predict disease risk [8,23-25].

1.3.4 Surgery

Surgery was the primary and only form of treatment for all MB patients up until the use of craniospinal radiation in the 1970's. Increased survival was documented in MB patients that underwent radical tumour resection. Recent studies have demonstrated that near total resection (wherein residual tumour is $\leq 1.5 \text{ cm}^2$) of tumour and gross total resection provide MB patients with similar progression free survival or overall survival. With the recent classification of MB, GTR was found to offer a better progression free survival outcome compared to sub-total resection (residual tumour $\geq 1.5 \text{ cm}^2$) in a large cohort of MB patients. More specifically, Group 4 MB patients have benefited with increased progression free survival and overall survival when they underwent gross total resection or near total resection procedures. Although gross total resection is considered the gold standard, more data from other MB cohorts is required to validate the benefits of progression free survival [6,18,26,27].

A surgical decision needs to be made to weight the benefits when performing gross total resection procedure, since complete resection of the tumour might lead to neurological deficits in MB patients. For the purpose of biopsy to study the histological and molecular signatures of the tumour, sufficient tissue needs to be resected from the specific area of the tumour. This process

could be challenging due to the high-level of spatial and temporal heterogeneity exhibited by these tumours. While some studies have implied the advantage of resecting recurrent tumours, it is yet to be evaluated in a large cohort of MB patients by controlling for their molecular characteristics [6,16,18,28,29].

1.3.5 Radiotherapy

Surgery followed by craniospinal radiation enhanced the overall survival of MB patients as they focused on eliminating remnant tumour cells. Irradiation on the complete craniospinal axis was performed as a prophylactic treatment to target tumour cells that have invaded to the spinal cord and the leptomeninges. Initially, high doses of irradiation were administered to all MB patients, but this led to severe side-effects such as neurocognitive impairment, growth disruption and deformities, infertility, cardio toxicity, endocrine disorders and secondary tumours. The standard craniospinal radiation dose is 24 gray (Gy) with a 54 Gy radiation boost to the tumour bed for patients with no metastatic disease. A higher irradiation dose of 36 Gy is administered to high-risk patients that exhibit metastasis [6,21,29].

With the recent classification of MB and proposed risk stratification based on their molecular signatures, efforts were taken to reduce or abstain from administering irradiation unless required, particularly in infants and children <5 years of age and for low-risk categories. Additionally, MB patients carrying *TP53* mutations are more prone to DNA damage and development of secondary cancers when radiotherapy is administered, therefore risk needs to be determined prior to treatment. A few clinical trials are investigating de-escalation of intensive treatment in patients with WNT MB given their excellent 5-year survival rate [21,30]. Alternative irradiation techniques such as proton radiotherapy and intensity-modulated radiation therapy are

currently used in clinical trials to study the effects of minimal radiation exposure on normal cells surrounding the tumour to prevent the harmful side-effects experienced by MB patients [31]. Irradiation protocol needs to be modified and tailored to each individual MB patient based on their clinical attributes and risk categories to avoid unwarranted toxicities from radiotherapy [18,29,32,33].

1.3.6 Chemotherapy

Chemotherapy is one of the principal modes of cancer treatment. The main class of drugs used to treat MB patients are cytotoxic agents that destroy proliferating cells by interfering with DNA replication and synthesis. Vincristine, cisplatin, lomustine and cyclophosphamide are some of the drugs approved to use for the treatment of MB patients. The chemotherapeutic regimen is determined based on age, risk category, molecular and clinical attributes including histology, amount of tumour resected and occurrence of metastasis [29]. Due to the harmful side effects from radiation, infants are primarily treated with an intensive chemotherapeutic regimen after surgical resection [34]. For children (> 3years of age) and adolescents that have undergone near total surgical resection and have no metastasis at diagnosis, they are treated with 24 Gy irradiation with a 54 Gy boosted tumour bed followed by 4-9 cycles of vincristine, cisplatin or cyclophosphamide, and autologous stem cell rescue. MB patients that present with metastasis post-surgery are treated with similar cycles of chemotherapy with an increased craniospinal radiation (36 Gy) and a 54 Gy boost to the tumour bed, and radiation at the secondary site of tumour [6,35]. In Europe, small doses of radiation daily (1.6 Gy to 1.8 Gy) is administered post chemotherapy to MB patients. However, studies have demonstrated that chemotherapy administered post-radiation results in a significantly better outcome compared to pre-radiotherapy [36]. Although, chemotherapy is one

of the most effective ways to target cancer cells, its effectiveness is often limited by acquired drug resistance or intolerable toxicity effects.

In North America, several clinical trials are ongoing for the treatment of MB to alleviate toxicity and improve the survival outcome of MB patients. For example, clinical trial NCT01878617 (SJMB03) is a clinical and molecular risk-directed therapy for newly diagnosed MB. Patients enrolled in this trial are grouped into specific strata based on their risk category and subgroup classification. All the patients undergo maximal surgical resection followed by radiation and chemotherapy. Craniospinal radiation with boost to the primary tumour bed is administered 5 days a week for 6 weeks followed by chemotherapy once every 4 weeks for 4 cycles. Some of the objectives of this clinical trial are to evaluate the toxicity of adjuvant chemotherapy, impact of physical exercise and to evaluate the cognitive function of patients. Another clinical trial, NCT02212574 is assessing the feasibility of surgery and chemotherapy-only in children with WNT positive medulloblastoma. WNT patients are often low-risk and do not require aggressive treatment. Patients that are WNT positive will undergo 9 cycles of chemotherapy regimen without radiation or the weekly chemotherapy administered alongside radiation. The objective of this study is to measure the progression free survival of patients with WNT MB [6,16,18,29].

1.4 Molecular classification of medulloblastoma

In the recent decade, high-throughput transcriptomics, genome-wide methylation arrays and advanced molecular tools have been used by several groups to classify MB into various subgroups [37-41]. In particular, next-generation sequencing studies by the Pediatric Cancer Genome Project, the International Cancer Genome Consortium for medulloblastoma and the Medulloblastoma Advanced Genomics Consortium facilitated broad classification of MB into four

distinct subgroups- WNT, SHH, Group 3 and Group 4. Advancement in integrative genomics has led to further classification of the subgroups into subtypes detailing differential prognosis, clinical presentation and genetic landscapes [42,43]. A detailed discussion of the various subgroups will be provided in the sections below and also illustrated in Figure 1.1.

MB Subgroup	WNT	SHH	Group 3	Group 4
% of cases	~10%	~30%	~25%	~35%
Age at diagnosis				
Gender	♂:♀	♂:♀	♂♂:♀	♂♂♂:♀
Prognosis				
Histology	Classic	Desmoplastic, Classic, LCA	Classic, LCA	Classic, LCA
Metastasis	5-10% Rare, Local	15-20% Local	40-45% Distant	35-40% Distant
Cell origin	Progenitor cells in lower rhombic lip	Granule precursors of external granule layer	Neural stem cells	Unipolar brush cells
Recurrent gene amplification	-	MYCN, GLI1 or GLI2	MYC, MYCN, OTX2	SNCAIP, MYCN, OTX2, CDK6
Recurrent SNVs	CTNNB1, DDX3X, SMARCA4, TP53	PTCH1, TERT, SUFU, SMO, TP53	SMARCA4, KBTBD4, CTDNEP1, KMT2D	KDM6A, ZMYM3, KTM2C, KBTBD4
Cytogenetic events	6	9q, 10q, 17p 3q, 9p	8, 10q, 11, 18q 1q, 7, 18 i17q	8, 11p, X 7, 18q i17q

Figure 1.1: A summary of the molecular and clinical features of the subgroups of MB. Figure is adapted from Juraschka *et al.* [6] (Created with BioRender).

1.4.1 WNT

The WNT subgroup represents approximately 10% of all MBs. WNT MBs are rarely metastatic at diagnosis and have the most favourable outcome, with a 5-year overall survival greater than 90%. The fatalities observed in this subgroup are mostly due to development of secondary tumours or consequences of aggressive therapy. These tumours often occur in children and young adults over the age of 4 and the typical male to female ratio is 1:1. WNT MB tumours are postulated to arise from the progenitor cells in the lower rhombic lip located in the midline of the brain. They display undeviating histology, with uniform clinical and molecular characteristics. Histologically, the classic subtype is highly prevalent in WNT MB tumours, with a rare presentation of the large cell anaplastic subtype in some tumours. Although large cell anaplastic subtype is associated with worse prognosis, WNT MBs with large cell anaplastic subtype was reported to have good outcomes [18,29,37,40,41,44,45].

Suggestive of the name, the WNT subgroup is driven by the activation of canonical WNT signaling pathway (Figure 1.2). Inactivation or loss of the tumour suppressor gene, adenomatous polyposis coli (APC), promotes hyperactivity of the WNT signaling pathway and progression of the tumour. Turcot Syndrome (TS) often occurs in patients with germline mutations in the *APC* gene and they tend to develop numerous polyps that mostly progress to sporadic colon carcinomas. Increased occurrence of MB is also documented in patients with TS [46-48]. Additionally, somatic *CTNNB1* gene mutations were found in 86% of WNT MB patients. *CTNNB1* encodes β -catenin, a critical effector molecule of the WNT signaling pathway. Activating mutations in the *CTNNB1* gene promote stabilization and nuclear accumulation of β -catenin in WNT patients [49]. Nuclear-localized β -catenin interacts with TCF/LEF family transcription factors, and subsequent activation of WNT signaling pathway [38,43,50].

Monosomy 6 is a structural alteration observed in most WNT patients and is a specific marker for this subgroup [29,51,52]. WNT subgroup harbour a multitude of single nucleotide variants (SNV) when compared to other MB subgroups. *DDX3X* (encodes for DEAD-box RNA helicase), *SMARCA4* (chromatin modifier gene) and *PI3KCA* (encodes for the catalytic subunit of PI3K) are some commonly mutated genes that interact with β -catenin in a cooperative manner to facilitate progression of WNT MB tumours [29,47,53,54]. With the recent emergence of methylation-derived subtypes, WNT MB is further classified into WNT- α and WNT- β based on their median age at diagnosis and the frequency of monosomy 6 [42]. Further information regarding the subtypes and their associated features will be discussed in Chapter 4.

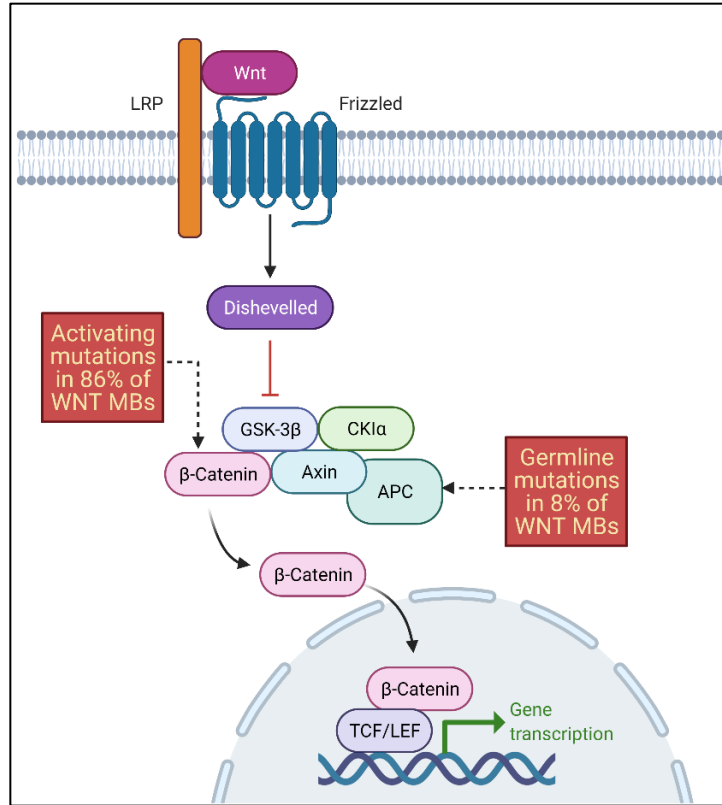


Figure 1.2: WNT signaling pathway.

β -catenin destruction complex comprising of Axin, APC, glycogen synthase kinase 3 (GSK3 β) and casein kinase 1 α (CK1 α) is disrupted when WNT binds to LRP and Frizzled (Fz) and activates Dishevelled (Dsh). β -catenin translocates into the nucleus and binds to TCF/LEF DNA binding transcription factors. This complex binds to the promoter region of target genes [18] (Created with BioRender).

1.4.2 SHH

The SHH MB subgroup constitute approximately one-third of all MB cases and this subgroup has a 5-year overall survival exceeding 75%. About 15-20% of SHH MBs are metastatic at diagnosis. Patients with SHH MB have variable outcome attributed to their age, clinical presentation and molecular abnormalities at the time of diagnosis. These tumours exhibit a slight male predominance with a gender ratio of male to female at 1.5:1. Age at diagnosis is represented as a bimodal distribution in SHH MBs as they generally occur in infants (<3 years of age) and adults (>16 years of age) with few cases found in children (3-16 years of age). SHH MBs are

postulated to arise from the granule neuronal precursor cells located in the external granule-cell layer of the cerebellar hemisphere. Unlike WNT MBs, all four histological subtypes (classic, nodular desmoplastic, large cell anaplastic, MB with extensive nodularity) are found among SHH MB tumours. Nodular desmoplastic and MB with extensive nodularity histological phenotypes are restricted to SHH MBs and are not prevalent in other MB subgroups. Although large cell anaplastic and classic subtypes have been associated with worse outcome, their contribution to the outcome of SHH MB tumours is unknown [18,39-41,44,45,55-57].

The SHH pathway plays a crucial role in normal cerebellar development. The receptor Patched 1 (PTCH1) interacts with the smoothed homologue (SMO) in the absence of the activating ligand, thereby preventing signal transduction and activation of the SHH signaling pathway (Figure 1.3). Aberrant signaling of the SHH pathway is the key driver of tumorigenesis in this specific subgroup. Mutations or deletions of *PTCH1*, SUPPRESSOR OF FUSED (*SUFU*), and *SMO* are characteristic of SHH MBs. Amplification of downstream transcription factors like *GLI1*, *GLI2* and *MYCN* are predominantly found in children with SHH MB [46-48,58]. In contrast, mutations in the telomerase reverse transcriptase (TERT) promotor region are commonly found in adults with SHH MB [59]. Recent data suggests that activating mutations in phosphatidylinositol 3-kinases (*PI3K*) and the *TP53* signaling pathway also play a significant role in the progression of some SHH MB tumours. Patients with Gorlin syndrome exhibiting nevoid basal cell carcinoma and germline mutations in *PTCH1*, *PTCH2* or *SUFU* tumour suppressor gene have a strong predisposition to SHH MB tumours [60,61]. About 30% of SHH MB patients associated with poor outcome of the disease have Li Fraumeni syndrome. This syndrome is caused by frequent germline mutations in the *TP53* tumour suppressor gene and is associated with increased susceptibility to malignancies [9,29,62].

The genes encoding chromatin modifiers such as *KMT2D* and *BCOR* are also frequently mutated in SHH MBs and are not restricted to WNT MBs. Other commonly occurring mutations unrelated to the SHH signaling cascade are *DDX3X*, *LDB1* (responsible for intraneuronal development) and *GABRG1* (inhibits neurotransmission). Loss of 9q (*PTCH1*), 10q (*SUFU*), 17p (*TP53*) and gain of 3q and 9p were some of the unique cytogenetic events observed in SHH MBs [29,35,54,55,63,64]. SHH MBs were recently subclassified into 4 distinct subtypes: SHH α , SHH β , SHH γ and SHH δ based on gene expression and methylation data [42]. These subtypes will be discussed in detail in Chapter 4.

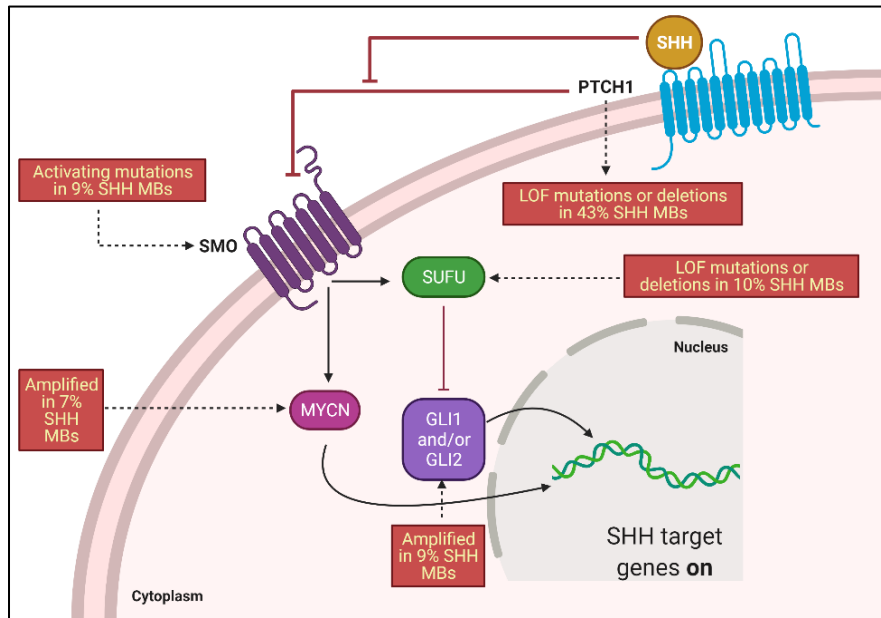


Figure 1.3: SHH signaling pathway.

PTCH inhibits SMO on the cell membrane. Binding of SHH to PTCH activates SMO and initiates downstream signaling. GLI is then activated and translocate to the nucleus to bind to promotor region of target genes. Activating and loss of function mutations of the SHH signaling components observed in SHH MB tumours are depicted in red boxes. Figure adapted from Northcott *et al.*[18] (Created with BioRender).

1.4.3 Group 3

Group 3 MBs constitute about 25% of all MB cases. These tumours are the most aggressive form of the disease, mostly metastatic at diagnosis (40-45%) with the least overall 5-year survival rate at about 50%. Group 3 MB tumours predominantly occur in infants and children, with a rare incidence in young adults. Group 3 MB tumours exhibit a sexual predominance with almost twice as many males affected than the female population. Classic or large cell anaplastic histological subtypes are commonly found in Group 3 MB tumours and are associated with poor prognosis of the disease. Group 3 MB tumours are postulated to arise from Prominin 1⁺ neural stem cells located in the 4th ventricle of the cerebellum. The true cell origin is unknown, but they possess similar transcriptional properties as photoreceptors and gamma aminobutyric acid-secreting (GABAergic) neurons [18,29,30,39,44,45,65-67].

In contrast to the WNT and SHH subgroups, there is no specific signaling pathway that is the potential driver of tumorigenesis in Group 3 MBs. However, recent studies on functional pathway analysis of various subgroups demonstrated that Notch and transforming growth factor beta (TGF- β) signaling are activated in this MB subgroup [18,29,30,43,68]. These tumours do not possess germline mutations that predispose them to developing into Group 3 MBs unlike the WNT and SHH subgroups. *MYC* amplification is frequently observed in Group 3 MBs. *MYC* is a proto-oncogene that is involved in a broad spectrum of cellular functions including cell-cycle progression, survival, protein translation and differentiation. Group 3 MB tumours with *MYC* amplicons often contain plasmacytoma variant translocation 1 (*PVT1*), which is required for the stabilization of myc protein. Orthodenticle homeobox 2 (*OTX2*) amplification is also observed in Group 3 MBs [29,30,43,69]. *OTX2* gene is crucial for brain development during embryogenesis

[70]. Both *MYC* and *OTX2* somatic gene aberrations are mutually exclusive and are used as prognostic markers for this subgroup [18,29,52].

Enhancer hijacking caused by structural changes in the DNA can lead to overexpression of growth factor independent 1 (*GFI1*) in Group 3 MBs [30,71]. Chromatin modifier and nucleosome remodelling genes like *KMT2D*, *SMARCA4*, *KBTBD4* and *CHD7* are frequently mutated in this subgroup. Group 3 MBs often present with a multitude of chromosomal aberrations including loss of 8, 10q and 16q, and, gain of 1q, 7 and 18. There is also a high prevalence of isochromosome 17q in a majority of Group 3 MB cases [18,29,30,35,43,54,64]. Subtype classification based on methylation data has led to further stratification of Group 3 MB into Group 3 α , Group 3 β and Group 3 γ [42]. Further insight into these subtypes will be provided in Chapter 4.

1.4.4 Group 4

Group 4 MB is the most common subgroup and represents approximately 35-40% of all MB cases. Although these tumours are frequently metastatic at diagnosis, patients with Group 4 MB demonstrate intermediate outcome (5-year survival >75%) with late recurrence of secondary tumours. Group 4 MB tumours typically occur in children and young adults, with a rare incidence in infants. These tumours exhibit a sexual predominance with almost thrice as many males affected than the female population. Histologically, the classic subtype is predominantly found in Group 4 MB tumours with rare cases of large cell anaplastic subtype. The true cell origin of Group 4 MB tumours is not established but they are thought to arise from primitive progenitors that exhibit transcriptional signatures of unipolar brush cells and are located in the upper rhombic lip. Group 4 MB patients are not predisposed to germline mutations [18,29,30,39,44,45,67,72].

Enhancer hijacking of the chromatin modifying protein PRDM6 occurs in a major subset of Group 4 MB patients [43]. Other recurrent somatic gene aberrations in *OTX2*, *SMARCA4*, *DDX3X*, *GFII1*, *KMT2D* and *KBTD4* are found in Group 4 MB. Amplification of *MYCN* and *CDK6* (cell cycle regulators), mutations in the *KDM6A* gene (encodes for histone modification enzyme), duplication of *SNCAIP* (encodes synuclein- α interacting protein associated with Parkinson's disease) are frequently observed in Group 4 MBs [18,29,30,43,54,67,69]. Isochromosome 17q, which is commonly observed in Group 3 MBs, is also prevalent in Group 4 MB tumours at a much higher frequency. Other cytogenetic events observed in Group 4 MBs are loss of 8q, 8p, 11p and X chromosome, and, gain of 7 and 18q chromosomes [29,30,39,64]. Despite being one of the most prevalent subgroup, the underlying biology is not well-established [23]. Many clinical and molecular signatures used to categorize patients into this subgroup overlap with Group 3 MB signatures despite the dissimilarity in outcome of the disease. Hence, more data are required to categorize patients efficiently into Group 4 MB subgroup. A study by Cavalli et al. further subclassified this group into Group 4 α , Group 4 β and Group 4 γ , which will be discussed in detail in Chapter 4 [42].

1.5 Molecular targeted therapy

The recent molecular classification of MB has provided key insights into the molecular drivers of the disease. However, more information is required to identify genetic drivers distinctive to each of the 4 subgroups. Currently, there are molecular targeted therapies in clinical trials for patients with SHH or Group 3 MBs. Molecular targeted therapies can be beneficial to patients in terms of alleviating toxicity associated with standard aggressive treatments, while retaining effectiveness in killing tumour cells [18,29,30].

SHH MB subgroups often carry activating mutations in *SMO* or loss-of-function mutations in *PTCH1*, as previously mentioned [6,73,74]. Pre-clinical trials investigating the role of SMO inhibitors showed that these inhibitors were effective only in SHH MB cases with mutations upstream of SMO. A first-generation oral inhibitor, Vismodegib, effectively inhibited SMO function in about 41% of treatment refractory SHH MB tumours. However, conformational changes in SMO due to mutations result in ineffective binding of inhibitors. Vismodegib-resistant SHH MBs are treated with second generation inhibitors such as MK-4101 that are structurally different from other SMO inhibitors [29,58,75-77].

GLI is a downstream effector of the SHH signaling pathway. GLI antagonist (GANT) and arsenic trioxide (ATO) are currently being investigated to effectively target GLI. GANT61 alone was found to increase apoptosis in some MB cell lines. Alternatively, combination treatment of ATO and cisplatin inhibited GLI activity and affected its stability [78,79]. Other pathways like PI3K play a role in tumour progression of some MBs. Combination treatment of PI3K inhibitors and SMO inhibitors were found to be effective in delaying the onset of resistance observed compared to treatment with a single agent [80]. Other class of inhibitors such as Aurora kinase A (AURKA) and Polo-like kinase (PLK) inhibitors are potent against SHH MBs. They behave in a synergistic manner with standard chemotherapeutic agents to inhibit tumour growth [35,81,82]. Combination therapies might help evade the challenges faced with the usage of single agent therapies.

Group 3 MB is defined by the amplification of the key driver gene, *MYC*. Bromodomain and extraterminal (BET) protein, BRD4, is instrumental in regulating the expression of MYC protein. BRD4 binds to acetylated lysines and recruits transcriptional regulators [83]. Among many bromodomain inhibitors, JQ1 has been shown to successfully breach the blood-brain barrier

(BBB) and inhibit MYC expression, resulting in decreased viability of Group 3 MB cells [6,84,85]. Other classes of inhibitors such as histone deacetylase (HDAC) inhibitors and PI3K inhibitors act in a synergistic manner to inhibit growth of Group 3 MB tumours [6,66,86]. Similar to SHH MB, Group 3 MB tumour growth is suppressed when the cells are treated with Aurora kinase inhibitors. MYC proteins are stabilized by binding to AURKA and regulate AURKB expression. Inhibitors of aurora kinase such as alisertib and CD532 have been potent in inhibiting tumour growth by facilitating degradation of MYC proteins and regulating their expression [87-90].

Cook Sangar *et al.* identified a CDK4/6 inhibitor called palbociclib that effectively enhanced apoptosis, decreased viability and prolonged survival of mice that had Group 3 MB and SHH MB. This phenomenon was also demonstrated by another research group, thereby substantiating CDK4/6 inhibition as a potent treatment for Group 3 MB and SHH MB [91,92]. As previously mentioned, over-expression of GFI1 proteins is often observed in Group 3 and Group 4 MBs. GFI1 is critical for the maintenance of MB tumours. Lysine demethylase 1 (LSD1) interacts with GFI1 to inhibit neuronal differentiation while promoting tumorigenesis. Inhibiting LSD1 (with GSK-LSD1 or ORY-1001) could be an effective treatment for GLI1 driven MB tumours but its efficacy is limited by its inability to infiltrate the brain tumours [6,93].

1.6 Chemoresistance

Chemotherapeutic resistance, or chemoresistance, remains one of the major obstacles faced in the clinical management of all cancers. Increased risk of disease relapse and poor clinical outcome are some of the consequences of tumours that are chemoresistant. Chemoresistance may be functionally categorized into innate and acquired chemoresistance, where innate chemoresistance is a form of resistance that exists before treatment, while acquired

chemoresistance typically arise after the tumour cells have been exposed to chemotherapy [94]. In general, cancer treatment is based on the target cancer cell population and the host environment. A combination of these factors leads to the development of resistance in cancer. An in-depth understanding of the molecular mechanisms contributing to the development of chemoresistance in cancer cells is crucial for utilization of molecular targeted therapies and design of novel therapeutic agents that could overcome chemoresistance and improve treatment outcomes [95] [96].

Multi-drug resistance is the ability of cancer cells to survive against multiple cytotoxic agents, each with a different mechanism of action. A major class of proteins associated with multi-drug resistance in malignancies is the ATP-binding cassette (ABC) transporters. These proteins can transport a variety of substrates, including chemotherapeutic agents, across the cell membrane through conformational changes. In particular, P-glycoprotein 1 (P-gp, ABCB1 or MDR1) is an ABC transporter that is frequently overexpressed in chemoresistant tumour cells that functionally works as an ATP-dependent efflux pump of cytotoxic drugs [95,96]. Immunohistochemical analysis revealed that P-gp is overexpressed in 43% of MB tumours, and that P-gp overexpression is significantly associated with high-risk MB [97]. The same study also found that inhibition of P-gp with vardenafil or verapamil in MB cell lines effectively increased their sensitivity to etoposide. Use of P-gp inhibitors might be an improved therapeutic option for treatment refractory MB tumours with increased P-gp expression.

Chemotherapeutic efficacy can also be decreased by mechanisms involving drug inactivation, or alteration in drug targets, that contribute to observed chemoresistance. For example, platinum drugs can be inactivated by binding to thiol molecules such as glutathione, and this enhances drug resistance [98]. Alternatively, alterations in drug target expression due to

genomic amplification events also leads to increased resistance to treatment. For example, amplifications of growth factor receptors including HER2 or EGFR in breast cancer cells results in increased resistance to tamoxifen [95].

Tumour cell chemoresistance may also result from inhibition of apoptotic cell death. Apoptosis can occur via the intrinsic or extrinsic pathways: the intrinsic pathway involves the BCL2 family proteins, mitochondrial release of cytochrome c, and subsequent activation of caspases, while the extrinsic pathway signals through death receptors expressed on the cell surface [95]. In this regard, the anti-apoptotic BCL2 protein that is expressed at high levels in certain tumours is potentially druggable. For example, SHH mediated signaling promotes the upregulation of BCL2 expression and survival of MB [99]. Inhibitors against BCL2 can be effective at inducing tumour cell apoptosis, however, prolonged use also contributed to increased resistance to the same therapeutic agents [97].

Therapy-imposed selective pressure and evolution of cancer cells results in treatment-refractory cancer cells that arise from pre-existing sub clonal populations. Accumulating genomic instability contributes to the development of tumour heterogeneity. Patients with tumours that have a high heterogenous population are predisposed to poor clinical outcome [100]. Given the different cell of origin and heterogenous nature of MB subgroups, it is vital to develop combinatorial chemotherapeutic agents that target drug sensitive populations in addition to cells that are more drug tolerant such as cancer stem cells (CSCs). CSCs and MB stem cells are tumour-initiating cells that also have the ability to sustain tumour growth and proliferation. CD133⁺ (Prominin 1) is a surface marker for MB stem cells. Group 3 MB with enriched CD133⁺ cell population was associated with higher incidence of metastasis and poor prognosis of the disease. Garg *et al.*, demonstrated that CD133⁺ MB cells are brain tumour-initiating cells that signal via the STAT3

pathway and contribute to MB recurrence. Targeting STAT3 using novel inhibitors led to the reduced tumour growth *in vivo* [101]. Hence, blocking STAT3 signaling in MB stem cells might be a novel therapeutic approach for treatment-refractory MB tumours.

1.7 Brain tumour microenvironment

The brain tumour microenvironment (TME) is comprised of several cellular components that play crucial roles in facilitating oncogenic transformation, tumour progression and treatment resistance. Of all the brain tumours, MB has the least amount of infiltrating immune cells. In addition to conventional cells such as fibroblasts, endothelial cells, and immune cells found in the TME, there are resident cell types that are exclusive to the brain TME. Microglia (resident brain macrophages), astrocytes and neurons are resident brain cells that are protected from circulating toxins and pathogens due to the blood-brain barrier (BBB). Tumour-associated macrophages (TAMs) and microglia can constitute up to 30% of the cells found in the TME. These immune cells are often involved in bidirectional cross-talk with tumour cells, wherein immune cells secrete soluble factors to promote tumorigenesis, while tumour cells secrete chemoattractants to recruit TAMs and microglia [102,103]. TAM-associated genes are upregulated in the TME of SHH MB compared to other subgroups [104].

Other immune cells such as dendritic cells in the brain TME can provoke an anti-tumour response by presenting tumour antigens to activated T-cells. Myeloid dendritic cells in the TME of Group 3 and Group 4 MBs were associated with a better survival outcome [105]. Additionally, neutrophils act as prognostic markers for brain malignancies [106]. They promote tumour growth and survival and also provide resistance to anti-angiogenic therapies in gliomas. Single-cell RNA sequencing data of 19 tumour samples revealed that Group 4 tumours have more neutrophils

compared to other MB subgroup tumours. Group 4 tumours also have higher immune cell infiltration in comparison to other subgroups. Notably, circulating neutrophils also facilitate metastasis by setting up a pre-metastatic niche for tumour cell colonization [103,107].

Tissue-specific cells such as astrocytes surrounding the brain interact with tumour cells via gap junctions and gather cytoplasmic calcium. Through this mechanism, astrocytes have been known to inhibit apoptosis in response to several chemotherapeutic agents [108]. Another study demonstrated that co-culture with astrocytes rendered glioma cells resistant to vincristine and temozolomide treatment by establishing gap junctions [109]. Blocking these interactions between astrocytes and tumour cells might help improve the response to cytotoxic drugs. In the case of MB, Liu *et al.* demonstrated that tumour associated astrocytes promote MB progression through SHH secretion. MB cells in the presence of these cells were found to exhibit increased proliferation, invasion and resistance to treatment [110].

Bockmayr *et al.* conducted a study surveying 10 cells in the microenvironment in 1422 brain tumours that included 763 cases of MB. This study revealed that MB tumours exhibited the least expression of immune cell signatures compared to gliomas. Compared to other MB subgroups, the TME of SHH MB comprises the highest number of fibroblasts, T cells and cells from the monocytic lineage, whereas the presence of neutrophils were scarce. In normal tissues, fibroblasts are required for the synthesis of components that make up the extracellular matrix. The desmoplastic histological subtype of MB is enriched with cancer associated fibroblasts (CAF), which are known to cause aberrant fibrosis [103,111,112]. Compared to other MB subgroups, the TME of Group 3 tumours had small amount of T cells and macrophages, while Group 4 tumours contained low numbers of fibroblasts. Both Group 3 and Group 4 MB were found to be enriched with cytotoxic T-lymphocytes in their TME [113].

T-lymphocytes can elicit an anti-tumour response in the brain TME. Compared to healthy subjects, MB patients exhibit increased regulatory T-cells (Tregs) near the tumour site and in peripheral blood. Tregs suppress cytotoxic T cell infiltration to promote tumour growth in an immunosuppressive environment. Activation of the SHH or β -catenin pathway preserves the immunosuppressive environment by recruiting Tregs. Recent advances in immunotherapy has impeded immune evasion by tumours. Programmed death (PD-1) pathway acts as an immune checkpoint and sends suppressive signals to effector T cells that dampen their anti-tumour activities in the TME. Blocking PD-1 signaling pathway resulted in an effective anti-tumour response in a variety of tumour types. Notably, expression of PD-L1 on cytotoxic T (CD8) cells reduces T-cell infiltration in the TME and was associated with poor prognosis in MB patients [114]. SHH and WNT MB tumours have the highest expression level of PD-L1 [113]. In an *in vitro* setting, MB cells can express higher PD-L1 in an anti-tumour response when stimulated with interferon γ . However, anti-PD1/PD-L1 therapy has been successful in only a subset of population and the rest display primary resistance to treatment [115]. Immunotherapy has been ineffective at treating tumours like MB due to their highly immunosuppressive environment. Understanding the constituents of the subgroup specific MB TME can yield benefits in understanding their pro- or anti-tumour effects that affect disease progression, as well as identify novel therapeutic strategies to counter MB that are refractory to conventional therapy [116].

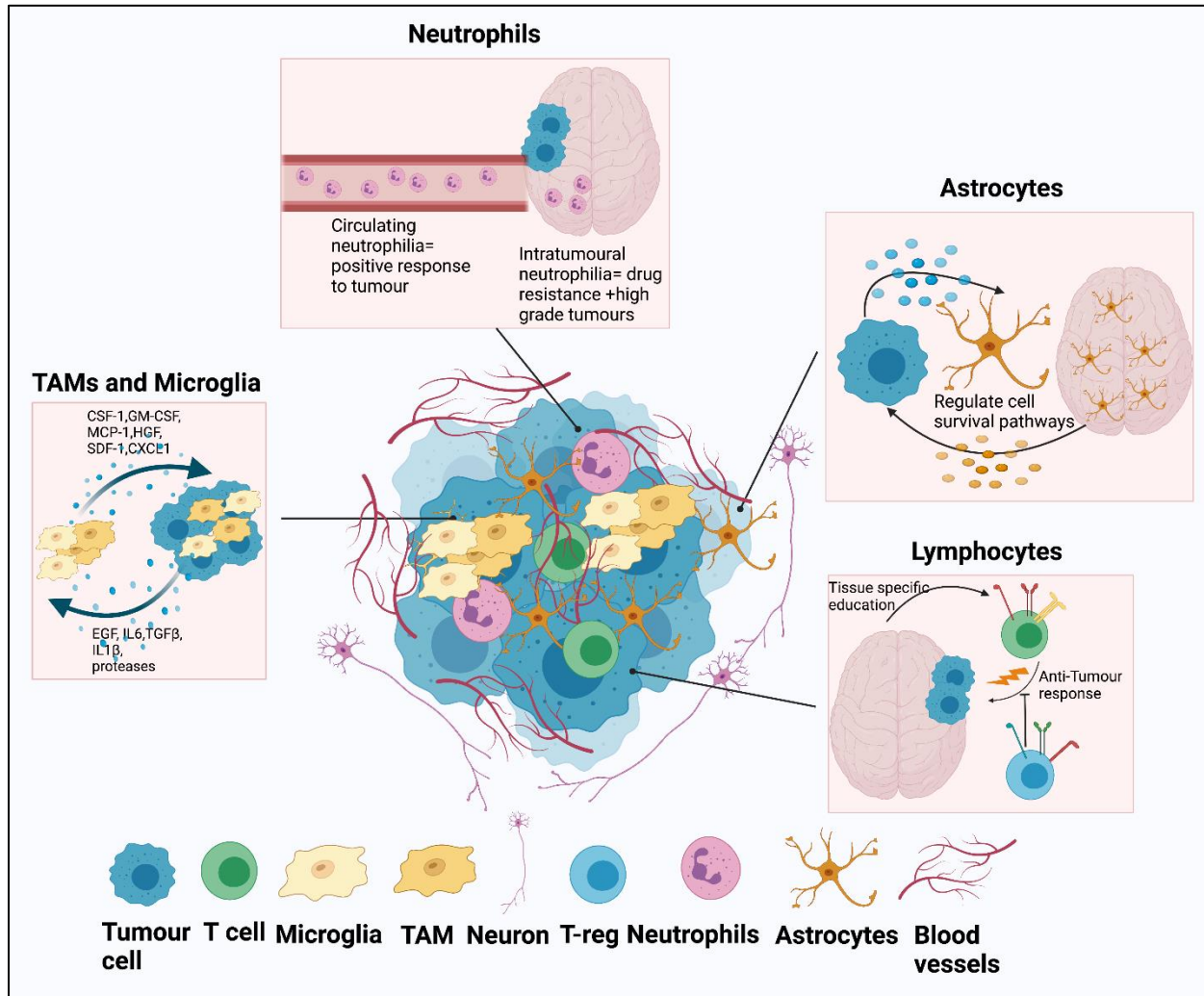


Figure 1.4: Cells in the brain tumour microenvironment.
 Figure adapted from Quail *et al.*[103] (Created with BioRender).

1.8 The IL-6/JAK/STAT3 signaling pathway

Interleukin 6 (IL-6) is a pleiotropic cytokine that plays a significant role in tumorigenesis. Indeed, high levels of serum IL-6 are correlated with shortened duration of overall survival in multiple malignancies [117]. IL-6 is also the best-established upstream regulator and activator of signal transducer and activator of transcription 3 (STAT3); IL-6 binding to its receptor IL-6R α induces dimerization of a receptor complex that includes glycoprotein 130 (gp130). This leads to

proximity-mediated transactivation of the gp130-associated Janus kinases (JAKs), and subsequent phosphorylation and dimerization of cytoplasmic STAT3, which then translocates into the nucleus, associates with transcription factors to control target gene expression. Whereas STAT3 is transiently phosphorylated in response to IL-6 stimulation in normal cells, constitutive activation of STAT3 is often implicated in treatment-refractory cancers [118]. As nuclear transcription factors that act to switch on expression of pro-survival and oncogenic proteins downstream of cytokine (growth factor) signaling, the IL-6/STAT3 pathway represents a promising molecular target for therapy. Tumour cells can exploit IL-6 to evade apoptosis by acquiring drug resistance through activation of pro-survival oncogenic pathways [119,120].

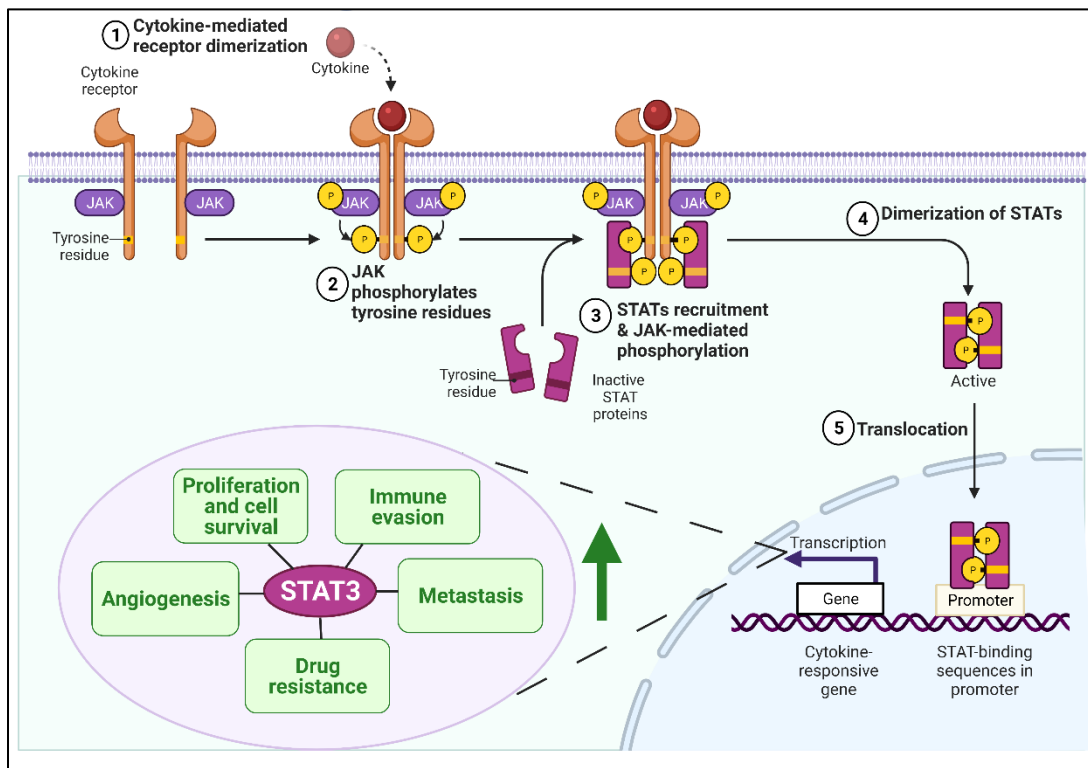


Figure 1.5: IL-6-JAK-STAT3 signaling pathway.

IL-6 binds to its receptor, IL-6R α , and gp130 to form a hexameric complex and initiate downstream signaling leading to autophosphorylation of JAKs. Inactive STAT3 proteins in the cytoplasm are recruited and phosphorylated by JAKs. Phosphorylated STAT3 dimers translocate to the nucleus where they bind to specific DNA binding sequence motifs to initiate gene expression. Proliferation, cell survival, immune evasion, metastasis, drug resistance and angiogenesis are some of the hallmarks of STAT3 protein (Created with BioRender).

1.8.1 Interleukin-6 family cytokines

The IL-6 family cytokines comprise of IL-6, IL-11, IL-27, IL-31, oncostatin M (OSM), leukemia inhibitory factor (LIF), ciliary neurotrophic factor (CNTF), cardiotrophin 1 (CT-1) and cardiotrophin-like cytokine factor 1 (CLCF1). The most striking feature of this group of cytokines is their shared common signal transducing receptor β -subunit, glycoprotein 130 (gp130). Gp130 (also known as IL-6ST or CD130) is a 130 kDa transmembrane protein that is ubiquitously expressed in all human cells [121,122]. The IL-6 family cytokines play crucial roles in early development, maintaining normal physiological homeostasis and inflammatory responses. These cytokines perform pleiotropic and redundant functions owing to their structural integrity and shared receptor subunit. They are widely used as indicators of disease onset or to predict outcome of the disease in the clinic [123,124].

The generic mechanism of signal transduction of IL-6 family cytokines is described below. The IL-6 family cytokines initiate the classic signaling cascade by binding to either a non-signaling α -receptor or to a β -receptor subunit (structurally similar to gp130) and gp130. For example, the ligands, IL-6 and IL-11 specifically bind to IL-6R α and IL-11R α respectively, to transduce the signal. OSM binds to OSMR β at a higher affinity but can also bind to LIFR β at a lower affinity. Alternatively, LIF can only bind to LIFR β and gp130 to form a signaling complex. Table 1.2 lists the IL-6 family cytokines and their receptor interactions.

There are three sites on IL-6 cytokine that play a role in receptor engagement. Sites 1 and 2 on the ligand interact with IL-6R α and gp130 respectively. Site 3 engages two of these trimetric complexes to form a hexameric signaling complex. The IL-6/IL-6R α /gp130 complex then initiates a downstream signaling cascade involving the JAK-STAT pathway. The IL-6 family cytokines also activate other prominent survival pathways including mitogen activated protein kinase

(MAPK), PI3K/AKT and Notch pathway via JAK or STAT activation through interaction with other pathway components [125,126].

Table 1.2: IL-6 family cytokines and their receptors.

Cytokine	Receptor
IL-6	IL-6R α
IL-11	IL-11R α
LIF	LIFR α
CT-1	
OSM	
OSM	OSMR β
IL-31	IL31-R α
IL-27	IL-27R α
CNTF	CNTFR α
CLCF-1	

In addition to the classic signaling mechanism, many of these cytokines can signal by two alternate mechanisms; trans-signaling and trans-presentation. Although gp130 is ubiquitously present in all human cell types, some cells lack the membrane bound non-signaling receptor subunit (such as IL-6R α or IL-11R α). In such cases, IL-6 binds to the soluble form of the receptor, sIL-6R α and the membrane bound gp130 to initiate the signaling cascade. This form of signaling is termed trans-signaling. The sIL-6R α is generated either by alternative splicing of mRNA, or by shedding of the membrane bound IL-6R α mediated by a protease called a disintegrin and metalloproteinase 17 (ADAM17) [127]. A third signaling mechanism, known as trans-presentation, involves the interaction of different cell types through the trimeric IL-6, IL-6R α and gp130 complex. For example, IL-6 binding to IL-6R α on the first cell facilitates their interaction with the membrane bound gp130 presented on a second cell, to trigger an intracellular signaling

cascade on the second cell. These three modes of signaling shed light on the unique role of the gp130 receptor subunit and its contribution to IL-6 family cytokine signaling [122,125,126].

Due to their role in a broad range of physiological conditions, development of therapeutic agents to target the IL-6 family cytokines are of high importance [122,124]. Monoclonal antibodies, recombinant cytokines and small molecule inhibitors are widely used to target the cytokines or their respective receptors to block function. For example, tocilizumab is a monoclonal antibody that binds to IL-6R to prevent binding of IL-6 and signal transduction. However, constant exposure to tocilizumab treatment leads to weight gain or increase in cholesterol in some patients [128]. Because these cytokines function in a complex network and affect systemic functions, caution is required when administering therapeutic agents to target them.

1.8.2 Glycoprotein 130

Gp130 is expressed in all human cells. Gp130 is classified as type 1 cytokine receptor based on specific conserved domains. It is involved in multiple physiological functions due to its role as a common signal transducer to the IL-6 family cytokines [125,129]. As previously described in section 1.8, the hexameric complex formed between gp130 and the cytokine/receptor triggers activation of downstream targets such as JAKs. Although JAKs are constitutively associated with gp130, receptor complex formation is a prerequisite event that triggers phosphorylation of JAKs. STATs are subsequently phosphorylated and initiate transcription in the nucleus. Gp130 activation also leads to phosphorylation of Src homology 2-containing phosphotyrosine phosphatase (SHP2) and downstream activation of Ras-MAPK-ERK signaling. Due to the involvement of gp130 in a wide range of signaling cascades, a negative feedback system is present to restrict constitutive cytokine-mediated signaling in order to maintain homeostasis. One example is suppressor of

cytokine signaling 3 (SOCS3), which directly interacts with gp130 to prevent phosphorylation of JAKs and STATs [130].

Dysregulation of gp130-mediated signaling has been implicated in numerous diseases including autoimmune diseases, chronic inflammatory diseases and cancer [122,131]. Recent studies have demonstrated the efficacy of inhibitors that target gp130 signaling in multiple malignancies. Bazedoxifene is an FDA-approved selective estrogen receptor modulator (SERM) that has been repurposed for use as a gp130 inhibitor. This inhibitor has a robust effect in various cancer cell lines and could be a potential therapy for some types of cancer [132-136]. SC144 is another inhibitor used in preclinical studies that also effectively targets gp130 [137].

1.8.3 Janus kinase

Janus kinases (JAKs) are non-receptor tyrosine kinases that are required for crucial functions such as growth, development and immune response. Generally, JAKs associate with the intracellular domains of cell membrane cytokine receptors to relay signals [138]. Ligand binding initiated receptor dimerization causes cross-phosphorylation of JAKs, followed by activation of numerous signaling cascades including those initiated by STAT, PI3K, and ERK. JAKs regulate numerous functions including proliferation, differentiation and chronic inflammation. The JAK family comprises of 4 members, namely JAK1, JAK2, JAK3 and tyrosine-protein activated kinase 2 (TYK2) [138,139].

Structurally, the JAK protein consists of 7 JAK homology (JH) domains. The most important domains of JAKs are JH1, JH2, Src homology (SH2) domain (JH3 and JH4), and band four-point-one, ezrin, radixin, moesin (FERM) domain (JH5, JH6 and JH7) (Figure 1.6). Ligand binding to the cytokine receptor causes transphosphorylation at the JH1 domain of JAKs. The JH2 domain is only present in JAK2 and is thought to play an inhibitory role because loss of JH2 leads

to constitutive activity. Mutation in the JH2 domain of JAK2 leads to autophosphorylation of JAK2 resulting in increased activation of STAT5 [140]. JAK-mediated phosphorylation of STATs at a site on the SH2 domain creates ligands for the STAT SH2 domains, and this allows STAT dimerization. The FERM domain interacts with the SH2 domain to form the receptor binding domain for distinct receptor interactions. Clinically, mutations in JAKs has resulted in aberrant downstream signaling and disease progression [138,140].

SOCS1 can act as a negative feedback regulator in two ways. Firstly, SOCS1 can interact with JAK to competitively inhibit STAT3 binding and activation. Secondly, SOCS1 can promote ubiquitination-mediated proteasomal degradation of JAKs [141,142]. JAK1 inhibition with RNAi or inhibitors has been shown to attenuate STAT3 phosphorylation and inhibit cell growth [143]. Activating mutations of JAK2 have also been reported as key drivers of tumorigenesis in myeloproliferative neoplasms [144]. In the clinic, JAKs are commonly targeted with a single therapeutic agent or may be used synergistically with cytotoxic agents to enhance the anti-tumour activity in some cancers. Most prominently used is Ruxolitinib, a potent but selective JAK1/JAK2 inhibitor that has been used to treat myeloproliferative disorders and cancers by inhibiting cell growth [145]. Thus, targeting JAKs with small molecule inhibitors holds potential as therapeutic options to help alleviate the treatment burden and tumorigenesis for JAK-involved tumours.

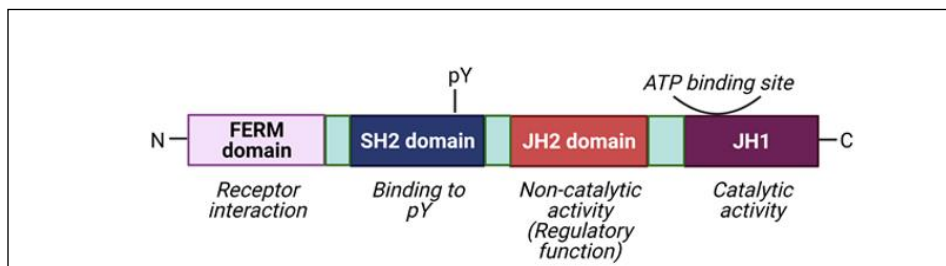


Figure 1.6: Structural components of JAK protein.

(Created with BioRender).

1.8.4 Signal transducers and activators of transcription

Signal transducer and activator of transcription (STAT) proteins are often implicated in tumorigenesis of multiple malignancies [146-148]. Of the seven STATs, STAT3 and STAT5 play a predominant role in tumour cell proliferation and survival. Increased STAT3 phosphorylation, which occurs downstream of JAK, is commonly associated with drug-resistant recurrent tumours, when compared to primary tumours [149]. STAT3 is also required for the recruitment of stromal and immune cells to the TME to facilitate tumour progression [150]. STAT3 is a negative regulator of T-helper cell mediated inflammation and activates genes crucial for immunosuppression. Aberrant STAT3 signaling also enables tumour cells to secrete immunosuppressive factors that activate STAT3 in immune cells and restricts its anti-tumour response. The immunosuppressive TME helps tumours cells to evade immune attack by blocking inflammatory signals, thereby making STAT3 a promising target for cancer immunotherapy [151].

The structural domains of the STAT3 protein and their functions are illustrated in Figure 1.7. STAT3 structure-function is defined by phosphorylation by JAKs, protein dimerization, and subsequent nuclear translocation to activate transcriptional expression of downstream genes. Following cytokine receptor dimerization, the first step in STAT3 activation is the recruitment of its latent cytoplasmic form by phosphorylated JAK proteins. Canonical STAT3 activation is regulated by two phosphorylation sites located near the C-terminus, Y705 and S727. STAT3 Y705 is phosphorylated by several kinases including EGFR, Src and JAK [152-154]. STAT3 S727 is phosphorylated by kinases including PKC, ERK and mTOR [155-158]. Of particular functional significance, pY705-STAT3 has been linked to drug resistance in multiple malignancies, whereas pS727-STAT3 is required for maximal transcriptional activation [158,159]. As key a driver of

oncogenesis, STAT3 activity promotes increased expression of downstream target genes that include *cyclin D1*, *c-myc*, *bcl-2*, *survivin*, *bcl-XL*, and *VEGF* [160].

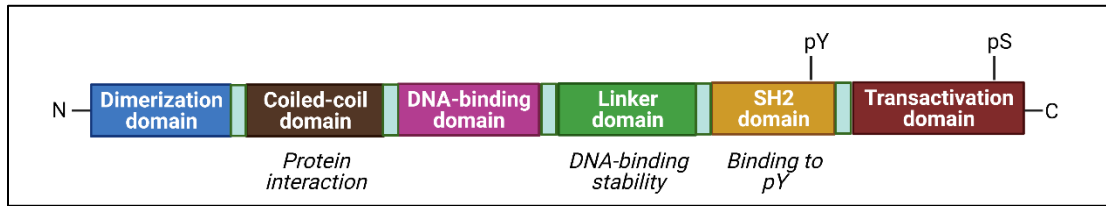


Figure 1.7: Structural components of STAT3 protein.
(Created with BioRender).

In summary, STAT3 is a transcription factor that can both activate and repress gene expression patterns to promote tumour survival and growth. Additionally, several upstream regulators such as cytokines and cytokine receptors converge on the JAK-STAT3 pathway, hence targeting STAT3 might be a novel cancer therapeutic approach with a potential for broad clinical impact. Previous studies have shown that STAT3 inhibitors were able to prevent phosphorylation of STAT3 Y705 and suppress cell proliferation and growth in MB [161,162]. For example, small molecule inhibitors such as niclosamide block the phosphorylation and nuclear translocation of STAT3 in multiple malignancies [163,164]. Although there are several STAT3 inhibitors that have shown efficacy in *in vitro* studies, there is yet any clinical evidence in terms of their *in vivo* efficacy. Thus, further refinement and evaluation of STAT3 inhibitors is required for their development as clinically relevant anti-cancer therapies [165].

1.9 Research objectives and hypothesis

1.9.1 Overview of the problem

MB is a high-grade pediatric brain malignancy with an overall 5-year survival rate of 60–80%, depending on the molecular classification. The four molecular subgroups of MB demand

specific molecular targeted therapies to treat each subgroup distinctly to improve the prognosis of the disease [45,69]. MB is primarily treated with a combination of conventional therapies including surgery, craniospinal irradiation, and cytotoxic chemotherapy [166]. While intensification of non-specific conventional therapies has led to significant improvements in patient survival, this achievement is accompanied by more severe long-term sequelae of survivors. As MB more commonly afflicts infants and children under 4 years old, aggressive chemotherapies also lead to harmful side effects [21,167]. The current clinical implications of molecular subgroups need to be considered to improve the quality of treatment for MB patients. Among the four molecular subgroups, Group 3 has been molecularly classified as the most aggressive type of MB, with metastases found in most patients at the time of diagnosis. Group 3 MB also has the worst overall survival (below 50%) and is predominantly found in infants and children [40].

My overall doctorate thesis objective is to evaluate if targeting the major components of the IL-6/STAT3 signaling pathway may be an improved therapeutic strategy to circumvent drug resistance in Group 3 MB. My overarching hypothesis is that the IL-6/STAT3 signaling axis contributes to chemoresistance in Group 3 MB via autocrine and paracrine signaling mechanisms. The following sections detail the rationale and research objectives for each chapter.

1.9.2 Chapter 2: Rationale and hypothesis

Chemotherapy is one of the principal modes of treatment for cancer, but its effectiveness is often limited by drug resistance. Constitutive activation of STAT3 is often implicated in promoting tumorigenesis. Drug-resistant recurrent tumours often have increased STAT3 phosphorylation as compared to primary chemosensitive tumours. Although the significance of increased STAT3 signaling in survival, proliferation and drug resistance has been well documented

in multiple malignancies, significant gaps remain in our understanding of the upstream regulators and of JAK-STAT3 signaling. IL-6 is a pleiotropic cytokine that signals by binding to the extracellular domain of the heterodimeric receptor IL-6R/gp130, leading to subsequent activation of JAK and the downstream effectors including STAT3. In Chapter 2:, I examine the hypothesis that an IL-6/STAT3 autocrine signaling mechanism contributes to acquired drug resistance in Group 3 MB. Therein, I assessed the possibility that IL-6 stimulation of STAT3 phosphorylation in MB cells results in further secretion of IL-6 in an autocrine feedback loop that sustains and amplifies the oncogenic activity of STAT3.

1.9.3 Chapter 3: Rationale and hypothesis

The finding that autocrine IL-6 activity promotes development of acquired drug resistance led to my studies outlined in Chapter 3, which examine the role of IL-6 family cytokines as paracrine mediators originating from the tumour microenvironment (TME). The TME is a fundamental regulator of tumour progression that has the potential to significantly modulate therapeutic efficacy in primary and metastatic brain malignancies. Gaining mechanistic insights into the tumour-promoting role of the individual components of the brain TME will help us design potential therapeutics to combat drug resistance and understand the pathogenesis of the disease [103].

My focus here is on the role of microglia, brain-resident macrophages known to secrete soluble factors that can facilitate tumour growth and survival in a bidirectional crosstalk manner. Hence, I evaluated the contribution of microglia in the development of chemoresistance in Group 3 MB cells. Additionally, the presence of IL-6 family cytokines in the brain TME has gained interest for its newly recognized role in CNS homeostasis and pathogenesis of diseases [168-170]. As upstream regulators of STAT3 signaling, I assessed the contribution of several members of the

IL-6 family cytokines to acquired chemoresistance in Group 3 MB cells. In Chapter 3:, I investigated the hypothesis that microglia contribute to tumour drug resistance by secreting cytokines that activate the IL-6/gp130/STAT3 signaling cascade in Group 3 MB cells.

1.9.4 Chapter 4: Rationale and hypothesis

In the past decade, numerous transcriptome studies have led to the discovery and stratification of MB into four distinct molecular subgroups with distinct biology and clinical behaviour. Understanding the regulatory circuitry that govern the transcriptional landscapes of MB subgroups, and how they relate to their respective developmental origins will be essential in identifying novel candidate targets for therapy [42,43,101]. My objective in Chapter 4 was to further validate the functional biological context of the work provided in Chapters 2 and 3 by using gene expression array data from existing published GEO datasets to probe for IL-6/STAT3 signaling axis components in Group 3 MB.

Chapter 2: Autocrine IL-6/STAT3 signaling aids development of acquired drug resistance in Group 3 medulloblastoma.

2.1 Chapter Overview

IL-6 stimulation of JAK/STAT3 signaling can occur via an autocrine (cell response to its own secreted signal) manner, subsequently contributing to cellular growth and transformation [171]. In this chapter, I focus on the preclinical approaches that help predict the emergence of drug resistance via IL-6/STAT3 autocrine signaling in human Group 3 MB. Using incremental drug selection, we generated chemoresistant MB cell lines with enhanced IL-6/STAT3 activity. Conversely, cytokine conditioning without drug pre-exposure was sufficient to convert chemosensitive MB cells to a chemoresistant variety. The critical requirement of the IL-6/STAT3 signaling axis in MB cell survival and drug resistance was evaluated using CRISPR-Cas9 engineered cells with loss of IL-6R or STAT3 function. My study highlights the pro-tumorigenic role of IL-6/STAT3 signaling, and implicate the potential for molecular targeted therapies to counter acquired drug resistance in Group 3 MB.

2.2 Materials and methods

2.2.1 Cells and tissue culture

MED-MEB-8A [172], referred to as Med8A-S, is a MB cell line derived from a 1-year old male (RRID: CVCL_M137). Med8A-R cells were derived from Med8A-S by incremental selection over a period of 4 months with vincristine (Sigma) at concentrations starting at 0.01 µg/mL and ending at 0.16 µg/mL. Med8A-S and Med8A-R were confirmed to have identical STR profiles (ATCC). Med8A-S and derived variants were cultured in 10% fetal bovine serum

(FBS, Invitrogen) DMEM (Sigma) supplemented with 1% penicillin–streptomycin (Pen-Strep, Gibco) and non-essential amino acids (NEAA, Invitrogen).

D341 Med (ATCC HTB187™) and D283 Med (ATCC HTB185™) are MB cell lines derived from 3.5-year old and 6-year old male, respectively. D341 and D283 were cultured in 20% FBS EMEM (Sigma) and 10% FBS EMEM, respectively. DAOY (ATCC HTB-186) is a MB cell line derived from a 4-year old male. Daoy was cultured in 10% FBS DMEM, all with 1% Pen-Strep and NEAA. D341, D283, and DAOY were purchased from ATCC, and used for experiments within passages 3–12.

Med8A-S cells were passaged once every three days (doubling time ~ 1 day) at 90% confluency. Old media is discarded and cells were washed with PBS. Since they are adherent cells, trypsin was used to lift the cells off the plate and neutralized using fresh media. 1 mL of Med8A-S cells was plated with 9 mL of fresh media in a 100 mm dish. Med8A-R, STAT3^{-/-} and IL-6R^{-/-} cells were passaged using the same conditions as Med8A-S. D283 and D341 grow as clusters in suspension with partially adherent cells. Cluster cells have high viability compared to single cells. The attached cells were removed from the flask base by using a cell scrapper. Cell culture was maintained by adding fresh media. D283 and D341 cell cultures should be maintained between 4×10^4 to 8×10^5 cells/mL. Cell viability between passages was assessed using Trypan blue.

IL-6 conditioning of cells (denoted as IL-6+) was achieved by culturing each cell line for 4 weeks in media supplemented with 2 ng/mL recombinant human IL-6 (Genscript). Following this conditioning, cells were cultured a further 2 weeks without IL-6 addition before being used for experiments.

For conditioning using the coculture system, I refer to target cells as ones being conditioned, while donor cells represent the source of stimulatory cytokines. Target cells were

plated at a density of 10^5 cells/well in a 6-well plate. Donor cells (e.g., IL-6+ cells already pre-conditioned with IL-6), were plated at a density of 10^5 cells within a Transwell insert (Greiner ThinCert) that was then placed into the well to co-incubate with the target cells in fresh culture media (with no added cytokine). Following the coculture for 3 days, the Transwell insert was removed, the target cells rinsed with blank media, and replenished with fresh media for another 3 days. Cells were either harvested for protein analysis, or the media supernatant analysed for secreted cytokines.

2.2.2 Cell viability assays

Cells were seeded in 96-well plates at a density of 10^5 cells/well, allowed to adhere for 16 hours before addition of drugs at various concentrations. After 48 hours, the fluorometric reagent Cell Titer Blue (Promega) was added according to manufacturer's protocol and fluorescence ($560_{\text{Ex}}/590_{\text{Em}}$) measured on a spectrophotometer (Enspire) after 4 hours. In this assay, live cell metabolites convert a redox dye (resazurin) to a fluorescent compound (resosurfin). The fluorescence emitted by live cells is plotted as relative fluorescence units (RFU). In addition to vincristine (Sigma), cells were also treated with cisplatin, idarubicin, mitoxantrone, or niclosamide (Selleckchem). All assays were conducted as 3 replicates per treatment condition and graphs were plotted using GraphPad Prism.

2.2.3 Radiation assay

Cells were seeded in 6-well plates at a density of 2.5×10^5 cells/well, allowed to adhere for 4 hours before administration of ionizing radiation at various doses. After 72 hours, cells were resuspended and incubated with AnnexinV-FITC (BD Biosciences) according to manufacturer's

instructions prior to flow cytometry analysis. All assays were conducted as 3 replicates per treatment condition and graphs were plotted using GraphPad Prism.

2.2.4 Western blots

Cell lysates were prepared in PN lysis buffer (10 mM PIPES, 50 mM NaCl, 150 mM sucrose, 50 mM NaF, 40 mM Na₄P₂O₇·10H₂O, 1 mM Na₃VO₄, 1% Triton X-100, Complete protease inhibitors (Sigma)). Total protein (30 µg) was separated by SDS-PAGE, and transferred to nitrocellulose using the Trans-Blot Turbo Transfer System (Bio-Rad). Blots were blocked in blocking buffer 5% bovine serum albumin (BSA, Fisher) in TBS-T (TBS-T is 50 mM Tris-HCl, 150 mM NaCl, pH 8 with 0.1% Tween20) for 1 hour at 22 °C, then incubated overnight at 4 °C with primary antibodies diluted in blocking buffer. Blots were further incubated with secondary goat anti-mouse or -rabbit fluorophore-conjugated antibodies (Dylight 800 or Dylight 680, ThermoFisher) in 2% non-fat milk in TBS-T, and scanned on the Licor Odyssey.

The following primary antibodies were used (complete details in Appendix B.1): pY705-STAT3, pS727-STAT3, STAT3, pAKT (S473), pAKT (T308), BAD, BCL-xl, MCL1, SOCS3, pErk1/2 and MDR1 (Cell Signaling Technologies); and GAPDH (Biolegend). In some experiments, cells were treated with IL-6 at the indicated concentrations and time prior to preparation of cell lysates.

2.2.5 Plasmids and CRISPR

Guide RNA (gRNA) mediated CRISPR-Cas9 gene editing was used to generate null cell lines. To target exon 2 of *STAT3*, DNA corresponding to 5' GCAGGAAGCGGCTATACTGC 3' gRNA sequence was cloned into plasmid pX330 (Addgene #42230). To target exon 1 of *IL-6Rα*, 5' GGCCGTCGGCTGCGCGCTGC 3' was cloned into pX458 (Addgene #48138). Med8A-R cells

were transfected with the respective plasmids using Lipofectamine 2000 (ThermoFisher) as per manufacturer's instructions. After 1 day, cells were clonally sorted by flow into 96-well plates (FacsAria, BD Biosciences). Screening for *STAT3*^{-/-} clones involved immunofluorescence evaluation for STAT3 expression, followed by western blot confirmation. Screening for *IL-6Rα*^{-/-} clones was done by flow cytometry. To identify indel mutations within the targeted genomic loci, I sequenced a genomic amplicon generated by polymerase chain reaction using the following primers: 5' CACCGGGCCGTCGGCTGCGCGCTGC 3' (Fwd) and 3' AAACGCAGCGCGCAGCCGACGGCCC 5' (Rev) for *STAT3*, and 5' TTCCTATCAGTGGACCGCGT 3' (Fwd) and 3' ACATTGATGGCATTATTGCTGA 5' (Rev) for *IL-6Rα*. Sequence alignments of the CRISPR generated mutants and parental strain were performed using CLC Main Workbench to confirm the knockout.

2.2.6 Flow cytometry

To evaluate cell surface *IL-6R* expression, cells were suspended, washed with phosphate buffered saline and stained with anti-human *IL-6Rα* antibody (R&D Systems) followed by secondary antibody (Dylight 488; ThermoFisher). Flow cytometry was conducted on the Accuri C6 (BD Biosciences) and analysis was conducted using FlowJo (Tree Star). Fluorescence activated cell sorting of CRISPR generated cells was conducted on the FacsAria (BD Biosciences) in the BCCHRI Flow Core facility.

2.2.7 Real Time PCR

Total RNA was extracted from Med8A-S, Med8A-R, and Med8A-IL6+ cells using the RNeasy mini plus kit (Cat# 74136; Qiagen). 1 μg RNA was reverse-transcribed into cDNA using the iScript cDNA synthesis kit (1708891; Biorad) and real-time PCR was performed using

TaqMan Fast Advanced Mastermix (# 4444556, Applied Biosystems) on the ABI StepOne System (Applied Biosystems). Pre-designed human PrimeTime qPCR Probe Assays (Integrated DNA Technologies) was used to measure gene expression of IL-6R (Hs.PT.58.3039085) and E2F3 (Hs.PT.58.22827120), and normalized to HPRT1 (Hs.PT.58 v.45621572). The relative changes in target gene were analyzed using the $2^{-\Delta\Delta C_t}$ method.

2.2.8 Cell proliferation and colony forming assay

Cell proliferation was assessed by seeding 5×10^3 cells/well in a 96-well plate and cell density monitored for 5 days. Using the in-built IncuCyte (Sartorius) analysis software, the cell proliferation rate was calculated by measuring the phase area confluence of cells over a period of time. Colony forming assay was performed by seeding 200 cells/well in a 96-well plate and monitored for 7 days. Both assays were performed and analyzed on the IncuCyte live-cell imaging platform (Sartorius).

2.2.9 Invasion and Migration assay

For the scratch-wound assay, 1.5×10^6 cells were plated on dishes coated with 10 $\mu\text{g/mL}$ fibronectin and incubated overnight. The cells were then washed with PBS and replenished with fresh media before performing the scratch using a 200 μL pipette tip. The wells were then imaged at 4-hour intervals for 24 hours. The migration index was quantified and measured as area (pixel^2) using Image J.

For the invasion assay, the cells were serum starved overnight and replenished with 2% FBS DMEM. 10^6 cells were plated on an 8 μm pore Transwell insert coated with different concentrations of Matrigel. The bottom well was supplemented with the chemoattractant (10% FBS DMEM). At 72 hours, the Transwell inserts were removed and stained with crystal violet to

visualize the invaded cells. The invasion index was quantified and measured as area (pixel²) using Image J.

2.2.10 ELISA and cytokine array

IL-6 cytokine secreted by cells was quantified using LEGEND MAX Human IL-6 ELISA Kit (Biolegend #430507). Media supernatant collected from culture of various cells were incubated and stained with reagents on a pre-coated 96-well strip plate as per manufacturer's instructions. A microplate reader (Enspire) was used to measure the absorbance at 450 nm. Quantibody[®] Human Cytokine Array 1 (RayBiotech) is a multiplex ELISA system for quantitative measurement of multiple cytokines simultaneously. Sample preparation and analysis was performed according to the manufacturer's instructions. Further statistical analysis was performed using GraphPad.

2.2.11 Statistical data analysis

All data are representative of at least three independent experiments. Graphs were plotted and statistical significance calculated using GraphPad, with *** $p < 0.001$, ** $p < 0.01$, * $p < 0.05$, ns – not significant. The statistical tests used is indicated in each figure legend.

2.3 Results

2.3.1 Drug resistant MB is correlated with increased IL-6/STAT3 activity

Initially, I evaluated the sensitivity of two human MB cell lines to vincristine, a vinca alkaloid that destabilizes microtubules and is one of the primary agents for clinical treatment of MB [166,173]. Med8A, which belongs to Group 3 MB, appears to be highly sensitive to vincristine when compared to DAOY, an SHH subgroup MB (Figure 2.1A) [174]. This presented an opportunity to contrast pathway changes resulting from acquired drug resistance, thus we subjected the chemosensitive parental line (herein referred to as Med8A-S) to gradual incremental selection with vincristine, and derived a stably chemoresistant variant termed Med8A-R (Figure 2.1B). Despite being selected with only vincristine, I found that Med8A-R exhibited significant resistance to other agents including cisplatin, mitoxantrone, and idarubicin (Figure 2.1C-F). Furthermore, I also assessed radio-sensitivity of Med8A-S and Med8A-R cells. These cells were irradiated at various doses and apoptosis assay was performed after 72 hours to assess cell death. My analysis revealed that Med8A-R cells were more resistant to irradiation when compared to Med8A-S at 10 Gy (Appendix A.9).

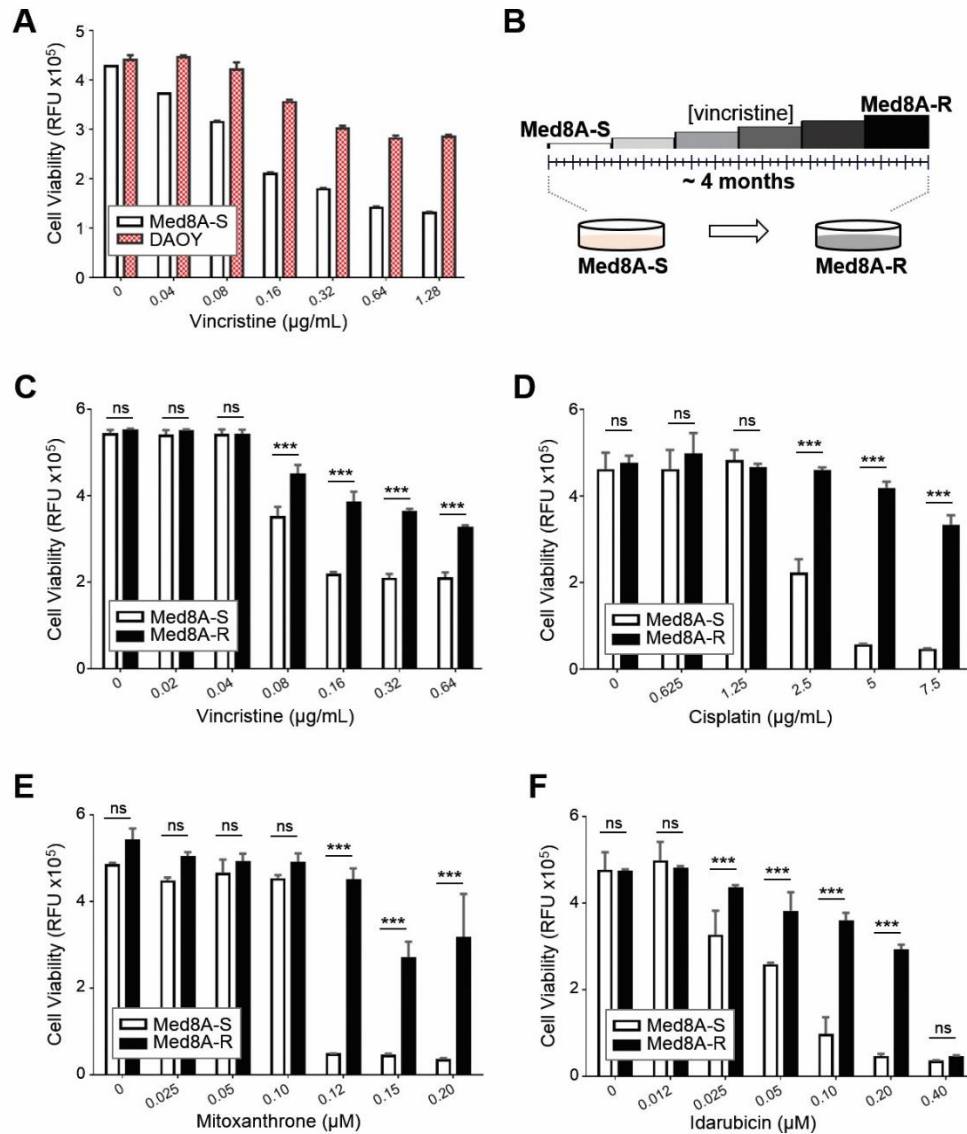


Figure 2.1: Derivation of a chemoresistant variant of Med8A MB.

(A) Med8A-S and DAOY cells were treated with vincristine at the indicated concentrations for 48 hours, and cell viability assessed by measuring the fluorescence after incubation with Cell Titer-Blue (CTB) for 4 hours. As plotted is the mean \pm SD of an experiment performed in triplicates, representative of at least 3 independent experiments. (B) Schematic for derivation of drug resistant Med8A cells. The chemosensitive parental cell line, Med8A-S, was subjected to incremental selection in vincristine over a period of 4 months to derive the stable chemoresistant variant Med8A-R. The endpoint vincristine concentration was at 0.16 μ g/mL. Med8A-S and Med8A-R were treated with (C) vincristine (D) cisplatin (E) mitoxantrone and (F) idarubicin for 48 hours and cell viability assessed with CTB. The fluorescence emitted by live cells is plotted as relative fluorescence units (RFU). The data represent the mean \pm SD of three replicates; *** p < 0.001, two-way ANOVA with Bonferroni's multiple comparison test [120].

Increased STAT3 activity is known to regulate most tumourigenic functions and promote drug resistance in gliomas and multiple other malignancies [87,162,175-178]. To infer the role of STAT3 in drug resistance of MB, I profiled the phosphorylation status at Tyr705 (pY705-STAT3) and Ser727 (pS727-STAT3) in lysates of Med8A and DAOY cells by western blot analysis. Under non-stimulated basal culture conditions, DAOY exhibited higher pY705-STAT3 levels when compared to Med8A-S (Figure 2.2A), suggesting that enhanced STAT3 activity may be involved in enhanced drug resistance of DAOY. Next, I titrated the concentration and duration of IL-6 treatment to optimize conditions able to stimulate pY705-STAT3 in Med8A cells in a non-saturating manner (Figure 2.2B). Even though non-stimulated Med8A-S and Med8A-R cells expressed comparable levels of STAT3 and pY705-STAT3; IL-6 treatment at 5 ng/mL invoked a stronger pY705-STAT3 response in Med8A-R compared to Med8A-S (Figure 2.2C, D), implicating enhanced sensitivity of the chemoresistant variant to IL-6/STAT3 signaling. Under basal conditions, I observed no difference in levels of pY705-STAT3 between Med8A-S and Med8A-R cells, however, treatment with the tyrosine phosphatase inhibitor, sodium vanadate, revealed a noticeable and significant increase of pY705-STAT3 in Med8A-R cells (Figure 2.2E), suggesting the chemoresistant line have a low albeit intrinsically enhanced level of STAT3 activity.

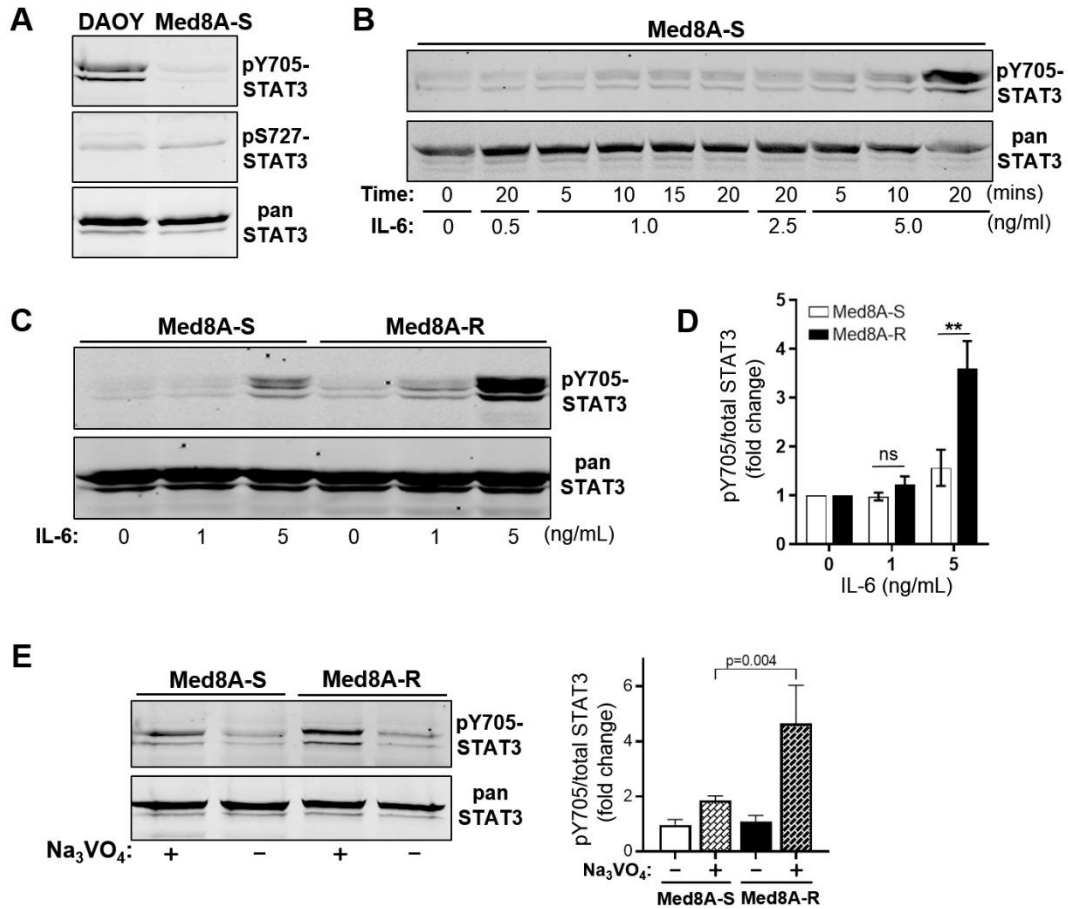


Figure 2.2: Chemoresistant MB is associated with enhanced STAT3 activity.

(A) Lysates of DAOY and Med8A-S cells under basal, non-stimulated conditions were assessed for levels of phosphorylated (pY705 and pS727) and total STAT3 by Western blot analysis. (B) Med8A-S was treated with IL-6 at various concentrations for various times to identify conditions promoting optimal but non-saturating stimulation of pY705-STAT3. (C) Med8A-S and Med8A-R cells were treated with IL-6 at 1 or 5 ng/mL for 10 min and cell lysates immunoblotted for pY705 and total STAT3. As shown is representative of 3 independent replicates. (D) Quantitation of pY705-STAT3 over total STAT3, reflected as fold change, from the data shown in (C). ** $p < 0.01$, two-way ANOVA with Bonferroni's post-test. (E) Med8A-S and Med8A-R cells were treated with 2 mM sodium vanadate for 20 min, and cell lysates immunoblotted for pY705 and total STAT3. Left panel: As shown is representative of 3 independent replicates. Right panel: Quantitation of pY705-STAT3 over total STAT3, reflected as fold change. Significance determined by two-way ANOVA with Bonferroni's multiple comparison test [120].

2.3.2 Loss of STAT3 or IL-6R in drug resistant MB led to restored sensitivity to vincristine

To further assess the requirement of STAT3 and IL-6 in drug resistance, I used CRISPR-Cas9 gene editing to generate clonal STAT3^{-/-} and IL-6Rα^{-/-} derivatives in the stably resistant Med8A-R cell background (Figure 2.3). Med8A-R cells lacking STAT3 or IL-6R (receptor for IL-6) expression (Figure 2.4A, B) showed increased sensitivity to vincristine when compared to the parental Med8A-R cells (Figure 2.4C, D). In addition, treatment of IL-6Rα^{-/-} cells with IL-6 failed to stimulate any increase in pY705-STAT3 levels (Figure 2.4E), indicating loss of IL-6R led to complete blockade of IL-6 mediated STAT3 activity. I assessed and found that Med8A-R cells expressed higher cell surface levels of IL-6R compared to Med8A-S, suggesting the increased STAT3 activity observed was due to increased IL-6 receptor function (Figure 2.4F). Furthermore, IL-6R expression was lower in STAT3^{-/-} cells when compared to the parental Med8A-R, but remain adequately expressed relative to Med8A-S cells (Figure 2.4F), suggesting that IL-6 activity cannot overcome loss of STAT3 in promoting drug resistance. In summary, MB cells with blockade of IL-6 stimulation of STAT3 activity exhibited increased susceptibility to vincristine treatment. Taken together, my results provide evidence that increased IL-6/STAT3 signaling enhances vincristine resistance in MB, and implicates the IL-6/STAT3 signaling axis as a novel therapeutic pathway to circumvent drug resistance.

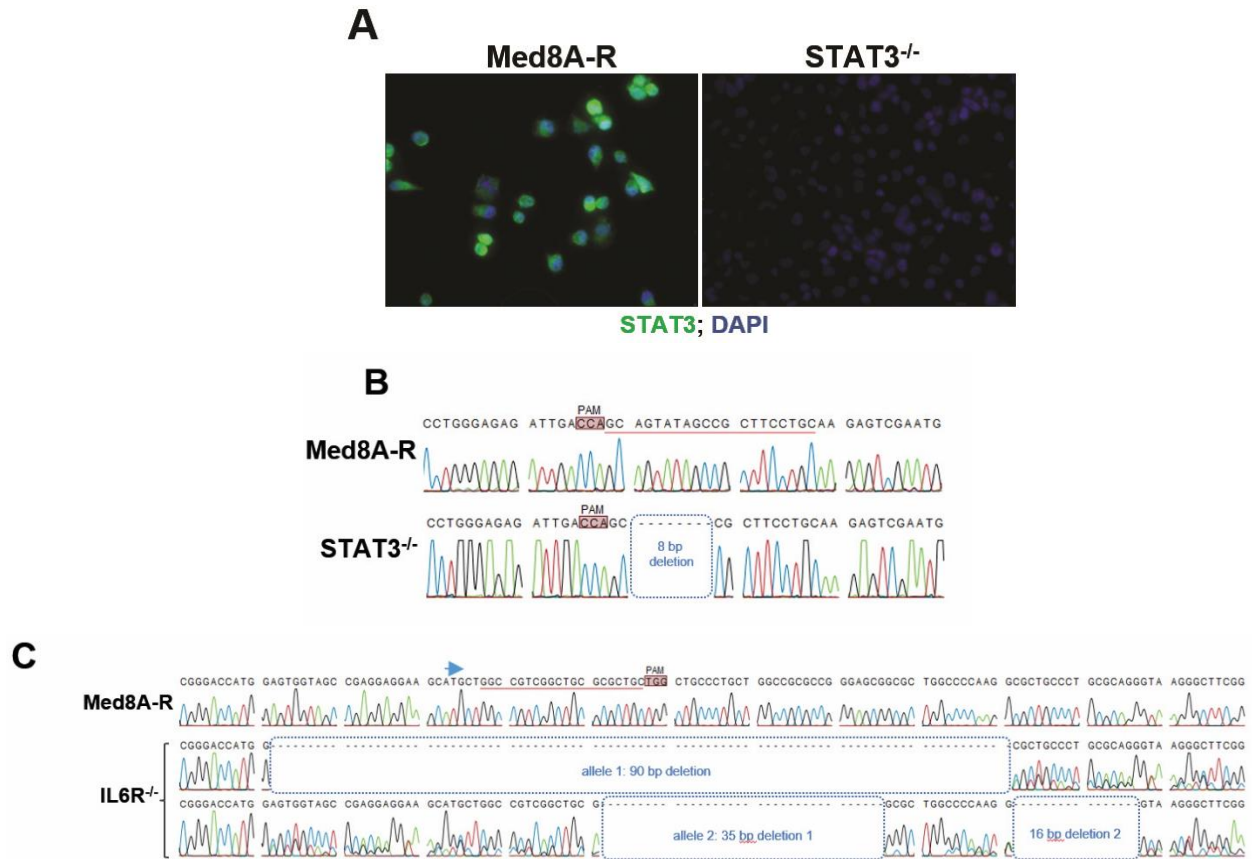


Figure 2.3: CRISPR-Cas9 generation of STAT3^{-/-} or IL-6R α ^{-/-} in Med8A-R cells.

(A) Immunofluorescence staining of Med8A-R (WT) and a clonal STAT3^{-/-} derivative for STAT3 (green) and nucleus (DAPI, blue). (B) Sequencing of the Med8A-R and STAT3^{-/-} cells revealed a homozygous 8bp missense deletion within the second coding exon of STAT3 at the gRNA targeted site (gRNA underlined, PAM motif highlighted). (C) The 1st coding exon of IL-6R α was similarly targeted using CRISPR-Cas9 in Med8A-R cells. As shown is the sequencing alignment for a single IL-6R α ^{-/-} clone showing the indicated deletions within each allele [120].

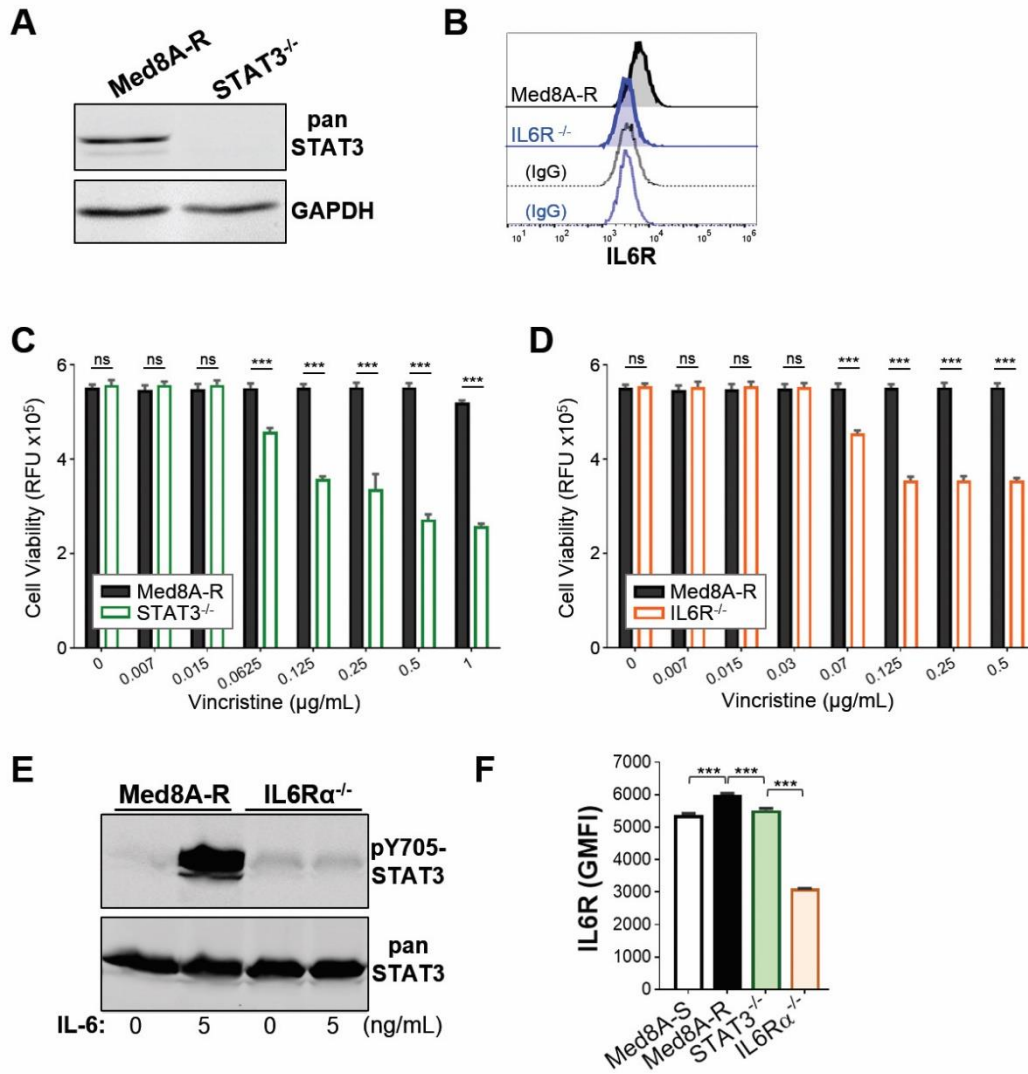


Figure 2.4: Loss of STAT3 or IL-6R restores chemosensitivity in Med8A-R cells.

(A) Western blot analysis of lysates of Med8A-R and STAT3^{-/-} cells for STAT3 and GAPDH expression. (B) Flow cytometry analysis of Med8A-R and IL-6Rα^{-/-} cells for cell surface expression of IL-6R, with corresponding IgG controls. Cell viability assay to assess the sensitivity of (C) STAT3^{-/-} and Med8A-R and (D) IL-6R^{-/-} and Med8A-R cells to vincristine. As plotted is the mean ± SD of an experiment performed in triplicates, representative of at least 3 independent experiments. ****p* < 0.001, two-way ANOVA with Bonferroni's multiple comparison test. (E) Lysates of Med8A-R and IL-6Rα^{-/-} untreated or treated with IL-6 were assessed for pY705-STAT3 and total STAT3 by western blot analysis. (F) Flow cytometry analysis of IL-6R expression of Med8A-S, Med8A-R, STAT3^{-/-}, and IL-6R^{-/-} cells. As plotted is the mean ± SD of the geometric mean fluorescence intensity (GMFI) for an experiment performed in triplicates; ****p* < 0.001, one-way ANOVA with Bonferroni's multiple comparison test [120].

2.3.3 Conditioning with exogenous IL-6 is sufficient to promote acquired drug resistance

Incremental vincristine selection resulted in the resistant Med8A-R variant that exhibit enhanced IL-6/STAT3 activity compared to Med8A-S, but without changes in STAT3 expression levels (Figure 2.5). I postulated that constant exposure to IL-6 stimuli may be a sufficient driver of drug resistance in MB. To evaluate this, Med8A-S cells were conditioned with 2 ng/mL IL-6 for 4 weeks to derive the subline known as Med8A-IL6+ (Figure 2.6A). Following the conditioning stint, Med8A-IL6+ cells were weaned off the exogenous IL-6 prior to further assays. At basal conditions, I found that Med8A-IL6+ cells exhibit increased pY705-STAT3 levels compared to the nonconditioned Med8A-S cells (Figure 2.6B). I performed qPCR to evaluate IL-6R mRNA expression in Med8A variants. Chemoresistant variants Med8A-R and Med8A-IL6+ exhibit significantly higher IL-6R mRNA expression compared to chemosensitive, Med8A-S. These results correlate with increased IL-6R protein expression observed in Med8A-R and Med8A-IL6+ cells (Figure 2.6B). Increased IL-6R expression in Med8A-R and Med8A-IL6+ cells may be due increased expression and activity of the transcription factor E2F3. A study by Libertini *et al.* showed that E2F3 directly binds and transactivate the IL-6R promotor region in prostate cancer cells [179]. QPCR analysis revealed that that both Med8A-R and Med8A-S-IL6+ cells have elevated E2F3 mRNA expression when compared to Med8A-S (Appendix A.4).

Med8A-IL6+ cells expressed correspondingly higher levels of IL-6R protein and mRNA when compared to both Med8A-S and Med8A-R (Figure 2.6C). Despite not having been selected with vincristine, I found that the relatively short term of conditioning with low levels of IL-6 was sufficient to render the Med8A-IL6+ cells highly resistant to vincristine (Figure 2.6D). IL-6 conditioning of Med8A-R cells appeared to elevate vincristine resistance, but the difference was not always evident given the already resistant nature of these cells (Figure 2.6E). IL-6 conditioning

mediated drug resistance is dependent on IL-6R as the receptor, since IL-6R $\alpha^{-/-}$ cells similarly conditioned with IL-6 exhibited no detectable enhancement of vincristine resistance (Figure 2.6E). STAT3 is also required, since IL-6 conditioning of STAT3 $^{-/-}$ cells failed to enhance resistance to vincristine (Figure 2.6F).

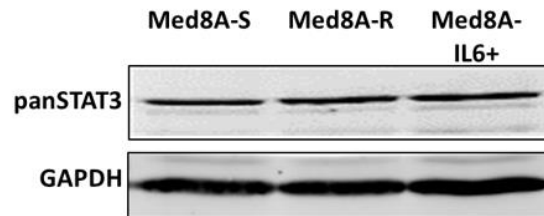


Figure 2.5: Comparison of STAT3 expression in chemosensitive parental and chemoresistant derivatives of Med8A cell lines.

Immunoblot of the indicated cell lysates were probed with antibodies against total STAT3 and GAPDH [120].

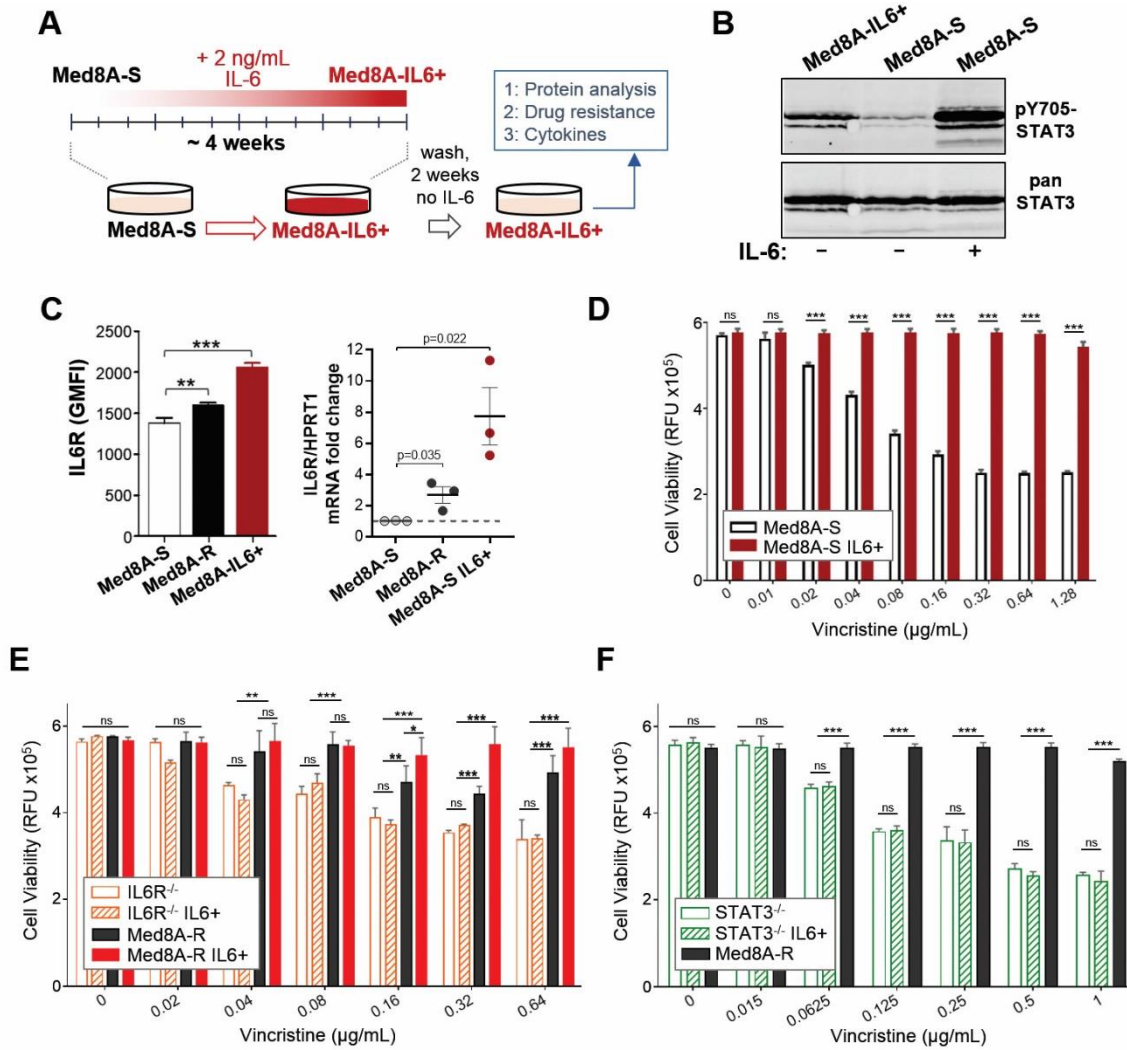


Figure 2.6: Exogenous IL-6 conditioning promotes drug resistance.

(A) Schematic for IL-6 conditioning of MB cells. The chemosensitive Med8A-S cells were cultured for 4 weeks in media supplemented with 2 ng/mL IL-6. Following the conditioning stint, the cells were cultured a further 2 weeks without exogenous IL-6 to yield Med8A-IL6+ variant used for subsequent assays. (B) Western blot analysis of Med8A-S and Med8A-S-IL-6+ cells for pY705 and total STAT3 levels under basal conditions, or transiently stimulated with 5 ng/mL IL-6 for 10 mins. (C) Analysis of Med8A-S, Med8A-R, and Med8A-S-IL-6+ cells using flow cytometry for IL-6R protein expression (Left panel), and QPCR for IL-6R mRNA expression (Right panel). Error bars represent mean \pm SD ($n = 3$); ** $p < 0.01$, *** $p < 0.001$, two tailed unpaired t-test. Cell viability assay to assess the sensitivity of (D) Med8A-S and Med8A-S-IL-6+ cells, (E) Med8A-R, Med8A-R-IL-6+, IL-6R^{-/-}, and IL-6R^{-/-}-IL-6+ cells, and, (F) Med8A-R, STAT3^{-/-} and STAT3^{-/-}-IL-6+ cells to vincristine. As plotted is the mean \pm SD of an experiment performed in triplicates, representative of at least 3 independent experiments. *** $p < 0.001$, two-way ANOVA with Tukey's multiple comparison test [120].

I had shown that Med8A cells selected only with vincristine also exhibited resistance to cisplatin, mitoxantrone, and idarubicin (Figure 2.1), agents that have different mechanisms of action [180] [181] [182]. To assess if IL-6 conditioning also rendered the cells multi-drug resistant, I tested and found that Med8A-IL6+ cells were also resistant to cisplatin, mitoxantrone and idarubicin treatment (Figure 2.7A, B, C).

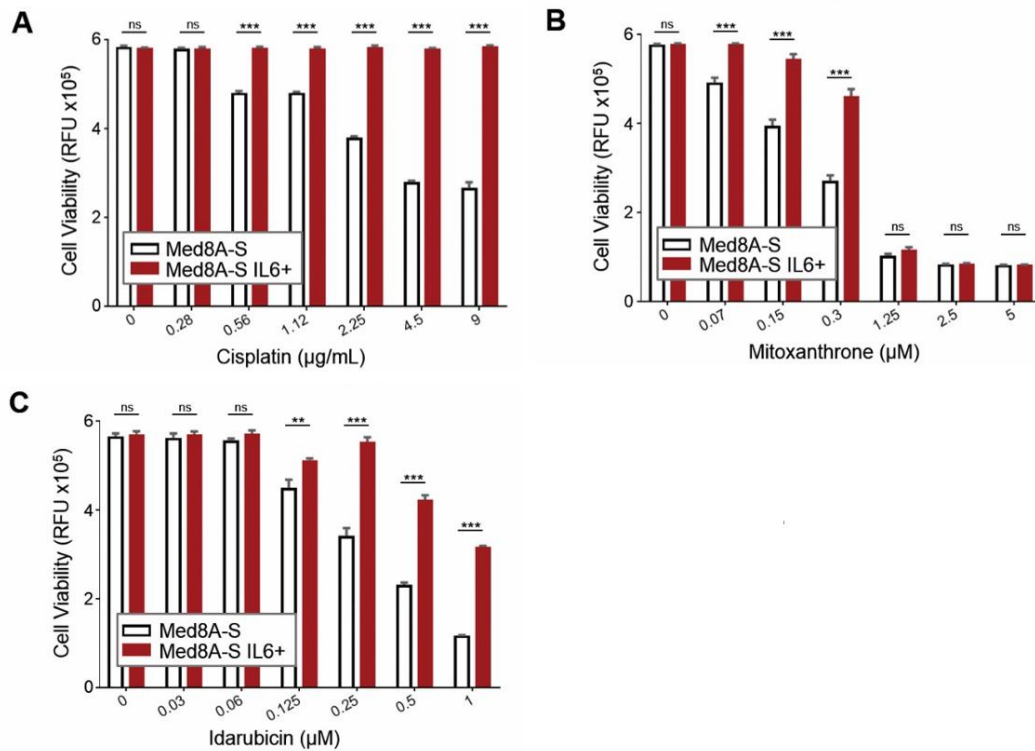


Figure 2.7: IL-6 conditioning promotes resistance to cisplatin, mitoxantrone and idarubicin.

Cell viability assay to assess the sensitivity of Med8A-S and Med8A-S-IL-6+ cells to (A) cisplatin, (B) mitoxantrone, and (C) idarubicin. As plotted is the mean +/- SD of an experiment performed in triplicates. *** $p < 0.001$, ** $p < 0.01$, two-way ANOVA with Bonferroni's multiple comparison test [120].

Differences in growth and proliferation for the cell lines used in the drug assays could affect perceived differences in drug sensitivity. I assessed and found that Med8A-S, Med8A-R,

and Med8A-IL6+ cells proliferated at the same rates (Figure 2.8A), thus the observed chemoresistance in Med8A-R and Med8A-IL6+ is not due to increased cell numbers alone. I do note that Med8A-R and Med8A-IL6+ exhibited an increased ability to grow clonally *in vitro*, suggestive of cooperative autocrine mediated effects (Figure 2.8B).

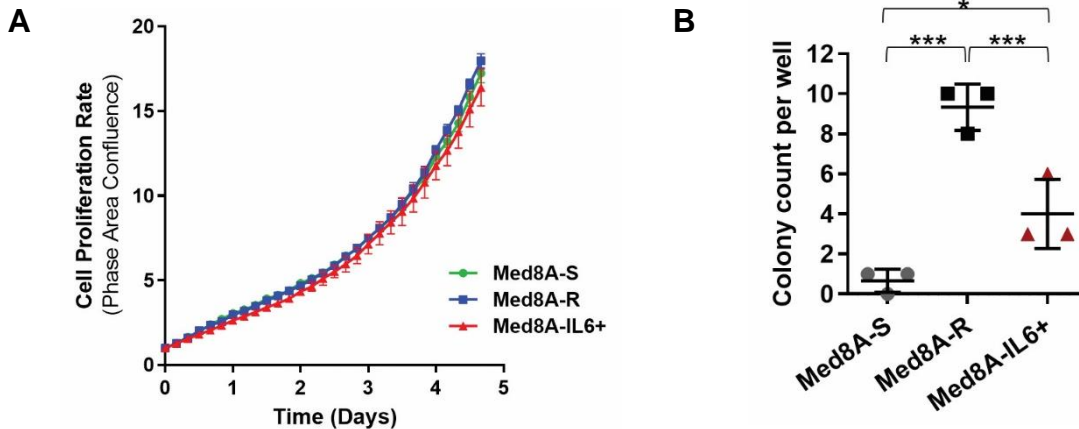


Figure 2.8 : Proliferation rate comparison of Med8A-S, Med8A-R and Med8A-IL6+ cells.

(A) Cells were plated at initial seeding of 5×10^3 cells per well in triplicates and proliferation monitored over 5 days using a live-imaging platform. As plotted are the phase area confluence (Mean \pm SD, $n=3$). The doubling time (in days) was derived from plotting an exponential growth curve; Med8A-S (1.111), Med8A-R (1.097) and Med8A-IL6+ (1.131). (B) Cells were plated at 200 cells per well and colony formation monitored over 7 days using a live-imaging platform. As plotted are the colony counts per well (minimum 25 cells per colony) at 7 days for triplicate experiments (Mean \pm SD, *** $p < 0.001$, ** $p < 0.01$, two-tailed unpaired t-test) [120].

2.3.4 MDR1 is positively associated with chemoresistant variants

Although selected with a single agent (i.e vincristine), Med8A-R cells demonstrated multi-drug resistance, as shown in Figure 2.1(C-F). Additionally, IL-6 conditioning of chemosensitive Med8A-S cells resulted in chemoresistant Med8A-IL6+ cells that also exhibit resistance in response to several drugs with different mechanisms of action (Figure 2.7). This led to us to explore the expression of multi-drug resistance 1 (MDR1) in the chemoresistant variants. MDR1 is a plasma membrane localized p-glycoprotein that function as an efflux pump to remove foreign

substrates from cells, thus reducing intracellular drug accumulation [183]. By western blot analysis (Figure 2.9), I found that MDR1 protein levels in the chemoresistant variants Med8A-R and Med8A-IL6+ cells were increased when compared to Med8A-S cells, suggesting that the observed multi-drug resistance is mediated by increased drug efflux due to MDR1.

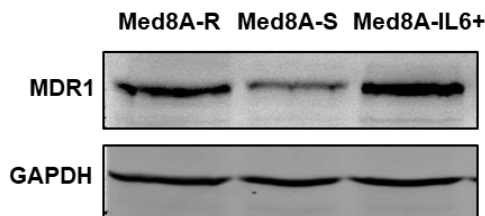


Figure 2.9: MDR1 expression in Med8A-S, Med8A-R and Med8A-IL6+.

Western blot analysis of Med8A-S, Med8A-R and Med8A-S-IL-6+ cells for MDR1 and GAPDH levels under basal conditions (n=1).

2.3.5 IL-6 conditioned cells exhibit increased migration and invasion

IL-6 has been known to play a significant role in promoting migration and invasion through the activation of STAT3 in multiple malignancies [184-186]. Initially, I compared the migratory and invasive potential of Med8A-S and Med8A-IL6+ cells using the scratch wound healing assay and the Transwell assay. When assessed as a scratch wound assay, Med8A-IL6+ cells exhibited increased migration when compared to Med8A-S cells (Figure 2.10A). To assess migration and invasion, cells were plated onto Transwell inserts, with and without Matrigel coating, and cells stimulated to migrate towards fetal bovine serum (FBS) as a chemoattractant. On uncoated inserts, Med8A-IL6+ cells exhibited increased migration when compared to Med8A-S cells (Figure 2.10B). Introduction of a Matrigel coating simulates the process of invasion *in vitro*, whereby cells need to degrade and then migrate through the matrix barrier. Indeed, increasing Matrigel concentrations hindered migration to an extent, but overall, Med8A-IL6+ cells displayed increased

invasion compared to Med8A-S cells (Figure 2.10B). In addition, I also assessed the invasion index of Med8A-R, IL-6R^{-/-}, and STAT3^{-/-} cells. While Med8A-R and IL-6R^{-/-} cells showed no remarkable difference in their invasion indexes, STAT3^{-/-} cells exhibited significantly decreased invasion compared to Med8A-R (Figure 2.10C). These results provide evidence that IL-6/STAT3 signaling pathway may contribute to tumorigenic properties of Med8A cells by enhancing tumour cell migration and invasion.

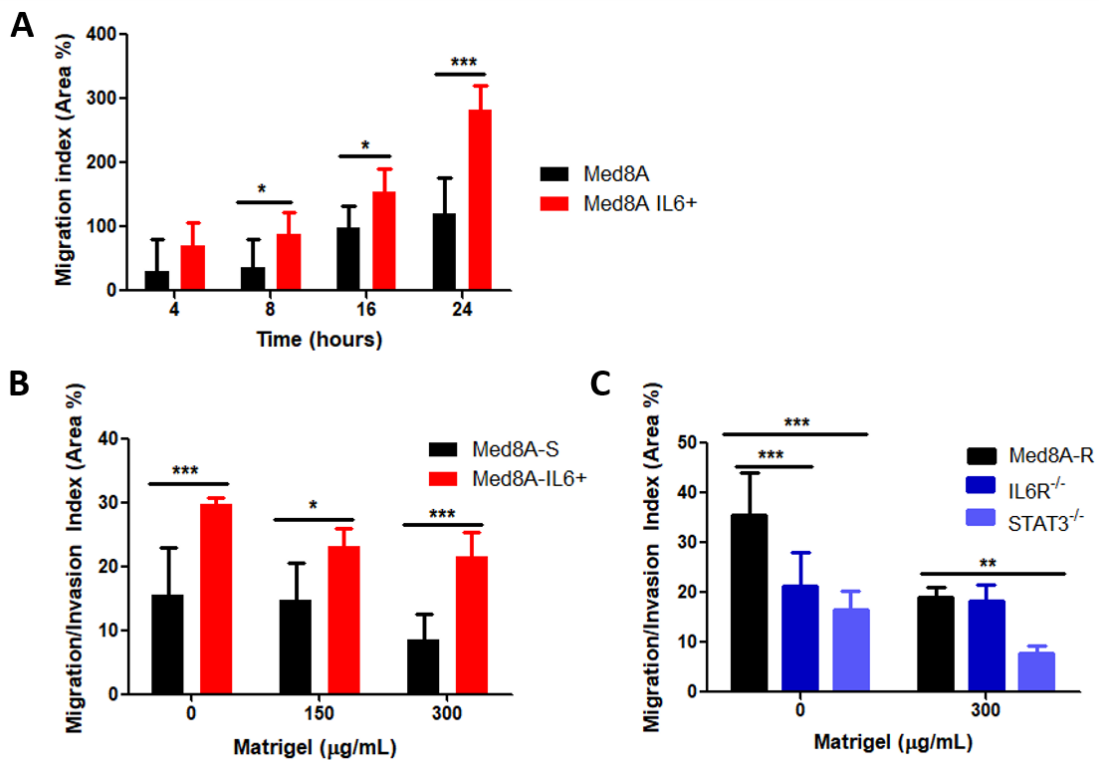


Figure 2.10: Cell migration assays.

(A) Med8A-S and Med8A-IL6⁺ cells were plated on fibronectin coated dishes and incubated overnight, scratched with a pipet tip to form a wound, and images taken at 4 hr intervals to monitor cell migration. The images were analyzed using Image J, and the results plotted as the migration index. As plotted is the mean \pm SD of three replicates; *** $p < 0.001$, ** < 0.01 , * < 0.05 , two-way ANOVA with Dunnett's multiple comparison test. (B) Med8A-S and Med8A-IL6⁺ cells or (C) Med8A-R, IL-6R^{-/-} and STAT3^{-/-} cells were plated on 8um pore Transwell inserts coated with different concentrations of Matrigel, and invasive migration stimulated using 10% FBS in the bottom well as a chemoattractant. At 72 hours, the Transwell inserts were removed and stained with crystal violet to visualize the invaded cells. The invasion index was quantified and measured

as area (pixel²) using Image J. As plotted is the mean \pm SD of three replicates; *** $p < 0.001$, ** < 0.01 , * < 0.05 , two-way ANOVA with Dunnett's multiple comparison test.

2.3.6 Chemoresistant MB is susceptible to combination treatment of vincristine with cisplatin or niclosamide

Since Med8A-R and Med8A-IL6+ exhibited resistance to several drugs when given as monotherapies (Figure 2.1, Figure 2.7), I assessed if combined therapy may be able to overcome the observed resistance. As shown in Figure 2.11A, combined treatment of vincristine and cisplatin effectively overcame the resistance observed for Med8A-R and Med8A-IL6+ to vincristine or cisplatin alone. In addition, I evaluated the effect of the selective STAT3 inhibitor, niclosamide, alone and in combination with vincristine. I assayed niclosamide at 0.3 and 0.6 $\mu\text{g/mL}$, since it was shown that concentrations below 1 $\mu\text{g/mL}$ is subtoxic to healthy human neural stem cells [187]. As shown in Figure 2.11B, Med8A-S, Med8A-R, and Med8A-IL6+ cells were not susceptible to low doses of niclosamide as a monotherapy. However, when used in combination, niclosamide effectively overcame the resistance observed for Med8A-R and Med8A-IL6+ cells to vincristine (Figure 2.11B). My findings suggest that sub-toxic levels of a STAT3 inhibitor as well as another chemotherapeutic used in combination with lower concentrations of vincristine greatly enhances the susceptibility of chemoresistant MB.

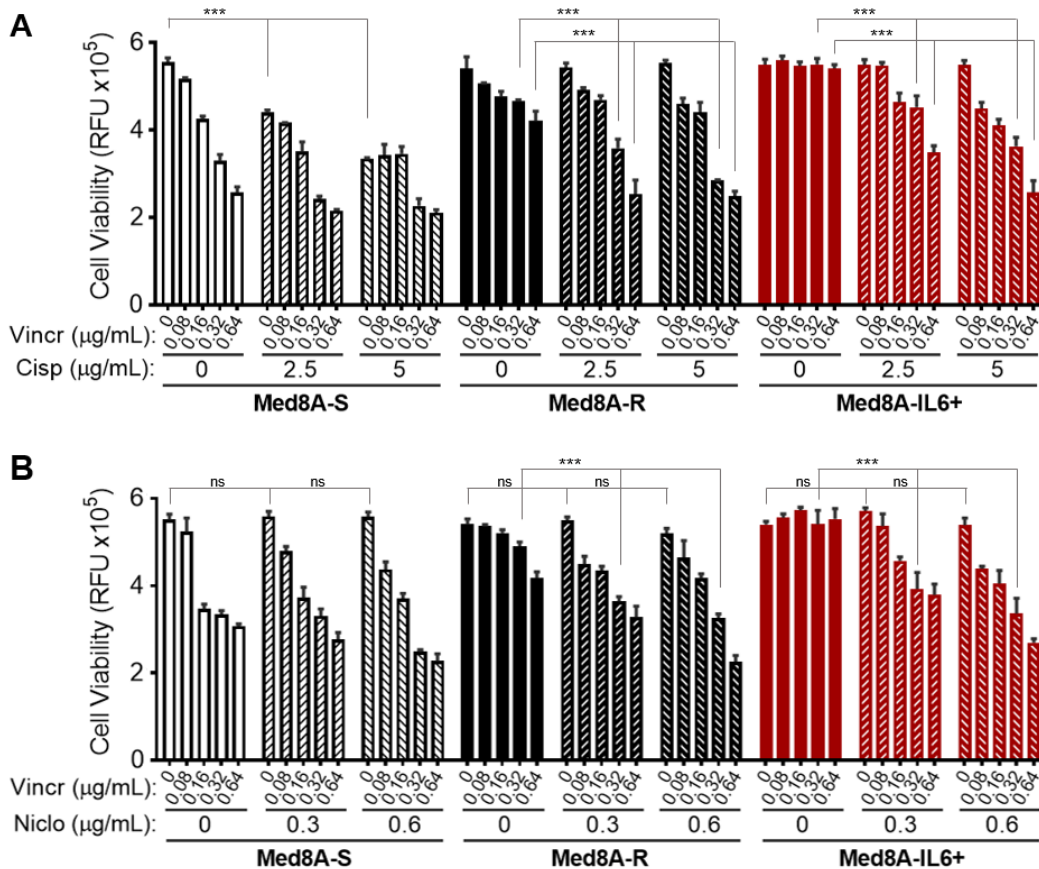


Figure 2.11: Chemoresistant MB is susceptible to combination treatment of vincristine with cisplatin or niclosamide.

Med8A-S, Med8A-R, and Med8A-S-IL-6+ cells were treated with vincristine alone or in combination with (A) cisplatin and (B) niclosamide at the indicated concentrations for 48 h and cell viability assessed with CTB. As plotted is the mean \pm SD of three replicates; *** $p < 0.001$, two-way ANOVA with Tukey's multiple comparison test (Significance not highlighted in the figure is presented as supplemental material in the publication [108]).

2.3.7 Autocrine IL-6 signaling promotes drug resistance in MB

To evaluate the possibility that IL-6 autocrine signaling in Med8A cells can promote drug resistance, I adopted a no-contact coculture system where a drug resistant derivative is used as cytokine “donor” cells to condition the target cell population. Nonconditioned Med8A-S or Med8A-R cells were plated in the bottom treatment chamber, while conditioned Med8A-S-IL-6+ or Med8A-R-IL-6+ cells were placed within hanging tissue

culture inserts, which effectively separated the cells while enabling exchange of media and soluble factors within the system (

Figure 2.12A). In this manner, I found that Med8A-S and Med8A-R cells cocultured for 3 days with their corresponding IL-6 conditioned cells exhibited robust activation of pY705-STAT3 compared with the absence of coculture (Figure 2.12B). As a control, IL-6R α ^{-/-} cells remain nonresponsive to coculture conditioning by Med8A-IL6⁺ cells, suggesting that IL-6/IL-6R is a potent cytokine stimulatory pathway promoting STAT3 activity (Figure 2.12 B).

Next, I assayed for cytokines as soluble autocrine factors released by the drug resistant cells. I profiled the culture supernatant of Med8A-S, Med8A-R, and Med8A-S-IL-6⁺ cells using an antibody-based quantitative cytokine array platform. Of the 20 cytokines examined using the array, four achieved quantifiable levels that was deemed statistically significant (Figure 2.12C). Not surprisingly, IL-6 levels were greatly elevated (over 10,000-fold) in the supernatant of Med8A-IL6⁺ cells when compared to Med8A-S or Med8A-R, indicating that exogenous IL-6 conditioning resulted in cells that secreted more IL-6. Compared to Med8A-S, Med8A-R cells secreted significantly higher amounts (over 20-fold) of MCP-1 (monocyte chemoattractant protein-1), but not of IL-6. Both Med8A-R and Med8A-S-IL-6⁺ cells secreted significantly higher levels of VEGF (vascular endothelial growth factor) when compared to Med8A-S, but at no greater than twofold maximum difference. The levels of RANTES were not significantly different between the 3 cell types assayed.

The cytokine array analysis provided strong evidence that IL-6 is the most prominent cytokine released by IL-6 conditioned Med8A cells that can function in an autocrine manner. Thus, I focused analysis on secreted IL-6 found in the conditioned media. Under non-stimulated

conditions, Med8A-S, Med8A-R, STAT3^{-/-}, and IL-6R^{-/-} cells secrete very low levels of IL-6, while DAOY secrete high levels of IL-6 (Figure 2.12D). The IL-6 conditioned Med8A-S-IL-6+ and Med8A-R-IL-6+ cells appear to sustain increased IL-6 secretion even after removal of the IL-6 stimuli. Increased IL-6 secretion was also detected for Med8A-S cells that had been cocultured with either Med8A-S-IL-6+ or DAOY cells, but not when cocultured with Med8A-R cells (Figure 2.12D). Finally, neither STAT3^{-/-} nor IL-6R^{-/-} cells respond to coculture mediated stimulation of IL-6 secretion, lending further support that an intact IL-6R/STAT3 signaling pathway is required to sustain autocrine IL-6 activity. Taken together, my data provide strong evidence that IL-6 signals in an autocrine manner to promote increased pY705-STAT3 activity, IL-6 secretion and acquired drug resistance in Med8A cells.

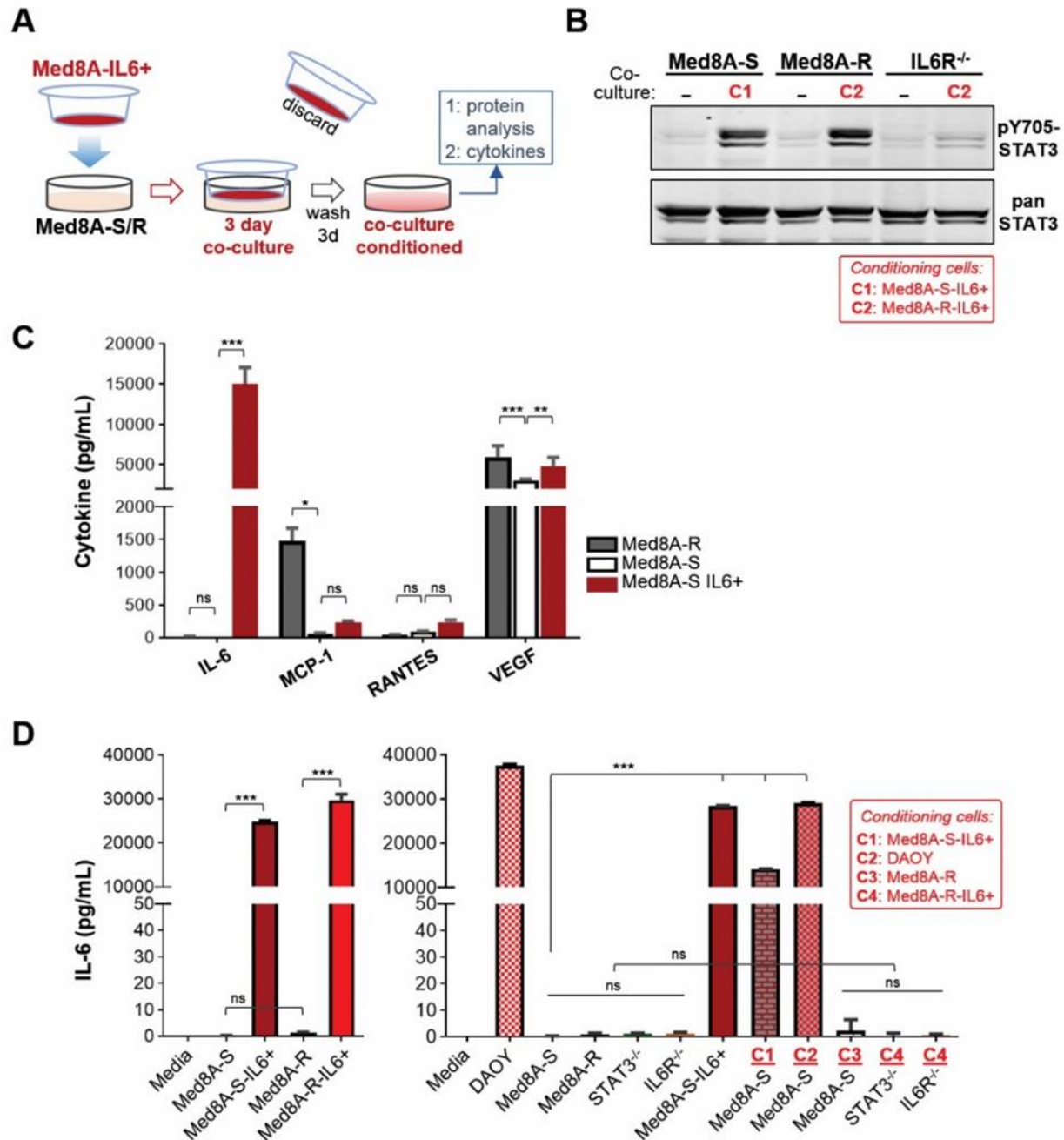


Figure 2.12: Autocrine IL-6 secretion promotes IL-6/STAT3 activity.

A) Schematic of coculture system for cell-based conditioning of MB cells. Cells (e.g., Med8A-S) targeted for conditioning are plated in the bottom well, while pre-conditioned Med8A-IL6+ cells are plated in the top Transwell insert with non-passable 1 μ m pores that allow media exchange between the two cell populations. After 3 days in coculture, the insert is discarded, cells in the treatment well washed, and fresh media added (with no IL-6). After 3 days, cells are harvested for protein analysis while the conditioned media used for cytokine assays. B) Western blot analysis

for pY705 and total STAT3 levels of Med8A-S, Med8A-R and IL-6R^{-/-} cells without (-) or with coculture treatment with Med8A-S-IL-6+ (C1) or Med8A-R-IL-6+ (C2) cells. C) Secreted cytokine analysis of conditioned media from Med8A-S, Med8A-R, and Med8A-S-IL-6+ cells. As shown are four cytokines, IL-6, MCP-1, RANTES, and VEGF, from the panel of 20 cytokines that achieved significant quantifiable levels. D) Secreted IL-6 analysis of conditioned media using an ELISA-based kit for the various cells, as indicated. Coculture cells plated in the Transwell inserts are as follows: Med8A-S-IL-6+ (C1); DAOY (C2); Med8A-R (C3); Med8A-R-IL-6+ (C4). As plotted is the mean ± SD of three replicates; *** $p < 0.001$, ** < 0.01 , * < 0.05 , two-way ANOVA with Dunnett's multiple comparison test [120].

2.3.8 Pro-survival and pro-apoptotic signaling pathways in MB cells

As mentioned earlier, Med8A-R and DAOY cells are chemoresistant, while Med8A-S cells are chemosensitive. I undertook a western blot screen for select pathways involved in pro-survival and pro-apoptotic signaling to identify additional pathways in addition to IL-6/STAT3 signaling. Lysates were collected from control and IL-6-stimulated cells, and probed with the indicated antibodies as shown in Figure 2.13.

In sum, the results were unremarkable to reveal change between Med8A-S and Med8A-R cells that would add to our understanding of the involved pathways in chemoresistance. I noted some differences that exist between DAOY and Med8A-S/R cells, summarized as follows. Compared to the Med8A cells, levels of pS473-Akt and pT308-Akt were higher in DAOY, while pERK was lower (Figure 2.13A). In addition, IL-6 stimulation appeared to dampen phosphorylated Akt in Med8A-S and Med8A-R cells. Levels of the Bcl2 family proteins, BCL-x1, MCL1 and Bad, were higher in Med8A-S/R when compared to DAOY (Figure 2.13B). Levels of SOCS3 are somewhat higher in Med8A-S/R when compared to DAOY (Figure 2.13C).

These results reveal little new information to account for the difference in survival of the drug resistant Med8A-R when compared to Med8A-S. The differences seen between DAOY and Med8A variants is most likely attributable to cell line differences. If anything, the results shown

here lend support to the notion that the IL-6/STAT3 pathway is an important if not critical player in regulating acquired drug resistance in MB.

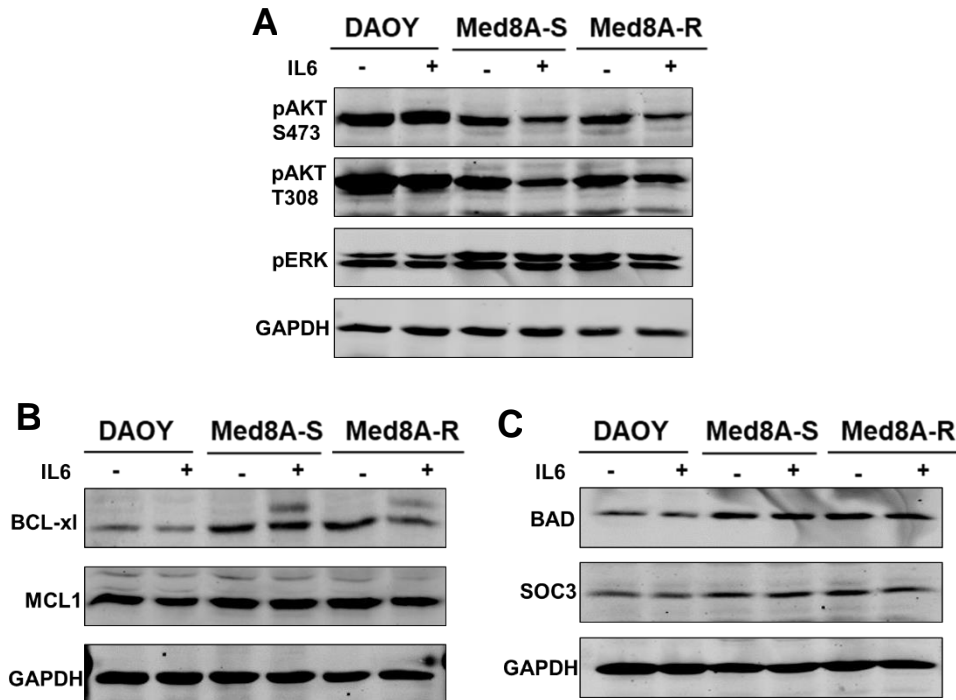


Figure 2.13: Survey of pro-survival and pro-apoptotic signaling in DAOY, Med8A-S and Med8A-R cells.

Western blot analysis for A) pAKT (S473), pAKT (Thr308), pERk, B) BCL-xL, MCL2, C) BAD, SOCS3 and total GAPDH levels of DAOY, Med8A-S and Med8A-R cells without (-) or with (+) IL-6 stimulus. Results shown is representative of at least 2 independent replicate experiments performed.

2.3.9 IL-6 conditioning leads to increased STAT3 activity, IL-6R expression, and acquired drug resistance in other Group 3 MB cell lines

My work with the Group 3 MB Med8A cell line has demonstrated a vital role of the IL-6/STAT3 pathway in the development of acquired drug resistance. To assess if this may be a generally applicable phenomenon, I profiled the expression of STAT3 and assessed the effects of IL-6 conditioning on D283 and D341, cell lines that also belong to Group 3 MB. IL-6 conditioned D283 and D341 cells showed no detectable difference in total STAT3 expression when compared

to the parental nonconditioned cells (Figure 2.14). Similar to Med8A cells, D283 and D341 cells exhibit low pY705-STAT3 levels at basal state, and that is rapidly inducible with bolus IL-6 treatment (Figure 2.15A). Similar to Med8A-S cells, IL-6 conditioning of D283 and D341 cells resulted in significant increases in IL-6R expression when compared to the nonconditioned cells (Figure 2.15B). IL-6 conditioning of D283 and D341 cells also resulted in cells exhibiting enhanced resistance to vincristine treatment (Figure 2.15C, D). Lastly, I assessed the ability of the drug resistant derivatives to condition the chemosensitive ones using the coculture model. When cocultured with their respective IL-6 conditioned cells, D283 and D341 exhibited increased pY705-STAT3 levels (Figure 2.15E) and increased secretion of IL-6 (Figure 2.15F). Hence, the results provide a consensus that Group 3 MB cell lines are highly responsive to IL-6 stimulation and promotion of STAT3 signaling that plays a prominent role in the development of acquired drug resistance in Group 3 cell lines.

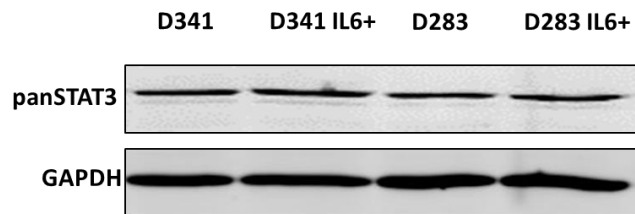
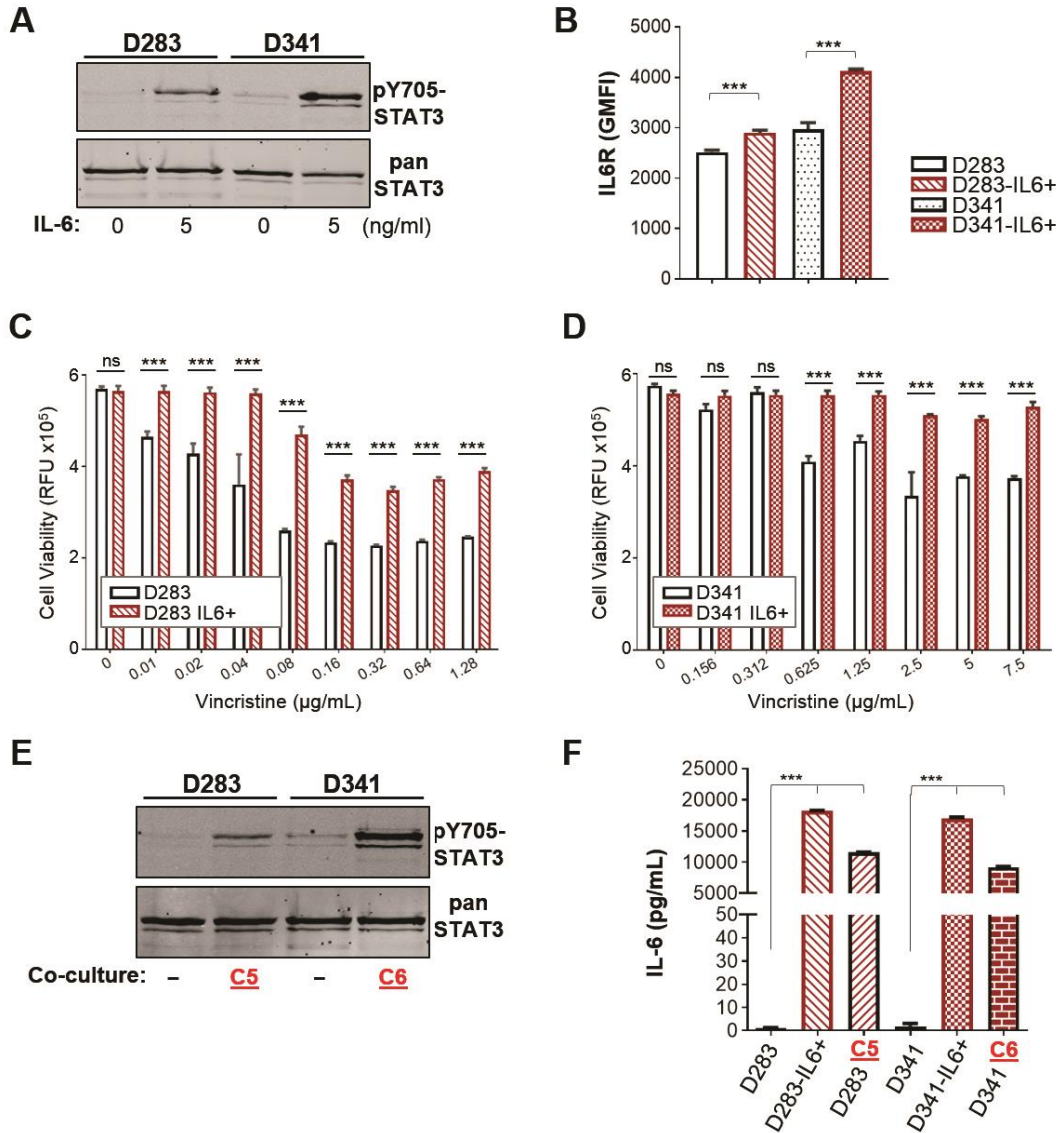


Figure 2.14: Comparison of STAT3 expression in chemosensitive parental and chemoresistant derivatives of D341 and D283 cell lines.

Immunoblot of the indicated cell lysates were probed with antibodies against total STAT3 and GAPDH [120].

Figure 2.15: Group 3 MB cell lines D283 and D341 exhibit similar responses to IL-6/STAT3 signaling.

A) D283 and D341 MB cells were treated with IL-6 at 5 ng/mL for 10 min and cell lysates



immunoblotted for pY705 and total STAT3. Left panel: Representative blot of 3 independent replicates. Right panel: Quantitation of pY705-STAT3 over total STAT3 (mean \pm SD, $n = 3$, $***p < 0.001$, one-way ANOVA with Bonferroni's post-test). B) Flow cytometry analysis for expression of IL-6R for D283 and D341 cells without and with IL-6 conditioning. As plotted is the GMFI mean \pm SD of an experiment performed in triplicates, and representative of 3 independent experiments ($***p < 0.001$, one-way ANOVA with Bonferroni's post-test). Cell viability assay to assess the sensitivity of (C) D283 and D283-IL-6+ and, (D) D341 and D341-IL-6+ cells to vincristine. As plotted is the mean \pm SD of an experiment performed in triplicates, representative of 2 independent experiments ($***p < 0.001$), one-way ANOVA with Bonferroni's multiple comparison test. E) Western blot analysis for pY705 and total STAT3 levels of D283 and

D341 cells without (-) or with coculture treatment with D283-IL-6+ (C1) or D341-IL-6+ (C2) cells, respectively. F) Secreted IL-6 analysis of conditioned media from D283 or D341 cells, their IL-6 conditioned derivatives, and upon coculture with D283-IL-6+ (C1) or D341-IL-6+ (C2) cells. Plotted is mean \pm SD of triplicate experiments; *** $p < 0.001$, two-way ANOVA with Dunnett's multiple comparison test [120].

2.4 Discussion

Our study highlights a prominent role for IL-6 -mediated activation of oncogenic STAT3 signaling that gives rise to acquired drug resistance in MB cell lines belonging to Group 3. In this context, IL-6 is a potential stimulatory cytokine found within the MB tumour microenvironment. We developed two model systems with a goal to identify a central pathway contributing to drug resistance. By subjecting the chemosensitive MB cell line, Med8A-S, to incremental selection with vincristine, we derived the variant Med8A-R that exhibited resistance to not only vincristine, but also to agents with different mechanisms of action. Characterization of this stably resistant derivative identified enhanced sensitivity to IL-6 mediated activation of STAT3, attributed in part to enhanced expression of IL-6R. Loss of STAT3 or IL-6R expression nullified the drug resistance of Med8A-R cells, indicating that IL-6/STAT3 signaling is a major driver of acquired drug resistance.

Notably, the chemoresistant DAOY cells exhibit constitutive pY705-STAT3 levels, while basal pY705-STAT3 in Med8A-R remains low, requiring IL-6 stimuli to provoke an enhanced response. This observation suggested that constant stimulation of the pathway may suffice to generate drug resistance. I confirmed this by using chronic low-level IL-6 stimuli to condition chemosensitive cells for 4 weeks, and found this method was highly effective in generating vincristine-resistant cells, despite not having been selected with the drug. Chemoresistance mediated by IL-6 conditioning similarly required IL-6R or STAT3, again highlighting the indispensable nature of both proteins that likely function in a linear fashion, with IL-6 as the

extracellular upstream cytokine, IL-6R as the receptor that activate JAKs, and subsequent phosphorylation and activation of STAT3.

Although the significance of STAT3 signaling in survival, proliferation, drug resistance, migration and invasion is well known, gaps remain in our understanding of the upstream regulators and activation of JAK-STAT3 signaling in MB [118,188]. In particular, pY705-STAT3 has been linked to drug resistance in multiple malignancies, whereas pS727-STAT3 is required for maximal transcriptional activation [158]. My study with Group 3 MB cell lines indicated that cells rendered drug resistant, either by drug selection or with sustained cytokine conditioning, exhibit low basal levels of pY705-STAT3 that remains inducible at enhanced levels by IL-6. Importantly, this mechanism invoked sustained activation of STAT3 dependent on elevated cytokine production, and not necessarily via mutational events of upstream regulators that result in constitutively activated STAT3. My knockout studies highlight the requirement of not only STAT3 in drug resistance mediated by IL-6 conditioning, but that includes IL-6R as a signaling intermediary. My data also shed light on STAT3 and IL-6 in promoting migration and invasion in MB cells. The mechanism of invasion and migration needs to be further investigated by evaluating the role of certain downstream effectors of the IL-6/STAT3 pathway. For example, STAT3 is a critical upstream regulator of several proteins including matrix metalloproteinases (MMP2 and MMP9), which have been known to play a vital role in cancer invasion and migration [189,190].

STAT3 activity promotes upregulation of oncogenic downstream targets that include *cyclin D1*, *c-myc*, *bcl-2*, *survivin*, *bcl-XL*, and *VEGF* [160]. MYC amplification in a subset of Group 3 MB contributes to poor disease outcome, and IL-6 is known to stimulate translation of c-Myc [42,85]. The MB cell lines used in this study exhibit high basal levels of c-Myc, and IL-6 stimulated significant increases of c-Myc in Med8A-S, Med8A-R and D341 (Appendix A.3).

Interestingly, MYC amplified MB may be targeted with BET and HDAC inhibitors, presenting a therapeutic option for chemoresistant MB driven by IL-6/STAT3 signaling [85,191].

Studies have shown that novel STAT3 inhibitors are able to disrupt pY705-STAT3 activity and suppress cell proliferation and growth in MB [87,165,192,193]. However, single pathway inhibition of STAT3 has led to feedback activation of other prominent survival pathways including EGFR and MEK/ERK, with ensuing reduced effectiveness of further STAT3 inhibition [194,195]. Similarly, IL-6 blockade therapy led to upregulation of EGFR signaling [196]. One strategy to mitigate development of resistance to any one agent is to use combination therapy. I showed that chemoresistant variants Med8A-R and Med8A-IL6+ cells were susceptible to combined vincristine and STAT3 inhibition with sub-toxic doses of niclosamide. Similarly, combined use of vincristine and cisplatin was effective at overcoming resistance observed for either agent when used as a monotherapy. Additional therapeutic options could include targeting of upstream or downstream components of the pathway, for example, inhibition of IL-6R or JAK kinases in the IL-6/STAT3 pathway, as well as co-inhibition of other prominent pro-survival pathways such as EGFR/ERK [194,195].

Tumour cells have been known to exploit IL-6 to evade apoptosis by acquiring drug resistance through activation of pro-survival oncogenic pathways [119]. In my study, prolonged exposure to IL-6 promotes resistance to treatment in several Group 3 MB cell lines. IL-6 conditioned cells exhibit increased pY705-STAT3 activity, IL-6R expression, elevated levels of IL-6 secreted and acquired resistance to vincristine. The cytokine array assay also revealed increased levels of RANTES (CCL5), monocyte chemoattractant protein 1 (MCP1), and VEGF secreted by Med8A-IL6+ in response to IL-6 conditioning. RANTES is a chemokine that facilitates leukocyte infiltration and inflammation [197]. MCP1 promotes recruitment of immune

cells in the tumour microenvironment [198]. VEGF is an angiogenic factor that facilitates the formation of blood vessels and supplies nutrients to the tumour cells. In sum, these cytokines are potential downstream targets of STAT3 known to promote tumorigenesis and metastasis in multiple malignancies [149,199-201].

Our study also supports the notion that IL-6 can function in an autocrine fashion. IL-6 conditioned MB cells secrete high levels of IL-6, while increased expression of IL-6R is indicative of an auto-feedback loop akin to oncogene-addiction, albeit one employing a cytokine-receptor pair. Similar mechanistic signaling has been reported to facilitate malignant transformation and activation of STAT3 in other tumours. Lung adenocarcinomas with activating mutations in EGFR was found to produce high IL-6 levels responsible for constitutive pY705-STAT3 activity [202]. In basal-like breast carcinomas, autocrine IL-6 sustains Notch-mediated promotion of proliferative self-renewal and increased invasiveness [203].

Several clinically approved monoclonal antibodies and inhibitors have been developed to target IL-6R and IL-6 [204]. Due to the clinical correlation of increased levels of IL-6 in serum and poor prognosis of tumours, blocking the IL-6/STAT3 signaling axis could be beneficial in improving treatment refractory cancers [205-207]. Other Group 3 MB cell lines evaluated in my study exhibited a similar phenotype when exposed to IL-6 conditioning, including increased pY705-STAT3 activity, IL-6R expression, IL-6 secretion and vincristine resistance.

In summary, my study demonstrated the functional consequence of targeting autocrine IL-6/STAT3 signaling in development of chemoresistance in Group 3 MB cell lines. I found that knocking out IL-6R or STAT3 was sufficient to circumvent drug resistance, highlighting their potential for targeting in treatment of refractory MB. My findings underscore how exogenous IL-6 was able to initiate an autocrine signaling machinery to evade drug-induced toxicity and promote

sustained cell growth. MB cells exposed to and surviving chemotherapy, as well as cells conditioned to stimulatory cytokines present in the tumour microenvironment might pave the way to resistant clonal selection and constitutive activation of pro-survival pathways. My study does not yet address the potential role of pro-inflammatory cells in the tumour microenvironment that may act via paracrine signaling to initiate and promote sustained cell growth and transformation in MB. Future studies could include investigation of brain tumour microenvironmental cells that include tumour associated macrophages and microglia, T-lymphocytes, neutrophils, and astrocytes, as possible sources of IL-6 and other inflammatory cytokines.

Chapter 3: Targeting gp130/STAT3 signaling axis attenuates tumour microenvironment mediated chemoresistance in Group 3 MB.

3.1 Chapter overview

The tumour microenvironment (TME) is a fundamental regulator of cancer progression that also governs therapeutic efficacy in primary and metastatic brain malignancies [103]. Mechanistic insights into the tumour-promoting role of the individual components of the brain TME will aid in identifying key survival pathways and design of potential therapeutics to combat drug resistance and pathogenesis of the disease.

In Chapter 2, I presented evidence that Group 3 MB cells subjected to chronic low-level IL-6 stimuli resulted in chemoresistant cells exhibiting enhanced STAT3 activity, and that secreted IL-6 can also act in autocrine positive feedback loop to constitutively activate STAT3. In contrast, the chemosensitive parental cells secreted little IL-6, raising the question of the cellular source for the initiating cytokine stimuli. In this chapter, I investigate the role of microglia (brain resident macrophages) as a source of cytokines that can promote STAT3 activation and chemotherapeutic resistance in Group 3 MB. In addition to evaluating this paracrine-based mechanism, I also evaluate the potential for targeting the IL-6/STAT3 signaling axis using inhibitors against gp130 and JAKs as an improved therapeutic strategy to circumvent drug resistance in medulloblastoma.

3.2 Materials and methods

3.2.1 Cells and tissue culture

Tissue culture methods for Med8A, Med8A-IL6+, IL-6R^{-/-} cells, and, D283 and D341 cell lines are as detailed in section 2.2.1 of this thesis. Human microglia cell line, HMC3 (ATCC CRL-3304™) were cultured in 10% FBS EMEM (Sigma), 1% Pen-Strep and NEAA. HMC3 was

purchased from ATCC and used for experiments within passages 3-12. HMC3 cells were passaged once every 4 days at 90% confluency, using trypsin to lift the cells, and cells reseeded at 10% confluency.

3.2.2 Co-culture system and cytokine conditioning

Cytokine conditioning of cells (denoted as IL-6+, LIF+, OSM+ and IL-11+) was achieved by culturing each cell line for 2 weeks in media supplemented with 2 ng/mL recombinant human IL-6, LIF, OSM and IL-11 (Genscript), respectively. Following this conditioning, cells were cultured a further 2 weeks without cytokine supplementation before being used for experiments.

For conditioning using the coculture system, I refer to target cells as ones being conditioned, while microglia represent the source of stimulatory cytokines. Target cells were plated at a density of 10^5 cells/well in a 6-well plate. Microglia were plated at a density of 10^4 cells within a Transwell insert (Greiner ThinCert) that was then placed into the well to co-incubate with the target cells in fresh culture media (with no added cytokine). Following the coculture for 3 days, the Transwell insert was removed, the target cells rinsed with blank media, and replenished with fresh media for another 3 days. Cells were either harvested for protein analysis, or the media supernatant analysed for secreted cytokines.

3.2.3 Cell viability assays

Cells were seeded in 96-well plates at a density of 10^5 cells/well, allowed to adhere for 16 h before addition of drugs at various concentrations. After 48 h, the fluorometric reagent Cell Titer Blue (Promega) was added according to manufacturer's protocol and fluorescence ($560_{Ex}/590_{Em}$) measured on a spectrophotometer (Enspire) after 4 h. In addition to vincristine (Sigma), cells were

also treated with ruxolitinib, bazedoxifene and SC144 (Selleckchem). All assays were conducted as 3 replicates per treatment condition and graphs were plotted using GraphPad Prism.

3.2.4 Western blots

Cell lysates were prepared in PN lysis buffer (10 mM PIPES, 50 mM NaCl, 150 mM sucrose, 50 mM NaF, 40 mM $\text{Na}_4\text{P}_2\text{O}_7 \cdot 10\text{H}_2\text{O}$, 1 mM Na_3VO_4 , 1% Triton X-100, Complete protease inhibitors (Sigma)). Total protein (30 μg) was separated by SDS-PAGE, and transferred to nitrocellulose using the Trans-Blot Turbo Transfer System (Bio-Rad). Blots were blocked in blocking buffer 5% bovine serum albumin (BSA, Fisher) in TBS-T (TBS-T is 50 mM TrisHCl, 150 mM NaCl, pH 8 with 0.1% Tween20) for 1 h at 22 °C, then incubated overnight at 4 °C with primary antibodies diluted in blocking buffer. Blots were further incubated with secondary goat anti-mouse or -rabbit fluorophore-conjugated antibodies (Dylight 800 or Dylight 680, ThermoFisher) in 2% non-fat milk in TBS-T, and scanned on the Licor Odyssey.

The following primary antibodies were used (complete details in Appendix B.1): pY705-STAT3, STAT3 (Cell Signaling Technologies); and GAPDH (Biolegend). In some experiments, cells were treated with IL-6, LIF, OSM, IL-11 (Genscript) at the indicated concentrations and time prior to preparation of cell lysates.

3.2.5 Plasmids and CRISPR

Guide RNA (gRNA) mediated CRISPR-Cas9 gene editing was used to generate null cell lines. To target exon 2 of *gp130*, 5' GGTGAACTTCTAGATCCATG 3' or 3' TGTGGTTATATCAGTCCTGA 5' was cloned into pX458 (Addgene #48138). Med8A-S cells were transfected with the respective plasmids using Lipofectamine 2000 (ThermoFisher) as per manufacturer's instructions. After 1 day, cells were clonally sorted by flow into 96-well plates

(FacsAria, BD Biosciences). Screening for gp130 null clones was done by flow cytometry. To identify indel mutations within the targeted genomic loci, I sequenced a genomic amplicon generated by polymerase chain reaction using the following primers: 5' GTTGACGTTGCAGACTTGG 3' (Fwd) and 3' CCTTCCACCATCCCACTCAC 5' (Rev) for *gp130*. Sequence alignments of the CRISPR generated mutants and parental strain were performed using CLC Main Workbench to confirm the knockout. Please refer to section 2.2.5 for more information regarding generation of IL-6R^{-/-} cells used in this chapter.

3.2.6 Flow cytometry

To evaluate cell surface gp130, IL-6R, OSMR, LIFR and IL11R expression, cells were suspended, washed with phosphate buffered saline and stained with anti-human IL-6R α antibody (R&D Systems), OSMR β (ThermoFisher), IL-11R α (ThermoFisher), LIFR α (Bioss), gp130 (Biolegend) followed by secondary antibody (Dylight 488; ThermoFisher). Flow cytometry was conducted on the Accuri C6 (BD Biosciences) and analysis was conducted using FlowJo (Tree Star). Fluorescence activated cell sorting of CRISPR generated cells was conducted on the FacsAria (BD Biosciences) in the BCCHRI Flow Core facility.

3.2.7 ELISA and cytokine array

IL-6, IL-11, LIF, OSM cytokines secreted by cells was quantified using LEGEND MAX Human IL-6 ELISA Kit (Biolegend #430507), Human LIF ELISA kit (Raybiotech #ELH-LIF-1): Human OSM ELISA kit (Raybiotech #ELH-OSM-1), and Human IL-11 ELISA kit (Raybiotech #ELH-IL11-1). Media supernatant collected from the culture of various cells were incubated and stained with reagents on a pre-coated 96-well strip plate as per manufacturer's instructions. A microplate reader (Enspire) was used to measure the absorbance at 450 nm. Quantibody[®] Human

Cytokine Array 1 (RayBiotech) is a multiplex ELISA system for quantitative measurement of multiple cytokines simultaneously. Sample preparation and analysis was performed according to the manufacturer's instructions. Further statistical analysis was performed using GraphPad.

3.2.8 Statistical data analysis

All data are representative of at least three independent experiments. Graphs were plotted and statistical significance calculated using GraphPad, with $***p < 0.001$, $**p < 0.01$, $*p < 0.05$, ns – not significant. The statistical tests used is indicated in each figure legend.

3.3 Results

3.3.1 MB cells co-cultured with microglia exhibit increased STAT3 activity and chemoresistance.

Activated microglia in the brain TME contribute to a cytokine rich environment [103,112]. As a potential source of IL-6 in the TME of Group 3 MB, I assessed the role of microglia and their contribution to drug resistance in Med8A-S cells via a paracrine signaling mechanism. As illustrated in Figure 3.1A, I used a no-contact co-culture system whereby the human microglia cell line, HMC3, is seeded in the upper chamber with Group 3 MB cells in the bottom chamber, thus allowing cell exposure to secreted factors. Med8A-S cells when co-cultured with HMC3 demonstrated significant resistance to vincristine treatment when compared to Med8A-S that were not subjected to co-culture (Figure 3.1B). The observed chemoresistance was not as high when compared to IL-6 conditioned cells (termed Med8A-IL6+ cells), but still remarkable given that co-culture with HMC3 for only 3 days was sufficient to achieve this phenomenon. In Chapter 2, I showed that IL-6R^{-/-} cells failed to respond to IL-6 conditioning and remained susceptible to vincristine treatment (see Figure 2.4D). Interestingly, IL-6R^{-/-} cells when co-cultured with HMC3 were found to exhibit significant resistance to vincristine treatment (Figure 3.1C). This finding suggests that soluble factors in addition to IL-6 released by microglia promote chemoresistance in Med8A-S and IL-6R^{-/-} cells.

Next, I evaluated if co-culture of MB with microglia promoted STAT3 activity that can be correlated with the observed chemoresistance. Indeed, both Med8A-S and IL-6R^{-/-} cells that were co-cultured with HMC3 exhibited elevated levels of pY705-STAT3 expression (Figure 3.1D). As expected, bolus IL-6 treatment resulted in increased pY705-STAT3 expression in Med8A-S cells that was not seen in IL-6R^{-/-} cells. In addition, HMC3 cells not subjected to exogenous stimuli

appear to have elevated pY705-STAT3, suggesting that HMC3 may be responsive to secreted factors in an autocrine fashion. To assess if secreted IL-6 contributes to sustained signaling, I measured IL-6 in tissue culture supernatant of HMC3 and Med8A cells, either alone or when co-cultured together. As shown in Figure 3.1E, HMC3 cells secreted high levels of IL-6 that is likely to act in paracrine fashion to activate IL-6/STAT3 signaling in Med8A-S cells. Indeed, Med8A-S cells that had been co-cultured with HMC3 also secreted measurable quantities of IL-6. I also found that IL-6R^{-/-} cells that had been co-cultured with HMC3 also secreted significant amounts of IL-6 despite lacking IL-6R expression, strongly suggesting that IL-6 secretion by MB cells could be triggered by cytokine-receptor pairs in addition to the IL-6/IL-6R combination.

Taken together, these results demonstrate that HMC3 microglia is a source of stimulatory cytokines, including IL-6, that act in paracrine fashion to stimulate STAT3 activity of Med8A MB cells, in turn promoting further secretion of IL-6, and possibly other cytokines, that can act in an autocrine manner and enable tumour cells to gain chemoresistance. Importantly, these results further suggest that therapeutic blockade of any one cytokine receptor, such as IL-6R, may not be sufficient to reduce the possibility of acquired drug resistance in these cells. This led to further investigation into the possibility of other cytokines able to stimulate STAT3 activity and drive development of chemoresistance in Group 3 MB cells.



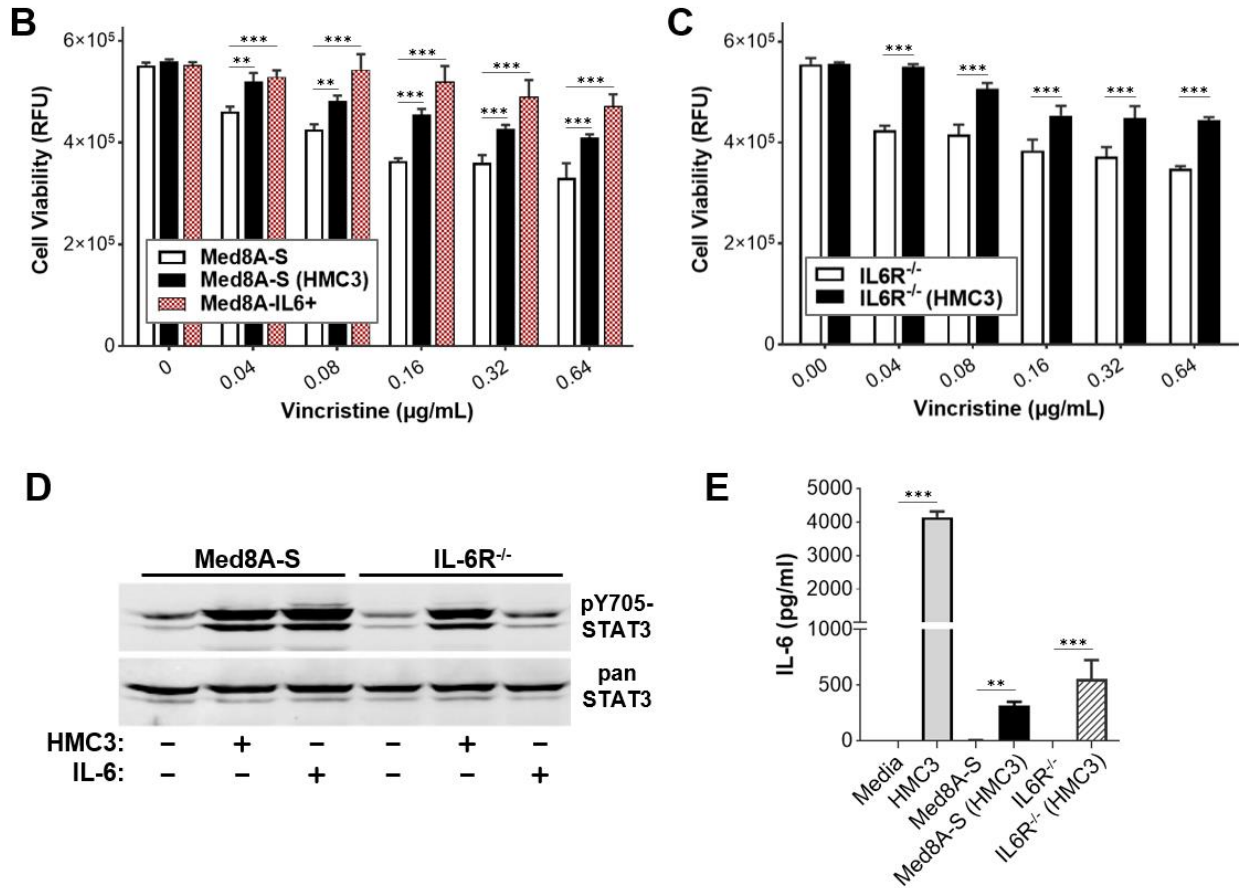


Figure 3.1: Exposure to microglia render Med8A cells chemoresistant concurrent with enhanced STAT3 activity.

(A) Schematic representation of co-culture system used to study the effect of microglia on Group 3 MB cell lines. Cells (e.g., Med8A-S) targeted for conditioning are plated in the bottom well, while microglia (HMC3) cells are plated in the top Transwell insert with non-passable 1 µm pores that allow media exchange between the two cell populations. After 3 days in co-culture, the insert is discarded, cells in the treatment well washed, and fresh media added. After 3 days, cells are harvested for protein analysis while the conditioned media used for cytokine assays. Cell viability assay to assess the sensitivity of (B) Med8A-S and (C) IL-6R^{-/-} to vincristine with or without co-culture with HMC3 cells. In (B), Med8A-IL6+ cells refer to Med8A-S cells conditioned with IL-6 for 4 weeks. As plotted is the mean ± SD of an experiment performed in triplicates, representative of at least 3 independent experiments. *** $p < 0.001$, two-way ANOVA with Bonferroni's multiple comparison test. (D) Western blot analysis of lysates of Med8A-S, IL-6R^{-/-} and HMC3 cells for pY705-STAT3 and STAT3 expression. (E) Analyses for secreted IL-6 in culture supernatant of the indicated cells and co-culture combination. As plotted is the mean ± SD of three replicates; *** $p < 0.001$, ** < 0.01 , * < 0.05 , two-way ANOVA with Tukey's multiple comparison test.

3.3.2 JAK inhibitor ruxolitinib diminishes STAT3 activity and reverts acquired drug resistance.

Janus kinases (JAK1, JAK2 and TYK2) are crucial signal transducers that link cytokine-bound receptors to activation of STAT proteins [138]. An initial western blot analysis of Med8A-S cells revealed that bolus IL-6 treatment upregulated levels of phosphorylated JAK1 (pY1034/1035-JAK1 referred to as pJAK1 in this thesis) and pY705-STAT3, but not the phosphorylation of the other JAKs assayed (Figure 3.2A). As expected, bolus IL-6 treatment failed to stimulate pJAK1 or pY705-STAT3 in IL-6R^{-/-} cells. Additionally, I found that Med8A-S and IL-6R^{-/-} cells that had been co-cultured with HMC3 exhibited increased pJAK1 and pY705-STAT3 expression (Figure 3.2A). This finding suggested that JAK inhibition may be a sufficient and preferred strategy to block STAT3 activation and development of acquired resistance that can occur downstream of signaling by multiple cytokine receptors.

Hence, I used a commercially available JAK1/2 inhibitor, ruxolitinib, to study the effects of blocking JAK1 activity in MB cells [145,208]. As shown in Figure 3.2B, ruxolitinib significantly diminished the levels of pY705-STAT3 of Med8A-S cells stimulated with bolus IL-6. Ruxolitinib also significantly diminished the levels of pY705-STAT3 in Med8A-S or IL-6R^{-/-} cells induced by co-culture with HMC3 microglia (Figure 3.2B). Since ruxolitinib effectively reduced pY705-STAT3 expression, I assessed if combination treatment with vincristine could overcome the resistance exhibited by these cells when exposed to HMC3 cells. As shown in Figure 3.2C and D, combined treatment with vincristine and a non-toxic dose of ruxolitinib (2 μM) effectively overcame the chemoresistance observed in both Med8A-S and IL-6R^{-/-} cells that had been co-cultured with HMC3. These results indicate that targeting JAKs is sufficient to overcome

acquired chemoresistance in Med8A-S and IL-6R^{-/-} cells exposed to soluble factors secreted by HMC3 microglia.

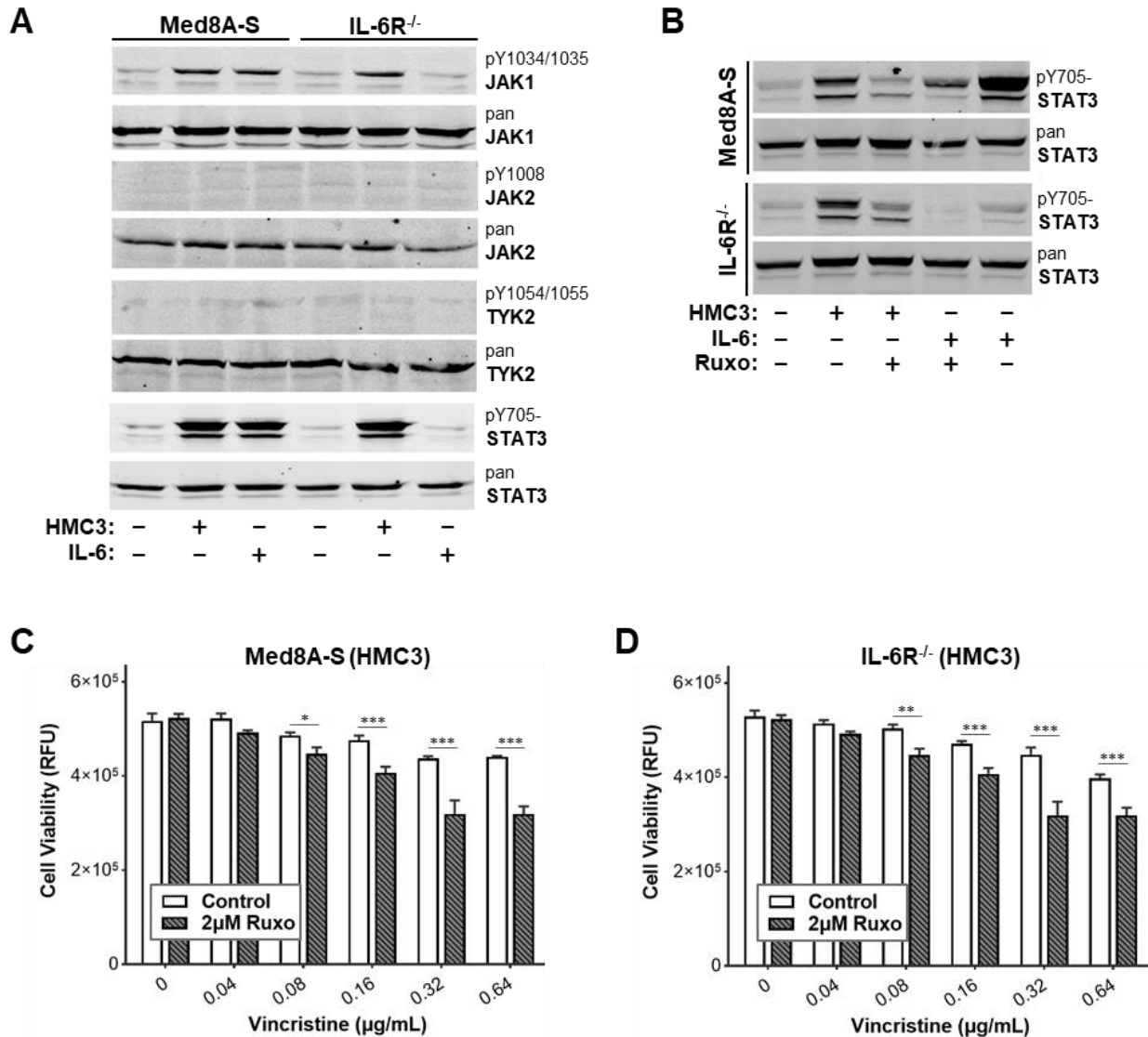


Figure 3.2: JAK inhibitor suppresses STAT3 activity and overcomes microglia-induced chemoresistance of MB cells.

Western blot analysis of lysates of (A) Med8A-S and IL-6R^{-/-} cells when co-cultured with HMC3 or stimulated with 5 ng/mL IL-6 for pJAK1, JAK1, pJAK2, JAK2, pTYK2, TYK2, pY705-STAT3 and STAT3 expression. (B) Med8A-S, Med8A-IL6+ and IL-6R^{-/-} cells were untreated or subjected to treatments that include co-culture with HMC3, or stimulation with 5 ng/mL IL-6. Where indicated, cells were then treated with 2 µM ruxolitinib for 20 mins prior to western blot analysis of lysates for pY705-STAT3 and STAT3 expression. Cell viability assay to assess chemosensitivity to vincristine of (C) Med8A-S or (D) IL-6R^{-/-} cells that had been co-cultured with HMC3 with or without treatment with 2 µM ruxolitinib. MB cells were co-cultured for 3 days

and replaced with fresh media. 2 μ M ruxolitinib was added to the media during the wean off period of 3 days prior to combination treatment. As plotted is the mean \pm SD of an experiment performed in triplicates, representative of at least 3 independent experiments. *** $p < 0.001$, ** <0.01 , * <0.05 , two-way ANOVA with Bonferroni's multiple comparison test.

3.3.3 The IL-6 family cytokines IL-6, LIF, OSM and IL-11 promote acquired resistance to vincristine treatment.

Stimulatory cytokines that belong to the IL-6 family signal through a common receptor β -subunit called gp130, which transduces the signal intracellularly to activate downstream targets such as JAKs and STAT3 [125,168]. Hence, I profiled the ability of several members of the IL-6 family cytokines, including IL-6, LIF, OSM, and IL-11, to stimulate phosphorylation of JAK1 and STAT3 in Med8A cells. Western blot analysis revealed that Med8A-S cells stimulated with bolus IL-6, LIF, OSM or IL-11 exhibited enhanced pJAK1 and pY705-STAT3 levels when compared to non-treated cells (Figure 3.3A). IL-6R^{-/-} cells similarly responded to stimulation with LIF, OSM or IL-11, but not to IL-6, which was expected (Figure 3.3A). Flow cytometry analysis revealed that Med8A-S cells expressed detectable cell surface levels of LIFR, OSMR and IL-11R (Figure 3.3B), a result that supports the ability of the cells to respond to cytokine stimuli.

I showed previously that IL-6 conditioned Med8A-S cells, but not cells lacking IL-6R, acquired resistance to vincristine treatment (see Chapter 2). As I had done before for IL-6, cells were subjected to low dose conditioning with IL-6, LIF, OSM and IL-11 for several weeks and weaned off this conditioning prior to conducting chemosensitivity and other assays. Previously, I showed that Med8A-IL6⁺ cells exhibited increased IL-6R expression in response to conditioning. However, no changes in receptor level expression was evident following cytokine conditioning of the Med8A-S cells to LIF, OSM or IL-11 (Figure 3.3B). In chemosensitivity assays, I found that both Med8A-S and IL-6R^{-/-} cells conditioned with LIF, OSM or IL-11 also exhibited significant

resistance to vincristine treatment (Figure 3.3C and D). These results further validate the possibility of stimulatory cytokines signaling through their specific α -receptors and common β -subunit to activate STAT3 and induce vincristine resistance in MB cells.

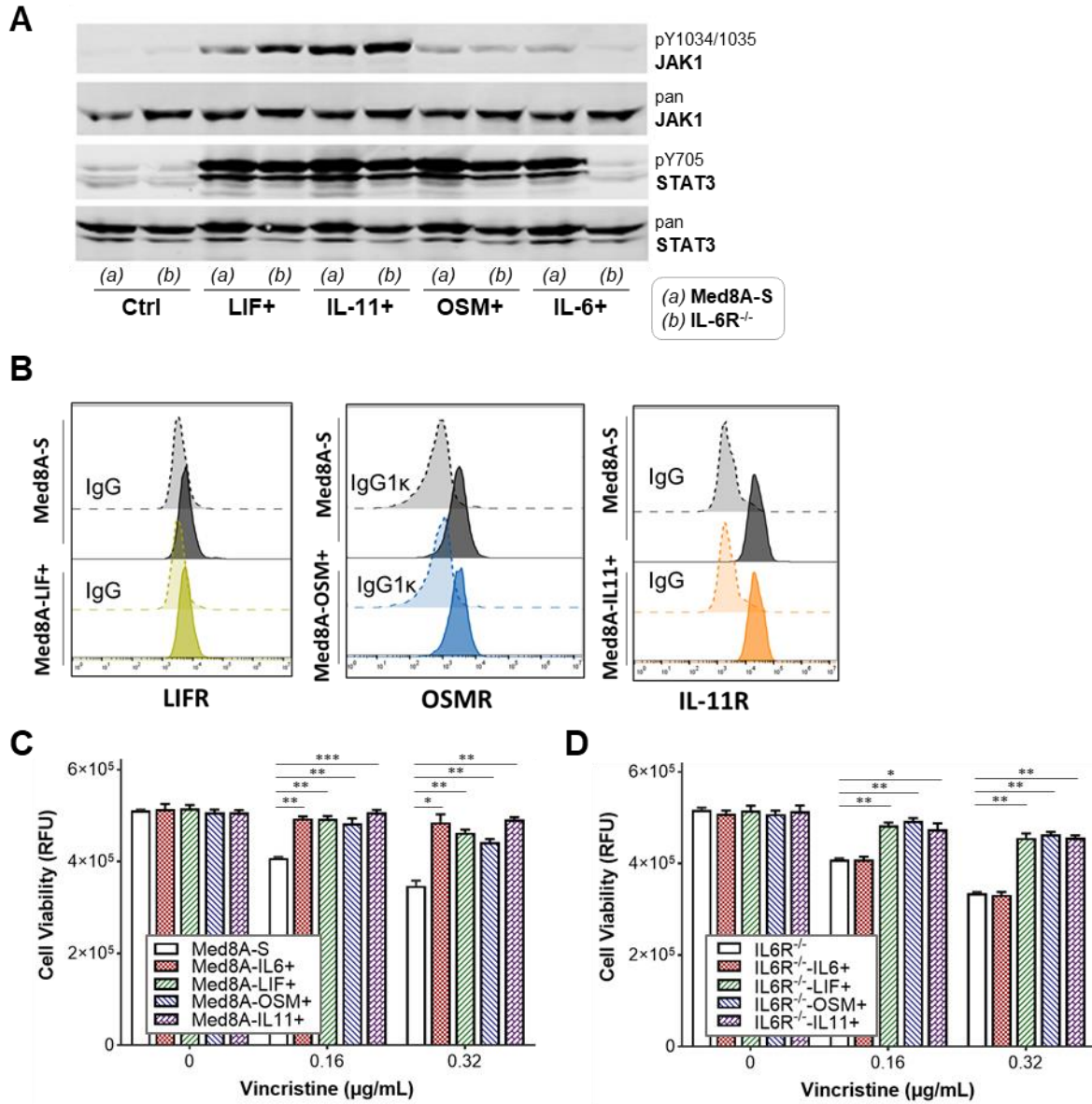


Figure 3.3: MB cells conditioned with IL-6 family cytokines enhance JAK1 and STAT3 activity and chemoresistance.

(A) Med8A-S and IL-6R^{-/-} cells untreated (Ctrl) or treated with bolus LIF, OSM, IL-11 or IL-6, and immunoblotted to detect pJAK1, JAK1, pY705-STAT3 and STAT3 expression. (B) Flow cytometry assay for cell surface expression of LIFR, OSMR and IL-11R in Med8A-S and cytokine conditioned cells (LIF, OSM or IL-11), with corresponding IgG controls. Cell viability assay to

assess vincristine sensitivity of (C) Med8A-S and (D) IL-6R^{-/-} cells not conditioned, or conditioned with IL-6, LIF, OSM or IL-11, as indicated. As plotted is the mean ± SD of an experiment performed in triplicates, representative of at least 3 independent experiments. ****p* < 0.001, **<0.01, *<0.05, two-way ANOVA with Bonferroni's multiple comparison test.

3.3.4 MB cells conditioned with one IL-6 family cytokine promote secretion of multiple IL-6 family cytokines.

In Chapter 2, I showed that Group 3 MB cells that had been conditioned with IL-6 secreted significant amounts of IL-6 that can act in feedback autocrine signaling (**Error! Reference source not found.**). Similarly, Med8A-S and IL-6R^{-/-} cells that had been co-cultured with HMC3 also secreted IL-6 (Figure 3.1E). To assess if this phenomenon is also applicable to other cytokines of the IL-6 family, I evaluated the secretion of LIF, OSM or IL-11 in response to exogenous cytokine conditioning of Med8A-S and IL-6R^{-/-} cells, as well as upon co-culture exposure to HMC3 microglia. The results are shown in Figure 3.4 (A, B and C for LIF, IL-11 and OSM, respectively). I found that HMC3 microglia secreted detectable amounts of LIF and IL-11, but not OSM, suggesting that LIF and IL-11 may also be significant contributors to paracrine signaling in the MB tumour microenvironment. However, Med8A-S or IL-6R^{-/-} cells that were co-cultured with HMC3 for 3 days did not secrete LIF, IL-11 or OSM in excess of non-co-cultured cells. Additionally, Med8A-S and IL-6R^{-/-} cells conditioned with LIF, OSM or IL-11 secreted high levels of the respective cytokine (eg. Med8A-LIF⁺ cells secreted LIF). Remarkably, compared to non-conditioned cells, Med8A-S cells conditioned with a single cytokine secreted significantly higher levels of other IL-6 family cytokines. For example, Med8A-IL6⁺ cells were found to secrete LIF, OSM and IL-11. This suggests that conditioning with one IL-6 family cytokine is sufficient to promote MB cell secretion of other cytokines belonging to the same family. It is worth noting that the weaker secretory response demonstrated by chemosensitive MB cells in response to microglia

could be attributed to the shorter exposure time (3 days) in comparison to exogenous cytokine conditioning (several weeks). Collectively, these results suggest that both paracrine and autocrine mechanisms involving IL-6 family cytokines is prevalent in the MB TME that given sufficient time, could promote transformation of chemosensitive tumour cells to chemoresistant variants.

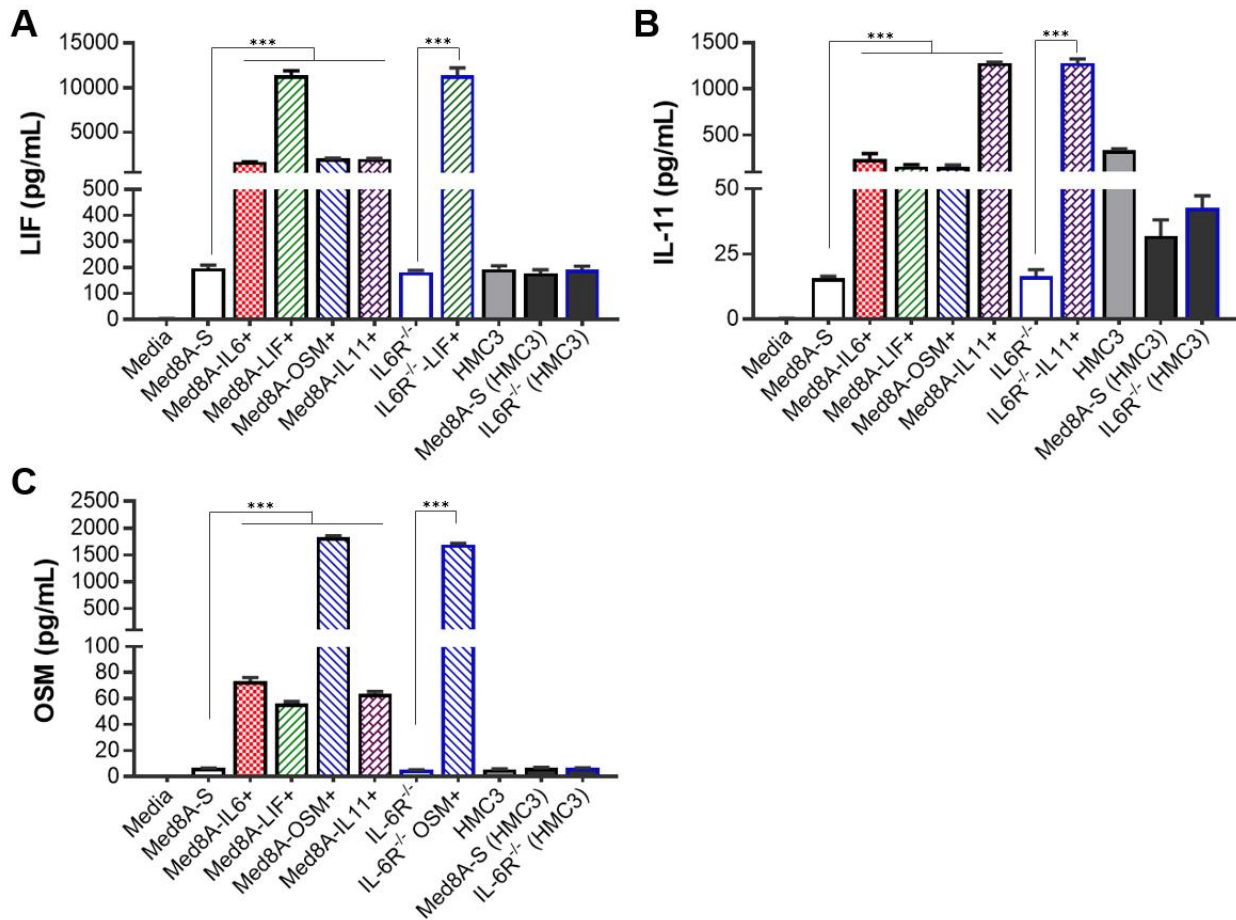


Figure 3.4: Chemoresistant MB cells secrete elevated levels of LIF, OSM and IL-11.

A) Secreted cytokine analysis of conditioned media from Med8A-S, IL-6R^{-/-}, Med8A-S-(LIF, OSM or IL11) +, IL-6R^{-/-}(LIF, OSM or IL11) + cells using an ELISA-based kit for the various cells, as indicated. Med8A-S and IL-6R^{-/-} cells were co-cultured with HMC3 prior to conditioned media collection. After 3 days in coculture, the insert was discarded, cells in the treatment well washed, and fresh media added. After 3 days, conditioned media used for cytokine assays. As plotted is the mean \pm SD of three replicates; *** $p < 0.001$, ** < 0.01 , * < 0.05 , ordinary one-way ANOVA with Bonferroni's multiple comparison test.

3.3.5 Ruxolitinib overcomes chemoresistance of IL-6 family cytokine conditioned MB cells.

When exposed to soluble factors secreted by HMC3 microglia, Med8A-S and IL-6R^{-/-} cells developed resistance to vincristine treatment that could be overcome with the JAK inhibitor ruxolitinib (Figure 3.2C, D). In Figure 3.3B, I showed that Med8A cells conditioned with IL-6 family cytokines were highly resistant to vincristine treatment. This raises the possibility that JAK inhibition can similarly overcome chemoresistance resulting from IL-6 family cytokine-conditioned MB cells. As shown in Figure 3.5, combination ruxolitinib and vincristine treatment of Med8A-IL6⁺, Med8A-LIF⁺, Med8A-OSM⁺ or Med8A-IL11⁺ cells effectively overcame the resistance observed with vincristine alone. In similar fashion, IL-6R^{-/-} cells conditioned with LIF, OSM or IL-11 also displayed enhanced sensitivity to combination vincristine and ruxolitinib treatment (Figure 3.6

). These results further confirm that combination treatment with ruxolitinib and vincristine is more effective compared to single agent treatment in overcoming acquired resistance in MB cells that had been exposed to cytokines for a prolonged period.

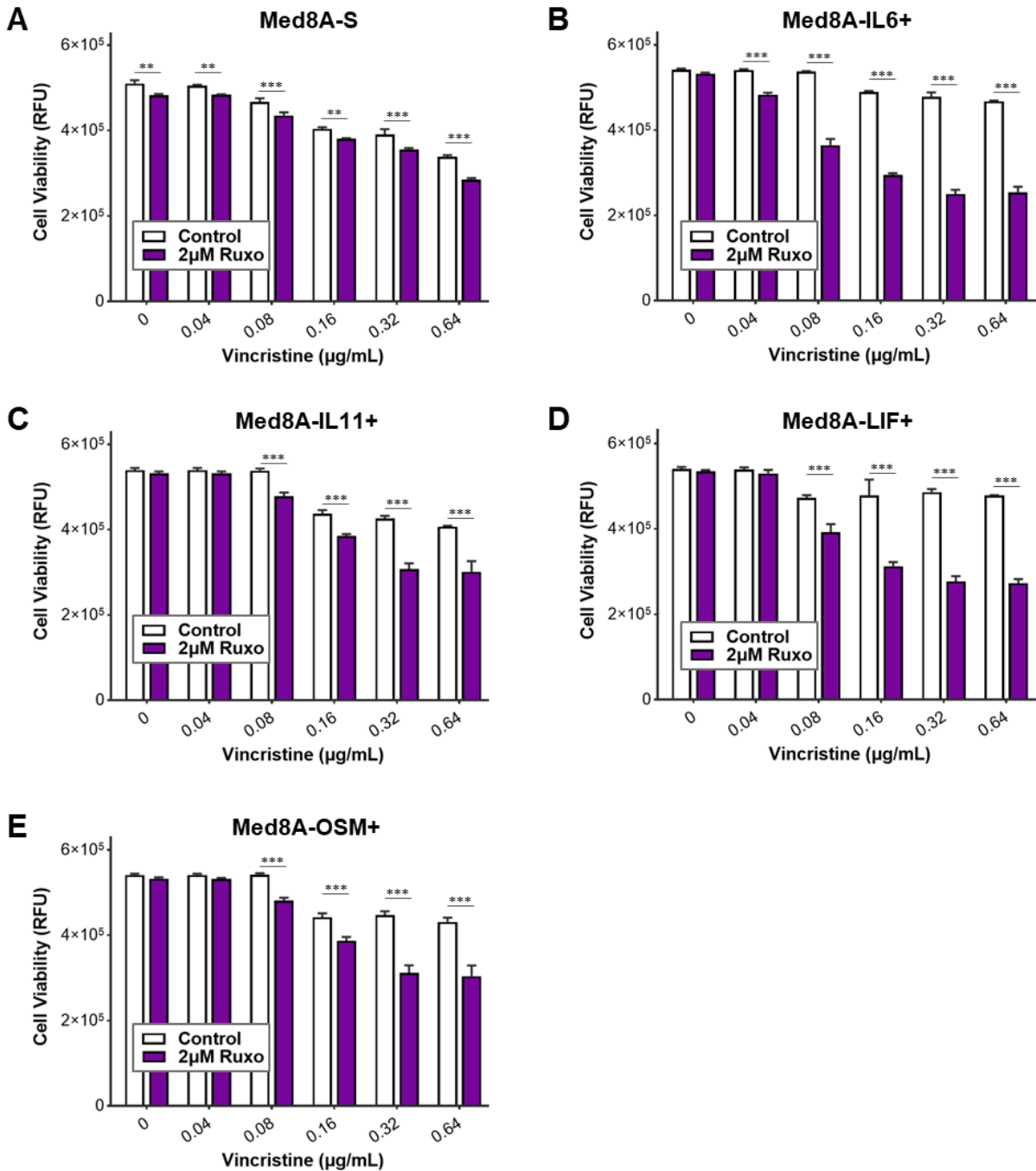


Figure 3.5: Combined treatment of vincristine with ruxolitinib in IL-6 family of cytokine conditioned Med8A-S cells.

Cell viability assay to assess the sensitivity of (A) Med8A-S, (B) Med8A-IL6+, (C) Med8A-IL11+, (D) Med8A-LIF+ and (E) Med8A-OSM+ to indicated concentrations of vincristine with and without 2 µM ruxolitinib. As plotted is the mean ± SD of an experiment performed in triplicates, representative of at least 3 independent experiments. *** $p < 0.001$, two-way ANOVA with Bonferroni's multiple comparison test.

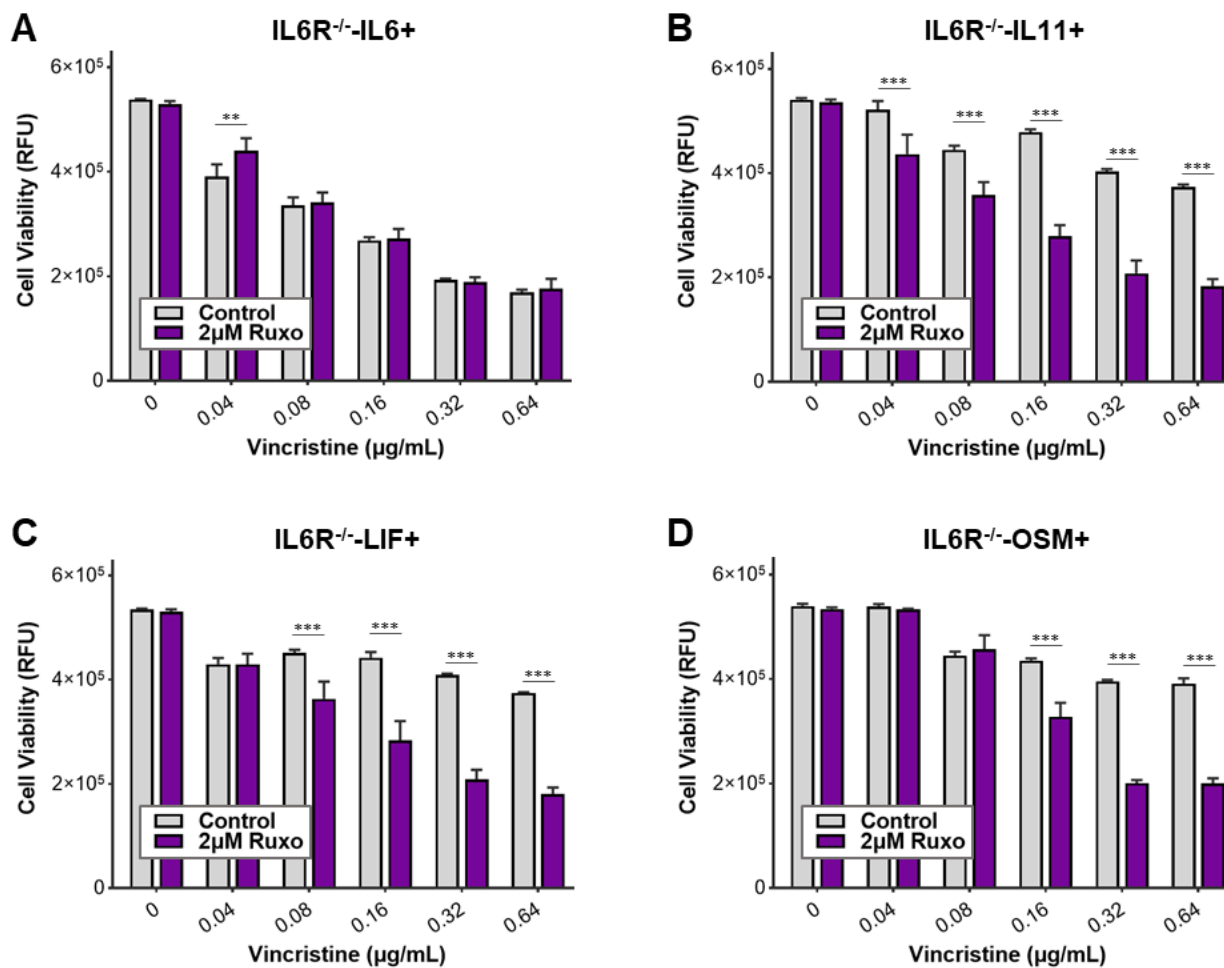


Figure 3.6: Combined treatment of vincristine with ruxolitinib in IL-6 family of cytokine conditioned IL6R^{-/-} cells.

Cell viability assay to assess the sensitivity of (A) IL-6R^{-/-}-IL6+, (B) IL-6R^{-/-}-IL11+, (C) IL-6R^{-/-}-LIF+ and (D) IL-6R^{-/-}-OSM+ cells to indicated concentrations of vincristine with and without 2 µM ruxolitinib. As plotted is the mean ± SD of an experiment performed in triplicates, representative of at least 3 independent experiments. ****p* < 0.001, two-way ANOVA with Bonferroni's multiple comparison test.

3.3.6 Targeting gp130 mitigates MB chemoresistance resulting from exposure to microglia.

My previous results suggested that more than one IL-6 family cytokine found in the TME can promote MB drug resistance. This finding bears significance for therapeutic considerations, since targeting any one IL-6 family cytokine, or its specific receptor, may not suffice as a strategy to overcome acquired drug resistance. Given that all receptors for the IL-6 family cytokines contain gp130 as the common β -subunit, I sought to evaluate the role of gp130, and its targeting, in chemoresistance. I used CRISPR-Cas9 gene editing technique to generate and then isolate Med8A-S clones lacking cell surface gp130 expression (Figure 3.7A), sequencing confirmation of targeted alleles shown in Appendix A.5). Unlike the parental Med8A-S cells, gp130^{-/-} cells co-cultured with HMC3 did not develop resistance to vincristine, suggesting that paracrine signaling was attenuated in cells lacking gp130 (Figure 3.7B). Western blot analysis also revealed that pY705-STAT3 expression was not induced in gp130^{-/-} cells co-cultured with HMC3 (Figure 3.7C).

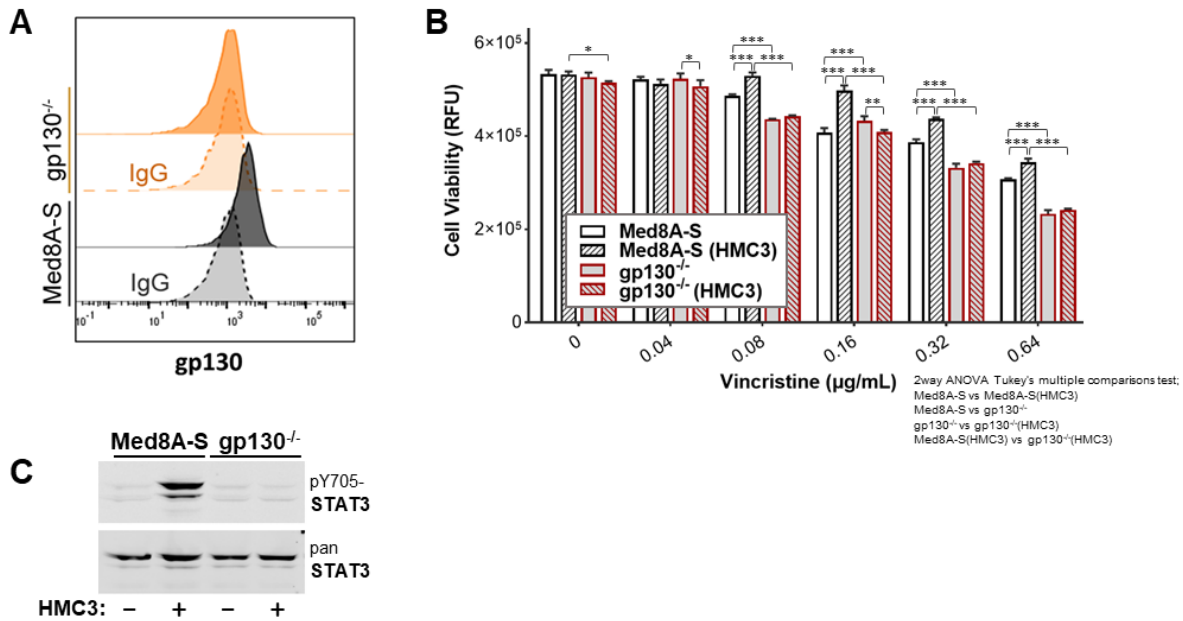


Figure 3.7: Loss of gp130 prevents microglia co-culture induced STAT3 signaling and chemoresistance in Med8A cells.

A) Flow cytometry assay for cell surface expression of gp130 in Med8A-S and gp130^{-/-} cells, with corresponding IgG controls. B) Cell viability assay to assess vincristine sensitivity of gp130^{-/-} and Med8A-S cells with or without HMC3 co-culture. As plotted is the mean \pm SD of an experiment performed in triplicates, representative of at least 3 independent experiments. *** $p < 0.001$, ** < 0.01 , * < 0.05 , two-way ANOVA with Bonferroni's multiple comparison test. C) Lysates of Med8A-S and gp130^{-/-} untreated or co-cultured with HMC3 were assessed for pY705-STAT3 and total STAT3 by western blot analysis.

Next, I evaluated the potential for targeting gp130 using commercially available small molecule inhibitors as a strategy to circumvent drug resistance exhibited by Med8A-S cells when exposed to HMC3 cells (Figure 3.8). Bazedoxifene is a selective estrogen receptor modulator (SERM) that had been repurposed as a gp130 inhibitor [132-134], while SC144 is a newer class and potent gp130 inhibitor that effectively blocks activation of downstream signaling such as AKT and STAT3 in ovarian cancer [137]. As shown in Figure 3.8A and B, both gp130 inhibitors enhanced sensitivity to vincristine treatment in Med8A-S cells that had been co-cultured with HMC3. Compared to SC144, bazedoxifene was less effective in overcoming resistance at lower concentrations of vincristine. Combined treatment of SC144 with vincristine was also effective in circumventing resistance of IL-6R^{-/-} cells that had been co-cultured with HMC3 cells (Figure 3.8D and E). Together, these results suggest that gp130 is a promising target to overcome resistance exhibited by chemoresistant MB cells.

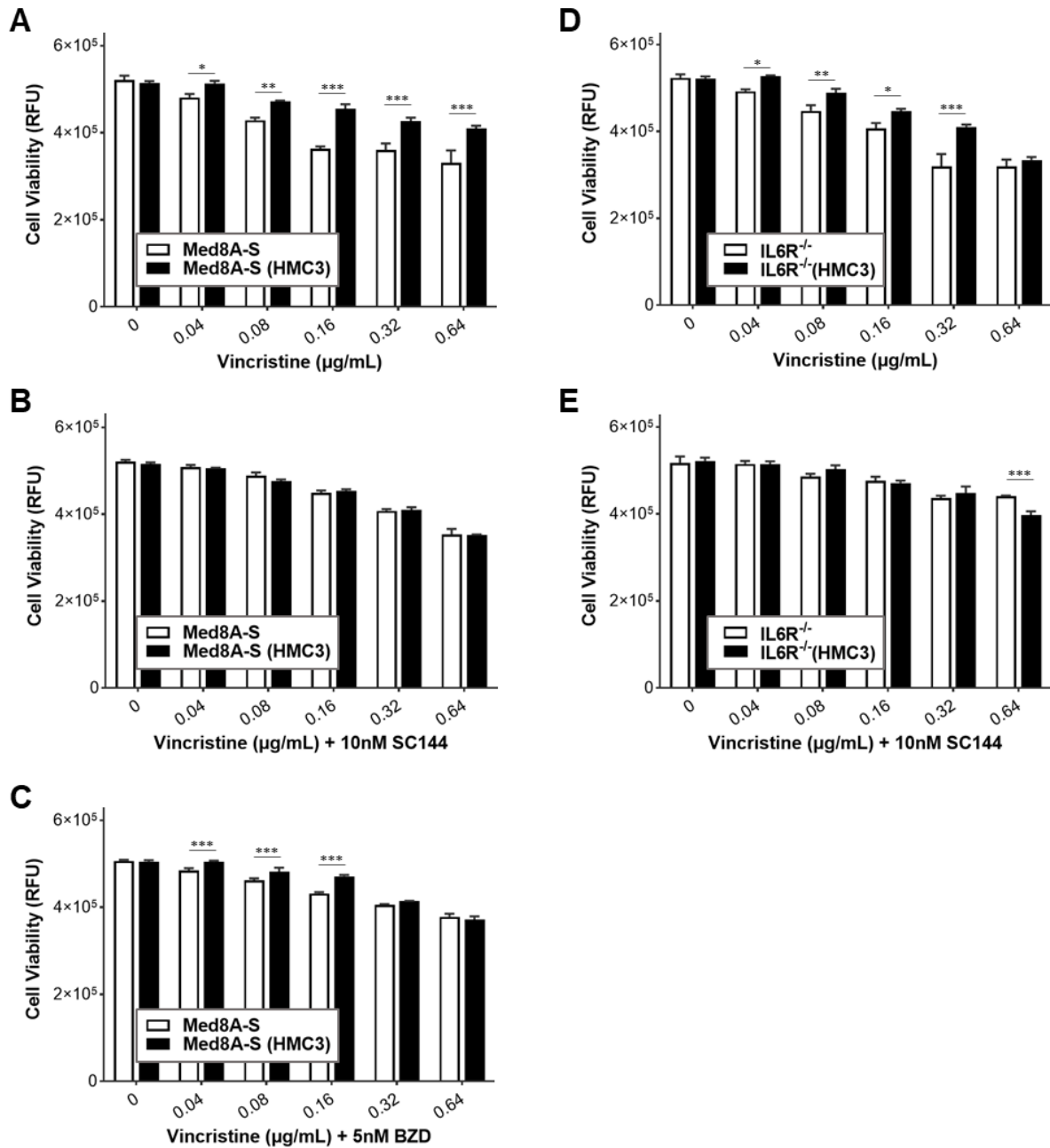


Figure 3.8: Gp130 inhibitors mitigates microglia co-culture induced chemoresistance in Med8A cells.

(A) Cell viability assay to assess the sensitivity of Med8A-S cells with or without HMC3 co-culture to vincristine alone, or, (B, C) in combination with gp130 inhibitors, SC144 or bazedoxifene (BZD), as indicated. (D) Cell viability assay to assess the sensitivity of IL-6R^{-/-} cells with or without HMC3 co-culture to vincristine alone, or, (E) in combination with SC144. As plotted is the mean ± SD of an experiment performed in triplicates, representative of at least 3 independent experiments. ****p* < 0.001, **<0.01, *<0.05, two-way ANOVA with Bonferroni's multiple comparison test.

3.3.7 Gp130 is essential for driving chemoresistance in other Group 3 MB cell lines.

My study demonstrated that gp130 plays an essential role in promoting chemotherapeutic resistance in Med8A cells in response to external stimuli. To evaluate if this may be a robust phenomenon demonstrated by other Group 3 MB cell lines, I assessed the requirement of gp130 in driving chemoresistance in D283 and D341 cells. To begin with, STAT3 expression profiling revealed that D283 and D341 cells exhibited increased pY705-STAT3 expression when co-cultured with HMC3 cells (Figure 3.9A). D283 and D341 cells when co-cultured with HMC3 also demonstrated significant resistance to vincristine treatment (Figure 3.9B and D). Finally, combination treatment using SC144 to target gp130, in conjunction with vincristine, was sufficient to overcome resistance of D283 and D341 cells that had been co-cultured with HMC3 microglia (Figure 3.9C and E). Taken together, my data demonstrate that microglia secrete soluble factors that promote chemotherapeutic resistance in Group 3 MB cell lines. Targeting gp130 in Group 3 MB cells holds potential to prevent TME-mediated development of chemoresistant variants of MB and improve overall therapeutic efficacy when used in combination with vincristine.

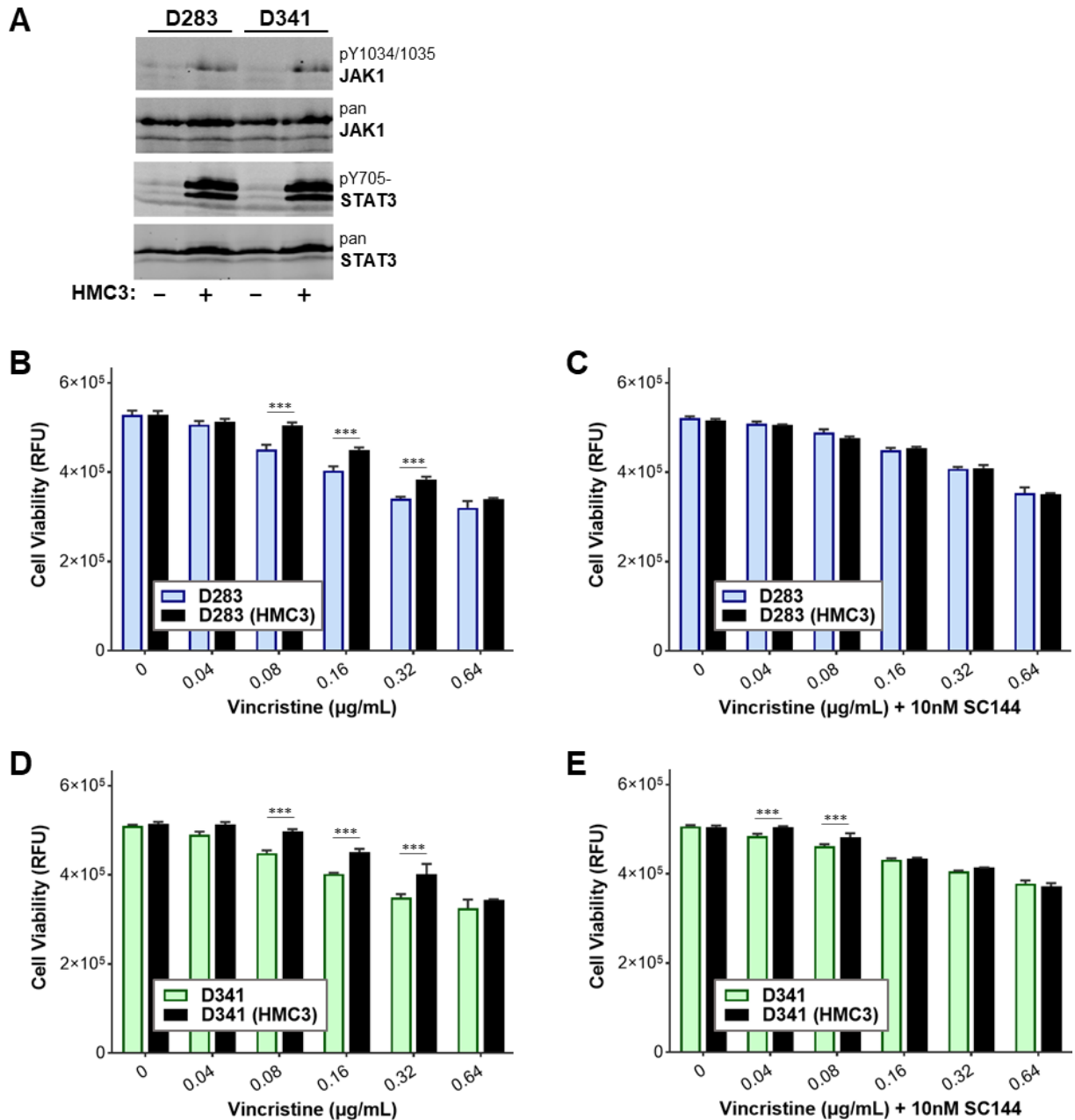


Figure 3.9: Combination SC144 and vincristine treatment mitigates microglia co-culture induced chemoresistance in D283 and D341 cells.

A) Lysates of D283 and D341 untreated or co-cultured with HMC3 were assessed for pY705-STAT3 and total STAT3 by western blot analysis. Cell viability assay to assess the sensitivity of (B) D283 and (C) D341 cells with or without HMC3 co-culture to vincristine alone, or, (D, E) in combination with SC144. As plotted is the mean \pm SD of an experiment performed in triplicates, representative of at least 3 independent experiments. *** $p < 0.001$, ** < 0.01 , * < 0.05 , two-way ANOVA with Bonferroni's multiple comparison test.

3.4 Discussion

The brain tumour microenvironment (TME) consists of several cellular components that are thought to play crucial roles in facilitating cellular transformation and tumour progression. Tumour-associated macrophages (TAMs) and microglia can constitute up to 30% of the cells found in the TME [103]. These immune cells are often involved in bidirectional cross-talk with tumour cells, wherein immune cells secrete soluble factors to promote tumorigenesis, while tumour cells secrete chemo-attractants to recruit TAMs and microglia [102]. For instance, gliomas and other cells in the TME can reprogram the microglia by releasing signals that can change the manner in which microglia function in a TME. Microglia can either aid or inhibit tumour growth and survival [209]. Extensive research over the years has highlighted the prognostic importance of immune cells and immunotherapy in cancer biology. Despite the characterization of MB into molecular subgroups, there is limited knowledge about the cellular players present in the MB TME and their contribution to tumour progression. Although subtle, understanding the constituents of the subgroup specific MB TME can yield benefits in understanding their pro- or anti-tumour effects that affect disease progression and also identify novel therapeutic strategies to counter MB that are refractory to conventional therapy [116].

My study highlights the contribution of microglia in the development of chemoresistance in Group 3 MB cells. The chemosensitive Group 3 MB cell line, Med8A-S, when co-cultured with microglia was found to be substantially resistant to vincristine treatment. Additionally, pY705-STAT3 activity was substantially elevated in Med8A-S cells exposed to microglia. This phenomenon is consistent with previous studies demonstrating the association of increased resistance to treatment with increased pY705-STAT3 activity [118,120].

In Chapter 2, I demonstrated that knockout of IL-6R (IL-6R^{-/-}) in a chemoresistant derivative of Med8A cells restored sensitivity to vincristine treatment, and that IL-6 conditioning of IL-6R^{-/-} cells failed to promote chemoresistance. Rather surprisingly, IL-6R^{-/-} cells co-cultured with microglia exhibited increased resistance to vincristine treatment and elevated pY705-STAT3 activity. This suggests that cells in the TME such as microglia likely secrete a wide range of stimulatory cytokines, in addition to IL-6, that can activate STAT3 and promote development of chemoresistance. An important implication is that blocking a single cytokine or its receptor may not be sufficient to abrogate STAT3 signaling and circumvent chemoresistance in tumour cells that are subjected to multiple cytokine stimuli that exists in the TME. Collectively, these results paved the way into the exploration of other upstream activators of STAT3 and its contribution to drug resistance in Group 3 MB cells.

The IL-6 family cytokines consist of several cytokines that activate STAT3 and play roles in a multitude of physiological functions [125]. Notably, IL-6 family cytokines in the brain TME contributes to CNS homeostasis and pathogenesis of diseases [168-170]. As upstream regulators of STAT3 signaling, I assessed the contribution of some members of this cytokine family, namely IL-6, LIF, OSM, and IL-11, in their ability to promote chemoresistance in the Group 3 MB cells. My findings showed that both chemosensitive Med8A cells (Med8A-S or IL-6R^{-/-}) acquired resistance to vincristine when subjected to exogenous cytokine conditioning for which the corresponding cytokine receptors are expressed. The chemoresistance observed in cytokine-conditioned cells was also associated with increased pJAK1 and pY705-STAT3 levels. These data suggest that IL-6 family cytokines can activate STAT3 in chemosensitive Group 3 MB cells and contribute to acquired drug resistance. More importantly, cells that lack one functional receptor can also develop drug resistance through STAT3 activation in response to other cytokines.

To assess paracrine signaling, I evaluated the secretion of IL-6, LIF, OSM, and IL-11 from microglia as well in chemosensitive MB cells co-cultured with microglia. HMC3 microglia secreted significantly more IL-6 and IL-11 when compared to non-co-cultured Med8A cells, indicating the potential that microglia-derived cells IL-6 and IL-11 can act as initiating cytokine stimuli to activate STAT3 signaling of MB cells in proximity. In addition, MB cells that had been co-cultured with microglia for 3 days was found to secrete significant quantities of IL-6, which now constitute a cytokine of tumour cell origin that can signal in autocrine fashion. It is intriguing to consider if this brief exposure to microglia may be sufficient to kick-start an autocrine signaling loop involving IL-6 family cytokines and further drive chemoresistance of MB. In particular, I found that Med8A cells that had been conditioned for 2 weeks with any one cytokine then secreted significant quantities of that same cytokine, as well as other cytokines in the IL-6 family. Thus, MB cell exposure to TME cytokines in paracrine signaling may over time result in sustained autocrine signaling and amplification through secretion of other cytokines, all of which with the potential to sustain STAT3 activity in a constitutive manner.

For technical reasons, the microglia conditioning experiments was limited to a 3-day exposure, in contrast to the 2-week long exogenous cytokine conditioning experiments. This limitation was due to MB cells reaching over-confluence if the co-culture were extended beyond 3-days. The brief exposure to microglia likely contributed to MB cells exhibiting a weaker to non-detectable secretory response of IL-6 family cytokines in comparison to cytokine conditioned cells. This phenomenon may also contribute to microglia conditioned MB cells that are resistant when compared to non-conditioned cells, but less resistant when compared to cytokine conditioned cells. It should be possible to extend the period of co-culture with MB cells with microglia by periodic passaging of MB cells and replacement of microglia inserts. This would allow assessment if

prolonged co-culture exposure to microglia can lead to increased cytokine secretion by MB cells and even further enhanced chemoresistance.

Gp130 is a ubiquitous protein that is part of a receptor complex involved in transducing JAK/STAT3 signaling initiated by IL-6 family cytokines [125,129]. Several studies have demonstrated that blocking gp130 signaling inhibits tumour growth and induces apoptosis *in vitro* and *in vivo* in multiple malignancies. Given that gp130 is a common signal transducer for the IL-6 family cytokines, I evaluated the effect of targeting gp130 in Group 3 MB cells. My findings demonstrate that Med8A cells lacking gp130 expression prevented microglia conditioning mediated acquired drug resistance, concomitant with blockade of STAT3 activity. To further validate the targeting gp130, I used two commercially available gp130 inhibitors, SC144 and bazedoxifene, in combination with vincristine to circumvent the observed chemoresistance [132-134,137]. Both inhibitors showed efficacy, with SC144 being more potent and exhibiting greater response at lower doses of vincristine when compared to bazedoxifene. Importantly, I used a titrated dose of SC144 or bazedoxifene that was not cytotoxic to Med8A cells when used as a mono-agent, thus potentially minimizing the deleterious side effects of an additional chemotherapeutic on non-tumour cells when used in combination with conventional agents such as vincristine. These striking results further validated the vital role of gp130 in IL-6 family cytokine mediated drug resistance in Group 3 MB cells that requires STAT3 activation.

Other potential drug targets that are downstream of multiple cytokine receptors are JAKs, which could be inhibited with ruxolitinib, a potent JAK inhibitor that has been shown to effectively block JAK1/2 activity [145,208]. Notably, a phase 1 trial demonstrated that ruxolitinib is safe to use in combination with multi-agent chemotherapy for children with acute lymphoblastic leukemia [210]. Hence, it might be closer to clinical translation for MB pediatric patients compared to other

inhibitors used in my study. Of the JAKs that were evaluated, I found that only JAK1 was inducibly phosphorylated in Med8A cells in response to IL-6 stimulation. A non-toxic dose of ruxolitinib effectively blocked IL-6 induced phosphorylation of STAT3, and when used in combination with vincristine, was able to overcome MB chemoresistance resulting from co-culture exposure to microglia. My experimental findings suggest that JAK1 could be a novel therapeutic target to effectively overcome chemoresistance in Group 3 MB cells.

In conclusion, my study demonstrated that targeting gp130/JAK/STAT3 signaling attenuates tumour microenvironment mediated chemoresistance in Group 3 MB. Blocking JAK1 activation with ruxolitinib led to diminished pY705-STAT3 activity and rendered chemoresistant Group 3 MB cells more susceptible to vincristine treatment. The evidence suggests that JAK1 might be a potential target to combat drug resistance in Group 3 MB. Additionally, prolonged exposure to stimulatory cytokines contributed by cells such as microglia present in the brain TME can promote chemoresistance via a paracrine signaling mechanism in Group 3 MB cells. Future studies could investigate the role of other cells in the brain TME that contribute to the development of drug resistance in Group 3 MB cells. Lack of gp130 resulted in diminished pY705-STAT3 activity and prevented acquired drug resistance in chemosensitive cells exposed to microglia. Notably, inhibiting gp130 signaling with targeted inhibitors such as bazedoxifene or SC144 in combination with vincristine can effectively overcome chemotherapeutic resistance. The multifaceted nature of gp130 makes it a promising therapeutic target for treatment of Group 3 MB tumours. Future studies are required to determine the efficacy of these inhibitors as a single agent and in combination with cytotoxic drugs in an *in vivo* setting.

Chapter 4: Data mining of MB transcriptional databases provides insight into components of the IL-6/STAT3 signaling cascade.

4.1 Chapter overview

Numerous transcriptome studies have led to stratification of MB into four distinct molecular subgroups: WNT, SHH, Group 3 and Group 4. Of these, Group 3 MB tumors are the most difficult to treat. To account for the high level of tumor heterogeneity, Cavalli *et al.* have classified Group 3 MB into additional subtypes, namely Groups 3 α , 3 β , and 3 γ [42]. Most notable is Group 3 γ that has high MYC amplification, high rates of metastasis, and worse overall survival. Group 3 α comprises of infants under the age of 3 with better clinical outcome. Although Group 3 α has a better prognosis compared to Group 3 γ , they are highly similar in terms of metastasis at diagnosis. Group 3 β also has a favourable outcome clinically but comprises of a slightly older population that present with infrequent metastasis.

In this Chapter, I aim to further validate the functional biological context of the work provided in Chapters 2 and 3 by using gene expression array data from existing published GEO datasets to probe for IL-6/STAT3 signaling axis components in Group 3 MB, in comparison to the other subgroups, as well as within the subtypes of Group 3. I analyzed the expression of select target genes relevant to my thesis using the GSE85217 gene expression database, comprising a cohort of 763 primary MB samples [42]. In addition to this large cohort database, I also probed other geo-datasets GSE21140 and GSE37418 to assess if the gene expression pattern is comparable among the molecular subgroups [40,211].

4.2 Methods

4.2.1 Data mining of gene expression profiles from GEO datasets

The functional genomics data repository available on Gene Expression Omnibus was used to query specific gene expression profiles of MB patients. GEO datasets GSE85217, GSE21140 and GSE37410 were specifically chosen for the analysis due to molecular subgroup classification of primary MB samples and large cohort. Clinical information for each primary MB tumour were downloaded from GEO and supplemental information provided by the authors for each dataset. More details regarding the GEO dataset is listed in Table 4.1

Table 4.1: Additional information of GEO datasets used in this study.

GEO Accession	GSE85217	GSE21140	GSE37418
Title	Expression data from primary medulloblastoma samples	Genomics of medulloblastoma identifies four distinct molecular variants	Novel mutations target distinct subgroups of medulloblastoma
PubMed ID	28609654;30324512	20823417	22722829;26199091
Series Type	Expression profiling by array	Expression profiling by array	Expression profiling by array
Platform	[HuGene-1_1-st] Affymetrix Human Gene 1.1 ST Array [HuGene11stv1_Hs_ENS G version 19.0.0]	[HuEx-1_0-st] Affymetrix Human Exon 1.0 ST Array [transcript (gene) version]	[HG-U133_Plus_2] Affymetrix Human Genome U133 Plus 2.0 Array
Taxonomy	Homo sapiens	Homo sapiens	Homo sapiens
Cohort size	763	103	76
Clinical information	Age, gender, histological subtype, metastatic status, molecular subgroup and subtype.	Age, gender, histological subtype and molecular subgroup.	Age, gender, ethnicity, metastatic stage and molecular subgroup.

4.2.2 Method of analysis

Raw Affymetrix CEL files consisting of exon array data primary MB specimens from the following GEO series (GSE85217, GSE21140, GSE37418) were extracted to perform gene-level analysis. Gene expression values were downloaded from the Matrix file and gene nomenclature was acquired from the SOFT file. The BioGPS website (<http://biogps.org/>) was used to collect information regarding each gene reporter probe for different Affymetrix platforms. *STAT3*, *STAT5A*, *STAT5B*, *IL6*, *LIF*, *OSM*, *IL11*, *IL6R α* , *IL11R α* , *LIFR α* , *OSMR β* , *Gp130*, *E2F3*, *JAK1*, *JAK2*, *TYK2*, *SOCS1*, *SOCS3*, *PIAS3* gene expression values were consolidated based on their subgroup classifications and plotted using GraphPad.

4.2.3 Statistical analysis

The gene expression values for individual patients were plotted with mean and one standard deviation. Ordinary one-way ANOVA followed by Tukey's multiple comparisons test was performed for analysis of each molecular subgroup. Statistical analysis was performed only between Group 3 MB and other subgroups (WNT, SHH and Group 4) for the purpose of this study. The p-value is considered significant when it is <0.05 and the actual number is displayed for each graph. Non-significant (ns) comparisons were not shown. All graphs were plotted using GraphPad Prism (v9.2.0).

4.3 Results

4.3.1 *STAT3* expression is significantly enriched in Group 3 γ MB

In the largest GSE85217 dataset that consists of 763 primary MB samples, *STAT3* expression was found to be enriched in Group 3 and Group 4 MB (Figure 4.1A). Within Group 3 MB, *STAT3* expression was highest for Group 3 γ (Figure 4.1B), a subtype that is associated with the worst prognosis. Group 4 had the highest *STAT3* expression, thus subtype analysis was also carried out. When compared to Group 4 α and Group 4 γ , Group 4 β had the highest *STAT3* expression (Figure 4.1B). The clinical significance of this finding is unclear, since all three subtypes of Group 4 MB are associated with similar overall survival as well as incidence of metastasis.

In GSE21140, both Group 3 and Group 4 MB displayed increased *STAT3* expression when compared to SHH MB (Figure 4.1C). In the smallest sized cohort, GSE37418, the only difference in *STAT3* expression with statistical significance is observed between Group 3 and Group 4 (Figure 4.1D). It should be noted that smaller sample size representations for WNT and SHH subgroups in GSE37418, and for WNT in GSE21140, likely contributed to the lack of statistically significant difference for *STAT3* expression when compared to Group 3 and Group 4. Overall, a consistent trend that is observed in my analyses of the 3 GEO MB datasets suggests that *STAT3* expression is highest in Groups 3 and 4.

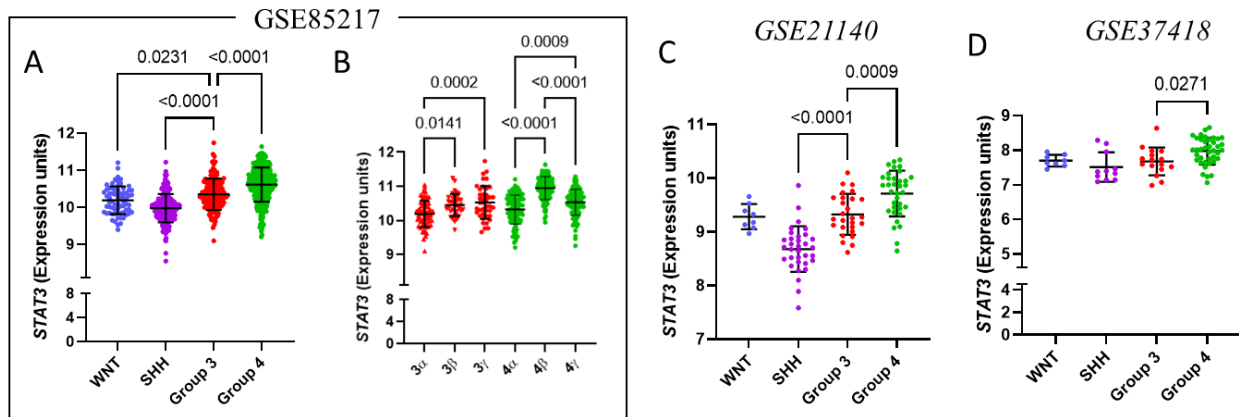


Figure 4.1: Expression of *STAT3* was analyzed according to their subgroup and subtype categorization.

The (A, B) GSE85217, (C) GSE21140 and (D) GSE37418 gene expression database is categorized into the 4 major subgroups WNT, SHH, Group 3 and Group 4. Group 3 MB from GSE85217 is further subcategorized into (B) 3 α , 3 β , and 3 γ subtypes for the purposes of this analysis. p-value (numbers) is displayed where significant ($p < 0.05$), one-way ANOVA with Tukey's post-test.

As reported by Cavalli *et al.* [42], analysis of the GSE85217 dataset revealed a worst overall 5-year survival for Group 3 MB patients when compared to other MB subgroups, and for Group 3 γ when compared to other subtypes within Group 3. Given that increased *STAT3* expression was observed in Group 3 and Group 3 γ (Figure 4.1A, B), I re-analyzed the GSE85217 dataset to determine if increased *STAT3* expression may correlate with poorer survival.

First, using the clinical dataset that accompanies GSE85217, I re-generated overall survival Kaplan-Meier plots that re-affirm the finding that Group 3 has the worst survival when compared with other MB subgroups (Figure 4.2A), while Group 3 γ has the worst survival when compared to other subtypes of Group 3 MB (Figure 4.2D). Then, I calculated the median expression for *STAT3* to facilitate survival analysis for MB patients categorized into high (upper 75% percentile) and low (lower 25% percentile) *STAT3* expression cohorts (Figure 4.2B, E and H). In this manner, no significant difference in 5-year overall survival was observed for all MB patients segregated into high or low *STAT3* expression (Figure 4.2C). Similarly, no significant difference in 5-year overall

survival was observed for Group 3 MB patients segregated into high or low *STAT3* expression (Figure 4.2F). Between the molecular subgroups, Group 4 MB patients have the highest *STAT3* levels. Survival analysis of Group 4 MB subtypes showed no significant difference in overall 5-year survival (Figure 4.2G). Additionally, for Group 4 MB, no significant difference in 5-year overall survival was observed between high and low *STAT3* expression (Figure 4.2I). In summary, *STAT3* expression levels at diagnosis do not serve as an indicator of overall survival in MB.

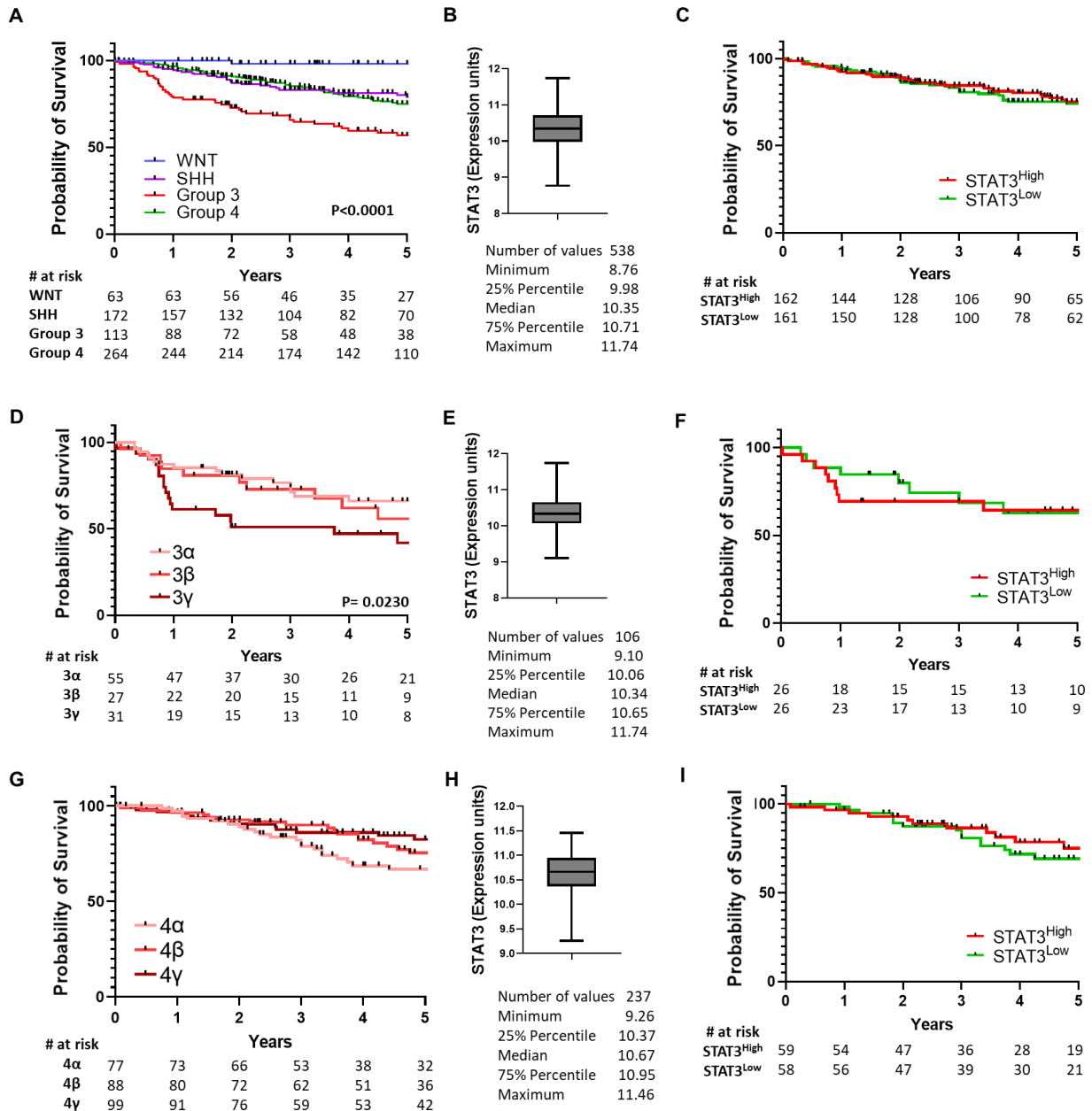


Figure 4.2: Correlation of *STAT3* expression with overall survival in MB.

Clinical data derived from GSE85217 dataset was used to generate Kaplan-Meier plots for 5-year survival of (A) MB subgroups, (D) Group 3 MB and (G) Group 4 MB subtypes. *STAT3* expression median with interquartile range was calculated for (B) all MB (n=538), (E) Group 3 MB (n=106) and (H) Group 4 MB (n=237). Kaplan-Meier plots for 5-year survival of (C) all MB, (F) Group 3 MB and (I) Group 4 MB divided into two populations designated with High (>75% percentile) or Low (<25% percentile) *STAT3* expression. Overall survival was right-censored at 5 years and *p*-values were reported (where significant) using the log-rank trend test. *Note that (A) and (B) is an independent reproduction of the plots originally published by Cavalli et al. [42] using the same dataset.*

In addition to *STAT3*, I also assessed the expression of *STAT5A* and *STAT5B* in the largest primary MB cohort (GSE85217). Similar to *STAT3*, constitutive activation of *STAT5* has been linked to disease progression in multiple malignancies [212], and *STAT5* is a known contributor to anti-tumour immunity by suppressing the immune response [213]. The analysis of GSE85217 revealed that Group 3 and Group 4 had elevated levels of *STAT5A* and *STAT5B* (Figure 4.3A and Figure 4.4A) Subtype analyses within Group 3 revealed that Group 3 γ expressed more *STAT5A* compared to Group 3 α and Group 3 β (Figure 4.3B), and more *STAT5B* compared to Group 3 β (Figure 4.4B). This suggests that increased levels of *STAT5A* and *STAT5B* associates with the worst prognosis in this cohort. No data was available for *STAT5A* or *STAT5B* in GSE21140. In GSE37418, *STAT5A* was significantly higher in Group 4 MB and *STAT5B* was significantly higher in Group 3 MB compared to WNT MB.

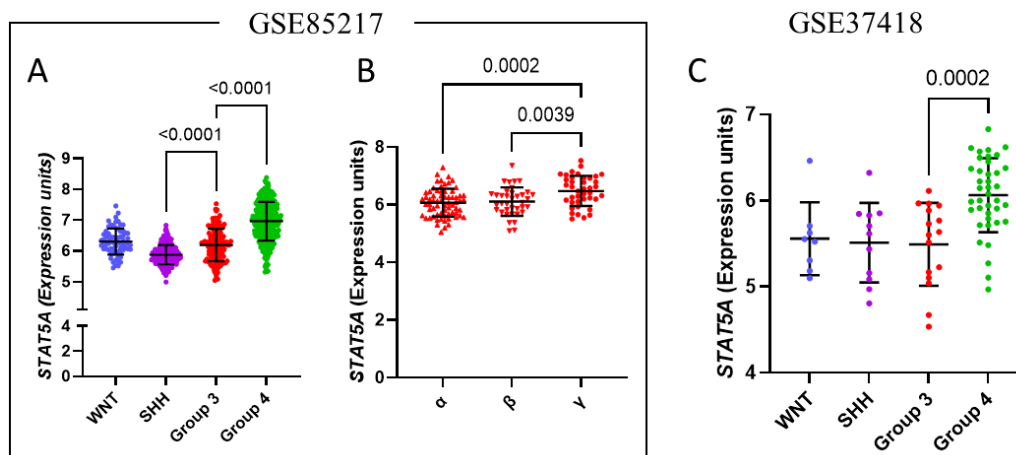


Figure 4.3: Expression of *STAT5A* was analyzed according to their subgroup and subtype categorization.

The (A, B) GSE85217 and (C) GSE37418 gene expression database is categorized into the 4 major subgroups WNT, SHH, Group 3 and Group 4. Group 3 MB from GSE85217 is further subcategorized into (B) 3 α , 3 β , and 3 γ subtypes for the purposes of this analysis. p-value (numbers) is displayed where significant ($p < 0.05$), one-way ANOVA with Tukey's post-test.

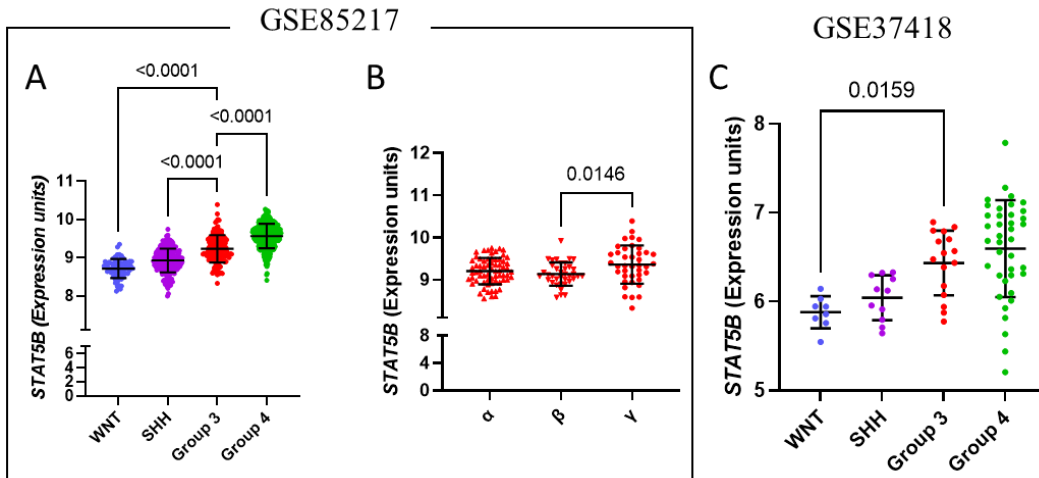


Figure 4.4: Expression of *STAT5B* was analyzed according to their subgroup and subtype categorization.

The (A, B) GSE85217 and (C) GSE37418 gene expression database is categorized into the 4 major subgroups WNT, SHH, Group 3 and Group 4. Group 3 MB from GSE85217 is further subcategorized into (B) 3 α , 3 β , and 3 γ subtypes for the purposes of this analysis. p-value (numbers) is displayed where significant ($p < 0.05$), one-way ANOVA with Tukey's post-test.

Among the three datasets, Group 4 MB exhibited the highest *STAT3* expression levels compared to other molecular subgroups. Cavalli *et al.* also found that there was a significant overlap across Group 3 MB and Group 4 MB at the sub clonal level. Further investigation is required at the cellular level like single-cell RNA sequencing data to bifurcate the subgroups efficiently to reveal common mechanisms and origins. A summary of key findings for *STAT3*, *STAT5A* and *STAT5B* expression in relation to Group 3 is also presented in Table 4.2.

Table 4.2: Summary of *STAT3*, *STAT5A* and *STAT5B* expression in GSE85217, GSE21140 and GSE37418 in comparison to Group 3 MB

Gene	Group 3 vs	GSE85217	GSE21140	GSE37418
<i>STAT3</i>	WNT	+	ns	ns
	SHH	+	+	ns
	Group 4	-	-	-
<i>STAT5A</i>	WNT	ns		ns
	SHH	+		ns
	Group 4	-		-
<i>STAT5B</i>	WNT	+		+
	SHH	+		ns
	Group 4	-		ns

+ indicates gene expression is **significantly higher** in Group 3

- indicates gene expression is **significantly lower** in Group 3

ns indicates no significant difference

blank space indicates no data available for analysis

4.3.2 Group 3 MB is associated with reduced *JAK1* expression.

Of the four JAKs, I performed analyses for *JAK1*, *JAK2* and *TYK2* expression on the basis of their association with class II cytokine receptors that contain gp130 [129]. In GSE85217 and GSE21140, *JAK1* expression was significantly lower in Group 3 MB when compared to the other subgroups (Figure 4.5A, C). Subtype analysis revealed that Group 3 γ exhibit reduced *JAK1* expression compared to Group 3 β (Figure 4.5B).

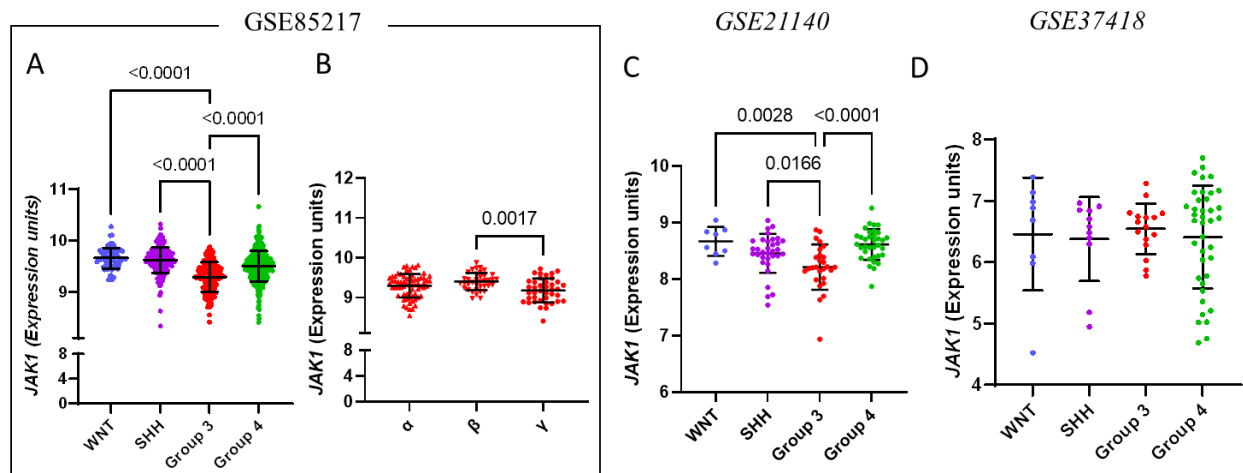


Figure 4.5: Expression of *JAK1* was analyzed according to their subgroup and subtype categorization.

The (A, B) GSE85217, (C) GSE21140 and (D) GSE37418 gene expression database is categorized into the 4 major subgroups WNT, SHH, Group 3 and Group 4. Group 3 MB from GSE85217 is further subcategorized into (B) 3 α , 3 β , and 3 γ subtypes for the purposes of this analysis. p-value (numbers) is displayed where significant ($p < 0.05$), one-way ANOVA with Tukey's post-test.

JAK2 expression was significantly lower in Group 3 MB when compared to Group 4 in GSE85217 and GSE21140 (Figure 4.6A, C), Within Group 3 MB, subtype 3 γ exhibited the lowest *JAK2* expression despite the unfavourable outcome depicted by this subtype (Figure 4.6B). *TYK2* expression was significantly elevated in Group 3 MB compared to Group 4 MB in all three datasets (Figure 4.7A, B, and C). Subtype analysis revealed that Group 3 γ exhibit reduced *TYK2* expression compared to Group 3 β (Figure 4.7B). Due to the smaller sample sizes and very large error bars, no interpretation could be derived from *JAK1* and *JAK2* analysis of the GSE37418 dataset. A summary of key findings for *JAK1*, *JAK2* and *TYK2* expression in relation to Group 3 is also presented in Table 4.3.

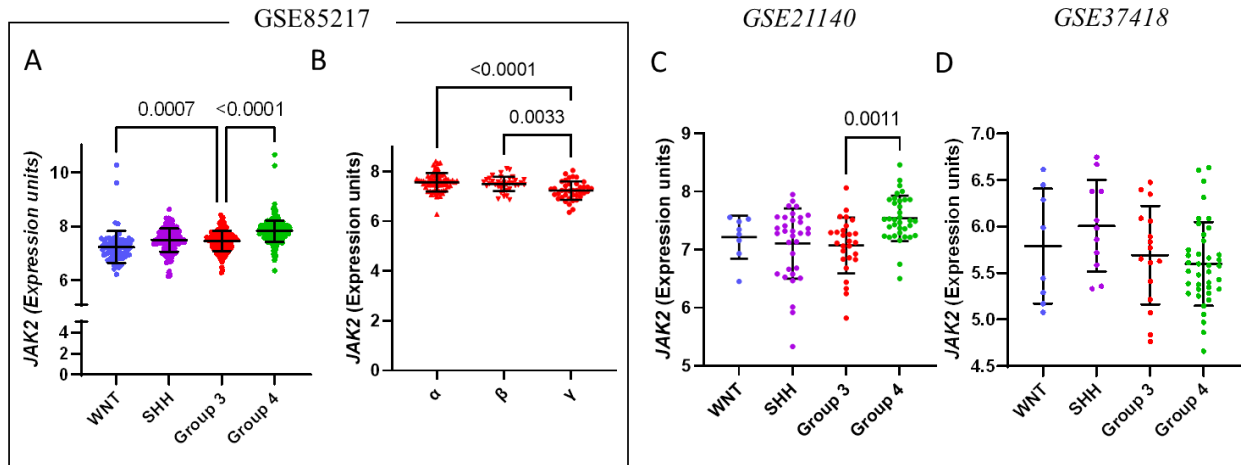


Figure 4.6: Expression of *JAK2* was analyzed according to their subgroup and subtype categorization.

The (A, B) GSE85217, (C) GSE21140 and (D) GSE37418 gene expression database is categorized into the 4 major subgroups WNT, SHH, Group 3 and Group 4. Group 3 MB from GSE85217 is further subcategorized into (B) 3 α , 3 β , and 3 γ subtypes for the purposes of this analysis. p-value (numbers) is displayed where significant ($p < 0.05$), one-way ANOVA with Tukey's post-test.

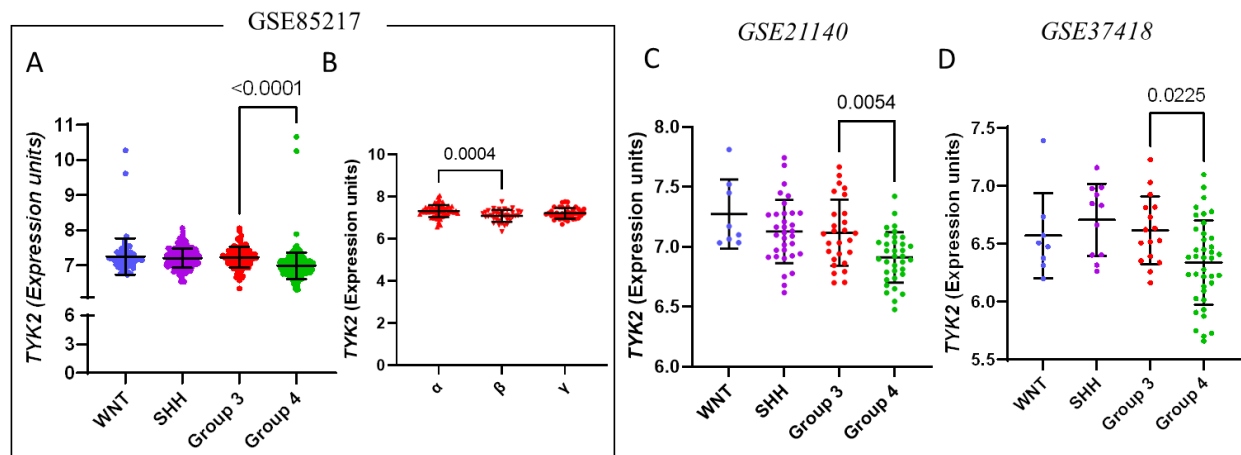


Figure 4.7: Expression of *TYK2* was analyzed according to their subgroup and subtype categorization.

The (A, B) GSE85217, (C) GSE21140 and (D) GSE37418 gene expression database is categorized into the 4 major subgroups WNT, SHH, Group 3 and Group 4. Group 3 MB from GSE85217 is further subcategorized into (B) 3 α , 3 β , and 3 γ subtypes for the purposes of this analysis. p-value (numbers) is displayed where significant ($p < 0.05$), one-way ANOVA with Tukey's post-test.

Table 4.3: Summary of *JAK1*, *JAK2* and *TYK2* expression in GSE85217, GSE21140 and GSE37418 in comparison to Group 3 MB.

Gene	Group 3 Vs	GSE85217	GSE21140	GSE37418
<i>JAK1</i>	<i>WNT</i>	-	-	ns
	<i>SHH</i>	-	-	ns
	<i>Group 4</i>	-	-	ns
<i>JAK2</i>	<i>WNT</i>	+	ns	ns
	<i>SHH</i>	ns	ns	ns
	<i>Group 4</i>	-	-	ns
<i>TYK2</i>	<i>WNT</i>	ns	ns	ns
	<i>SHH</i>	ns	ns	ns
	<i>Group 4</i>	+	+	+

+ indicates gene expression is **significantly higher** in Group 3 MB

- indicates gene expression is **significantly lower** in Group 3 MB

ns indicates no significant difference

blank space indicates no data available for analysis

4.3.3 Expression analyses of the IL-6 family cytokines and their receptors.

4.3.3.1 Expression analyses of *IL6*, *IL6R* and *E2F3*.

Expression of *IL6* was significantly higher in Group 3 MB only when compared to SHH MB in GSE85217, but were otherwise not remarkable between the different major groups, nor between the Group 3 subtypes (Figure 4.8A, C, D). For *IL6*, no significant difference was observed within the Group 3 MB subtypes (Figure 4.8B). Expression of the corresponding receptor, *IL6R* were not significantly different between all MB subgroups (Figure 4.9A). Within Group 3 MB, *IL6R* expression was higher in Group 3 γ and Group 3 β when compared to Group 3 α (Figure 4.9B).

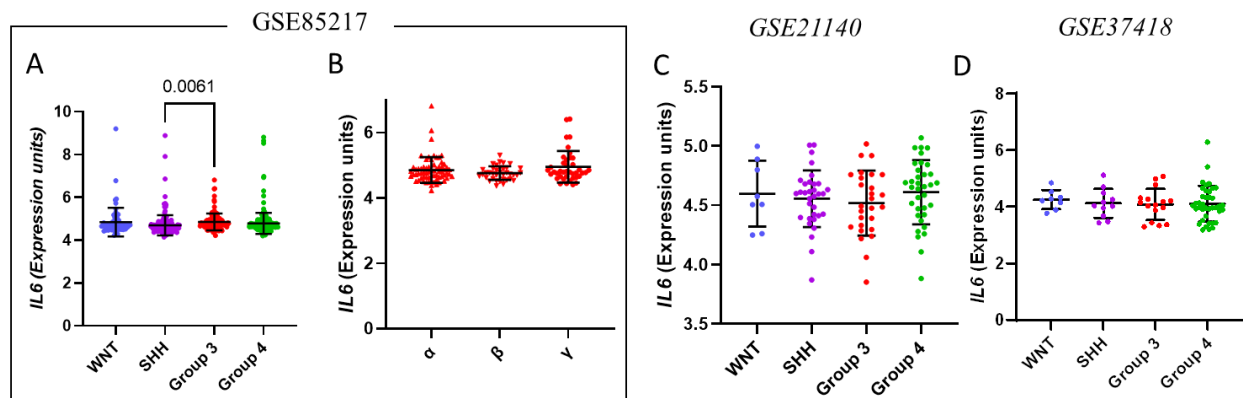


Figure 4.8: Expression of *IL6* was analyzed according to their subgroup and subtype categorization.

The (A, B) GSE85217, (C) GSE21140 and (D) GSE37418 gene expression database is categorized into the 4 major subgroups WNT, SHH, Group 3 and Group 4. Group 3 MB from GSE85217 is further subcategorized into (B) 3 α , 3 β , and 3 γ subtypes for the purposes of this analysis. p-value (numbers) is displayed where significant ($p < 0.05$), one-way ANOVA with Tukey's post-test.

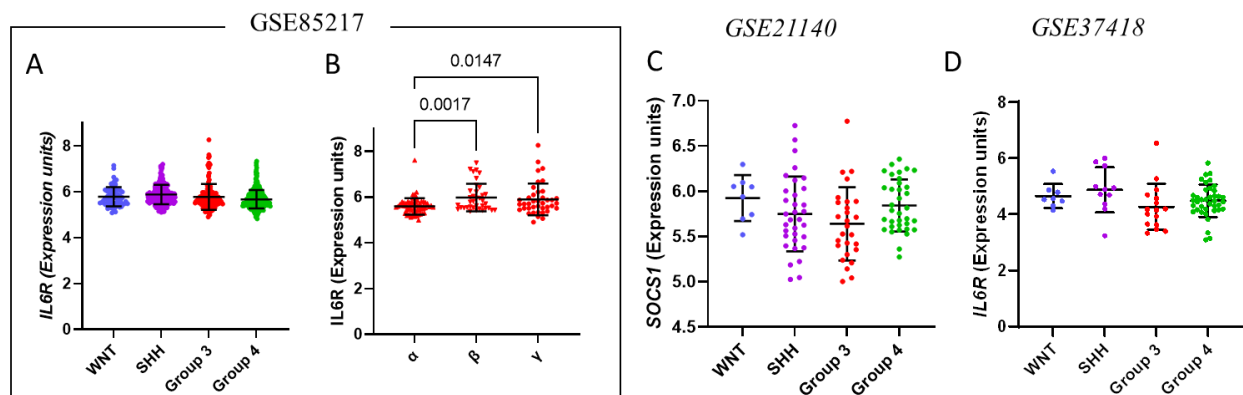


Figure 4.9: Expression of *IL6R* was analyzed according to their subgroup and subtype categorization.

The (A, B) GSE85217, (C) GSE21140 and (D) GSE37418 gene expression database is categorized into the 4 major subgroups WNT, SHH, Group 3 and Group 4. Group 3 MB from GSE85217 is further subcategorized into (B) 3 α , 3 β , and 3 γ subtypes for the purposes of this analysis. p-value (numbers) is displayed where significant ($p < 0.05$), one-way ANOVA with Tukey's post-test.

In addition, I assessed the expression of *E2F3*, a transcription factor shown to directly bind the promoter of *IL6R* and regulate its expression [179]. In GSE85719, *E2F3* expression was

elevated in Group 3 and Group 4 MB subgroups (Figure 4.10A). Within Group 3 MB, *E2F3* was significantly higher in Group 3 γ when compared to Group 3 α and Group 3 β (Figure 4.10B). In GSE21140 and GSE37418, *E2F3* was significantly elevated in Group 3 MB compared to WNT MB (Figure 4.10C, D). In summary, increased *STAT3* expression was correlated with increased *IL-6R* in subtype Group 3 γ when compared to Group 3 α , and is suggestive of increased sensitivity to *IL-6* cytokine stimulation of *STAT3* activity. A summary of key findings for *IL6*, *IL6R* and *E2F3* expression in relation to Group 3 is also presented in Table 4.4.

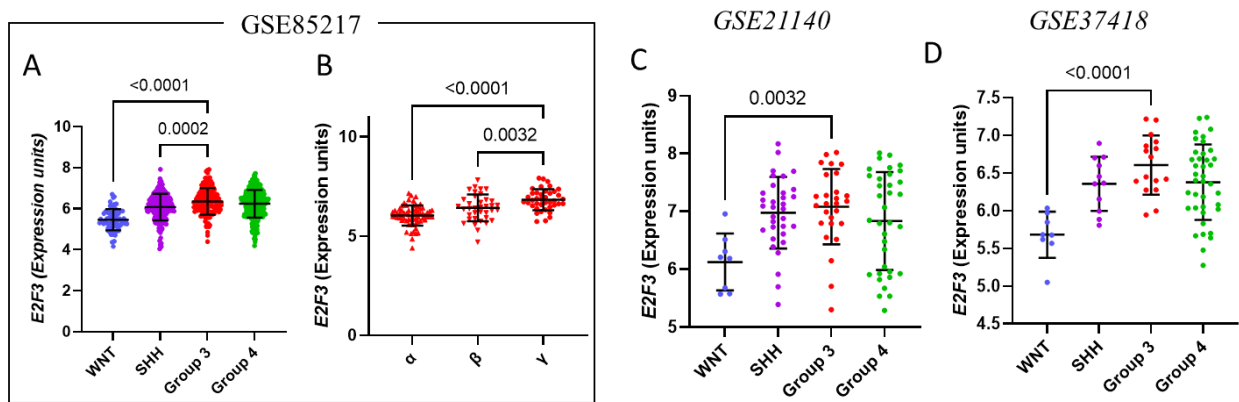


Figure 4.10: Expression of *E2F3* was analyzed according to their subgroup and subtype categorization.

The (A, B) GSE85217, (C) GSE21140 and (D) GSE37418 gene expression database is categorized into the 4 major subgroups WNT, SHH, Group 3 and Group 4. Group 3 MB from GSE85217 is further subcategorized into (B) 3 α , 3 β , and 3 γ subtypes for the purposes of this analysis. p-value (numbers) is displayed where significant ($p < 0.05$), one-way ANOVA with Tukey's post-test.

Table 4.4: Summary of *IL6*, *IL6R* and *E2F3* expression in GSE85217, GSE21140 and GSE37418 in comparison to Group 3 MB.

Gene	Group 3 Vs	GSE85217	GSE21140	GSE37418
<i>IL6</i>	<i>WNT</i>	ns	ns	ns
	<i>SHH</i>	+	ns	ns
	<i>Group 4</i>	ns	ns	ns
<i>IL6R</i>	<i>WNT</i>	ns	ns	ns
	<i>SHH</i>	ns	ns	ns
	<i>Group 4</i>	ns	ns	ns
<i>E2F3</i>	<i>WNT</i>	+	+	+
	<i>SHH</i>	+	ns	ns
	<i>Group 4</i>	ns	ns	ns

+ indicates gene expression is **significantly higher** in Group 3 MB

- indicates gene expression is **significantly lower** in Group 3 MB

ns indicates no significant difference

blank space indicates no data available for analysis

4.3.3.2 Expression analyses of *LIF*, *LIFR*, *OSM*, *OSMR*, *IL11*, *IL11R* and *Gp130*.

WNT MB was found to have elevated levels of *LIF* compared to Group 3 MB in GSE 85217 and GSE37418 (Figure 4.11A, D). *LIFR* expression was significantly lower in Group 3 MB when compared to SHH MB and was consistent among the three datasets (Figure 4.12A, C, D). Group 3 MB subtypes showed no remarkable difference in *LIF* and *LIFR* expression (Figure 4.11B and Figure 4.12B). Given that WNT is an MB subgroup associated with the best overall survival, high *LIF* expression may be suggestive of an improved outcome.

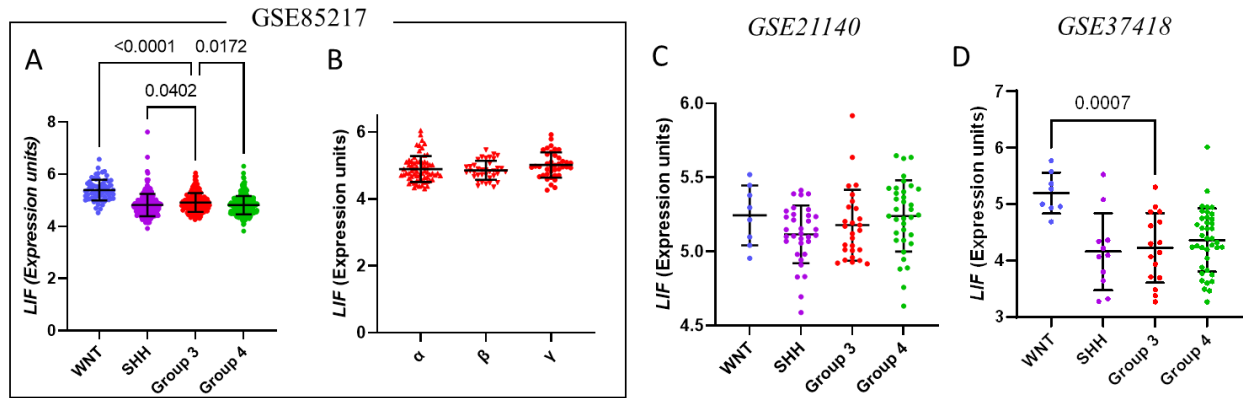


Figure 4.11: Expression of *LIF* was analyzed according to their subgroup and subtype categorization.

The (A, B) GSE85217, (C) GSE21140 and (D) GSE37418 gene expression database is categorized into the 4 major subgroups WNT, SHH, Group 3 and Group 4. Group 3 MB from GSE85217 is further subcategorized into (B) 3α , 3β , and 3γ subtypes for the purposes of this analysis. p-value (numbers) is displayed where significant ($p < 0.05$), one-way ANOVA with Tukey's post-test.

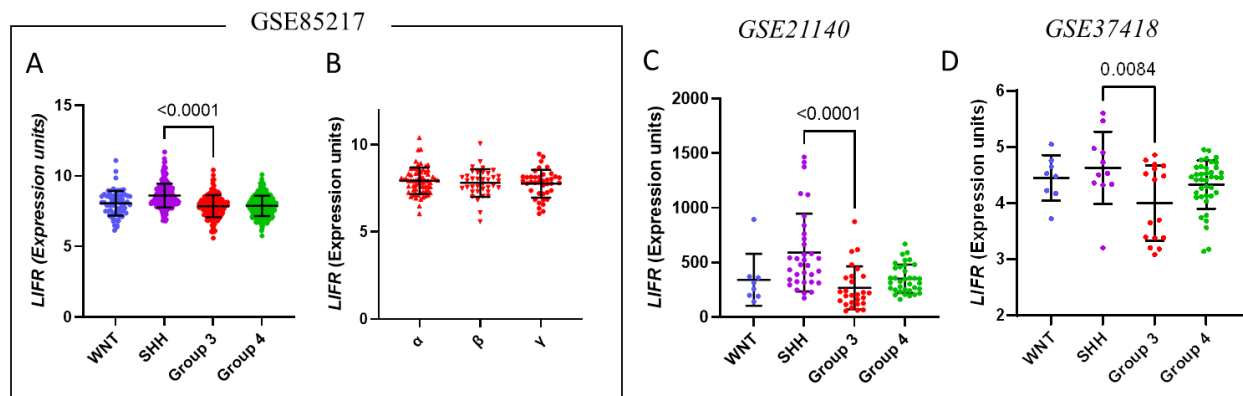


Figure 4.12: Expression of *LIFR* was analyzed according to their subgroup and subtype categorization.

The (A, B) GSE85217, (C) GSE21140 and (D) GSE37418 gene expression database is categorized into the 4 major subgroups WNT, SHH, Group 3 and Group 4. Group 3 MB from GSE85217 is further subcategorized into (B) 3α , 3β , and 3γ subtypes for the purposes of this analysis. p-value (numbers) is displayed where significant ($p < 0.05$), one-way ANOVA with Tukey's post-test.

OSM expression was reduced in Group 3 MB when compared to WNT MB in GSE85217, however this finding was not replicated in the other datasets with smaller cohort sizes (Figure 4.13). No notable difference in *OSM* levels was detected within the subtypes of Group 3 MB (Figure 4.13B) WNT MB exhibited increased levels of *OSMR* compared to Group 3 MB consistently among the three datasets (Figure 4.14A, C, D). Within the subtypes of Group 3, *OSMR* was significantly elevated in Group 3 γ , the subtype with the least favourable outcome (Figure 4.14B).

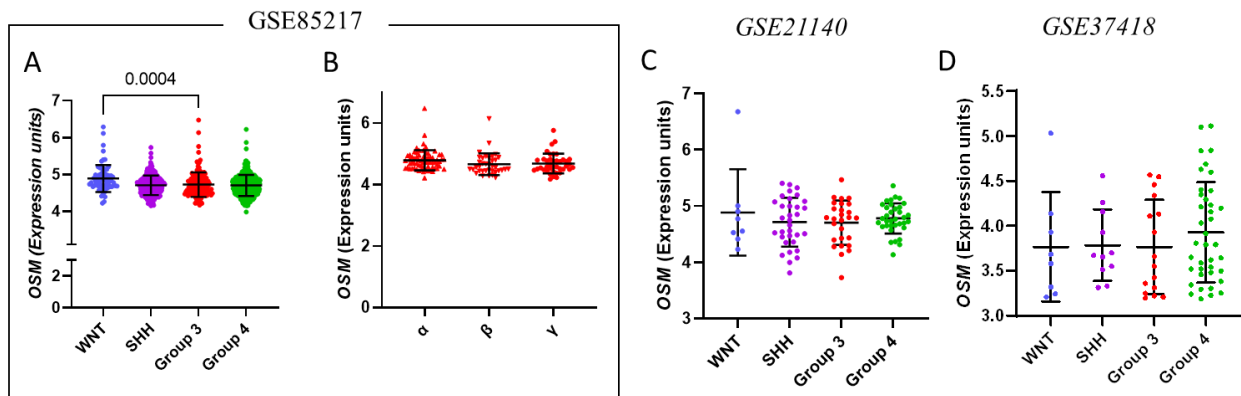


Figure 4.13: Expression of *OSM* was analyzed according to their subgroup and subtype categorization.

The (A, B) GSE85217, (C) GSE21140 and (D) GSE37418 gene expression database is categorized into the 4 major subgroups WNT, SHH, Group 3 and Group 4. Group 3 MB from GSE85217 is further subcategorized into (B) 3 α , 3 β , and 3 γ subtypes for the purposes of this analysis. p-value (numbers) is displayed where significant ($p < 0.05$), one-way ANOVA with Tukey's post-test.

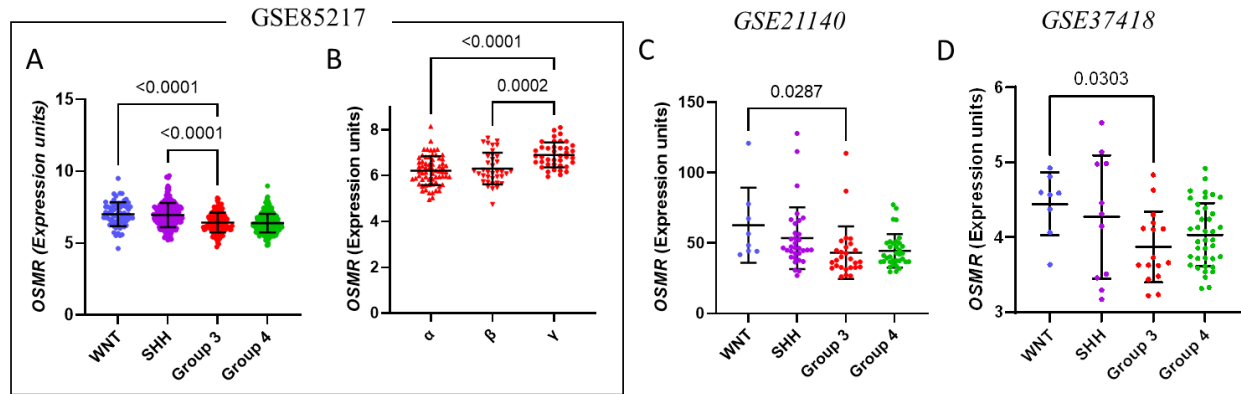


Figure 4.14: Expression of *OSMR* was analyzed according to their subgroup and subtype categorization.

The (A, B) GSE85217, (C) GSE21140 and (D) GSE37418 gene expression database is categorized into the 4 major subgroups WNT, SHH, Group 3 and Group 4. Group 3 MB from GSE85217 is further subcategorized into (B) 3 α , 3 β , and 3 γ subtypes for the purposes of this analysis. p-value (numbers) is displayed where significant ($p < 0.05$), one-way ANOVA with Tukey's post-test.

IL11 expression was significantly elevated in Group 3 MB when compared to SHH in GSE85217 and GSE21140, and when compared to Group 4 MB in GSE85217 (Figure 4.15A, C). Within Group 3, *IL11* was reduced in Group 3 γ in comparison to Group 3 α (Figure 4.15B). *IL11R* expression was consistently higher in Group 3 MB when compared to Group 4 MB in all three datasets, and when compared to SHH in GSE85217 and GSE21140 (Figure 4.16A, C). In contrast, *IL11R* expression was lower in Group 3 MB when compared to WNT MB in GSE85217 and GSE21140. In addition, a consistent trend observed in all three data sets suggested that *IL11R* expression was highest in WNT MB (Figure 4.16A, C, D). Within Group 3 MB, *IL11R* expression was highest in Group 3 α , and lowest in Group 3 β (Figure 4.16B).

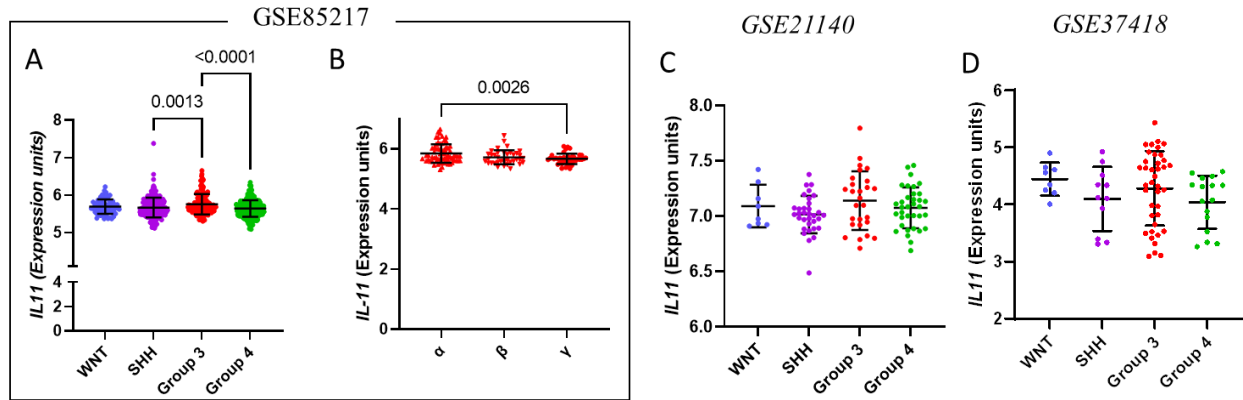


Figure 4.15: Expression of *IL11* was analyzed according to their subgroup and subtype categorization.

The (A, B) GSE85217, (C) GSE21140 and (D) GSE37418 gene expression database is categorized into the 4 major subgroups WNT, SHH, Group 3 and Group 4. Group 3 MB from GSE85217 is further subcategorized into (B) 3α , 3β , and 3γ subtypes for the purposes of this analysis. p-value (numbers) is displayed where significant ($p < 0.05$), one-way ANOVA with Tukey's post-test.

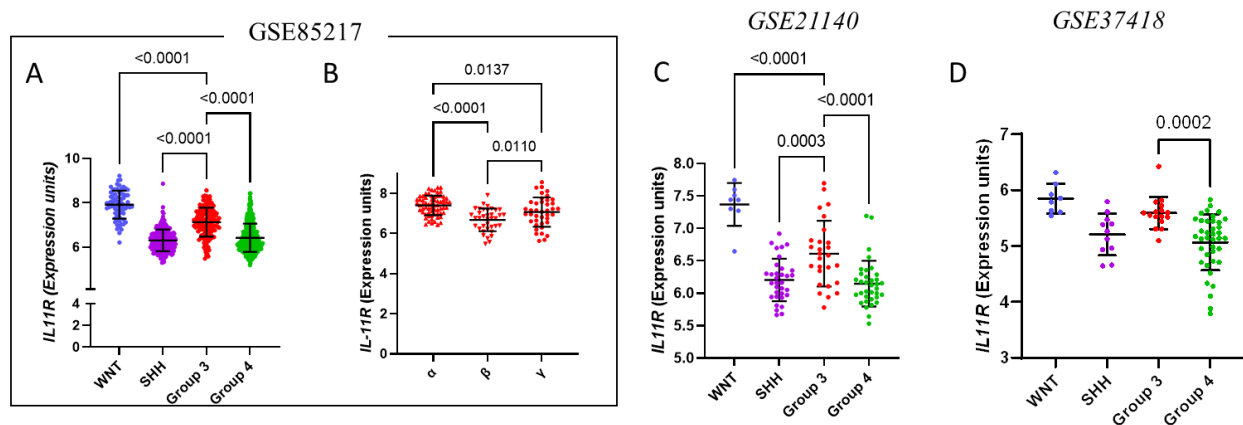


Figure 4.16: Expression of *IL11R* was analyzed according to their subgroup and subtype categorization.

The (A, B) GSE85217, (C) GSE21140 and (D) GSE37418 gene expression database is categorized into the 4 major subgroups WNT, SHH, Group 3 and Group 4. Group 3 MB from GSE85217 is further subcategorized into (B) 3α , 3β , and 3γ subtypes for the purposes of this analysis. p-value (numbers) is displayed where significant ($p < 0.05$), one-way ANOVA with Tukey's post-test.

As mentioned previously, Gp130 is a common subunit for the IL-6 subfamily of cytokine receptors, hence its expression might serve as a pan-indicator for the entire subfamily. In GSE85217, *GP130* expression was higher in comparison to Group 4, and lower in comparison to

WNT and SHH MB (Figure 4.17A). In GSE37418, *GP130* was reduced in Group 3 when compared to WNT, while no significant differences between the subgroups was evident in the GSE21140 dataset (Figure 4.17C, D). No significant differences in *GP130* levels was detected when comparing the subtypes of Group 3 MB (Figure 4.17B). Overall, some of the IL-6 family cytokines and their receptor gene expression was consistent across the three datasets. However, a larger primary MB sample size is required to derive conclusion from these data. A summary of key findings for expression of *LIF*, *LIFR*, *OSM*, *OSMR*, *IL11*, *IL11R* and *gp130* in relation to Group 3 is presented in Table 4.5.

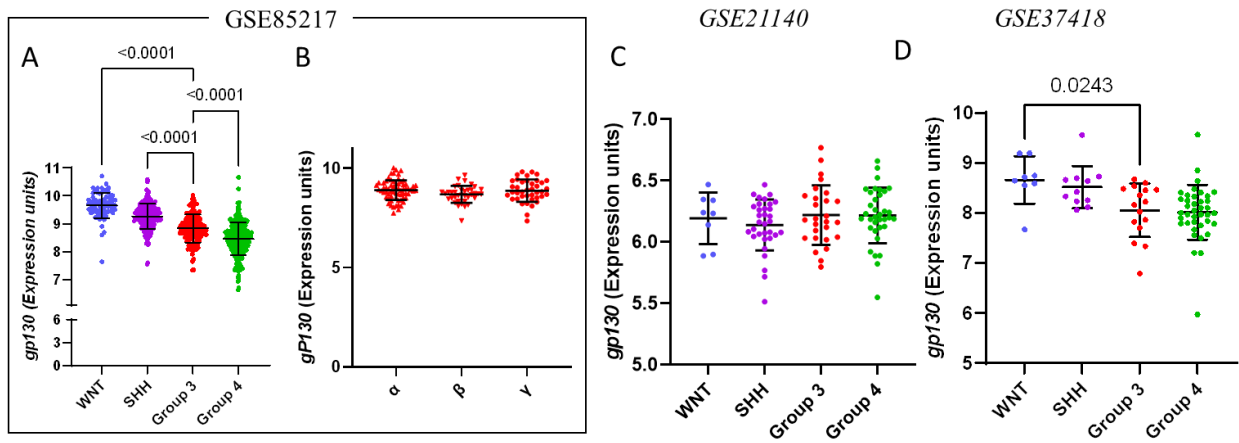


Figure 4.17: Expression of *GP130* was analyzed according to their subgroup and subtype categorization.

The (A, B) GSE85217, (C) GSE21140 and (D) GSE37418 gene expression database is categorized into the 4 major subgroups WNT, SHH, Group 3 and Group 4. Group 3 MB from GSE85217 is further subcategorized into (B) 3 α , 3 β , and 3 γ subtypes for the purposes of this analysis. p-value (numbers) is displayed where significant (p < 0.05), one-way ANOVA with Tukey's post-test.

Table 4.5: Summary of *LIF*, *LIFR*, *OSM*, *OSMR*, *IL11*, *IL11R* and *Gp130* expression in GSE85217, GSE21140 and GSE37418 in comparison to Group 3 MB.

Gene	Group 3 Vs	GSE85217	GSE21140	GSE37418
<i>LIF</i>	<i>WNT</i>	-	ns	-
	<i>SHH</i>	+	ns	ns
	<i>Group 4</i>	+	ns	ns
<i>LIFR</i>	<i>WNT</i>	ns	ns	ns
	<i>SHH</i>	-	-	-
	<i>Group 4</i>	ns	ns	ns
<i>OSM</i>	<i>WNT</i>	-	ns	ns
	<i>SHH</i>	ns	ns	ns
	<i>Group 4</i>	ns	ns	ns
<i>OSMR</i>	<i>WNT</i>	-	-	-
	<i>SHH</i>	-	ns	ns
	<i>Group 4</i>	ns	ns	ns
<i>IL11</i>	<i>WNT</i>	ns	ns	ns
	<i>SHH</i>	+	+	ns
	<i>Group 4</i>	+	ns	ns
<i>IL11R</i>	<i>WNT</i>	-	-	ns
	<i>SHH</i>	+	+	ns
	<i>Group 4</i>	+	+	+
<i>GPI30</i>	<i>WNT</i>	-	ns	-
	<i>SHH</i>	-	ns	ns
	<i>Group 4</i>	+	ns	ns

+ indicates gene expression is **significantly higher** in Group 3 MB

- indicates gene expression is **significantly lower** in Group 3 MB

ns indicates no significant difference

blank space indicates no data available for analysis

4.3.4 Expression analyses of negative feedback regulators of IL-6/STAT3 signaling.

In this section, I analyzed the expression of several key negative regulators of IL-6/STAT3 signaling, specifically *SOCS1*, *SOCS3* and *PIAS3* (Protein inhibitor of activated STAT3). As mentioned in section 1.7.3, *SOCS1* and *SOCS3* are cytokine inducible members of the STAT-induced STAT inhibitors (SSI). Mechanistically, *SOCS1* and *SOCS3* proteins can bind JAKs and gp130 respectively to inhibit their binding to STAT proteins [214,215]. *PIAS3* is a protein that can bind to the DNA-binding domain of STAT3 to repress its transcriptional activity, hence *PIAS3* is a direct and major negative regulator of STAT3 [216].

Analysis of GSE85217 revealed that *SOCS1* expression was lowest in Group 3 MB, a finding that is suggestive of a weaker negative feedback regulation of IL-6/STAT3 signaling in this MB subgroup with the worst prognosis (Figure 4.18A). Within Group 3 MB, subtype Group 3 β exhibited the highest level of *SOCS1* compared to the more metastatic subtypes, Group 3 α and Group 3 γ (Figure 4.18B). In the same dataset, *SOCS3* expression was found to be lower in Group 3 when compared to Group 4, but higher when compared to SHH (Figure 4.19A). Within Group 3 MB, subtype Group 3 γ exhibited higher *SOCS3* expression when compared to Group 3 β (Figure 4.19B). However, there was no remarkable difference in *SOCS1* or *SOCS3* expression found in primary MB samples from GSE21140 and GSE37418 (Figure 4.18C, D; Figure 4.19C, D).

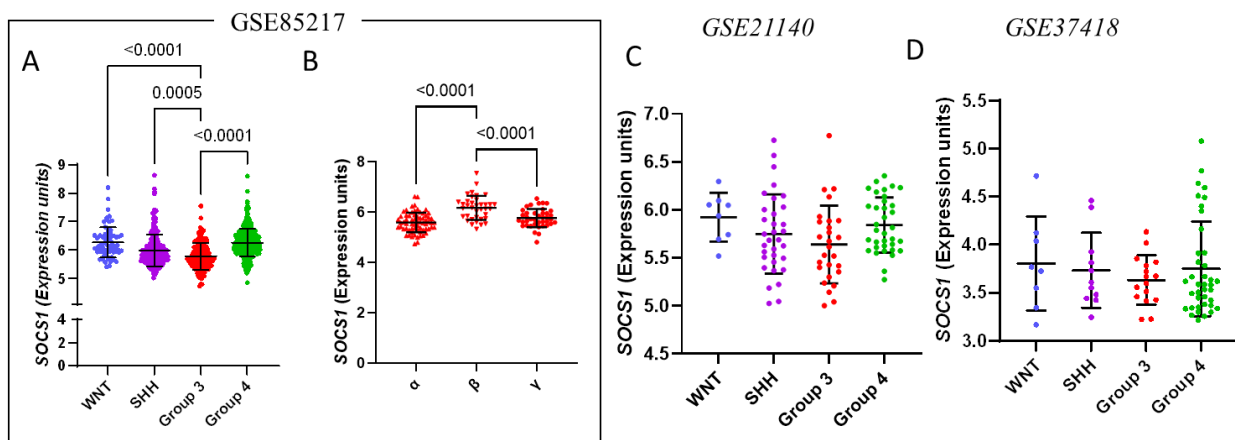


Figure 4.18: Expression of *SOCS1* was analyzed according to their subgroup and subtype categorization.

The (A, B) GSE85217, (C) GSE21140 and (D) GSE37418 gene expression database is categorized into the 4 major subgroups WNT, SHH, Group 3 and Group 4. Group 3 MB from GSE85217 is further subcategorized into (B) 3 α , 3 β , and 3 γ subtypes for the purposes of this analysis. p-value (numbers) is displayed where significant ($p < 0.05$), one-way ANOVA with Tukey's post-test.

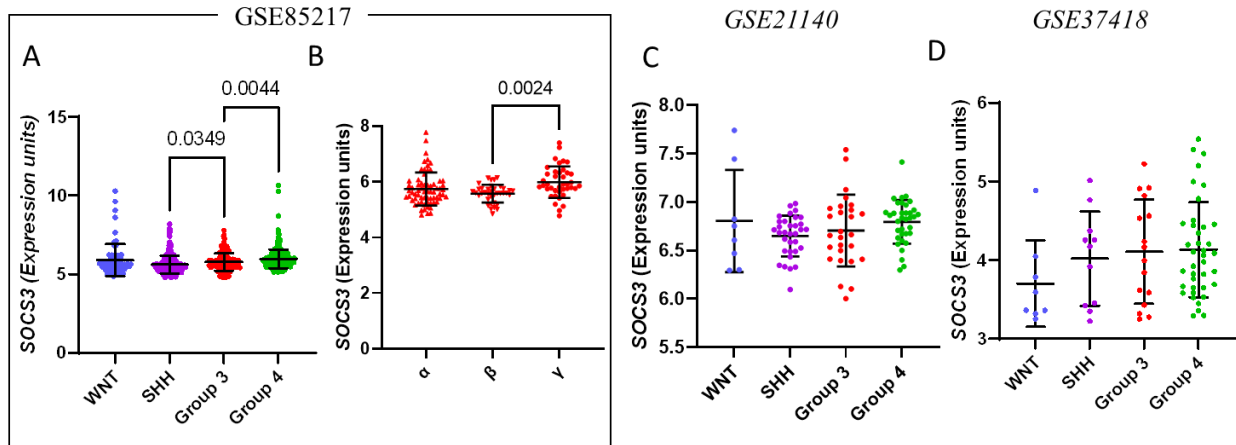


Figure 4.19: Expression of *SOCS3* was analyzed according to their subgroup and subtype categorization.

The (A, B) GSE85217, (C) GSE21140 and (D) GSE37418 gene expression database is categorized into the 4 major subgroups WNT, SHH, Group 3 and Group 4. Group 3 MB from GSE85217 is further subcategorized into (B) 3 α , 3 β , and 3 γ subtypes for the purposes of this analysis. p-value (numbers) is displayed where significant ($p < 0.05$), one-way ANOVA with Tukey's post-test.

PIAS3 expression was significantly lower in Group 3 MB when compared to SHH MB in all three datasets (Figure 4.20A, C, D). In addition, *PIAS3* expression was also lower in Group 3 MB when compared to WNT MB in GSE85217 and GSE21140 (Figure 4.20A, C). Lower *PIAS3* expression in Group 3 and Group 4 MB correlated with the enriched STAT3 expression observed in these molecular subgroups. Group 3 γ , an MB subtype with the lowest overall survival and high metastatic incidence, was found to have low *PIAS3* expression (Figure 4.20B). Overall, this analysis revealed that *PIAS3* and *SOCS1* gene expression is lower in Group 3 MB indicating a feeble negative feedback mechanism in this cohort. A summary of the key findings for expression of *SOCS1*, *SOCS3* and *PIAS3* in relation to Group 3 is presented in Table 4.6.

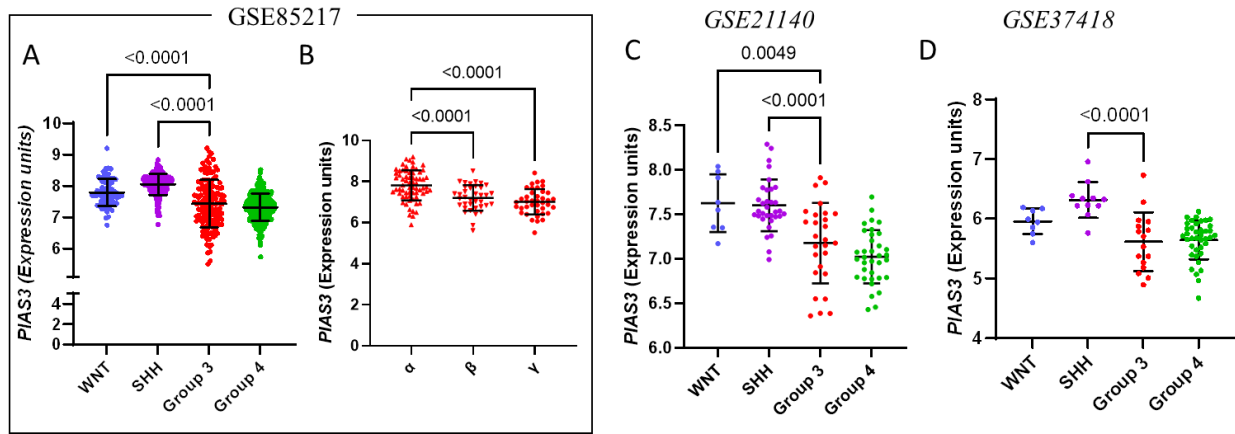


Figure 4.20: Expression of *PIAS3* was analyzed according to their subgroup and subtype categorization.

The (A, B) GSE85217, (C) GSE21140 and (D) GSE37418 gene expression database is categorized into the 4 major subgroups WNT, SHH, Group 3 and Group 4. Group 3 MB from GSE85217 is further subcategorized into (B) 3 α , 3 β , and 3 γ subtypes for the purposes of this analysis. p-value (numbers) is displayed where significant ($p < 0.05$), one-way ANOVA with Tukey's post-test.

Table 4.6: Summary of *SOCS1*, *SOCS3* and *PIAS3* expression in GSE85217, GSE21140 and GSE37418 in comparison to Group 3 MB.

Gene	Group 3 Vs	GSE85217	GSE21140	GSE37418
SOCS1	<i>WNT</i>	-	ns	ns
	<i>SHH</i>	-	ns	ns
	<i>Group 4</i>	-	ns	ns
SOCS3	<i>WNT</i>	ns	ns	ns
	<i>SHH</i>	+	ns	ns
	<i>Group 4</i>	-	ns	ns
PIAS3	<i>WNT</i>	-	ns	-
	<i>SHH</i>	-	-	-
	<i>Group 4</i>	ns	ns	ns

+ indicates gene expression is **significantly higher** in Group 3 MB

- indicates gene expression is **significantly lower** in Group 3 MB

ns indicates no significant difference

blank space indicates no data available for analysis

4.4 Discussion

Several recent landmark papers have contributed to an extraordinary amount of information regarding the four distinct molecular subgroups of MB. The molecular classification of MB that was based on transcriptional profiling has led to a better understanding of their disease origin, treatment response and clinical outcomes. Clinical characteristics and DNA methylation array documented along with microarray transcriptome data has provided a new perspective about the disease. In particular, the rich gene expression data will be beneficial to identify genes associated with pathogenesis of MB subgroups and pave the way to discovery of novel targeted therapeutic strategies.

Among the four molecular subgroups, Group 3 MB manifest as high-risk tumors due to poor overall survival and highest rates of metastasis at diagnosis [23,45]. WNT MB and SHH MB have a defined signaling pathway where mutations in the pathway components contributes to MB tumorigenesis and disease progression. In contrast, Group 3 and Group 4 MB harbour mutations and chromosomal aberrations that do not have a particular signaling pathway or pathways that define their pathogenesis. My experimental findings described in Chapters 2 and 3 showed that constant exposure of MB cells to pro-inflammatory cytokines found in the brain TME and activation of JAK/STAT3 signaling led to development of chemoresistance in Group 3 MB cell lines. To provide a functional biological context and assess the translational potential to our experimental findings, I analyzed the expression of major components involved in the IL-6/STAT3 signaling axis in MB transcriptome databases to gain some clinical insights.

Rationalizing that IL-6 signaling primarily feeds into activation of STAT3, I began my analysis by assessing if *STAT3* gene expression could be correlated to the MB subgroups, with particular emphasis on Group 3. Enriched *STAT3* levels was observed in Group 3 MB and Group

4 MB. Within the subgroup classification reported by Cavalli et al., Group 3 γ subtype has the least favorable outcome, with high *MYC* amplification and frequent metastasis that correlated with increased *STAT3* expression. It was also revealed that Group 3 α and Group 3 β patients are associated with loss of *MYC* and balanced *MYC* respectively. *MYC* amplified tumours were found to have the lowest overall survival compared to non-*MYC* amplified tumours in the 763 primary MB cohort [42]. As previously discussed in Chapter 2, *MYC* is a transcription factor that acts downstream of *STAT3* and that is a prominent driver of Group 3 MB. I assessed and found that the Group 3 MB cell lines used in this thesis (Med8A, D341 and D283) also exhibit high levels of c-myc protein. In addition, IL-6 stimulation of Med8A and D341 cells resulted in significantly enhanced c-myc levels (Appendix A.3). Overall, Group 4 MB depicted significantly higher *STAT3* level compared to other subgroups. Further analysis into Group 4 MB subtypes revealed that *STAT3* levels were significantly higher in Group 4 β compared to Group 4 α and Group 4 γ . GFI activation is another major characteristic of limited to Group 4 β subtype [42]. GFI1 is a zinc finger protein that interacts with PIAS3 (*STAT3* inhibitor) to enhance *STAT3* signaling [217]. Increased *STAT3* levels observed in these cells could be attributed to high GFI activation.

Survivorship analysis performed with clinical information provided by Cavalli *et al.* confirmed that Group 3 MB patients have the least favourable outcome compared to other MB subgroups [42]. My analysis revealed that increased *STAT3* levels was observed in Group 3 MB patients, thus correlating high *STAT3* expression with an MB subgroup with the poorest survival. Similarly, Group 3 γ , with the least overall survival within the Group 3 subtypes, were found to have high *STAT3* levels. This correlation did not hold for Group 4 MB: wherein Group 4 had the highest *STAT3* expression amongst the MB subgroups, the overall survival of Group 4 was improved when compared to Group 3 MB. In addition, 5-year survivorship analysis for all MB,

Group 3, and Group 4 MB, segregated into high or low *STAT3* expression cohorts was found to be not statistically significant. This data indicated that *STAT3* gene expression at disease diagnosis is not a clear indicator of overall survival in these MB subgroups. In future analysis, it would be informative to also include the expression of *STAT3* protein and its phosphorylation status to not only correlate with MB subgroups and subtypes, but also with survivorship outcomes.

Another major *STAT* protein involved in tumour progression is *STAT5*. Increasing evidence suggests that *STAT5* plays a significant role in tumour growth, metastasis and resistance to anti-cancer therapeutics. My analysis revealed that *STAT5* isoforms, *STAT5A* and *STAT5B* were both upregulated in non-WNT/SHH MB. Within Group 3 MB, both *STAT5A* and *STAT5B* were found to be significantly elevated in Group 3 γ that is correlated with lowest overall survival and higher incidence of metastasis.

Next, I focused analyses on the *IL-6* subfamily of cytokine expression, as well as their corresponding receptors, that were the subject of my thesis research presented in Chapters 2 and 3. Higher *IL6* expression in Group 3 MB over SHH MB also correlated with poor overall survival in Group 3 MB primary tumors. In contrast, *IL6R* levels was not significantly different between Group 3 MB and SHH MB. However, when considered within the subgroups, *IL6R* and *STAT3* levels in 3 β and 3 γ were significantly higher when compared to 3 α , which correlated to Group 3 subtypes with worse outcomes [42]. Thus, the increased expression of *IL-6R* may predict an enhanced response to the cytokine and subsequent *STAT3* activity leading to a worse outcome. In my Group 3 MB cell-based modeling studies, I found that *IL-6R* expression was also elevated in the chemoresistant Med8A-R and Med8A-IL6+ cells. I also found that expression of E2F3, a transcription factor able to transactivate *IL-6R* expression [179], is elevated in Group 3 γ MBs, and

in our chemoresistant Med8A derivatives. Taken together, the findings support the idea that increased IL-6 autocrine activity may be a driver of treatment resistance in Group 3 MB.

The analyses of *IL11*, *IL11R*, *OSM*, *OSMR*, *LIF* and *LIFR* expression in the GEO cohorts were mixed in terms of correlation with MB subgroups that have poorer outcomes. For example, I found that *IL11* was elevated, while *OSM* and *LIF* were decreased, in Group 3 MB relative to other subgroups with a better prognosis. *IL11R* was higher in Group 3 relative to SHH and Group 4, but lower relative to WNT MB. Generally, *LIFR* and *OSMR* expression was lower in Group 3 compared to some of the other subgroups. Within subtypes of Group 3 MB, *IL11* and *IL11R* expression was significantly higher in Group 3 α that has the most favourable outcome. In contrast, *OSMR* levels was significantly higher in Group 3 γ that has the least favourable outcome. My studies have shown that *IL11*, *LIF*, *OSM* and *IL-6* conditioning of Med8A-S yielded chemoresistant variants that secreted significant levels of the respective cytokines, suggesting that external stimuli might still play a crucial role in activating STAT3 signaling in MB cells that possess the required cytokine and/or receptor expression. It is important to note that the MB cohorts in the analyzed GEO datasets were predominantly based on patients with diagnosed disease that have not yet seen treatment, thus it would be of interest to ascertain if relapsed variants may exhibit enhanced expression of any of the genes analyzed.

Among the JAKs, I had observed that the IL-6 family cytokines could stimulate phosphorylation of JAK1 in Med8A cells, but not of JAK2 or TYK2, even though JAK2 and TYK2 protein expression was detectable. Analysis of the GEO datasets revealed that *JAK1* mRNA expression was lower in Group 3 MB compared to the other molecular subgroups, while *JAK2* was lower, and *TYK2* higher, in Group 3 when compared to Group 4. Within Group 3, *JAK1* and *JAK2* expression was lowest in Group 3 γ . I also found that the *JAK* associated cytokine receptor, *GP130*,

was reduced in Group 3 MB when compared to WNT MB. Thus, in sum, higher expression of JAKs do not correlate with MB subgroups with poorer outcomes. It is conceivable that cytokine mediated activation of JAKs, especially *JAK1*, may be a better predictor of oncogenic activity, and not its absolute expression. This may be resolved in future MB datasets that also incorporates whole- and phospho-proteome analysis that allow for resolution of the activated status of JAKs as well as other downstream proteins including the STATs.

A negative feedback mechanism is crucial to maintain physiological homeostasis and a key component of normal cellular signaling pathway. The result of a failed negative feedback mechanism could result in constitutive signaling that leads to uncontrolled proliferation and growth of tumour cells [218]. In that regard, *SOCS1*, *SOCS3* and *PIAS3* are major negative regulators of the IL-6/STAT3 signaling axis. Indeed, lower *SOCS1* and *PIAS3* expression was seen in Group 3 MB that is correlated with a poor survival outcome. Furthermore, Group 3 γ subtypes associated with the worst outcome also expressed significantly lower *PIAS3* expression. In contrast, *SOCS3* expression was higher in subtype Group 3 γ .

Although the transcriptome data provides insight into the abundance of mRNA, it does not necessarily correlate to protein expression in the cell. In a study by Rivero-Hinojosa *et al.*, qualitative proteomic analysis was performed in 41 primary MB tumours to investigate the correlation between mRNA and protein abundance. Their results demonstrated that there was positive correlation between mRNA and protein in 87% of the genes, however only 45% of the genes displayed statistical significance. Predicting functional biology solely based on transcriptome data is not advised and might be a poor predictor of protein abundance. Lack of difference in gene expression data between molecular subgroups might not reveal important proteins contributing to biology of those subgroups [219]. Future studies integrating genomic and

proteomic data will provide a better understanding of the biological determinants and their functional consequence.

A retrospective cohort study comprising of 428 primary MB samples by Schwalbe *et al.*, incorporated risk stratification into the current molecular classification. This resulted in seven clinically relevant molecular subgroups of MB - WNT, SHH (infant), SHH (child), Group 3 (low risk), Group 3 (high risk), Group 4 (low risk) and Group 4 (high risk). It could be informative to analyze the expression of key genes of the IL-6/STAT3 pathway in Group 3 (low risk) and Group 3 (high risk) subgroups as defined by this alternative subgroup classification [57].

To summarize, my analyses of MB transcriptome datasets unveiled certain correlations of expression of key components involved in IL-6/STAT3 signaling in Group 3 MB. However, there was ambiguity in gene expression of some components across the three different GEO databases. This could be attributed to the different microarray platforms used in obtaining gene expression data. In addition, the smaller sample sizes inherent in two of the datasets could also contribute to large variations in the expression analysis and lack of statistical significance of the resulting comparisons [220]. In conclusion, my analyses did reveal that *STAT3* and *STAT5* were upregulated in Group 3 γ , the MB subtype correlated with poor survival outcomes and increased incidence of metastasis. In turn, this could inform future studies unravel the potential role of *STAT5* isoforms and their contribution to treatment resistance in Group 3 MB.

Chapter 5: Conclusion

5.1 Chapter summaries and working models

For my thesis research, I chose to study Group 3 MB, given that it is the most aggressive form of the disease with the least overall 5-year survival. To this date, there is no defined signaling pathway associated with the pathogenesis of Group 3 MB. Through my research, I aimed to establish the role of prominent IL-6/STAT3 signaling in the development of chemotherapeutic resistance in Group 3 MB cells. Herein, I will summarize my experimental findings by chapter, and present working models based on these discoveries.

5.1.1 Autocrine IL-6 signaling mediates chemoresistance in MB cells.

Initially, I profiled two MB cell lines and found that under basal conditions, constitutive phosphorylation of STAT3 (pY705-STAT3) was correlated with chemoresistance. Exogenous IL-6 robustly induced pY705-STAT3 in the chemosensitive Med8A-S cells. Via incremental drug selection with vincristine, we derived the stably chemoresistant variant Med8A-R, that exhibited enhanced IL-6 stimulation of pY705-STAT3, increased IL-6R expression, and chemoresistance to several drugs with different mechanisms of action. Subsequent silencing of STAT3 or IL-6R expression restored the chemosensitivity of Med8A-R cells, highlighting the key involvement of the IL-6/STAT3 signaling axis in chemoresistance.

Given that vincristine selection resulted in the Med8A-R variant which exhibit increased sensitivity to IL-6 stimulation, I assessed and found that prolonged exposure of Med8A-S to IL-6 alone (termed IL-6 conditioning in this thesis) was sufficient to confer multi-drug resistance. Even upon weaning off the exogenously supplemented IL-6, the conditioning-derived Med8A-IL6+ cells had increased basal levels of pY705-STAT3 and increased IL-6R expression. IL-6

conditioning of IL-6R^{-/-} or STAT3^{-/-} cells failed to induce chemoresistance, a further indication of the critical involvement of IL-6R and STAT3. Moreover, Med8A-IL6⁺ cells now secreted significant levels of IL-6, an indication of sustained autocrine signaling involving IL-6 and constitutive activation of STAT3 that could drive chemoresistance. Using a co-culture system, I further demonstrated that Med8A-IL6⁺ cells ably invoked a strong pY705-STAT3 response in the parental Med8A-S cells, strongly indicating that chemoresistant MB may secrete autocrine factors, including IL-6, that could transform chemosensitive tumours to becoming chemoresistant. Importantly, combination treatment of vincristine with cisplatin (a cytotoxic agent) or niclosamide (a STAT3 inhibitor) effectively overcame the resistance observed for Med8A-R and Med8A-IL6⁺ cells. I validated key findings observed with the Med8A cells using D283 and D341, cell lines that also belong to Group 3 MB.

Overall in Chapter 2, my study unveiled autocrine IL-6 as a promoter of STAT3 signaling in development of drug resistance, and suggests therapeutic benefits for targeting the IL-6/STAT3 signaling axis in Group 3 MBs as illustrated in Figure 5.1.

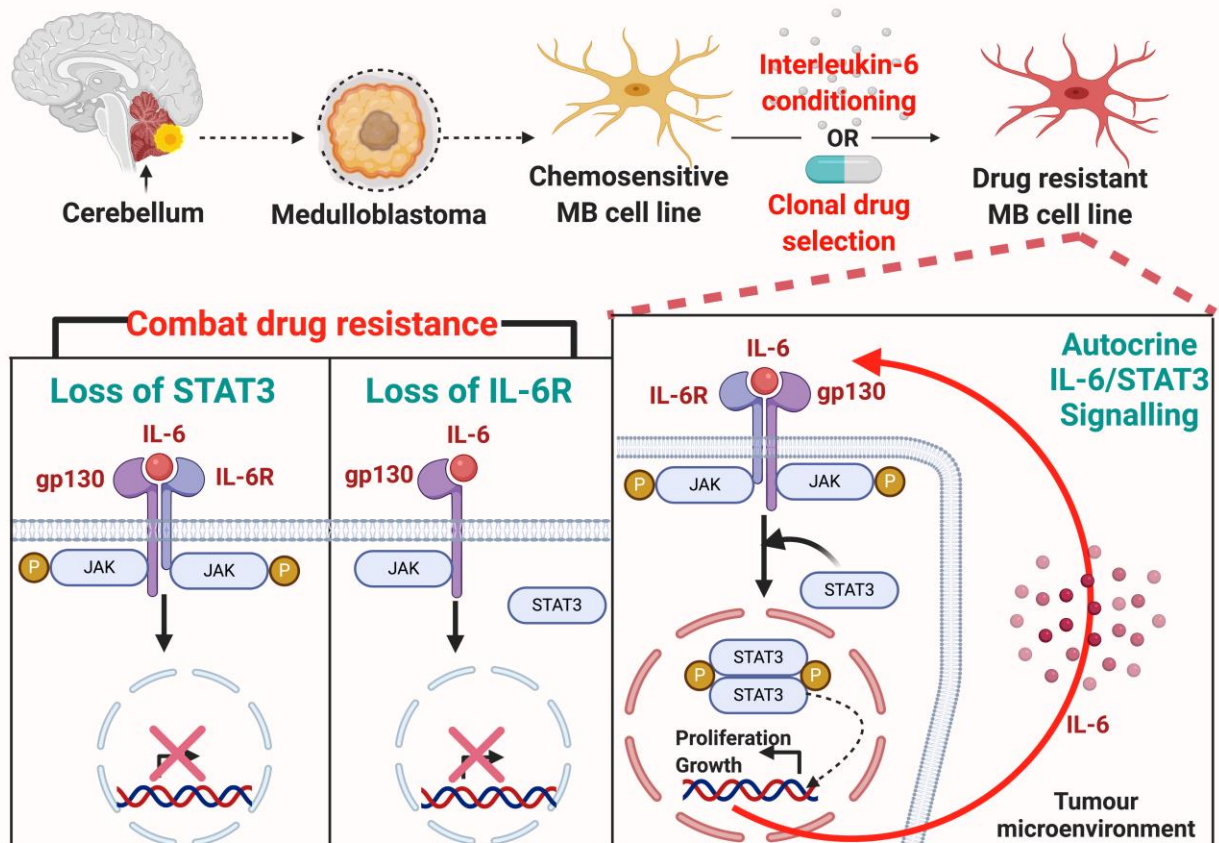


Figure 5.1: Graphical abstract depicts the experimental approach and mechanisms involved in autocrine IL-6/STAT3 signaling in the development of chemoresistance in Group 3 MB cells.

(Created with BioRender.com).

5.1.2 Paracrine IL-6 signaling originating from the brain TME.

To understand the role of paracrine signaling in the TME of MB, I evaluated if brain resident macrophages, microglia, may be a source of stimulatory cytokines that can induce STAT3 activity and promote MB chemoresistance. I found that Group 3 MB cells, Med8A-S, D283 and D341, exposed in a co-culture system to HMC3, a human microglia cell line, exhibited enhanced pY705-STAT3 expression and acquired drug resistance. Indeed, HMC3 cells were found to secrete high levels of IL-6. Unexpectedly, even though IL-6R^{-/-} cells do not respond to exogenous IL-6 conditioning, IL-6R^{-/-} cells co-cultured with HMC3 cells also exhibited increased pY705-STAT3

levels and chemoresistance, suggesting that other soluble factors released by microglia is sufficient to drive chemoresistance in Med8A cells. This finding also suggests that targeting IL-6 or its receptor alone may not be sufficient to abrogate drug resistance in these cells.

Next, I evaluated if the IL-6 family cytokines share a common ability to activate STAT3 signaling in Group 3 MB cells. Med8A-S and IL-6R^{-/-} cells conditioned with OSM, IL-11 or LIF also became chemoresistant and exhibited enhanced pY705-STAT3 levels. Cytokine secretion analysis revealed that the conditioned cells not only secreted increased levels of the respective cytokines they were conditioned with, but also of other IL-6 family cytokines. This finding suggested that IL-6 family cytokines can act in a complementary manner to amplify autocrine signaling and promote constitutive activation of STAT3. I also found that IL-6 family cytokine stimulation of STAT3 signaling involved JAK1. Indeed, combined treatment of the JAK inhibitor ruxolitinib with vincristine was effective in overcoming chemoresistance of IL-6 family cytokine conditioned Med8A cells.

HMC3 cells co-cultured Med8A cells also exhibited increased pJAK1 and pY705-STAT3 concomitant with chemoresistance, and that combination ruxolitinib and vincristine treatment overcame the observed chemoresistance to vincristine as a monoagent. I also showed that IL-6 was secreted at high levels in Med8A-S and IL-6R^{-/-} cells that had been co-cultured with HMC3. Although HMC3 was initially chosen as a major source of IL-6 and to demonstrate paracrine signaling mechanism, cytokine array analysis revealed that HMC3 secreted other soluble factors in addition to IL-6, such as GRO. Given that IL-6 family of receptors share a common beta subunit, gp130, I evaluated if targeting gp130 may effectively abrogate chemoresistance resulting from IL-6 family cytokine signaling. Co-culture with HMC3 failed to induce chemoresistance in Gp130^{-/-} cells. Furthermore, I evaluated the potential of targeting gp130 using commercially available

inhibitors, SC144 and Bazedoxifene (BZD). In combination with vincristine, subtoxic levels of SC144 or BZD proved to be effective in overcoming resistance depicted by chemoresistant Group 3 MB cells. This robust phenomenon was further validated in two other Group 3 MB cell lines, D283 and D341. Collectively, this data presented in Chapter 3 suggests that targeting JAK or gp130 in chemoresistant Group 3 MB cells is a novel approach to circumvent chemotherapeutic resistance and lower drug toxicity. A graphical abstract is presented in Figure 5.2.

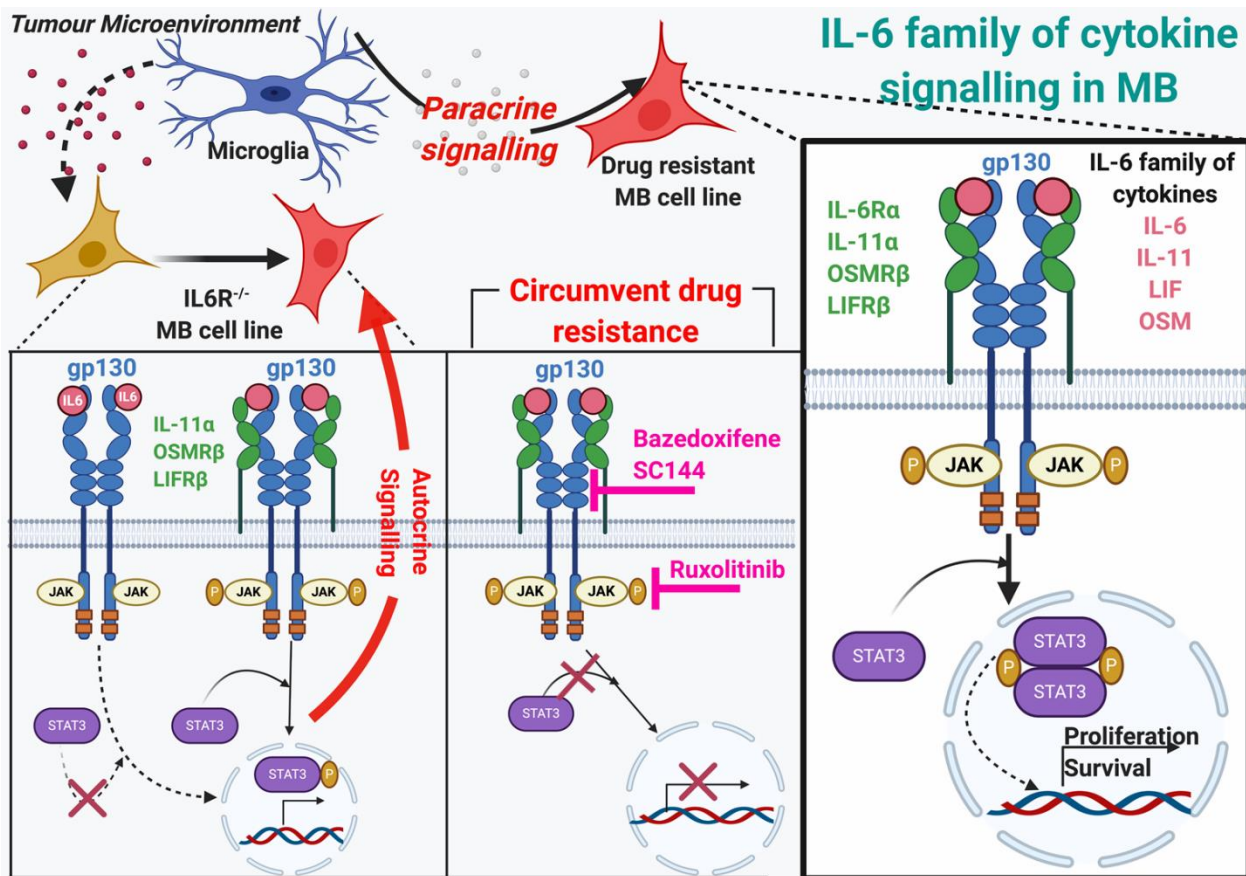


Figure 5.2: Graphical abstract depicts the experimental approach and mechanism involved in tumour microenvironment mediated chemotherapeutic resistance involving IL-6 family of cytokine signaling in Group 3 MB.

(Created with BioRender.com).

5.1.3 Correlative clinical evidence for IL-6/JAK/STAT signaling in subgroups of MB.

To provide a clinical perspective to the functional assays demonstrated in my study, I investigated several GEO databases and evaluated the gene expression patterns of select target genes associated with the IL-6/STAT3 signaling axis. In the largest cohort, my analysis revealed that *STAT3* levels were enriched in Group 3 and Group 4 MB and particularly in Group 3 γ subtype, which is associated with poor overall survival. Notably, STAT5 isoforms, *STAT5A* and *STAT5B* were both upregulated in non-WNT/SHH MB and significantly elevated in Group 3 γ subtype.

Stimulatory cytokines that belong to IL-6 family cytokines such as IL-6, LIF, IL-11 and OSM; and their corresponding receptors used in the thesis were also analyzed in the different GEO databases, with particular attention to elucidating significance between Group 3 with the other MB subgroups, and between Group 3 γ with the other subtypes, given that Group 3 and Group 3 γ were associated with worst survival [42]. Although there was positive correlation of some cytokines and receptors to poor survival outcome, there was huge variation in results across the different GEO databases. In the large 763 patient cohort, I found that *IL6* expression was significantly higher in Group 3 MB over SHH MB. But no remarkable difference was found in *IL6R* expression across the molecular subgroups. Within the subgroups, Group 3 γ and Group 3 β associated with the least favourable outcome were found to have significantly higher *IL6R* expression. On the contrary, other cytokines and receptors such as *IL11* and *IL11R* were found to be significantly higher in Group 3 α , a subtype associated with the most favourable outcome. Additionally, *GPI30* did not show any remarkable difference among the molecular subgroups.

My experimental findings revealed that only pJAK1 was significantly upregulated in Group 3 MB cell lines in response to external stimuli. However, *JAK1* expression was found to be lower in Group 3 MB compared to other molecular subgroups in two of the GEO databases.

Though *JAK1* expression is lower in Group 3 MB and is inversely correlated with poor outcome, their biological activity depends on their interaction with external stimuli. Increased pJAK1 was found to induce enhanced pY705-STAT3 and correlated with increased resistance to vincristine treatment. Another JAK member, *TYK2* was found to be significantly higher in Group 3 MB compared to Group 4 MB in all three datasets.

Analysis of negative feedback regulators of the IL-6/STAT3 signaling axis such as *SOCS1*, *SOCS3* and *PIAS3* was also carried out. Low *PIAS3* and *SOCS1* expression in Group 3 MB correlated with poor survival outcome. Furthermore, Group 3 γ subtypes associated with poor outcome also expressed significantly lower *PIAS3* and *SOCS1*. In contrast, *SOCS3* expression was higher in Group 3 γ . Protein expression analysis of negative feedback regulators in Group 3 MB cells and their chemoresistant variants will be beneficial to further understand their role. A summary of key gene expression analyses conducted for Chapter 4 presented as a heat map collated for MB subgroups and subtypes is presented in Figure 5.3. In conclusion, my analyses of MB transcriptome datasets unveiled certain correlations of expression of key components involved in IL-6/STAT3 signaling in Group 3 MB.

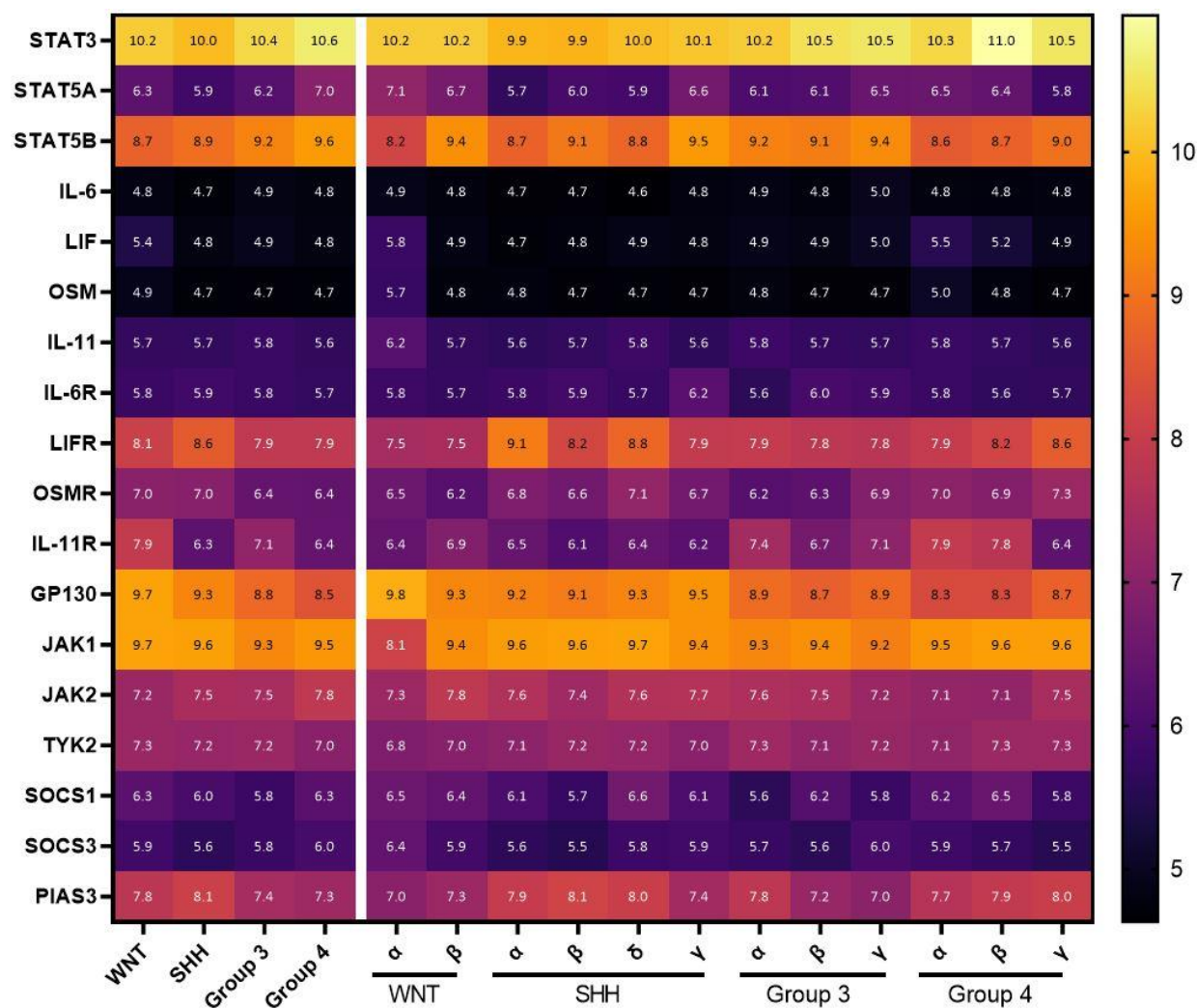


Figure 5.3: Heat map summary depiction of gene expression involved in the IL-6/STAT3 signaling pathway.

The mean values in expression units is plotted with the corresponding scale depicted on the right.

5.2 Significance of study

Transcriptional profiling of MB has led to categorization of four distinct molecular subgroups that will be instrumental to define risk in the clinical setting. However, therapeutic intervention linked to the risk stratification have yet to be refined to improve clinical outcomes and long-term sequelae of patients with more aggressive forms of MB. The conventional treatment approach is undermined by treatment refractory tumours and frequent occurrence of relapse, with

high variability in survival outcomes [21,39,40,45,47,52,69,221]. Hence, specific targeted therapies are currently required to efficiently treat this aggressive malignancy [222]. Importantly, knowledge of activated signaling pathways in promoting treatment resistance and pathogenesis of the disease is key to designing novel therapeutic options.

Patients with Group 3 MB have the least overall survival of about 60%. These tumours are the hardest to treat and are predominantly found in infants and children. Unlike WNT and SHH subgroups, Group 3 and Group 4 MB do not have a single definitive signaling pathway associated with tumour progression. My study has identified a prominent cancer survival pathway and its contribution to development of chemotherapeutic resistance in Group 3 MB. The IL-6/STAT3 signaling cascade is a well-established pathway that has been known to promote tumorigenesis in several malignancies. Through my findings, I have demonstrated that constant exposure to stimulatory cytokines secreted by immune cells in the tumour microenvironment contributed to drug resistance in Group 3 MB cells. I have established a direct correlation between constitutive activation of STAT3 and drug resistance in Group 3 MB cells. To circumvent chemoresistance, I targeted individual components of the IL-6/STAT3 signaling axis using loss-of-function approaches (CRISPR-Cas9 mediated knockouts) or small molecule inhibitors to evaluate their role in drug resistance. Cytotoxic drugs such as vincristine that is used to treat MB patients in the clinic was also used in my study to treat Group 3 MB cells. My research has demonstrated the targeting gp130, JAK1 or STAT3 using inhibitors diminished STAT3 signaling and thereby sensitizing chemoresistant cells to vincristine treatment. In addition, these inhibitors may be prophylactic to prevent the development of chemoresistance when given early during the treatment regime. Due to the high incidence of Group 3 MB particularly in infants and children, using combined treatment with sub-toxic levels of inhibitors and low dose of cytotoxic drugs could alleviate the post

treatment burden experienced by most patients, while also improving therapeutic options for relapsed and chemoresistant tumours.

5.3 Limitations of study

Drug resistance assays were primarily performed using 2-dimensional (2D) monolayer cell cultures. Although this technique is well established, inexpensive and highly replicable, it is not a good representative of the tumour cell environment. On the contrary, a 3D cell culture system is more relevant for pre-clinical screening of anti-cancer drugs. Spheroid 3D culture systems maintain structural complexity such as cell morphology or polarity. Cellular integrity and cell-cell interactions are well preserved in spheroid 3D cultures and influence intracellular pathway signaling [223]. 3D cell cultures also provide for the enrichment of CSC and MB stem cell populations [224]. In context of MB, enriched stem cell population in Group 3 MB contributes to increased resistance to treatment [101]. Additionally, SHH MB cell lines grown as spheroid 3D cultures were found to be significantly chemoresistant compared to monolayer culture system [225]. Hence, a 3D cell culture system might be a more suitable platform to evaluate drug resistance. Another major limitation in my study is the absence of healthy neural stem cells (NSCs) to study the effect of inhibitors and drugs on healthy brain cells. Neural stem cells are self-renewing, multipotent cells that give rise to cells of the central nervous system during development [226]. Healthy NSC as control in dose-response curves could be beneficial to understand neural toxicity, an important aspect to consider for MB that occurs frequently during the early developmental ages of children.

Although an *in vitro* setting allows for controlled experiments to study the TME (eg. microglia and MB interactions), it is not adequate to model the highly dynamic TME of a living

tumour that contains a plethora of other stimuli, including other immune cells, non-immune cells, role of the tumour vasculature, and other non-cellular factors such as nutrients, growth factors, cytokines and chemokines, ECM, oxygen and so on. In this context, an ideal model would be an immuno-competent murine-based model for MB tumorigenesis. Although transgenic models for Group 3 MB has been challenging to develop, limited *in vivo* modeling using immune-incompetent mice is possible [29]. In this regard, orthotopic CNS engraftment of human MB cells could be useful to assess their potential to recruit macrophages. Alternatively, overexpression of MYC and dominant negative forms of *TP53* in cerebellar stem cells or granule neuron precursors helped transform these cells to resemble Group 3 MB in mice [66]. Testing combination treatments targeting the IL-6/STAT3 signaling cascade in these *in vivo* model systems will be highly complementary to purely *in vitro* models, and represent next steps to further validate the findings of my research hypotheses.

The brain TME consists of multiple cell types including macrophages, microglia, astrocytes, lymphocytes, dendritic cells and neutrophils. In this thesis, I have only investigated the role of microglia and its contribution to chemoresistance in Group 3 MB cells. Microglia were chosen primarily due to their presence in the brain TME and as a source of IL-6. However, it is essential to understand the individual roles of these immune cells in the MB TME and their clinical implications. SHH MB tumours are known to have a rich infiltration of TAMs compared to Group 3 MB, but the latter had higher amount of CD8+ PD-1+ T cells in the TME [113]. Programmed death 1/programmed death ligand 1 (PD-1/ PD-L1) is an immune checkpoint pathway that is utilized by tumour cells to evade immune cell targeting. Expression of PD-L1 on cytotoxic T (CD8) cells reduces T-cell infiltration in the TME and was associated with poor prognosis in MB patients [114]. Using these immune cells might be a better model to mimic the Group 3 MB TME.

Additionally, assessment of cytokines secreted by the different immune cells also found in the TME could help to better understand their contribution to drug resistance in Group 3 MB cells.

In this thesis, a biased approach was used to identify the molecular signatures that contribute to drug resistance in Group 3 MB. Prior established knowledge of oncogenic pathways was utilized to design the experimental model systems to investigate drug resistance. Although this approach is notable from a mechanistic point of view, it fails to provide substantial information about other molecular alterations and oncogenic events occurring in this disease. However, an unbiased approach utilizes valuable tools such as high-throughput screening to identify significant cancer signatures and predict clinical outcome of the disease. A disadvantage of this method is the high genetic noise and the lack of strong evidence between cause and effect [227,228]. Given the strengths and caveats of both the approaches, an integrated approach should be used to identify and validate cancer signatures. The primary purpose for analyzing GEO datasets was to analyze the transcriptome data for the individual components of IL-6/STAT3 signaling cascade and provide clinical significance to functional protein data explored in this thesis. Analysis of GEO datasets did not provide a definite conclusion regarding the gene expression patterns and their association with outcome for certain genes in my thesis. However, it is to be noted that disease phenotypes cannot be inferred from genomic alterations alone. Stronger correlative information between clinical subgroups of MB, in particular for Group 3 MB, await future omics datasets that include the proteome (total and phospho-proteome expression) to confirm both mRNA and protein involvement [219]. In addition, single-cell sequencing could be a vital tool to distinguish tumour heterogeneity, lineages and identify sub-populations. This technology has been able to unravel specific molecular signatures and provide insights into pathway enrichment pertinent to Group 3 MB [229]. Identification of subgroup specific immune cell infiltration in the MB TME could form

the basis for *in vitro* reconstitution studies to evaluate the role of each of these immune cells found in the MB TME. [113].

Another limitation is that a microglia cell line was used to model one aspect of the immune cell-MB interaction that may occur within the brain TME to study drug resistance in Group 3 MB. It is essential to confirm the presence of microglia in the TME of Group 3 MB. Tumour microarray analysis of clinical biopsy formalin fixed paraffin embedded (FFPE) samples could be useful to identify immune cell populations enriched in Group 3 MB including microglia. Assessment of individual components of the IL-6/STAT3 signaling cascade including their expression levels and activity status (*eg* phosphorylated JAK or STAT3) in diagnostic and relapsed primary MB samples by immunohistochemical staining will serve to validate the clinical relevance of immune cell infiltrates in the MB TME that could modify chemotherapeutic response.

5.4 Future perspectives

Group 3 MB is frequently metastatic at initial diagnosis. I showed that IL-6 conditioned Group 3 MB cells exhibited enhanced migration and invasion potential. This raises the interesting possibility if clinically diagnosed metastatic Group 3 MB may already exhibit constitutive IL-6/JAK/STAT3 activity; genomic and proteomic profiling of Group 3 MB categorized into metastatic and non-metastatic variants might provide additional valuable insights. A recent study by Kumar *et al.*, investigated the clinical outcome and compared the molecular signatures of diagnostic and relapsed MB. This study highlights the need for verifying molecular targets in relapsed MB prior to deciding the treatment strategy. Divergence in some molecular features was found in patient-matched diagnostic and relapsed MB, however the subgroup was mostly preserved. When the gene expression dataset is made publicly available, it will be intriguing to

compare the expression of key genes of IL-6/STAT3 signaling pathway in diagnostic and relapsed MB patients [230]. Experimentally, it would be of interest to examine if other IL-6 family cytokines, as well as prolonged exposure to TME immune cells including microglia, also facilitate transformation of Group 3 MB cells into a more invasive phenotype. It would also be of interest to examine if TME cytokine induced STAT3 signaling leads to increased expression of proteolytic enzymes commonly implicated in metastasis [231].

In chapter 2, I showed that multi-drug resistance protein (MDR1; also known as ABCB1, Pgp) was upregulated in multi drug resistant MB cells. MDR1 belongs to the ATP binding cassette family and acts as a drug efflux transporter to decrease intracellular concentrations of several drugs. In some types of cancer, overexpression of MDR1 is a marker for treatment refractory tumour cell population [232]. Overexpression of MDR1 has also been known to promote chemotherapeutic resistance against a variety of cancer drugs such as taxanes, vinca alkaloids and anthracyclines [233]. In my thesis, I have demonstrated that Med8A-R and Med8A-IL6+ cells are resistant to cytotoxic drugs such as vinca alkaloids (vincristine) and anthracyclines (idarubicin and mitoxantrone). Future studies examining the use of MDR1 inhibitors alone or in combination with cytotoxic drugs may be explored to effectively overcome resistance in Group 3 MB cells through an alternate signaling mechanism.

In addition to IL-6, cytokine array analysis also revealed that HMC3 secreted high levels of the chemokine, GRO (also known as CXCL1) (Appendix A.8). Furthermore, Med8A-S and IL-6R^{-/-} cells co-cultured with HMC3 also secreted significant levels of GRO (Appendix A.8). GRO is known to activate STAT3 in an autocrine manner and induce cancer stem like characteristics in tumour cells [234]. In addition to TAMs and microglia, activation of STAT3 in Th17 cells produce IL-17A that induces astrocytes to secrete GRO in the brain TME. The presence of GRO in the

brain TME could play a significant role in the recruitment of neutrophils [235]. Circulating neutrophils play a role to facilitate metastasis by setting up a pre-metastatic niche for tumour cell colonization, while intratumoral neutrophils correlate with increased incidence of drug resistance [103]. Given the high level of GRO secreted by Group 3 MB cells in response to HMC3, it might be worthy to assess GRO signaling and its contribution to chemoresistance in these cells.

5.5 Closing remarks

MB is the most common pediatric brain malignancy and it is categorized into four distinct molecular subgroups. Of the subgroups, Group 3 MB patients have the least favourable outcome and frequent recurrence of disease. Acquired treatment resistance is a common feature of recurrent tumours that is usually treated with an intensive regimen of chemotherapy. Due to the occurrence of Group 3 MB predominantly in infants and young children, these aggressive treatments often lead to severe long-term side effects for survivors. Unlike WNT and SHH MB, Group 3 MB does not have a defined signaling pathway contributing to the pathogenesis of the disease. In search of a potentially targetable signaling pathway, I investigated the role of IL-6/STAT3 signaling and its contribution to chemoresistance in Group 3 MB cells. To study chemoresistance, I developed two unique model systems to assess gain-of-function and loss-of-function of critical genes in the IL-6/STAT3 signaling pathway. My research findings demonstrated that an autocrine signaling mechanism involving IL-6 was crucial for sustained signaling and subsequent development of chemotherapeutic resistance. Additionally, stimulatory cytokines secreted by certain cells in the brain TME initiated paracrine signaling with Group 3 MB cells and promoted chemoresistance in Group 3 MB. Overall, I demonstrated that acquired chemoresistance in Group 3 MB cells can be initiated by the IL-6/STAT3 signaling cascade. As a novel and potentially improved treatment

approach, I demonstrated that targeting individual components of IL-6/STAT3 signaling axis such as JAK, gp130 or STAT3 using inhibitors at sub toxic doses in combination with a conventional cytotoxic agent circumvented acquired chemoresistance in Group 3 MB cells. In the future, this treatment regimen could possibly be used in the clinic to treat treatment refractory Group 3 MB tumours and lower the chemotherapeutic burden on pediatric patients.

Bibliography

1. LJ Rubinstein and DW Northfield. *The Medulloblastoma and the So-Called "Arachnoidal Cerebellar Sarcoma"*. Brain. 1964; **87**:379-412.
2. BS Brody and WJ German. *Medulloblastoma of the Cerebellum: A Report of 15 Cases*. Yale J Biol Med. 1933; **6**(1):19-29.
3. H Cushing and P Bailey, *Tumors Arising from the Blood-Vessels of the Brain. Angiomatous Malformations and Hemangioblastomas*. 1928: Charles C Thomas.
4. LJ Kunschner. *Harvey Cushing and medulloblastoma*. Arch Neurol. 2002; **59**(4):642-5.
5. JT Rutka and HJ Hoffman. *Medulloblastoma: a historical perspective and overview*. J Neurooncol. 1996; **29**(1):1-7.
6. K Juraschka and MD Taylor. *Medulloblastoma in the age of molecular subgroups: a review*. J Neurosurg Pediatr. 2019; **24**(4):353-363.
7. E Paterson and RF Farr. *Cerebellar medulloblastoma: treatment by irradiation of the whole central nervous system*. Acta radiol. 1953; **39**(4):323-36.
8. NE Millard and KC De Braganca. *Medulloblastoma*. J Child Neurol. 2016; **31**(12):1341-53.
9. DN Louis, A Perry, G Reifenberger, A von Deimling, D Figarella-Branger, WK Cavenee, H Ohgaki, OD Wiestler, P Kleihues, and DW Ellison. *The 2016 World Health Organization Classification of Tumors of the Central Nervous System: a summary*. Acta Neuropathol. 2016; **131**(6):803-20.
10. DT Jones, PA Northcott, M Kool, and SM Pfister. *The role of chromatin remodeling in medulloblastoma*. Brain Pathol. 2013; **23**(2):193-9.
11. QT Ostrom, H Gittleman, G Truitt, A Boscia, C Kruchko, and JS Barnholtz-Sloan. *CBTRUS Statistical Report: Primary Brain and Other Central Nervous System Tumors Diagnosed in the United States in 2011-2015*. Neuro Oncol. 2018; **20**(suppl_4):iv1-iv86.
12. DL Johnston, D Keene, M Kostova, D Strother, L Lafay-Cousin, C Fryer, K Scheinmann, AS Carret, A Fleming, V Percy, S Afzal, B Wilson, L Bowes, S Zelcer, C Mpofo, M Silva, V Larouche, J Brossard, and E Bouffet. *Incidence of medulloblastoma in Canadian children*. J Neurooncol. 2014; **120**(3):575-9.
13. MT Giordana, P Schiffer, and D Schiffer. *Prognostic factors in medulloblastoma*. Childs Nerv Syst. 1998; **14**(6):256-62.
14. V Khanna, RL Achey, QT Ostrom, H Block-Beach, C Kruchko, JS Barnholtz-Sloan, and PM de Blank. *Incidence and survival trends for medulloblastomas in the United States from 2001 to 2013*. J Neurooncol. 2017; **135**(3):433-441.
15. S Ezzat, M Kamal, N El-Khateeb, M El-Beltagy, H Taha, A Refaat, M Awad, S Abouelnaga, and MS Zaghoul. *Pediatric brain tumors in a low/middle income country: does it differ from that in developed world?* J Neurooncol. 2016; **126**(2):371-6.
16. A Thomas and G Noel. *Medulloblastoma: optimizing care with a multidisciplinary approach*. J Multidiscip Healthc. 2019; **12**:335-347.
17. WR Polkinghorn and NJ Tarbell. *Medulloblastoma: tumorigenesis, current clinical paradigm, and efforts to improve risk stratification*. Nat Clin Pract Oncol. 2007; **4**(5):295-304.

18. PA Northcott, GW Robinson, CP Kratz, DJ Mabbott, SL Pomeroy, SC Clifford, S Rutkowski, DW Ellison, D Malkin, MD Taylor, A Gajjar, and SM Pfister. *Medulloblastoma*. Nat Rev Dis Primers. 2019; **5**(1):11.
19. DW Ellison, M Kocak, J Dalton, H Megahed, ME Lusher, SL Ryan, W Zhao, SL Nicholson, RE Taylor, S Bailey, and SC Clifford. *Definition of disease-risk stratification groups in childhood medulloblastoma using combined clinical, pathologic, and molecular variables*. J Clin Oncol. 2011; **29**(11):1400-7.
20. V Ramaswamy, M Remke, E Bouffet, S Bailey, SC Clifford, F Doz, M Kool, C Dufour, G Vassal, T Milde, O Witt, K von Hoff, T Pietsch, PA Northcott, A Gajjar, GW Robinson, L Padovani, N Andre, M Massimino, B Pizer, R Packer, S Rutkowski, SM Pfister, MD Taylor, and SL Pomeroy. *Risk stratification of childhood medulloblastoma in the molecular era: the current consensus*. Acta Neuropathol. 2016; **131**(6):821-31.
21. A Gajjar, M Chintagumpala, D Ashley, S Kellie, LE Kun, TE Merchant, S Woo, G Wheeler, V Ahern, MJ Krasin, M Fouladi, A Broniscer, R Krance, GA Hale, CF Stewart, R Dauser, RA Sanford, C Fuller, C Lau, JM Boyett, D Wallace, and RJ Gilbertson. *Risk-adapted craniospinal radiotherapy followed by high-dose chemotherapy and stem-cell rescue in children with newly diagnosed medulloblastoma (St Jude Medulloblastoma-96): long-term results from a prospective, multicentre trial*. Lancet Oncol. 2006; **7**(10):813-20.
22. CS McManamy, J Pears, CL Weston, Z Hanzely, JW Ironside, RE Taylor, RG Grundy, SC Clifford, DW Ellison, and G Clinical Brain Tumour. *Nodule formation and desmoplasia in medulloblastomas-defining the nodular/desmoplastic variant and its biological behavior*. Brain Pathol. 2007; **17**(2):151-64.
23. PA Northcott, A Korshunov, SM Pfister, and MD Taylor. *The clinical implications of medulloblastoma subgroups*. Nat Rev Neurol. 2012; **8**(6):340-51.
24. S Rutkowski, K von Hoff, A Emser, I Zwiener, T Pietsch, D Figarella-Branger, F Giangaspero, DW Ellison, ML Garre, V Biassoni, RG Grundy, JL Finlay, G Dhall, MA Raquin, and J Grill. *Survival and prognostic factors of early childhood medulloblastoma: an international meta-analysis*. J Clin Oncol. 2010; **28**(33):4961-8.
25. ML Garre, A Cama, F Bagnasco, G Morana, F Giangaspero, M Brisigotti, C Gambini, M Forni, A Rossi, R Haupt, P Nozza, S Barra, G Piatelli, G Viglizzo, V Capra, W Bruno, L Pastorino, M Massimino, M Tumolo, P Fidani, S Dallorso, RF Schumacher, C Milanaccio, and T Pietsch. *Medulloblastoma variants: age-dependent occurrence and relation to Gorlin syndrome--a new clinical perspective*. Clin Cancer Res. 2009; **15**(7):2463-71.
26. A Gajjar, RA Sanford, R Bhargava, R Heideman, A Walter, Y Li, JW Langston, JJ Jenkins, M Muhlbauer, J Boyett, and LE Kun. *Medulloblastoma with brain stem involvement: the impact of gross total resection on outcome*. Pediatr Neurosurg. 1996; **25**(4):182-7.
27. EM Thompson, T Hielscher, E Bouffet, M Remke, B Luu, S Gururangan, RE McLendon, DD Bigner, ES Lipp, S Perreault, YJ Cho, G Grant, SK Kim, JY Lee, AAN Rao, C Giannini, KKW Li, HK Ng, Y Yao, T Kumabe, T Tominaga, WA Grajkowska, M Perek-Polnik, DCY Low, WT Seow, KTE Chang, J Mora, IF Pollack, RL Hamilton, S Leary, AS Moore, WJ Ingram, AR Hallahan, A Jouviet, M Fevre-Montange, A Vasiljevic, C Faure-Conter, T Shofuda, N Kagawa, N Hashimoto, N Jabado, AG Weil, T Gayden, T Wataya, T Shalaby, M Grotzer, K Zitterbart, J Sterba, L Kren, T Hortobagyi, A Klekner, B Laszlo, T Poczka, P Hauser, U Schuller, S Jung, WY Jang, PJ French, JM Kros, MC van Veelen, L Massimi, JR Leonard, JB Rubin, R Vibhakar, LB Chambless, MK Cooper, RC Thompson,

- CC Faria, A Carvalho, S Nunes, J Pimentel, X Fan, KM Muraszko, E Lopez-Aguilar, D Lyden, L Garzia, DJH Shih, N Kijima, C Schneider, J Adamski, PA Northcott, M Kool, DTW Jones, JA Chan, A Nikolic, ML Garre, EG Van Meir, S Osuka, JJ Olson, A Jahangiri, BA Castro, N Gupta, WA Weiss, I Moxon-Emre, DJ Mabbott, A Lassaletta, CE Hawkins, U Tabori, J Drake, A Kulkarni, P Dirks, JT Rutka, A Korshunov, SM Pfister, RJ Packer, V Ramaswamy and MD Taylor. *Prognostic value of medulloblastoma extent of resection after accounting for molecular subgroup: a retrospective integrated clinical and molecular analysis*. *Lancet Oncol*. 2016; **17**(4):484-495.
28. EM Thompson, A Bramall, JE Herndon, 2nd, MD Taylor, and V Ramaswamy. *The clinical importance of medulloblastoma extent of resection: a systematic review*. *J Neurooncol*. 2018; **139**(3):523-539.
 29. J Wang, A Garancher, V Ramaswamy, and RJ Wechsler-Reya. *Medulloblastoma: From Molecular Subgroups to Molecular Targeted Therapies*. *Annu Rev Neurosci*. 2018; **41**:207-232.
 30. AJ Gajjar and GW Robinson. *Medulloblastoma-translating discoveries from the bench to the bedside*. *Nat Rev Clin Oncol*. 2014; **11**(12):714-22.
 31. WH St Clair, JA Adams, M Bues, BC Fullerton, S La Shell, HM Kooy, JS Loeffler, and NJ Tarbell. *Advantage of protons compared to conventional X-ray or IMRT in the treatment of a pediatric patient with medulloblastoma*. *Int J Radiat Oncol Biol Phys*. 2004; **58**(3):727-34.
 32. TE Merchant, LE Kun, MJ Krasin, D Wallace, MM Chintagumpala, SY Woo, DM Ashley, M Sexton, SJ Kellie, V Ahern, and A Gajjar. *Multi-institution prospective trial of reduced-dose craniospinal irradiation (23.4 Gy) followed by conformal posterior fossa (36 Gy) and primary site irradiation (55.8 Gy) and dose-intensive chemotherapy for average-risk medulloblastoma*. *Int J Radiat Oncol Biol Phys*. 2008; **70**(3):782-7.
 33. I Moxon-Emre, E Bouffet, MD Taylor, N Laperriere, N Scantlebury, N Law, BJ Spiegler, D Malkin, L Janzen, and D Mabbott. *Impact of craniospinal dose, boost volume, and neurologic complications on intellectual outcome in patients with medulloblastoma*. *J Clin Oncol*. 2014; **32**(17):1760-8.
 34. AE Evans, RD Jenkin, R Sposto, JA Ortega, CB Wilson, W Wara, IJ Ertel, S Kramer, CH Chang, SL Leikin, and et al. *The treatment of medulloblastoma. Results of a prospective randomized trial of radiation therapy with and without CCNU, vincristine, and prednisone*. *J Neurosurg*. 1990; **72**(4):572-82.
 35. V Ramaswamy, M Remke, E Bouffet, CC Faria, S Perreault, YJ Cho, DJ Shih, B Luu, AM Dubuc, PA Northcott, U Schuller, S Gururangan, R McLendon, D Bigner, M Fouladi, KL Ligon, SL Pomeroy, S Dunn, J Triscott, N Jabado, A Fontebasso, DT Jones, M Kool, MA Karajannis, SL Gardner, D Zagzag, S Nunes, J Pimentel, J Mora, E Lipp, AW Walter, M Ryzhova, O Zheludkova, E Kumirova, J Alshami, SE Croul, JT Rutka, C Hawkins, U Tabori, KE Codispoti, RJ Packer, SM Pfister, A Korshunov, and MD Taylor. *Recurrence patterns across medulloblastoma subgroups: an integrated clinical and molecular analysis*. *Lancet Oncol*. 2013; **14**(12):1200-7.
 36. RD Kortmann, J Kuhl, B Timmermann, U Mittler, C Urban, V Budach, E Richter, N Willich, M Flentje, F Berthold, I Slavic, J Wolff, C Meisner, O Wiestler, N Sorensen, M Warmuth-Metz, and M Bamberg. *Postoperative neoadjuvant chemotherapy before radiotherapy as compared to immediate radiotherapy followed by maintenance*

- chemotherapy in the treatment of medulloblastoma in childhood: results of the German prospective randomized trial HIT '91.* Int J Radiat Oncol Biol Phys. 2000; **46**(2):269-79.
37. YJ Cho, A Tsherniak, P Tamayo, S Santagata, A Ligon, H Greulich, R Berhoukim, V Amani, L Goumnerova, CG Eberhart, CC Lau, JM Olson, RJ Gilbertson, A Gajjar, O Delattre, M Kool, K Ligon, M Meyerson, JP Mesirov, and SL Pomeroy. *Integrative genomic analysis of medulloblastoma identifies a molecular subgroup that drives poor clinical outcome.* J Clin Oncol. 2011; **29**(11):1424-30.
 38. DW Ellison, J Dalton, M Kocak, SL Nicholson, C Fraga, G Neale, AM Kenney, DJ Brat, A Perry, WH Yong, RE Taylor, S Bailey, SC Clifford, and RJ Gilbertson. *Medulloblastoma: clinicopathological correlates of SHH, WNT, and non-SHH/WNT molecular subgroups.* Acta Neuropathol. 2011; **121**(3):381-96.
 39. M Kool, A Korshunov, M Remke, DT Jones, M Schlanstein, PA Northcott, YJ Cho, J Koster, A Schouten-van Meeteren, D van Vuurden, SC Clifford, T Pietsch, AO von Bueren, S Rutkowski, M McCabe, VP Collins, ML Backlund, C Haberler, F Bourdeaut, O Delattre, F Doz, DW Ellison, RJ Gilbertson, SL Pomeroy, MD Taylor, P Lichter, and SM Pfister. *Molecular subgroups of medulloblastoma: an international meta-analysis of transcriptome, genetic aberrations, and clinical data of WNT, SHH, Group 3, and Group 4 medulloblastomas.* Acta Neuropathol. 2012; **123**(4):473-84.
 40. PA Northcott, A Korshunov, H Witt, T Hielscher, CG Eberhart, S Mack, E Bouffet, SC Clifford, CE Hawkins, P French, JT Rutka, S Pfister, and MD Taylor. *Medulloblastoma comprises four distinct molecular variants.* J Clin Oncol. 2011; **29**(11):1408-14.
 41. P Gibson, Y Tong, G Robinson, MC Thompson, DS Currle, C Eden, TA Kranenburg, T Hogg, H Poppleton, J Martin, D Finkelstein, S Pounds, A Weiss, Z Patay, M Scoggins, R Ogg, Y Pei, ZJ Yang, S Brun, Y Lee, F Zindy, JC Lindsey, MM Taketo, FA Boop, RA Sanford, A Gajjar, SC Clifford, MF Roussel, PJ McKinnon, DH Gutmann, DW Ellison, R Wechsler-Reya, and RJ Gilbertson. *Subtypes of medulloblastoma have distinct developmental origins.* Nature. 2010; **468**(7327):1095-9.
 42. FMG Cavalli, M Remke, L Rampasek, J Peacock, DJH Shih, B Luu, L Garzia, J Torchia, C Nor, AS Morrissy, S Agnihotri, YY Thompson, CM Kuzan-Fischer, H Farooq, K Isaev, C Daniels, BK Cho, SK Kim, KC Wang, JY Lee, WA Grajkowska, M Perek-Polnik, A Vasiljevic, C Faure-Conter, A Jouvett, C Giannini, AA Nageswara Rao, KKW Li, HK Ng, CG Eberhart, IF Pollack, RL Hamilton, GY Gillespie, JM Olson, S Leary, WA Weiss, B Lach, LB Chambless, RC Thompson, MK Cooper, R Vibhakar, P Hauser, MC van Veelen, JM Kros, PJ French, YS Ra, T Kumabe, E Lopez-Aguilar, K Zitterbart, J Sterba, G Finocchiaro, M Massimino, EG Van Meir, S Osuka, T Shofuda, A Klekner, M Zollo, JR Leonard, JB Rubin, N Jabado, S Albrecht, J Mora, TE Van Meter, S Jung, AS Moore, AR Hallahan, JA Chan, DPC Tirapelli, CG Carlotti, M Fouladi, J Pimentel, CC Faria, AG Saad, L Massimi, LM Liau, H Wheeler, H Nakamura, SK Elbabaa, M Perezpena-Diazconti, F Chico Ponce de Leon, S Robinson, M Zapotocky, A Lassaletta, A Huang, CE Hawkins, U Tabori, E Bouffet, U Bartels, PB Dirks, JT Rutka, GD Bader, J Reimand, A Goldenberg, V Ramaswamy, and MD Taylor. *Intertumoral Heterogeneity within Medulloblastoma Subgroups.* Cancer Cell. 2017; **31**(6):737-754 e6.
 43. PA Northcott, I Buchhalter, AS Morrissy, V Hovestadt, J Weischenfeldt, T Ehrenberger, S Grobner, M Segura-Wang, T Zichner, VA Rudneva, HJ Warnatz, N Sidiropoulos, AH Phillips, S Schumacher, K Kleinheinz, SM Waszak, S Erkek, DTW Jones, BC Worst, M Kool, M Zapatka, N Jager, L Chavez, B Hutter, M Bieg, N Paramasivam, M Heinold, Z

- Gu, N Ishaque, C Jager-Schmidt, CD Imbusch, A Jugold, D Hubschmann, T Risch, V Amstislavskiy, FGR Gonzalez, UD Weber, S Wolf, GW Robinson, X Zhou, G Wu, D Finkelstein, Y Liu, FMG Cavalli, B Luu, V Ramaswamy, X Wu, J Koster, M Ryzhova, YJ Cho, SL Pomeroy, C Herold-Mende, M Schuhmann, M Ebinger, LM Liau, J Mora, RE McLendon, N Jabado, T Kumabe, E Chuah, Y Ma, RA Moore, AJ Mungall, KL Mungall, N Thiessen, K Tse, T Wong, SJM Jones, O Witt, T Milde, A Von Deimling, D Capper, A Korshunov, ML Yaspo, R Kriwacki, A Gajjar, J Zhang, R Beroukhim, E Fraenkel, JO Korbel, B Brors, M Schlesner, R Eils, MA Marra, SM Pfister, MD Taylor, and P Lichter. *The whole-genome landscape of medulloblastoma subtypes*. Nature. 2017; **547**(7663):311-317.
44. C Raybaud, V Ramaswamy, MD Taylor, and S Laughlin. *Posterior fossa tumors in children: developmental anatomy and diagnostic imaging*. Childs Nerv Syst. 2015; **31**(10):1661-76.
45. MD Taylor, PA Northcott, A Korshunov, M Remke, YJ Cho, SC Clifford, CG Eberhart, DW Parsons, S Rutkowski, A Gajjar, DW Ellison, P Lichter, RJ Gilbertson, SL Pomeroy, M Kool, and SM Pfister. *Molecular subgroups of medulloblastoma: the current consensus*. Acta Neuropathol. 2012; **123**(4):465-72.
46. TJ Pugh, SD Weeraratne, TC Archer, DA Pomeranz Krummel, D Auclair, J Bochicchio, MO Carneiro, SL Carter, K Cibulskis, RL Erlich, H Greulich, MS Lawrence, NJ Lennon, A McKenna, J Meldrim, AH Ramos, MG Ross, C Russ, E Shefler, A Sivachenko, B Sogoloff, P Stojanov, P Tamayo, JP Mesirov, V Amani, N Teider, S Sengupta, JP Francois, PA Northcott, MD Taylor, F Yu, GR Crabtree, AG Kautzman, SB Gabriel, G Getz, N Jager, DT Jones, P Lichter, SM Pfister, TM Roberts, M Meyerson, SL Pomeroy, and YJ Cho. *Medulloblastoma exome sequencing uncovers subtype-specific somatic mutations*. Nature. 2012; **488**(7409):106-10.
47. G Robinson, M Parker, TA Kranenburg, C Lu, X Chen, L Ding, TN Phoenix, E Hedlund, L Wei, X Zhu, N Chalhoub, SJ Baker, R Huether, R Kriwacki, N Curley, R Thiruvankatam, J Wang, G Wu, M Rusch, X Hong, J Becksfort, P Gupta, J Ma, J Easton, B Vadodaria, A Onar-Thomas, T Lin, S Li, S Pounds, S Paugh, D Zhao, D Kawauchi, MF Roussel, D Finkelstein, DW Ellison, CC Lau, E Bouffet, T Hassall, S Gururangan, R Cohn, RS Fulton, LL Fulton, DJ Dooling, K Ochoa, A Gajjar, ER Mardis, RK Wilson, JR Downing, J Zhang, and RJ Gilbertson. *Novel mutations target distinct subgroups of medulloblastoma*. Nature. 2012; **488**(7409):43-8.
48. DT Jones, N Jager, M Kool, T Zichner, B Hutter, M Sultan, YJ Cho, TJ Pugh, V Hovestadt, AM Stutz, T Rausch, HJ Warnatz, M Ryzhova, S Bender, D Sturm, S Pleier, H Cin, E Pfaff, L Sieber, A Wittmann, M Remke, H Witt, S Hutter, T Tzaridis, J Weischenfeldt, B Raeder, M Avci, V Amstislavskiy, M Zapatka, UD Weber, Q Wang, B Lasitschka, CC Bartholomae, M Schmidt, C von Kalle, V Ast, C Lawerenz, J Eils, R Kabbe, V Benes, P van Sluis, J Koster, R Volckmann, D Shih, MJ Betts, RB Russell, S Coco, GP Tonini, U Schuller, V Hans, N Graf, YJ Kim, C Monoranu, W Roggendorf, A Unterberg, C Herold-Mende, T Milde, AE Kulozik, A von Deimling, O Witt, E Maass, J Rossler, M Ebinger, MU Schuhmann, MC Fruhwald, M Hasselblatt, N Jabado, S Rutkowski, AO von Bueren, D Williamson, SC Clifford, MG McCabe, VP Collins, S Wolf, S Wiemann, H Lehrach, B Brors, W Scheurlen, J Felsberg, G Reifenberger, PA Northcott, MD Taylor, M Meyerson, SL Pomeroy, ML Yaspo, JO Korbel, A Korshunov, R

- Eils, SM Pfister, and P Lichter. *Dissecting the genomic complexity underlying medulloblastoma*. Nature. 2012; **488**(7409):100-5.
49. DW Ellison, OE Onilude, JC Lindsey, ME Lusher, CL Weston, RE Taylor, AD Pearson, SC Clifford, and C United Kingdom Children's Cancer Study Group Brain Tumour. *beta-Catenin status predicts a favorable outcome in childhood medulloblastoma: the United Kingdom Children's Cancer Study Group Brain Tumour Committee*. J Clin Oncol. 2005; **23**(31):7951-7.
 50. MC Thompson, C Fuller, TL Hogg, J Dalton, D Finkelstein, CC Lau, M Chintagumpala, A Adesina, DM Ashley, SJ Kellie, MD Taylor, T Curran, A Gajjar, and RJ Gilbertson. *Genomics identifies medulloblastoma subgroups that are enriched for specific genetic alterations*. J Clin Oncol. 2006; **24**(12):1924-31.
 51. SC Clifford, ME Lusher, JC Lindsey, JA Langdon, RJ Gilbertson, D Straughton, and DW Ellison. *Wnt/Wingless pathway activation and chromosome 6 loss characterize a distinct molecular sub-group of medulloblastomas associated with a favorable prognosis*. Cell Cycle. 2006; **5**(22):2666-70.
 52. PA Northcott, DJ Shih, J Peacock, L Garzia, AS Morrissy, T Zichner, AM Stutz, A Korshunov, J Reimand, SE Schumacher, R Beroukhim, DW Ellison, CR Marshall, AC Lionel, S Mack, A Dubuc, Y Yao, V Ramaswamy, B Luu, A Rolider, FM Cavalli, X Wang, M Remke, X Wu, RY Chiu, A Chu, E Chuah, RD Corbett, GR Hoad, SD Jackman, Y Li, A Lo, KL Mungall, KM Nip, JQ Qian, AG Raymond, NT Thiessen, RJ Varhol, I Birol, RA Moore, AJ Mungall, R Holt, D Kawauchi, MF Roussel, M Kool, DT Jones, H Witt, LA Fernandez, AM Kenney, RJ Wechsler-Reya, P Dirks, T Aviv, WA Grajkowska, M Perek-Polnik, CC Haberler, O Delattre, SS Reynaud, FF Doz, SS Pernet-Fattet, BK Cho, SK Kim, KC Wang, W Scheurlen, CG Eberhart, M Fevre-Montange, A Jouvet, IF Pollack, X Fan, KM Muraszko, GY Gillespie, C Di Rocco, L Massimi, EM Michiels, NK Kloosterhof, PJ French, JM Kros, JM Olson, RG Ellenbogen, K Zitterbart, L Kren, RC Thompson, MK Cooper, B Lach, RE McLendon, DD Bigner, A Fontebasso, S Albrecht, N Jabado, JC Lindsey, S Bailey, N Gupta, WA Weiss, L Bogner, A Klekner, TE Van Meter, T Kumabe, T Tominaga, SK Elbabaa, JR Leonard, JB Rubin, LM Liau, EG Van Meir, M Fouladi, H Nakamura, G Cinalli, M Garami, P Hauser, AG Saad, A Iolascon, S Jung, CG Carlotti, R Vibhakar, YS Ra, S Robinson, M Zollo, CC Faria, JA Chan, ML Levy, PH Sorensen, M Meyerson, SL Pomeroy, YJ Cho, GD Bader, U Tabori, CE Hawkins, E Bouffet, SW Scherer, JT Rutka, D Malkin, SC Clifford, SJ Jones, JO Korbel, SM Pfister, MA Marra and MD Taylor. *Subgroup-specific structural variation across 1,000 medulloblastoma genomes*. Nature. 2012; **488**(7409):49-56.
 53. S Oh, RA Flynn, SN Floor, J Purzner, L Martin, BT Do, S Schubert, D Vaka, S Morrissy, Y Li, M Kool, V Hovestadt, DT Jones, PA Northcott, T Risch, HJ Warnatz, ML Yaspo, CM Adams, RD Leib, M Breese, MA Marra, D Malkin, P Lichter, JA Doudna, SM Pfister, MD Taylor, HY Chang, and YJ Cho. *Medulloblastoma-associated DDX3 variant selectively alters the translational response to stress*. Oncotarget. 2016; **7**(19):28169-82.
 54. A Gajjar, GW Robinson, KS Smith, T Lin, TE Merchant, M Chintagumpala, A Mahajan, J Su, E Bouffet, U Bartels, T Schechter, T Hassall, T Robertson, W Nicholls, S Gururangan, K Schroeder, M Sullivan, G Wheeler, JR Hansford, SJ Kellie, G McCowage, R Cohn, MJ Fisher, MJ Krasin, CF Stewart, A Broniscer, I Buchhalter, RG Tatevossian, BA Orr, G Neale, P Klimo, Jr., F Boop, A Srinivasan, SM Pfister, RJ Gilbertson, A Onar-Thomas, DW Ellison, and PA Northcott. *Outcomes by Clinical and Molecular Features in Children*

- With Medulloblastoma Treated With Risk-Adapted Therapy: Results of an International Phase III Trial (SJMB03)*. J Clin Oncol. 2021; **39**(7):822-835.
55. J Garcia-Lopez, R Kumar, KS Smith, and PA Northcott. *Deconstructing Sonic Hedgehog Medulloblastoma: Molecular Subtypes, Drivers, and Beyond*. Trends Genet. 2021; **37**(3):235-250.
 56. PA Northcott, T Hielscher, A Dubuc, S Mack, D Shih, M Remke, H Al-Halabi, S Albrecht, N Jabado, CG Eberhart, W Grajkowska, WA Weiss, SC Clifford, E Bouffet, JT Rutka, A Korshunov, S Pfister, and MD Taylor. *Pediatric and adult sonic hedgehog medulloblastomas are clinically and molecularly distinct*. Acta Neuropathol. 2011; **122**(2):231-40.
 57. EC Schwalbe, JC Lindsey, S Nakjang, S Crosier, AJ Smith, D Hicks, G Rafiee, RM Hill, A Iliasova, T Stone, B Pizer, A Michalski, A Joshi, SB Wharton, TS Jacques, S Bailey, D Williamson, and SC Clifford. *Novel molecular subgroups for clinical classification and outcome prediction in childhood medulloblastoma: a cohort study*. Lancet Oncol. 2017; **18**(7):958-971.
 58. M Kool, DT Jones, N Jager, PA Northcott, TJ Pugh, V Hovestadt, RM Piro, LA Esparza, SL Markant, M Remke, T Milde, F Bourdeaut, M Ryzhova, D Sturm, E Pfaff, S Stark, S Hutter, H Seker-Cin, P Johann, S Bender, C Schmidt, T Rausch, D Shih, J Reimand, L Sieber, A Wittmann, L Linke, H Witt, UD Weber, M Zapatka, R Konig, R Beroukhim, G Bergthold, P van Sluis, R Volckmann, J Koster, R Versteeg, S Schmidt, S Wolf, C Lawrenz, CC Bartholomae, C von Kalle, A Unterberg, C Herold-Mende, S Hofer, AE Kulozik, A von Deimling, W Scheurlen, J Felsberg, G Reifenberger, M Hasselblatt, JR Crawford, GA Grant, N Jabado, A Perry, C Cowdrey, S Croul, G Zadeh, JO Korbel, F Doz, O Delattre, GD Bader, MG McCabe, VP Collins, MW Kieran, YJ Cho, SL Pomeroy, O Witt, B Brors, MD Taylor, U Schuller, A Korshunov, R Eils, RJ Wechsler-Reya, P Lichter, SM Pfister, and IPT Project. *Genome sequencing of SHH medulloblastoma predicts genotype-related response to smoothed inhibition*. Cancer Cell. 2014; **25**(3):393-405.
 59. JC Lindsey, EC Schwalbe, S Potluri, S Bailey, D Williamson, and SC Clifford. *TERT promoter mutation and aberrant hypermethylation are associated with elevated expression in medulloblastoma and characterise the majority of non-infant SHH subgroup tumours*. Acta Neuropathol. 2014; **127**(2):307-9.
 60. K Fujii and T Miyashita. *Gorlin syndrome (nevoid basal cell carcinoma syndrome): update and literature review*. Pediatr Int. 2014; **56**(5):667-74.
 61. MD Taylor, L Liu, C Raffel, CC Hui, TG Mainprize, X Zhang, R Agatep, S Chiappa, L Gao, A Lowrance, A Hao, AM Goldstein, T Stavrou, SW Scherer, WT Dura, B Wainwright, JA Squire, JT Rutka, and D Hogg. *Mutations in SUFU predispose to medulloblastoma*. Nat Genet. 2002; **31**(3):306-10.
 62. N Zhukova, V Ramaswamy, M Remke, E Pfaff, DJ Shih, DC Martin, P Castelo-Branco, B Baskin, PN Ray, E Bouffet, AO von Bueren, DT Jones, PA Northcott, M Kool, D Sturm, TJ Pugh, SL Pomeroy, YJ Cho, T Pietsch, M Gessi, S Rutkowski, L Bogнар, A Klekner, BK Cho, SK Kim, KC Wang, CG Eberhart, M Fevre-Montange, M Fouladi, PJ French, M Kros, WA Grajkowska, N Gupta, WA Weiss, P Hauser, N Jabado, A Jouvet, S Jung, T Kumabe, B Lach, JR Leonard, JB Rubin, LM Liau, L Massimi, IF Pollack, Y Shin Ra, EG Van Meir, K Zitterbart, U Schuller, RM Hill, JC Lindsey, EC Schwalbe, S Bailey, DW Ellison, C Hawkins, D Malkin, SC Clifford, A Korshunov, S Pfister, MD Taylor, and U

- Tabori. *Subgroup-specific prognostic implications of TP53 mutation in medulloblastoma*. J Clin Oncol. 2013; **31**(23):2927-35.
63. DM Patmore, A Jassim, E Nathan, RJ Gilbertson, D Tahan, N Hoffmann, Y Tong, KS Smith, TD Kanneganti, H Suzuki, MD Taylor, P Northcott, and RJ Gilbertson. *DDX3X Suppresses the Susceptibility of Hindbrain Lineages to Medulloblastoma*. Dev Cell. 2020; **54**(4):455-470 e5.
 64. DJ Shih, PA Northcott, M Remke, A Korshunov, V Ramaswamy, M Kool, B Luu, Y Yao, X Wang, AM Dubuc, L Garzia, J Peacock, SC Mack, X Wu, A Rolider, AS Morrissy, FM Cavalli, DT Jones, K Zitterbart, CC Faria, U Schuller, L Kren, T Kumabe, T Tominaga, Y Shin Ra, M Garami, P Hauser, JA Chan, S Robinson, L Bognar, A Klekner, AG Saad, LM Liau, S Albrecht, A Fontebasso, G Cinalli, P De Antonellis, M Zollo, MK Cooper, RC Thompson, S Bailey, JC Lindsey, C Di Rocco, L Massimi, EM Michiels, SW Scherer, JJ Phillips, N Gupta, X Fan, KM Muraszko, R Vibhakar, CG Eberhart, M Fouladi, B Lach, S Jung, RJ Wechsler-Reya, M Fevre-Montange, A Jouvet, N Jabado, IF Pollack, WA Weiss, JY Lee, BK Cho, SK Kim, KC Wang, JR Leonard, JB Rubin, C de Torres, C Lavarino, J Mora, YJ Cho, U Tabori, JM Olson, A Gajjar, RJ Packer, S Rutkowski, SL Pomeroy, PJ French, NK Kloosterhof, JM Kros, EG Van Meir, SC Clifford, F Bourdeaut, O Delattre, FF Doz, CE Hawkins, D Malkin, WA Grajkowska, M Perek-Polnik, E Bouffet, JT Rutka, SM Pfister, and MD Taylor. *Cytogenetic prognostication within medulloblastoma subgroups*. J Clin Oncol. 2014; **32**(9):886-96.
 65. D Kawauchi, RJ Ogg, L Liu, DJH Shih, D Finkelstein, BL Murphy, JE Rehg, A Korshunov, C Calabrese, F Zindy, T Phoenix, Y Kawaguchi, J Gronych, RJ Gilbertson, P Lichter, A Gajjar, M Kool, PA Northcott, SM Pfister, and MF Roussel. *Novel MYC-driven medulloblastoma models from multiple embryonic cerebellar cells*. Oncogene. 2017; **36**(37):5231-5242.
 66. Y Pei, CE Moore, J Wang, AK Tewari, A Eroshkin, YJ Cho, H Witt, A Korshunov, TA Read, JL Sun, EM Schmitt, CR Miller, AF Buckley, RE McLendon, TF Westbrook, PA Northcott, MD Taylor, SM Pfister, PG Febbo, and RJ Wechsler-Reya. *An animal model of MYC-driven medulloblastoma*. Cancer Cell. 2012; **21**(2):155-67.
 67. PA Northcott, AM Dubuc, S Pfister, and MD Taylor. *Molecular subgroups of medulloblastoma*. Expert Rev Neurother. 2012; **12**(7):871-84.
 68. M Kool, J Koster, J Bunt, NE Hasselt, A Lakeman, P van Sluis, D Troost, NS Meeteren, HN Caron, J Cloos, A Mrsic, B Ylstra, W Grajkowska, W Hartmann, T Pietsch, D Ellison, SC Clifford, and R Versteeg. *Integrated genomics identifies five medulloblastoma subtypes with distinct genetic profiles, pathway signatures and clinicopathological features*. PLoS One. 2008; **3**(8):e3088.
 69. PA Northcott, DT Jones, M Kool, GW Robinson, RJ Gilbertson, YJ Cho, SL Pomeroy, A Korshunov, P Lichter, MD Taylor, and SM Pfister. *Medulloblastomics: the end of the beginning*. Nat Rev Cancer. 2012; **12**(12):818-34.
 70. F Beby and T Lamonerie. *The homeobox gene Otx2 in development and disease*. Exp Eye Res. 2013; **111**:9-16.
 71. PA Northcott, C Lee, T Zichner, AM Stutz, S Erkek, D Kawauchi, DJ Shih, V Hovestadt, M Zapatka, D Sturm, DT Jones, M Kool, M Remke, FM Cavalli, S Zuyderduyn, GD Bader, S VandenBerg, LA Esparza, M Ryzhova, W Wang, A Wittmann, S Stark, L Sieber, H Seker-Cin, L Linke, F Kratochwil, N Jager, I Buchhalter, CD Imbusch, G Zipprich, B Raeder, S Schmidt, N Diessl, S Wolf, S Wiemann, B Brors, C Lawerenz, J Eils, HJ

- Warnatz, T Risch, ML Yaspo, UD Weber, CC Bartholomae, C von Kalle, E Turanyi, P Hauser, E Sanden, A Darabi, P Siesjo, J Sterba, K Zitterbart, D Sumerauer, P van Sluis, R Versteeg, R Volckmann, J Koster, MU Schuhmann, M Ebinger, HL Grimes, GW Robinson, A Gajjar, M Mynarek, K von Hoff, S Rutkowski, T Pietsch, W Scheurlen, J Felsberg, G Reifenberger, AE Kulozik, A von Deimling, O Witt, R Eils, RJ Gilbertson, A Korshunov, MD Taylor, P Lichter, JO Korbel, RJ Wechsler-Reya, and SM Pfister. *Enhancer hijacking activates GFII family oncogenes in medulloblastoma*. *Nature*. 2014; **511**(7510):428-34.
72. CY Lin, S Erkek, Y Tong, L Yin, AJ Federation, M Zapatka, P Haldipur, D Kawauchi, T Risch, HJ Warnatz, BC Worst, B Ju, BA Orr, R Zeid, DR Polaski, M Segura-Wang, SM Waszak, DT Jones, M Kool, V Hovestadt, I Buchhalter, L Sieber, P Johann, L Chavez, S Groschel, M Ryzhova, A Korshunov, W Chen, VV Chizhikov, KJ Millen, V Amstislavskiy, H Lehrach, ML Yaspo, R Eils, P Lichter, JO Korbel, SM Pfister, JE Bradner, and PA Northcott. *Active medulloblastoma enhancers reveal subgroup-specific cellular origins*. *Nature*. 2016; **530**(7588):57-62.
73. JT Romer, H Kimura, S Magdaleno, K Sasai, C Fuller, H Baines, M Connelly, CF Stewart, S Gould, LL Rubin, and T Curran. *Suppression of the Shh pathway using a small molecule inhibitor eliminates medulloblastoma in Ptc1(+/-)p53(-/-) mice*. *Cancer Cell*. 2004; **6**(3):229-40.
74. DM Berman, SS Karhadkar, AR Hallahan, JI Pritchard, CG Eberhart, DN Watkins, JK Chen, MK Cooper, J Taipale, JM Olson, and PA Beachy. *Medulloblastoma growth inhibition by hedgehog pathway blockade*. *Science*. 2002; **297**(5586):1559-61.
75. G Filocamo, M Brunetti, F Colaceci, R Sasso, M Tanori, E Pasquali, R Alfonsi, M Mancuso, A Saran, A Lahm, L Di Marcotullio, C Steinkuhler, and S Pazzaglia. *MK-4101, a Potent Inhibitor of the Hedgehog Pathway, Is Highly Active against Medulloblastoma and Basal Cell Carcinoma*. *Mol Cancer Ther*. 2016; **15**(6):1177-89.
76. A Gajjar, CF Stewart, DW Ellison, S Kaste, LE Kun, RJ Packer, S Goldman, M Chintagumpala, D Wallace, N Takebe, JM Boyett, RJ Gilbertson, and T Curran. *Phase I study of vismodegib in children with recurrent or refractory medulloblastoma: a pediatric brain tumor consortium study*. *Clin Cancer Res*. 2013; **19**(22):6305-12.
77. GW Robinson, BA Orr, G Wu, S Gururangan, T Lin, I Qaddoumi, RJ Packer, S Goldman, MD Prados, A Desjardins, M Chintagumpala, N Takebe, SC Kaste, M Rusch, SJ Allen, A Onar-Thomas, CF Stewart, M Fouladi, JM Boyett, RJ Gilbertson, T Curran, DW Ellison, and A Gajjar. *Vismodegib Exerts Targeted Efficacy Against Recurrent Sonic Hedgehog-Subgroup Medulloblastoma: Results From Phase II Pediatric Brain Tumor Consortium Studies PBTC-025B and PBTC-032*. *J Clin Oncol*. 2015; **33**(24):2646-54.
78. M Lauth, A Bergstrom, T Shimokawa, and R Toftgard. *Inhibition of GLI-mediated transcription and tumor cell growth by small-molecule antagonists*. *Proc Natl Acad Sci U S A*. 2007; **104**(20):8455-60.
79. Z Lin, S Li, H Sheng, M Cai, LY Ma, L Hu, S Xu, LS Yu, and N Zhang. *Suppression of GLI sensitizes medulloblastoma cells to mitochondria-mediated apoptosis*. *J Cancer Res Clin Oncol*. 2016; **142**(12):2469-2478.
80. S Buonamici, J Williams, M Morrissey, A Wang, R Guo, A Vattay, K Hsiao, J Yuan, J Green, B Ospina, Q Yu, L Ostrom, P Fordjour, DL Anderson, JE Monahan, JF Kelleher, S Peukert, S Pan, X Wu, SM Maira, C Garcia-Echeverria, KJ Briggs, DN Watkins, YM Yao, C Lengauer, M Warmuth, WR Sellers, and M Dorsch. *Interfering with resistance to*

- smoothened antagonists by inhibition of the PI3K pathway in medulloblastoma.* Sci Transl Med. 2010; **2**(51):51ra70.
81. SL Markant, LA Esparza, J Sun, KL Barton, LM McCoig, GA Grant, JR Crawford, ML Levy, PA Northcott, D Shih, M Remke, MD Taylor, and RJ Wechsler-Reya. *Targeting sonic hedgehog-associated medulloblastoma through inhibition of Aurora and Polo-like kinases.* Cancer Res. 2013; **73**(20):6310-22.
 82. J Triscott, C Lee, C Foster, B Manoranjan, MR Pambid, R Berns, A Fotovati, C Venugopal, K O'Halloran, A Narendran, C Hawkins, V Ramaswamy, E Bouffet, MD Taylor, A Singhal, J Hukin, R Rassekh, S Yip, P Northcott, SK Singh, C Dunham, and SE Dunn. *Personalizing the treatment of pediatric medulloblastoma: Polo-like kinase 1 as a molecular target in high-risk children.* Cancer Res. 2013; **73**(22):6734-44.
 83. A Henssen, T Thor, A Odersky, L Heukamp, N El-Hindy, A Beckers, F Speleman, K Althoff, S Schafers, A Schramm, U Sure, G Fleischhack, A Eggert, and JH Schulte. *BET bromodomain protein inhibition is a therapeutic option for medulloblastoma.* Oncotarget. 2013; **4**(11):2080-95.
 84. M Magistri, D Velmeshev, M Makhmutova, P Patel, GC Sartor, CH Volmar, C Wahlestedt, and MA Faghihi. *The BET-Bromodomain Inhibitor JQ1 Reduces Inflammation and Tau Phosphorylation at Ser396 in the Brain of the 3xTg Model of Alzheimer's Disease.* Curr Alzheimer Res. 2016; **13**(9):985-95.
 85. P Bandopadhyay, G Bergthold, B Nguyen, S Schubert, S Gholamin, Y Tang, S Bolin, SE Schumacher, R Zeid, S Masoud, F Yu, N Vue, WJ Gibson, BR Paoletta, SS Mitra, SH Cheshier, J Qi, KW Liu, R Wechsler-Reya, WA Weiss, FJ Swartling, MW Kieran, JE Bradner, R Beroukhi, and YJ Cho. *BET bromodomain inhibition of MYC-amplified medulloblastoma.* Clin Cancer Res. 2014; **20**(4):912-25.
 86. K Sun, R Atoyian, MA Borek, S Dellarocca, ME Samson, AW Ma, GX Xu, T Patterson, DP Tuck, JL Viner, A Fattaey, and J Wang. *Dual HDAC and PI3K Inhibitor CUDC-907 Downregulates MYC and Suppresses Growth of MYC-dependent Cancers.* Mol Cancer Ther. 2017; **16**(2):285-299.
 87. D Yang, H Liu, A Goga, S Kim, M Yuneva, and JM Bishop. *Therapeutic potential of a synthetic lethal interaction between the MYC proto-oncogene and inhibition of aurora-B kinase.* Proc Natl Acad Sci U S A. 2010; **107**(31):13836-41.
 88. RJ Diaz, B Golbourn, C Faria, D Picard, D Shih, D Raynaud, M Leadly, D MacKenzie, M Bryant, M Bebenek, CA Smith, MD Taylor, A Huang, and JT Rutka. *Mechanism of action and therapeutic efficacy of Aurora kinase B inhibition in MYC overexpressing medulloblastoma.* Oncotarget. 2015; **6**(5):3359-74.
 89. MW Richards, SG Burgess, E Poon, A Carstensen, M Eilers, L Chesler, and R Bayliss. *Structural basis of N-Myc binding by Aurora-A and its destabilization by kinase inhibitors.* Proc Natl Acad Sci U S A. 2016; **113**(48):13726-13731.
 90. WC Gustafson, JG Meyerowitz, EA Nekritz, J Chen, C Benes, E Charron, EF Simonds, R Seeger, KK Matthay, NT Hertz, M Eilers, KM Shokat, and WA Weiss. *Drugging MYCN through an allosteric transition in Aurora kinase A.* Cancer Cell. 2014; **26**(3):414-427.
 91. AR Hanaford, TC Archer, A Price, UD Kahlert, J Maciaczyk, G Nikkhah, JW Kim, T Ehrenberger, PA Clemons, V Dancik, B Seashore-Ludlow, V Viswanathan, ML Stewart, MG Rees, A Shamji, S Schreiber, E Fraenkel, SL Pomeroy, JP Mesirov, P Tamayo, CG Eberhart, and EH Raabe. *DiSCoVERing Innovative Therapies for Rare Tumors:*

- Combining Genetically Accurate Disease Models with In Silico Analysis to Identify Novel Therapeutic Targets.* Clin Cancer Res. 2016; **22**(15):3903-14.
92. ML Cook Sangar, LA Genovesi, MW Nakamoto, MJ Davis, SE Knobluagh, P Ji, A Millar, BJ Wainwright, and JM Olson. *Inhibition of CDK4/6 by Palbociclib Significantly Extends Survival in Medulloblastoma Patient-Derived Xenograft Mouse Models.* Clin Cancer Res. 2017; **23**(19):5802-5813.
 93. C Lee, VA Rudneva, S Erkek, M Zapatka, LQ Chau, SK Tacheva-Grigorova, A Garancher, JM Rusert, O Aksoy, R Lea, HP Mohammad, J Wang, WA Weiss, HL Grimes, SM Pfister, PA Northcott, and RJ Wechsler-Reya. *Lsd1 as a therapeutic target in Gfi1-activated medulloblastoma.* Nat Commun. 2019; **10**(1):332.
 94. X Wang, H Zhang, and X Chen. *Drug resistance and combating drug resistance in cancer.* Cancer Drug Resist. 2019; **2**:141-160.
 95. C Holohan, S Van Schaeybroeck, DB Longley, and PG Johnston. *Cancer drug resistance: an evolving paradigm.* Nat Rev Cancer. 2013; **13**(10):714-26.
 96. N Vasani, J Baselga, and DM Hyman. *A view on drug resistance in cancer.* Nature. 2019; **575**(7782):299-309.
 97. RT Othman, I Kimishi, TD Bradshaw, LC Storer, A Korshunov, SM Pfister, RG Grundy, ID Kerr, and B Coyle. *Overcoming multiple drug resistance mechanisms in medulloblastoma.* Acta Neuropathol Commun. 2014; **2**:57.
 98. C Meijer, NH Mulder, H Timmer-Bosscha, WJ Sluiter, GJ Meersma, and EG de Vries. *Relationship of cellular glutathione to the cytotoxicity and resistance of seven platinum compounds.* Cancer Res. 1992; **52**(24):6885-9.
 99. EE Bar, A Chaudhry, MH Farah, and CG Eberhart. *Hedgehog signaling promotes medulloblastoma survival via Bc/II.* Am J Pathol. 2007; **170**(1):347-55.
 100. I Dagogo-Jack and AT Shaw. *Tumour heterogeneity and resistance to cancer therapies.* Nat Rev Clin Oncol. 2018; **15**(2):81-94.
 101. N Garg, D Bakhshinyan, C Venugopal, S Mahendram, DA Rosa, T Vijayakumar, B Manoranjan, R Hallett, N McFarlane, KH Delaney, JM Kwiecien, CC Arpin, PS Lai, RF Gomez-Biagi, AM Ali, ED de Araujo, OA Ajani, JA Hassell, PT Gunning, and SK Singh. *CD133(+) brain tumor-initiating cells are dependent on STAT3 signaling to drive medulloblastoma recurrence.* Oncogene. 2017; **36**(5):606-617.
 102. RL Bowman, F Klemm, L Akkari, SM Pyonteck, L Sevenich, DF Quail, S Dhara, K Simpson, EE Gardner, CA Iacobuzio-Donahue, CW Brennan, V Tabar, PH Gutin, and JA Joyce. *Macrophage Ontogeny Underlies Differences in Tumor-Specific Education in Brain Malignancies.* Cell Rep. 2016; **17**(9):2445-2459.
 103. DF Quail and JA Joyce. *The Microenvironmental Landscape of Brain Tumors.* Cancer Cell. 2017; **31**(3):326-341.
 104. AS Margol, NJ Robison, J Gnanachandran, LT Hung, RJ Kennedy, M Vali, G Dhall, JL Finlay, A Erdreich-Epstein, MD Krieger, R Drissi, M Fouladi, FH Gilles, AR Judkins, R Sposto, and S Asgharzadeh. *Tumor-associated macrophages in SHH subgroup of medulloblastomas.* Clin Cancer Res. 2015; **21**(6):1457-65.
 105. S Anguille, EL Smits, E Lion, VF van Tendeloo, and ZN Berneman. *Clinical use of dendritic cells for cancer therapy.* Lancet Oncol. 2014; **15**(7):e257-67.
 106. M Massara, P Persico, O Bonavita, V Mollica Poeta, M Locati, M Simonelli, and R Bonecchi. *Neutrophils in Gliomas.* Front Immunol. 2017; **8**:1349.

107. S Diao, C Gu, H Zhang, and C Yu. *Immune cell infiltration and cytokine secretion analysis reveal a non-inflammatory microenvironment of medulloblastoma*. *Oncol Lett*. 2020; **20**(6):397.
108. Q Lin, K Balasubramanian, D Fan, SJ Kim, L Guo, H Wang, M Bar-Eli, KD Aldape, and IJ Fidler. *Reactive astrocytes protect melanoma cells from chemotherapy by sequestering intracellular calcium through gap junction communication channels*. *Neoplasia*. 2010; **12**(9):748-54.
109. W Chen, D Wang, X Du, Y He, S Chen, Q Shao, C Ma, B Huang, A Chen, P Zhao, X Qu, and X Li. *Glioma cells escaped from cytotoxicity of temozolomide and vincristine by communicating with human astrocytes*. *Med Oncol*. 2015; **32**(3):43.
110. Y Liu, LW Yuelling, Y Wang, F Du, RE Gordon, JA O'Brien, JMY Ng, S Robins, EH Lee, H Liu, T Curran, and ZJ Yang. *Astrocytes Promote Medulloblastoma Progression through Hedgehog Secretion*. *Cancer Res*. 2017; **77**(23):6692-6703.
111. RL Bowman and JA Joyce. *Therapeutic targeting of tumor-associated macrophages and microglia in glioblastoma*. *Immunotherapy*. 2014; **6**(6):663-6.
112. T Byrd, RG Grossman, and N Ahmed. *Medulloblastoma-biology and microenvironment: a review*. *Pediatr Hematol Oncol*. 2012; **29**(6):495-506.
113. M Bockmayr, M Mohme, F Klauschen, B Winkler, J Budczies, S Rutkowski, and U Schuller. *Subgroup-specific immune and stromal microenvironment in medulloblastoma*. *Oncoimmunology*. 2018; **7**(9):e1462430.
114. D Murata, Y Mineharu, Y Arakawa, B Liu, M Tanji, M Yamaguchi, KI Fujimoto, N Fukui, Y Terada, R Yokogawa, M Yamaguchi, S Minamiguchi, and S Miyamoto. *High programmed cell death 1 ligand-1 expression: association with CD8+ T-cell infiltration and poor prognosis in human medulloblastoma*. *J Neurosurg*. 2018; **128**(3):710-716.
115. AM Martin, CJ Nirschl, MJ Polanczyk, WR Bell, TR Nirschl, S Harris-Bookman, J Phallen, J Hicks, D Martinez, A Ogurtsova, H Xu, LM Sullivan, AK Meeker, EH Raabe, KJ Cohen, CG Eberhart, PC Burger, M Santi, JM Taube, DM Pardoll, CG Drake, and M Lim. *PD-L1 expression in medulloblastoma: an evaluation by subgroup*. *Oncotarget*. 2018; **9**(27):19177-19191.
116. TF Kabir, CA Kunos, JL Villano, and A Chauhan. *Immunotherapy for Medulloblastoma: Current Perspectives*. *Immunotargets Ther*. 2020; **9**:57-77.
117. BE Lippitz and RA Harris. *Cytokine patterns in cancer patients: A review of the correlation between interleukin 6 and prognosis*. *Oncoimmunology*. 2016; **5**(5):e1093722.
118. HJ Lee, G Zhuang, Y Cao, P Du, HJ Kim, and J Settleman. *Drug resistance via feedback activation of Stat3 in oncogene-addicted cancer cells*. *Cancer Cell*. 2014; **26**(2):207-21.
119. DR Hodge, EM Hurt, and WL Farrar. *The role of IL-6 and STAT3 in inflammation and cancer*. *Eur J Cancer*. 2005; **41**(16):2502-12.
120. L Sreenivasan, H Wang, SQ Yap, P Leclair, A Tam, and CJ Lim. *Autocrine IL-6/STAT3 signaling aids development of acquired drug resistance in Group 3 medulloblastoma*. *Cell Death Dis*. 2020; **11**(12):1035.
121. PC Heinrich, I Behrmann, S Haan, HM Hermanns, G Muller-Newen, and F Schaper. *Principles of interleukin (IL)-6-type cytokine signaling and its regulation*. *Biochem J*. 2003; **374**(Pt 1):1-20.
122. SA Jones and BJ Jenkins. *Recent insights into targeting the IL-6 cytokine family in inflammatory diseases and cancer*. *Nat Rev Immunol*. 2018; **18**(12):773-789.
123. CA Dinarello. *Historical insights into cytokines*. *Eur J Immunol*. 2007; **37** **Suppl 1**:S34-45.

124. C Garbers, HM Hermanns, F Schaper, G Muller-Newen, J Grotzinger, S Rose-John, and J Scheller. *Plasticity and cross-talk of interleukin 6-type cytokines*. Cytokine Growth Factor Rev. 2012; **23**(3):85-97.
125. M Murakami, D Kamimura, and T Hirano. *Pleiotropy and Specificity: Insights from the Interleukin 6 Family of Cytokines*. Immunity. 2019; **50**(4):812-831.
126. S Kang, T Tanaka, M Narazaki, and T Kishimoto. *Targeting Interleukin-6 Signaling in Clinic*. Immunity. 2019; **50**(4):1007-1023.
127. S Rose-John. *Interleukin-6 Family Cytokines*. Cold Spring Harb Perspect Biol. 2018; **10**(2).
128. L Melton and A Coombs. *Actemra poised to launch IL-6 inhibitors*. Nat Biotechnol. 2008; **26**(9):957-9.
129. PC Heinrich, I Behrmann, G Muller-Newen, F Schaper, and L Graeve. *Interleukin-6-type cytokine signaling through the gp130/Jak/STAT pathway*. Biochem J. 1998; **334** (Pt 2):297-314.
130. RD Metcalfe, TL Putoczki, and MDW Griffin. *Structural Understanding of Interleukin 6 Family Cytokine Signaling and Targeted Therapies: Focus on Interleukin 11*. Front Immunol. 2020; **11**:1424.
131. T Omokehinde and RW Johnson. *GP130 Cytokines in Breast Cancer and Bone*. Cancers (Basel). 2020; **12**(2).
132. X Wu, Y Cao, H Xiao, C Li, and J Lin. *Bazedoxifene as a Novel GP130 Inhibitor for Pancreatic Cancer Therapy*. Mol Cancer Ther. 2016; **15**(11):2609-2619.
133. H Xiao, HK Bid, X Chen, X Wu, J Wei, Y Bian, C Zhao, H Li, C Li, and J Lin. *Repositioning Bazedoxifene as a novel IL-6/GP130 signaling antagonist for human rhabdomyosarcoma therapy*. PLoS One. 2017; **12**(7):e0180297.
134. J Tian, X Chen, S Fu, R Zhang, L Pan, Y Cao, X Wu, H Xiao, HJ Lin, HW Lo, Y Zhang, and J Lin. *Bazedoxifene is a novel IL-6/GP130 inhibitor for treating triple-negative breast cancer*. Breast Cancer Res Treat. 2019; **175**(3):553-566.
135. W Song, K Gao, P Huang, Z Tang, F Nie, S Jia, and R Guo. *Bazedoxifene inhibits PDGF-BB induced VSMC phenotypic switch via regulating the autophagy level*. Life Sci. 2020; **259**:118397.
136. RA Hill, K Kouremenos, D Tull, A Maggi, A Schroeder, A Gibbons, J Kulkarni, S Sundram, and X Du. *Bazedoxifene - a promising brain active SERM that crosses the blood brain barrier and enhances spatial memory*. Psychoneuroendocrinology. 2020; **121**:104830.
137. S Xu, F Grande, A Garofalo, and N Neamati. *Discovery of a novel orally active small-molecule gp130 inhibitor for the treatment of ovarian cancer*. Mol Cancer Ther. 2013; **12**(6):937-49.
138. E Bousoik and H Montazeri Aliabadi. *"Do We Know Jack" About JAK? A Closer Look at JAK/STAT Signaling Pathway*. Front Oncol. 2018; **8**:287.
139. F Seif, M Khoshmirsafa, H Aazami, M Mohsenzadegan, G Sedighi, and M Bahar. *The role of JAK-STAT signaling pathway and its regulators in the fate of T helper cells*. Cell Commun Signal. 2017; **15**(1):23.
140. R Ferrao and PJ Lupardus. *The Janus Kinase (JAK) FERM and SH2 Domains: Bringing Specificity to JAK-Receptor Interactions*. Front Endocrinol (Lausanne). 2017; **8**:71.
141. C Liongue and AC Ward. *Evolution of the JAK-STAT pathway*. JAKSTAT. 2013; **2**(1):e22756.

142. J Pencik, HT Pham, J Schmoellerl, T Javaheri, M Schleederer, Z Culig, O Merkel, R Moriggl, F Grebien, and L Kenner. *JAK-STAT signaling in cancer: From cytokines to non-coding genome*. Cytokine. 2016; **87**:26-36.
143. L Song, B Rawal, JA Nemeth, and EB Haura. *JAK1 activates STAT3 activity in non-small-cell lung cancer cells and IL-6 neutralizing antibodies can suppress JAK1-STAT3 signaling*. Mol Cancer Ther. 2011; **10**(3):481-94.
144. C Nielsen, HS Birgens, BG Nordestgaard, L Kjaer, and SE Bojesen. *The JAK2 V617F somatic mutation, mortality and cancer risk in the general population*. Haematologica. 2011; **96**(3):450-3.
145. J Mascarenhas, TI Mughal, and S Verstovsek. *Biology and clinical management of myeloproliferative neoplasms and development of the JAK inhibitor ruxolitinib*. Curr Med Chem. 2012; **19**(26):4399-413.
146. J Abdulghani, L Gu, A Dagvadorj, J Lutz, B Leiby, G Bonuccelli, MP Lisanti, T Zellweger, K Alanen, T Mirtti, T Visakorpi, L Bubendorf, and MT Nevalainen. *Stat3 promotes metastatic progression of prostate cancer*. Am J Pathol. 2008; **172**(6):1717-28.
147. WM Burke, X Jin, HJ Lin, M Huang, R Liu, RK Reynolds, and J Lin. *Inhibition of constitutively active Stat3 suppresses growth of human ovarian and breast cancer cells*. Oncogene. 2001; **20**(55):7925-34.
148. U Holtick, M Vockerodt, D Pinkert, N Schoof, B Sturzenhofecker, N Kussebi, K Lauber, S Wesselborg, D Loffler, F Horn, L Trumper, and D Kube. *STAT3 is essential for Hodgkin lymphoma cell proliferation and is a target of tyrphostin AG17 which confers sensitization for apoptosis*. Leukemia. 2005; **19**(6):936-44.
149. H Yu, D Pardoll, and R Jove. *STATs in cancer inflammation and immunity: a leading role for STAT3*. Nat Rev Cancer. 2009; **9**(11):798-809.
150. P Grosse-Gehling, CA Fargeas, C Dittfeld, Y Garbe, MR Alison, D Corbeil, and LA Kunz-Schughart. *CD133 as a biomarker for putative cancer stem cells in solid tumours: limitations, problems and challenges*. J Pathol. 2013; **229**(3):355-78.
151. H Yu, M Kortylewski, and D Pardoll. *Crosstalk between cancer and immune cells: role of STAT3 in the tumour microenvironment*. Nat Rev Immunol. 2007; **7**(1):41-51.
152. R Garcia, CL Yu, A Hudnall, R Catlett, KL Nelson, T Smithgall, DJ Fujita, SP Ethier, and R Jove. *Constitutive activation of Stat3 in fibroblasts transformed by diverse oncoproteins and in breast carcinoma cells*. Cell Growth Differ. 1997; **8**(12):1267-76.
153. C Lutticken, UM Wegenka, J Yuan, J Buschmann, C Schindler, A Ziemiecki, AG Harpur, AF Wilks, K Yasukawa, T Taga, and et al. *Association of transcription factor APRF and protein kinase Jak1 with the interleukin-6 signal transducer gp130*. Science. 1994; **263**(5143):89-92.
154. LA Megeney, RL Perry, JE LeCouter, and MA Rudnicki. *bFGF and LIF signaling activates STAT3 in proliferating myoblasts*. Dev Genet. 1996; **19**(2):139-45.
155. K Yokogami, S Wakisaka, J Avruch, and SA Reeves. *Serine phosphorylation and maximal activation of STAT3 during CNTF signaling is mediated by the rapamycin target mTOR*. Curr Biol. 2000; **10**(1):47-50.
156. AT Wierenga, I Vogelzang, BJ Eggen, and E Vellenga. *Erythropoietin-induced serine 727 phosphorylation of STAT3 in erythroid cells is mediated by a MEK-, ERK-, and MSK1-dependent pathway*. Exp Hematol. 2003; **31**(5):398-405.

157. N Jain, T Zhang, WH Kee, W Li, and X Cao. *Protein kinase C delta associates with and phosphorylates Stat3 in an interleukin-6-dependent manner*. J Biol Chem. 1999; **274**(34):24392-400.
158. Z Wen, Z Zhong, and JE Darnell, Jr. *Maximal activation of transcription by Stat1 and Stat3 requires both tyrosine and serine phosphorylation*. Cell. 1995; **82**(2):241-50.
159. J Sgrignani, M Garofalo, M Matkovic, J Merulla, CV Catapano, and A Cavalli. *Structural Biology of STAT3 and Its Implications for Anticancer Therapies Development*. Int J Mol Sci. 2018; **19**(6).
160. RL Carpenter and HW Lo. *STAT3 Target Genes Relevant to Human Cancers*. Cancers (Basel). 2014; **6**(2):897-925.
161. L Yang, S Lin, L Xu, J Lin, C Zhao, and X Huang. *Novel activators and small-molecule inhibitors of STAT3 in cancer*. Cytokine Growth Factor Rev. 2019; **49**:10-22.
162. X Chen, L Pan, J Wei, R Zhang, X Yang, J Song, RY Bai, S Fu, CR Pierson, JL Finlay, C Li, and J Lin. *LLL12B, a small molecule STAT3 inhibitor, induces growth arrest, apoptosis, and enhances cisplatin-mediated cytotoxicity in medulloblastoma cells*. Sci Rep. 2021; **11**(1):6517.
163. X Ren, L Duan, Q He, Z Zhang, Y Zhou, D Wu, J Pan, D Pei, and K Ding. *Identification of Niclosamide as a New Small-Molecule Inhibitor of the STAT3 Signaling Pathway*. ACS Med Chem Lett. 2010; **1**(9):454-9.
164. L Shi, H Zheng, W Hu, B Zhou, X Dai, Y Zhang, Z Liu, X Wu, C Zhao, and G Liang. *Niclosamide inhibition of STAT3 synergizes with erlotinib in human colon cancer*. Onco Targets Ther. 2017; **10**:1767-1776.
165. P Yue and J Turkson. *Targeting STAT3 in cancer: how successful are we?* Expert Opin Investig Drugs. 2009; **18**(1):45-56.
166. AM Martin, E Raabe, C Eberhart, and KJ Cohen. *Management of pediatric and adult patients with medulloblastoma*. Curr Treat Options Oncol. 2014; **15**(4):581-94.
167. DJ Mabbott, BJ Spiegler, ML Greenberg, JT Rutka, DJ Hyder, and E Bouffet. *Serial evaluation of academic and behavioral outcome after treatment with cranial radiation in childhood*. J Clin Oncol. 2005; **23**(10):2256-63.
168. A Lilja, C Nordborg, A Brun, LG Salford, and P Aman. *Expression of the IL-6 family cytokines in human brain tumors*. Int J Oncol. 2001; **19**(3):495-9.
169. E Houben, N Hellings, and B Broux. *Oncostatin M, an Underestimated Player in the Central Nervous System*. Front Immunol. 2019; **10**:1165.
170. UK Hanisch. *Microglia as a source and target of cytokines*. Glia. 2002; **40**(2):140-55.
171. S Grivennikov and M Karin. *Autocrine IL-6 signaling: a key event in tumorigenesis?* Cancer Cell. 2008; **13**(1):7-9.
172. W Hartmann, A Koch, H Brune, A Waha, U Schuller, I Dani, D Denkhau, W Langmann, U Bode, OD Wiestler, K Schilling, and T Pietsch. *Insulin-like growth factor II is involved in the proliferation control of medulloblastoma and its cerebellar precursor cells*. Am J Pathol. 2005; **166**(4):1153-62.
173. EK Rowinsky and RC Donehower. *The clinical pharmacology and use of antimicrotubule agents in cancer chemotherapeutics*. Pharmacol Ther. 1991; **52**(1):35-84.
174. DP Ivanov, B Coyle, DA Walker, and AM Grabowska. *In vitro models of medulloblastoma: Choosing the right tool for the job*. J Biotechnol. 2016; **236**:10-25.
175. RB Luwor, SS Stylli, and AH Kaye. *The role of Stat3 in glioblastoma multiforme*. J Clin Neurosci. 2013; **20**(7):907-11.

176. K Banerjee and H Resat. *Constitutive activation of STAT3 in breast cancer cells: A review.* Int J Cancer. 2016; **138**(11):2570-8.
177. G Niu, KL Wright, M Huang, L Song, E Haura, J Turkson, S Zhang, T Wang, D Sinibaldi, D Coppola, R Heller, LM Ellis, J Karras, J Bromberg, D Pardoll, R Jove, and H Yu. *Constitutive Stat3 activity up-regulates VEGF expression and tumor angiogenesis.* Oncogene. 2002; **21**(13):2000-8.
178. XT Ma, S Wang, YJ Ye, RY Du, ZR Cui, and M Somsouk. *Constitutive activation of Stat3 signaling pathway in human colorectal carcinoma.* World J Gastroenterol. 2004; **10**(11):1569-73.
179. SJ Libertini, H Chen, B al-Bataina, T Koilvaram, M George, AC Gao, and M Mudryj. *The interleukin 6 receptor is a direct transcriptional target of E2F3 in prostate tumor derived cells.* Prostate. 2012; **72**(6):649-60.
180. RJ Packer, LN Sutton, R Elterman, B Lange, J Goldwein, HS Nicholson, L Mulne, J Boyett, G D'Angio, K Wechsler-Jentsch, and et al. *Outcome for children with medulloblastoma treated with radiation and cisplatin, CCNU, and vincristine chemotherapy.* J Neurosurg. 1994; **81**(5):690-8.
181. S Dasari and PB Tchounwou. *Cisplatin in cancer therapy: molecular mechanisms of action.* Eur J Pharmacol. 2014; **740**:364-78.
182. C Marosi. *Complications of chemotherapy in neuro-oncology.* Handb Clin Neurol. 2012; **105**:873-85.
183. A Seelig. *P-Glycoprotein: One Mechanism, Many Tasks and the Consequences for Pharmacotherapy of Cancers.* Front Oncol. 2020; **10**:576559.
184. W Chen, T Xia, D Wang, B Huang, P Zhao, J Wang, X Qu, and X Li. *Human astrocytes secrete IL-6 to promote glioma migration and invasion through upregulation of cytomembrane MMP14.* Oncotarget. 2016; **7**(38):62425-62438.
185. GL Razidlo, KM Burton, and MA McNiven. *Interleukin-6 promotes pancreatic cancer cell migration by rapidly activating the small GTPase CDC42.* J Biol Chem. 2018; **293**(28):11143-11153.
186. WJ Azar, EL Christie, C Mitchell, DS Liu, G Au-Yeung, and DDL Bowtell. *Noncanonical IL6 Signaling-Mediated Activation of YAP Regulates Cell Migration and Invasion in Ovarian Clear Cell Cancer.* Cancer Res. 2020; **80**(22):4960-4971.
187. R Natarajan, V Singal, R Benes, J Gao, H Chan, H Chen, Y Yu, J Zhou, and P Wu. *STAT3 modulation to enhance motor neuron differentiation in human neural stem cells.* PLoS One. 2014; **9**(6):e100405.
188. H Yu, H Lee, A Herrmann, R Buettner, and R Jove. *Revisiting STAT3 signaling in cancer: new and unexpected biological functions.* Nat Rev Cancer. 2014; **14**(11):736-46.
189. F Zhang, Z Wang, Y Fan, Q Xu, W Ji, R Tian, and R Niu. *Elevated STAT3 Signaling-Mediated Upregulation of MMP-2/9 Confers Enhanced Invasion Ability in Multidrug-Resistant Breast Cancer Cells.* Int J Mol Sci. 2015; **16**(10):24772-90.
190. TX Xie, D Wei, M Liu, AC Gao, F Ali-Osman, R Sawaya, and S Huang. *Stat3 activation regulates the expression of matrix metalloproteinase-2 and tumor invasion and metastasis.* Oncogene. 2004; **23**(20):3550-60.
191. Y Pei, KW Liu, J Wang, A Garancher, R Tao, LA Esparza, DL Maier, YT Udaka, N Murad, S Morrissy, H Seker-Cin, S Brabetz, L Qi, M Kogiso, S Schubert, JM Olson, YJ Cho, XN Li, JR Crawford, ML Levy, M Kool, SM Pfister, MD Taylor, and RJ Wechsler-

- Reya. *HDAC and PI3K Antagonists Cooperate to Inhibit Growth of MYC-Driven Medulloblastoma*. *Cancer Cell*. 2016; **29**(3):311-323.
192. S Ball, C Li, PK Li, and J Lin. *The small molecule, LLL12, inhibits STAT3 phosphorylation and induces apoptosis in medulloblastoma and glioblastoma cells*. *PLoS One*. 2011; **6**(4):e18820.
193. H Xiao, HK Bid, D Jou, X Wu, W Yu, C Li, PJ Houghton, and J Lin. *A novel small molecular STAT3 inhibitor, LY5, inhibits cell viability, cell migration, and angiogenesis in medulloblastoma cells*. *J Biol Chem*. 2015; **290**(6):3418-29.
194. NS Nagathihalli, JA Castellanos, P Lamichhane, F Messaggio, C Shi, X Dai, P Rai, X Chen, MN VanSaun, and NB Merchant. *Inverse Correlation of STAT3 and MEK Signaling Mediates Resistance to RAS Pathway Inhibition in Pancreatic Cancer*. *Cancer Res*. 2018; **78**(21):6235-6246.
195. C Zhao, L Yang, F Zhou, Y Yu, X Du, Y Xiang, C Li, X Huang, C Xie, Z Liu, J Lin, L Wang, G Liang, and R Cui. *Feedback activation of EGFR is the main cause for STAT3 inhibition-irresponsiveness in pancreatic cancer cells*. *Oncogene*. 2020; **39**(20):3997-4013.
196. CS Milagre, G Gopinathan, G Everitt, RG Thompson, H Kulbe, H Zhong, RE Hollingsworth, R Grose, DD Bowtell, D Hochhauser, and FR Balkwill. *Adaptive Upregulation of EGFR Limits Attenuation of Tumor Growth by Neutralizing IL6 Antibodies, with Implications for Combined Therapy in Ovarian Cancer*. *Cancer Res*. 2015; **75**(7):1255-64.
197. V Appay and SL Rowland-Jones. *RANTES: a versatile and controversial chemokine*. *Trends Immunol*. 2001; **22**(2):83-7.
198. G Conductier, N Blondeau, A Guyon, JL Nahon, and C Rovere. *The role of monocyte chemoattractant protein MCP1/CCL2 in neuroinflammatory diseases*. *J Neuroimmunol*. 2010; **224**(1-2):93-100.
199. EH Yi, CS Lee, JK Lee, YJ Lee, MK Shin, CH Cho, KW Kang, JW Lee, W Han, DY Noh, YN Kim, IH Cho, and SK Ye. *STAT3-RANTES autocrine signaling is essential for tamoxifen resistance in human breast cancer cells*. *Mol Cancer Res*. 2013; **11**(1):31-42.
200. A Eichten, J Su, AP Adler, L Zhang, E Ioffe, AA Parveen, GD Yancopoulos, J Rudge, I Lowy, HC Lin, D MacDonald, C Daly, X Duan, and G Thurston. *Resistance to Anti-VEGF Therapy Mediated by Autocrine IL6/STAT3 Signaling and Overcome by IL6 Blockade*. *Cancer Res*. 2016; **76**(8):2327-39.
201. VS Jones, RY Huang, LP Chen, ZS Chen, L Fu, and RP Huang. *Cytokines in cancer drug resistance: Cues to new therapeutic strategies*. *Biochim Biophys Acta*. 2016; **1865**(2):255-65.
202. SP Gao, KG Mark, K Leslie, W Pao, N Motoi, WL Gerald, WD Travis, W Bornmann, D Veach, B Clarkson, and JF Bromberg. *Mutations in the EGFR kinase domain mediate STAT3 activation via IL-6 production in human lung adenocarcinomas*. *J Clin Invest*. 2007; **117**(12):3846-56.
203. P Sansone, G Storci, S Tavolari, T Guarnieri, C Giovannini, M Taffurelli, C Ceccarelli, D Santini, P Paterini, KB Marcu, P Chieco, and M Bonafe. *IL-6 triggers malignant features in mammospheres from human ductal breast carcinoma and normal mammary gland*. *J Clin Invest*. 2007; **117**(12):3988-4002.
204. Q Liu, S Yu, A Li, H Xu, X Han, and K Wu. *Targeting interleukin-6 to relieve immunosuppression in tumor microenvironment*. *Tumour Biol*. 2017; **39**(6):1010428317712445.

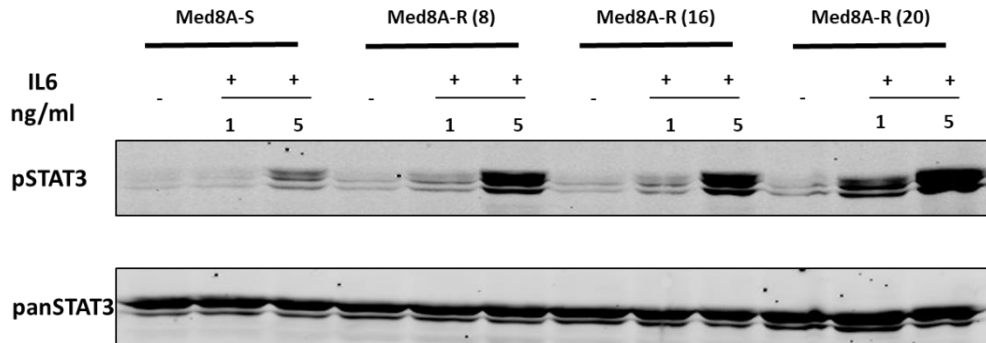
205. J Nakashima, M Tachibana, Y Horiguchi, M Oya, T Ohigashi, H Asakura, and M Murai. *Serum interleukin 6 as a prognostic factor in patients with prostate cancer*. Clin Cancer Res. 2000; **6**(7):2702-6.
206. Y Shan, X He, W Song, D Han, J Niu, and J Wang. *Role of IL-6 in the invasiveness and prognosis of glioma*. Int J Clin Exp Med. 2015; **8**(6):9114-20.
207. EM Silva, VS Mariano, PRA Pastrez, MC Pinto, AG Castro, KJ Syrjanen, and A Longatto-Filho. *High systemic IL-6 is associated with worse prognosis in patients with non-small cell lung cancer*. PLoS One. 2017; **12**(7):e0181125.
208. S Verstovsek. *Ruxolitinib: an oral Janus kinase 1 and Janus kinase 2 inhibitor in the management of myelofibrosis*. Postgrad Med. 2013; **125**(1):128-35.
209. DH Gutmann and H Kettenmann. *Microglia/Brain Macrophages as Central Drivers of Brain Tumor Pathobiology*. Neuron. 2019; **104**(3):442-449.
210. ML Loh, SK Tasian, KR Rabin, P Brown, D Magoon, JM Reid, X Chen, CH Ahern, BJ Weigel, and SM Blaney. *A phase I dosing study of ruxolitinib in children with relapsed or refractory solid tumors, leukemias, or myeloproliferative neoplasms: A Children's Oncology Group phase I consortium study (ADVL1011)*. Pediatr Blood Cancer. 2015; **62**(10):1717-24.
211. M Morfouace, S Cheepala, S Jackson, Y Fukuda, YT Patel, S Fatima, D Kawauchi, AA Shelat, CF Stewart, BP Sorrentino, JD Schuetz, and MF Roussel. *ABCG2 Transporter Expression Impacts Group 3 Medulloblastoma Response to Chemotherapy*. Cancer Res. 2015; **75**(18):3879-89.
212. S Igelmann, HA Neubauer, and G Ferbeyre. *STAT3 and STAT5 Activation in Solid Cancers*. Cancers (Basel). 2019; **11**(10).
213. A Rani and JJ Murphy. *STAT5 in Cancer and Immunity*. J Interferon Cytokine Res. 2016; **36**(4):226-37.
214. R Lang, AL Pauleau, E Parganas, Y Takahashi, J Mages, JN Ihle, R Rutschman, and PJ Murray. *SOCS3 regulates the plasticity of gp130 signaling*. Nat Immunol. 2003; **4**(6):546-50.
215. NPD Liao, A Laktyushin, IS Lucet, JM Murphy, S Yao, E Whitlock, K Callaghan, NA Nicola, NJ Kershaw, and JJ Babon. *The molecular basis of JAK/STAT inhibition by SOCS1*. Nat Commun. 2018; **9**(1):1558.
216. Z Yagil, H Nechushtan, G Kay, CM Yang, DM Kemeny, and E Razin. *The enigma of the role of protein inhibitor of activated STAT3 (PIAS3) in the immune response*. Trends Immunol. 2010; **31**(5):199-204.
217. B Rodel, K Tavassoli, H Karsunky, T Schmidt, M Bachmann, F Schaper, P Heinrich, K Shuai, HP Elsasser, and T Moroy. *The zinc finger protein Gfi-1 can enhance STAT3 signaling by interacting with the STAT3 inhibitor PIAS3*. EMBO J. 2000; **19**(21):5845-55.
218. N Perrimon and AP McMahon. *Negative feedback mechanisms and their roles during pattern formation*. Cell. 1999; **97**(1):13-6.
219. S Rivero-Hinojosa, LS Lau, M Stampar, J Staal, H Zhang, H Gordish-Dressman, PA Northcott, SM Pfister, MD Taylor, KJ Brown, and BR Rood. *Proteomic analysis of Medulloblastoma reveals functional biology with translational potential*. Acta Neuropathol Commun. 2018; **6**(1):48.
220. D Greenbaum, C Colangelo, K Williams, and M Gerstein. *Comparing protein abundance and mRNA expression levels on a genomic scale*. Genome Biol. 2003; **4**(9):117.

221. DW Parsons, M Li, X Zhang, S Jones, RJ Leary, JC Lin, SM Boca, H Carter, J Samayoa, C Bettegowda, GL Gallia, GI Jallo, ZA Binder, Y Nikolsky, J Hartigan, DR Smith, DS Gerhard, DW Fults, S VandenBerg, MS Berger, SK Marie, SM Shinjo, C Clara, PC Phillips, JE Minturn, JA Biegel, AR Judkins, AC Resnick, PB Storm, T Curran, Y He, BA Rasheed, HS Friedman, ST Keir, R McLendon, PA Northcott, MD Taylor, PC Burger, GJ Riggins, R Karchin, G Parmigiani, DD Bigner, H Yan, N Papadopoulos, B Vogelstein, KW Kinzler, and VE Velculescu. *The genetic landscape of the childhood cancer medulloblastoma*. Science. 2011; **331**(6016):435-9.
222. C Miranda Kuzan-Fischer, K Juraschka, and MD Taylor. *Medulloblastoma in the Molecular Era*. J Korean Neurosurg Soc. 2018; **61**(3):292-301.
223. KM Yamada and E Cukierman. *Modeling tissue morphogenesis and cancer in 3D*. Cell. 2007; **130**(4):601-10.
224. D Lv, Z Hu, L Lu, H Lu, and X Xu. *Three-dimensional cell culture: A powerful tool in tumor research and drug discovery*. Oncol Lett. 2017; **14**(6):6999-7010.
225. SJ Roper, F Linke, PJ Scotting, and B Coyle. *3D spheroid models of paediatric SHH medulloblastoma mimic tumour biology, drug response and metastatic dissemination*. Sci Rep. 2021; **11**(1):4259.
226. S Temple. *The development of neural stem cells*. Nature. 2001; **414**(6859):112-7.
227. DF Ransohoff. *Bias as a threat to the validity of cancer molecular-marker research*. Nat Rev Cancer. 2005; **5**(2):142-9.
228. F Bianchi, F Nicassio, and PP Di Fiore. *Unbiased vs. biased approaches to the identification of cancer signatures: the case of lung cancer*. Cell Cycle. 2008; **7**(6):729-34.
229. C Qin, Y Pan, Y Li, Y Li, W Long, and Q Liu. *Novel Molecular Hallmarks of Group 3 Medulloblastoma by Single-Cell Transcriptomics*. Front Oncol. 2021; **11**:622430.
230. R Kumar, KS Smith, M Deng, C Terhune, GW Robinson, BA Orr, APY Liu, T Lin, CA Billups, M Chintagumpala, DC Bowers, TE Hassall, JR Hansford, DA Khuong-Quang, JR Crawford, AE Bendel, S Gururangan, K Schroeder, E Bouffet, U Bartels, MJ Fisher, R Cohn, S Partap, SJ Kellie, G McCowage, AC Paulino, S Rutkowski, G Fleischhack, G Dhall, LJ Klesse, S Leary, J Nazarian, M Kool, P Wesseling, M Ryzhova, O Zheludkova, AV Golanov, RE McLendon, RJ Packer, C Dunham, J Hukin, M Fouladi, CC Faria, J Pimentel, AW Walter, N Jabado, YJ Cho, S Perreault, SE Croul, M Zapotocky, C Hawkins, U Tabori, MD Taylor, SM Pfister, P Klimo, Jr., FA Boop, DW Ellison, TE Merchant, A Onar-Thomas, A Korshunov, DTW Jones, A Gajjar, V Ramaswamy, and PA Northcott. *Clinical Outcomes and Patient-Matched Molecular Composition of Relapsed Medulloblastoma*. J Clin Oncol. 2021; **39**(7):807-821.
231. Y Teng, JL Ross, and JK Cowell. *The involvement of JAK-STAT3 in cell motility, invasion, and metastasis*. JAKSTAT. 2014; **3**(1):e28086.
232. A Vaidyanathan, L Sawers, AL Gannon, P Chakravarty, AL Scott, SE Bray, MJ Ferguson, and G Smith. *ABCBI (MDR1) induction defines a common resistance mechanism in paclitaxel- and olaparib-resistant ovarian cancer cells*. Br J Cancer. 2016; **115**(4):431-41.
233. AK Nanayakkara, CA Follit, G Chen, NS Williams, PD Vogel, and JG Wise. *Targeted inhibitors of P-glycoprotein increase chemotherapeutic-induced mortality of multidrug resistant tumor cells*. Sci Rep. 2018; **8**(1):967.
234. A Valeta-Magara, A Gadi, V Volta, B Walters, R Arju, S Giashuddin, H Zhong, and RJ Schneider. *Inflammatory Breast Cancer Promotes Development of M2 Tumor-Associated*

- Macrophages and Cancer Mesenchymal Cells through a Complex Chemokine Network.* Cancer Res. 2019; **79**(13):3360-3371.
235. Z Yan, SA Gibson, JA Buckley, H Qin, and EN Benveniste. *Role of the JAK/STAT signaling pathway in regulation of innate immunity in neuroinflammatory diseases.* Clin Immunol. 2018; **189**:4-13.

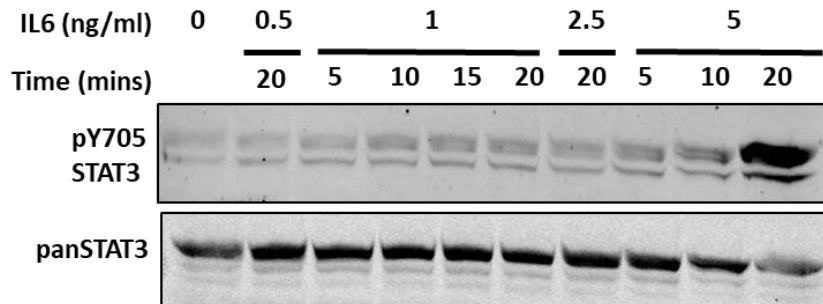
Appendix A

A.1



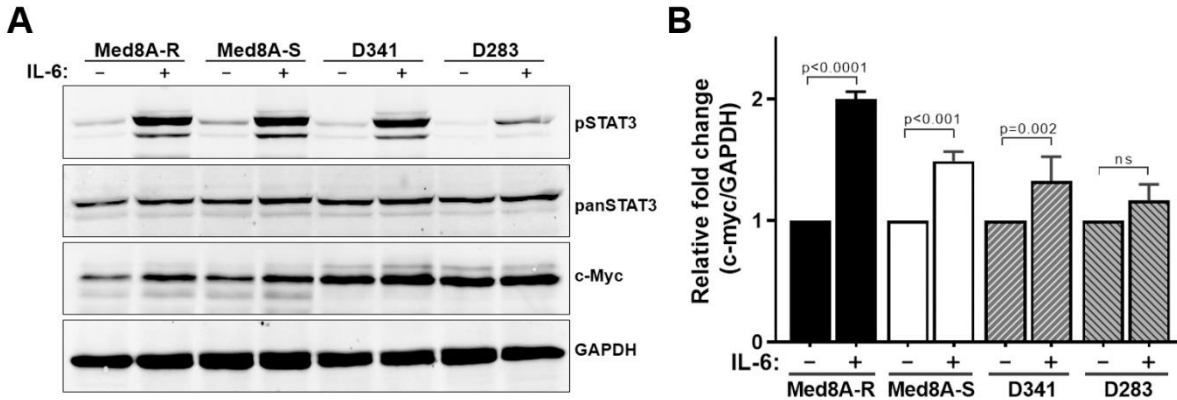
IL-6 stimulation of STAT3 expression in Med8A-S and Med8A-R variants. The indicated cells were untreated or treated with 1 ng/mL and 5 IL-6 ng/mL for 15 mins and lysates immunoblotted for pY705-STAT3, total STAT3 and GAPDH. As shown is representative of 3 independent replicates.

A.2



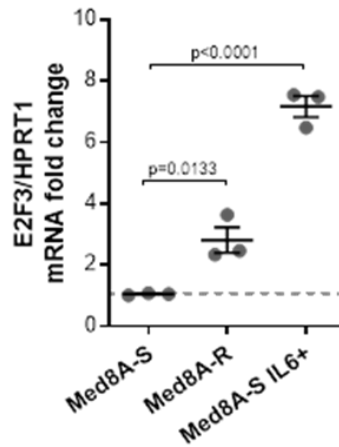
Concentration and time optimization for IL-6 stimulation. Med8A-R cells were untreated or treated with varying concentration of IL-6 for different time points (mentioned in the figure) and lysates immunoblotted for pY705-STAT3, total STAT3 and GAPDH. As shown is representative of 3 independent replicates.

A.3



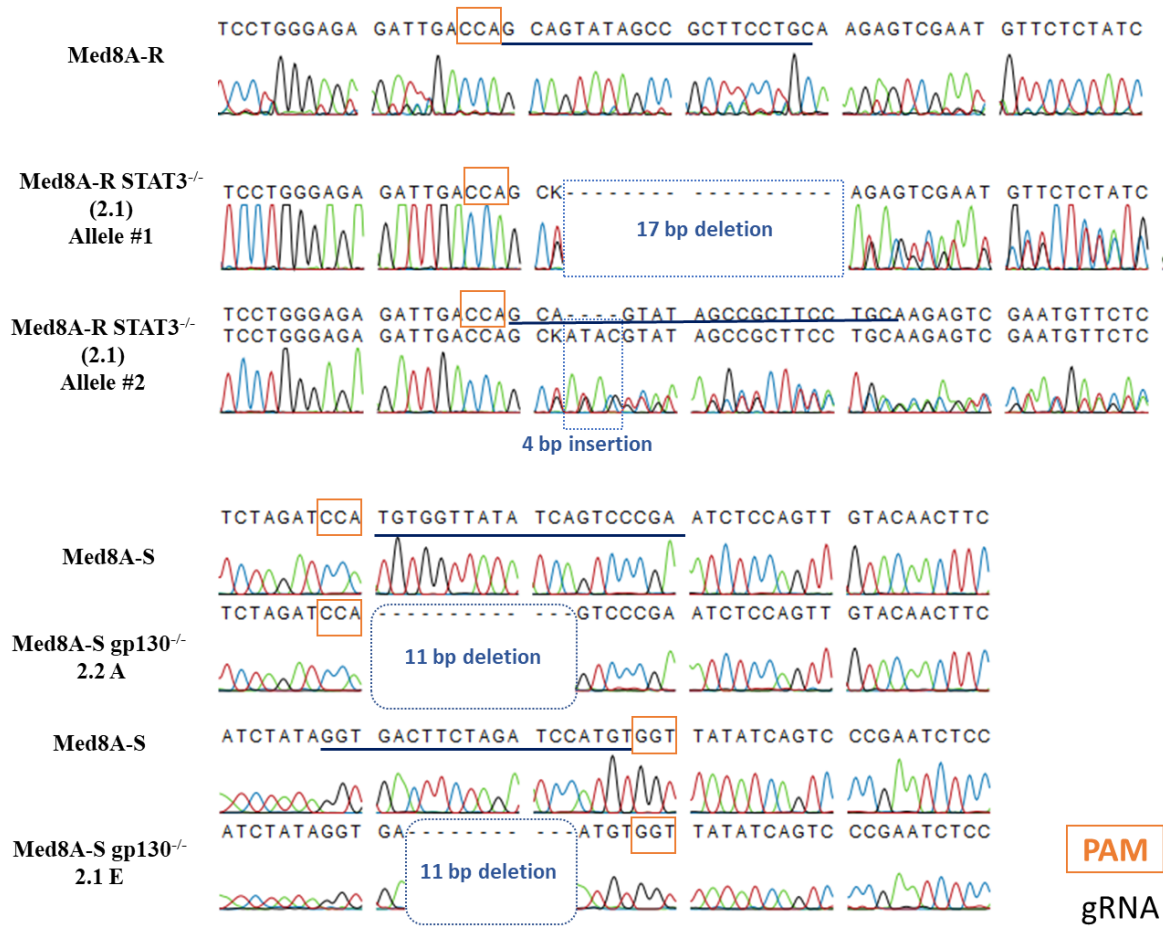
IL-6 stimulation of c-Myc expression. (A) The indicated cells were untreated or treated with 10 ng/mL IL-6 for 15 mins and lysates immunoblotted for pY705-STAT3, total STAT3, c-Myc and GAPDH. As shown is representative of 3 independent replicates. (B) Quantitation of c-Myc over GAPDH, reflected as fold change, from the data shown in A (Mean \pm SD, one-way ANOVA with Bonferroni's post-test).

A.4



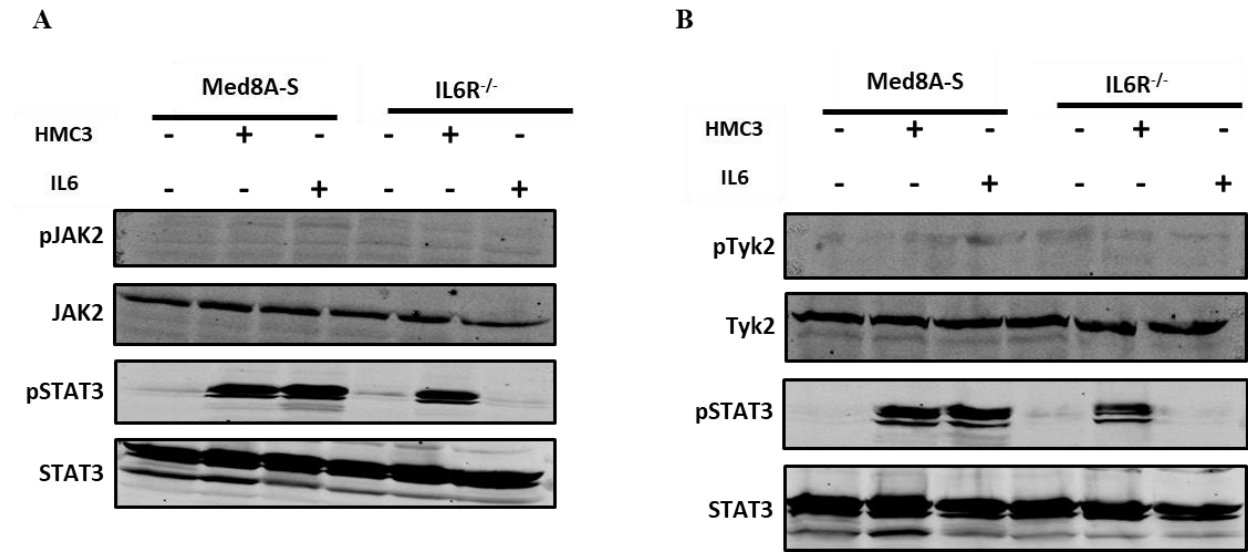
E2F3 mRNA expression. QPCR for IL6R mRNA expression. Error bars represent mean \pm SD ($n = 3$); ** $p < 0.01$, *** < 0.001 , two tailed unpaired t-test.

A.5



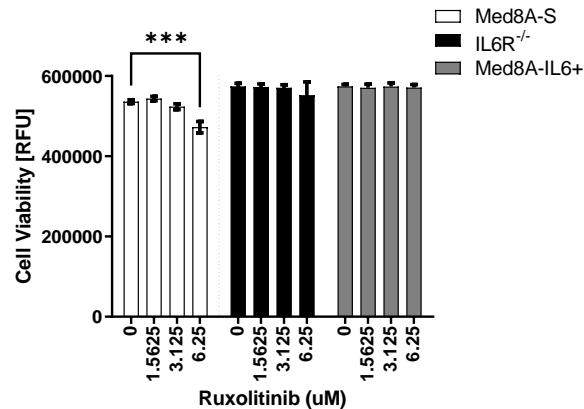
Sequencing of STAT3 and gp130 CRISPR clones: Sequencing of the Med8A-R and STAT3^{-/-} cells revealed a heterozygous indel within the second coding exon of *STAT3* at the gRNA targeted site. The 2nd coding exon of *gp130* was similarly targeted using CRISPR-Cas9 in Med8A-S cells. As shown is the sequencing alignment for a two homozygous deletion in gp130^{-/-} clones (gRNA underlined, PAM motif highlighted in orange).

A.6



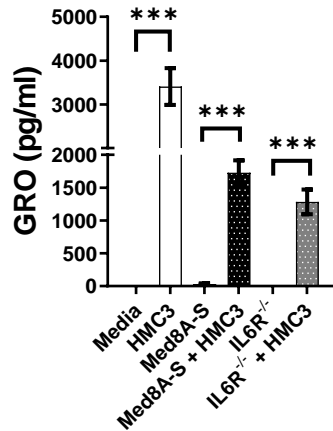
Phosphorylation of JAK2 and TYK2 expression. The indicated cells were co-cultured with HMC3 cells or conditioned with IL-6 for 2 weeks and weaned off for two weeks prior to harvesting lysates. (A) Immunoblotted for pJAK2, JAK2, pY705-STAT3, total STAT3. B) Immunoblotted for pTyk2, Tyk2, pY705-STAT3, total STAT3.

A.7



Optimization for sub toxic dose of ruxolitinib. Med8A-S, IL-6R^{-/-}, and Med8A-S-IL-6+ cells were treated with ruxolitinib alone at the indicated concentrations for 48 h and cell viability assessed with CTB. As plotted is the mean \pm SD of three replicates; *** $p < 0.001$, two-way ANOVA with bonferroni multiple comparison test. (##Significance are compared between 0 and other concentrations within each cell line).

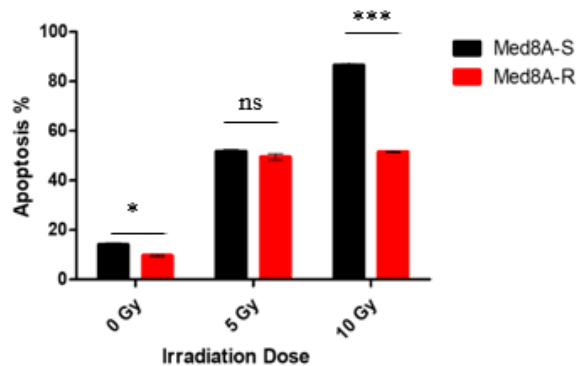
A.8



HMC3 and Med8A cells secrete GRO.

Analyses for secreted GRO in culture supernatant of the indicated cells and co-culture combination. As plotted is the mean \pm SD of three replicates; *** $p < 0.001$, ** < 0.01 , * < 0.05 , two-way ANOVA with Tukey's multiple comparison test.

A.9



Med8A-R cells exhibit resistance to irradiation.

Med8A-S and Med8A-R cells were plated at an initial seeding density of 2.5×10^5 cells per well in triplicates and subjected to 5 Gy and 10 Gy radiation. These cells were incubated at 37° C for 72 hours before performing Annexin V apoptosis assay.

Appendix B

B.1

Table: List of antibodies/kits used in the thesis.

Antibody	Catalog #	Application	Company
pY705-STAT3	9145	Western blot	Cell Signaling
pS727-STAT3	9134	Western blot	Cell Signaling
STAT3	9139	Western blot	Cell Signaling
pAKT (S473)	4060	Western blot	Cell Signaling
pAKT (T308)	2965	Western blot	Cell Signaling
BAD	sc-8044	Western blot	Santa Cruz
BCL-xL	2764	Western blot	Cell Signaling
MCL1	sc-819	Western blot	Santa Cruz
SOCS3	52113	Western blot	Cell Signaling
pERK1/2	4695	Western blot	Cell Signaling
MDR1	12273	Western blot	Cell Signaling
GAPDH	631402	Western blot	Biologend
c-MYC	13987	Western blot	Cell signaling
pJAK1	74129	Western blot	Cell signaling
pJAK2	8082	Western blot	Cell signaling
pTYK2	68790	Western blot	Cell signaling
JAK1	3344	Western blot	Cell signaling
JAK2	3230	Western blot	Cell signaling
TYK2	14193	Western blot	Cell signaling
IL-6R α	352802	Flow cytometry	R&D systems
IL-6	Z03034	Recombinant cytokine	Genscript
LIF	Z02681	Recombinant cytokine	Genscript
IL-11	Z03108	Recombinant cytokine	Genscript
OSM	Z03132	Recombinant cytokine	Genscript
LIFR α	BS-1458R	Flow cytometry	Bios USA
IL-11R α	10264-1-AP	Flow cytometry	Thermo Fisher
OSMR β	17-1303-42	Flow cytometry	Thermo Fisher
IL-6	362006	ELISA	Biologend
Gp130	362005	Flow cytometry	Biologend